FORCED SYNOPTIC COASTAL-TRAPPED WAVES ALONG THE SOUTHERN AFRICAN COASTLINE

Roy C. van Ballegooyen

Submitted in fulfilment of the requirements
for the
degree of Master of Science
in the
Faculty of Science, University of Cape Town

October 1995

Abstract

The presence of subinertial (2 to 20 day) oscillations in sea levels and currents over the continental shelf surrounding southern Africa is well-documented, however presently available observational data alone are largely unsuitable or insufficient to adequately characterise the shelf circulation in terms of coastal-trapped wave (CTW) theory. In this dissertation, an analysis of atmospheric pressure and sea level data from 1980 to 1990, a scale analysis of the equations of motion and numerical modelling are used to characterise the subinertial coastal-trapped wave motions off the west coast and south coasts of southern Africa.

Appropriate scaling of the equations of motion and numerical analyses of the subinertial CTW response at a number of locations along the west and south coasts of southern Africa indicate that the large scale response of shelf waters to synoptic scale or "weather band" atmospheric forcing is predominantly barotropic. This permits the use of the linear, vertically integrated, shallow water wave equations on a f-plane to model the response of the West Coast shelf waters to "weather band" atmospheric forcing. The CTW dispersion curves have been calculated for a number of shelf profiles along the West and South Coast and are used in the interpretation of the sea level analyses and the numerical modelling results, and further to investigate the effect of increasing water column stratification on the subinertial CTW response.

Both sea level analyses and the modelling results indicate that the sea level fluctuations associated with synoptic CTW motions off the West and South Coasts are quasi-periodic and predominantly locally forced. Seasonal and interannual changes in the atmospheric forcing are strongly reflected in the first order response of the shelf waters. The more energetic and extensive atmospheric forcing of winter and spring is clearly observed in the CTW sea level response at both West and South Coast locations. The effect of seasonal changes in the stratification of the shelf waters are more subtle. Increased stratification of the water column modifies the response of shelf waters mainly by altering the topographic scattering of CTW motions due to large alongshore changes in the bottom topography.

Theoretical considerations and the modelling results show that the extent and rapidity of changes in the wind fields over the shelf are strong factors in determining both the nature and amplitude of the CTW response. In general there is a resonance between the weather systems moving along the southern African coastline and the shelf waters, leading to a significant CTW response at subinertial frequencies. Smaller more rapid changes in the wind stress fields are less effective in generating CTW motions, except in the wider shelf regions which respond more readily to rapidly propagating weather systems. The efficiency of wind-forcing over wide, shallow shelf regions is clearly observed as an increased sea level variability over both the Orange River cone and Agulhas Bank which seem to be geographic origins for the CTW motions observed over southern African continental shelf. The effect of open ocean and remote forcing on the shelf circulation is evidenced as large, low frequency excursions of sea level all along the southern African coastline, especially along the East Coast where the Agulhas Current dramatically damps and slows the propagation of CTW's along the shelf.

The importance of the underlying bottom topography in determining the nature of the barotropic response over the shelf is clearly demonstrated in the numerical model results. The shorter wavelength, barotropic CTW motions are strongly scattered by large alongshore variations in the shelf topography, both inhibiting the propagation of CTW energy along the West Coast and resulting in the development of strong, almost steady-state, cross-shore velocities near the shelf edge. These large cross-shore velocities are particularly prominent south of Lüderitz, in the vicinity of Hondeklip Bay and to a lesser extent in the vicinity of Cape Columbine. The potential importance of stratification in modifying the topographic scattering of CTW motions is noted and the barotropic modelling results are interpreted accordingly, however the modelling results are well supported by oceanographic observations along the West Coast.

Finally, it should be noted that the lack of a detailed knowledge and understanding of the offshore and coastal marine wind fields along the southern African coast is a particularly limiting factor in both present and future studies of CTW motions and shelf circulation around southern Africa.

Acknowledgements

I thank my supervisor, Professor Geoff Brundrit, for his advice and guidance and Drs Frank Shillington and Dirk van Foreest for their encouragement and many discussions during this during the course of this research. I further thank Professor Johann Lutjeharms, Henry Valentine and Lesley Staegemann for providing an environment that expedited the completion of the dissertation.

The advice, information and data provided by Dr Mark Jury of the University of Cape Town, Greville Nelson of the Sea Fisheries Research Institute, Dr Eckart Schumann of the University of Port Elizabeth and Ian Hunter of the South African Weather Bureau, as well as many former colleagues at the former National Research Institue of Oceanology and the present EMATEK, is greatly appreciated. The assistance of the UCT Information Technology Services and Shaun Courtney with the computational aspects of the research and Sarah Searson with the initial processing of the sea level data, is acknowledged.

To Jean, thank you for your patience, support and encouragement during this period.

TABLE OF CONTENTS

List of symbols

x	cross-shore distance co-ordinate (m)
X	cross-shore spatial scale (m)
y	longshore distance co-ordinate (m)
Y	longshore spatial scale (m)
t	time (s)
T	temporal scale of the response (s)
η	sea level displacement (m)
η	sea level displacement height scale (m)
η'	pressure adjusted sea level displacement (m)
h	water depth (m)
H	water depth scale (m)
X_h	characteristic scale of cross-shore variations in bottom topography
Y_h	characteristic scale of alongshore variations in bottom topography
u	cross-shore velocity ($m.s^{-1}$)
U	cross-shore velocity scale ($m.s^{-1}$)
v	longshore velocity ($m.s^{-1}$)
V	longshore velocity scale ($m.s^{-1}$)
U	cross-shore volume transport ($m^3.s^{-1}$)
V	longshore volume transport ($m^3.s^{-1}$)
ρ	in-situ density
ρ'	perturbation density ($kg.m^{-3}$)
ρ_0	mean density ($kg.m^{-3}$)
f_0	Coriolis parameter at a specified latitude
β	beta parameter ($m^{-1}.s^{-1}$)
f	Coriolis parameter (s^{-1}) where $f = f_0 + \beta y$
f	characteristic magnitude of the Coriolis parameter (s^{-1})
g	gravitational constant ($m.s^{-2}$)
r	bottom friction coefficient ($m.s^{-1}$)

τ_b	bottom stress due to friction ($N.m^{-2}$)
τ_b	characteristic magnitude of bottom stress due to friction ($N.m^{-2}$)
τ_w	surface stress due to wind ($N.m^{-2}$)
τ_w	characteristic magnitude of surface stress due to wind ($N.m^{-2}$)
σ_n	frequency of n^{th} mode coastal-trapped wave (s^{-1})
k	cross-shore wavenumber (m^{-1})
ℓ	longshore wavenumber (m^{-1})
$F_n(x,\ell)$	offshore modal structure of the n^{th} mode barotropic CTW (m)
$F_n(x,z)$	offshore modal structure of the n^{th} mode stratified CTW (m)
C_{ph}	phase velocity of wave ($m.s^{-1}$) where $C_{ph} = \sigma/k$, σ/ℓ
C_g	group velocity of wave ($m.s^{-1}$) where $C_g = \partial\sigma/\partial k$, $\partial\sigma/\partial\ell$
C_f	phase velocity of moving wind stress field ($m.s^{-1}$)
E_{TOT}	total energy in a cross-shore transect (J)
E	energy density ($J.m^{-3}$)
$\bar{F}$	energy flux ($J.m^{-2}.s^{-1}$)
α	average cross-shore shelf slope, where $\alpha = \Delta h/\Delta x$
N	Brunt-Väisälä frequency (s^{-1}), where $N^2 = -g/\rho_0 \partial\rho_0/\partial z$,
N	characteristic magnitude of the Brunt-Väisälä frequency
N_s	characteristic magnitude of the shelf-averaged Brunt-Väisälä frequency (s^{-1})
E_K	kinetic energy averaged over a wave period
E_P	potential energy averaged over a wave period
R_{kp}	the ratio (averaged over a wave period), between kinetic energy (E_K) and potential energy (E_P), where $R_{kp} = E_K / E_P$.
R_0	Rossby radius of deformation, where $R_0^2 = gH/f^2$
ε	the divergence parameter, where $\varepsilon^2 = \left(\frac{X}{R_0}\right)^2 = \frac{f^2X^2}{gH}$
R_i	internal Rossby radius of deformation, where $R_i^2 = (NH/f)^2$
S	Burger number (stratification parameter) $S^2 = \left(\frac{R_i}{X_h}\right)^2 = \left(\frac{NH}{fX_h}\right)^2$

L_f	frictional decay length scale for coastal-trapped waves
T_f	frictional decay time scale for coastal-trapped waves
a_{nn}	frictional coupling coefficient for coastal-trapped waves
h_n	wind-forcing coupling coefficient for coastal-trapped waves
$\hat{P}_{xx}(f)$	autospectral estimate for time series *x(t)*
$\hat{P}_{yy}(f)$	autospectral estimate for time series *y(t)*
$\hat{P}_{xy}(f)$	cross-spectral estimate for time series *x(t)* and *y(t)*
$\hat{\theta}_{xy}(f)$	phase function estimate for time series *x(t)* and *y(t)*
$\hat{\gamma}^2_{xy}(f)$	coherence function for time series *x(t)* and *y(t)*
$\hat{C}_{xx}(i\Delta t)$	auto-covariance function for time series *x(t)* at lag $i\Delta t$
$\hat{C}_{yy}(i\Delta t)$	auto-covariance function for time series *y(t)* at lag $i\Delta t$
$\hat{C}_{xy}(i\Delta t)$	cross-covariance function for time series *x(t)* and *y(t)* at lag $i\Delta t$
$\hat{r}_{xx}(i\Delta t)$	normalised auto-covariance function for time series *x(t)*
$\hat{r}_{yy}(i\Delta t)$	normalised auto-covariance function for time series *y(t)*
$\hat{r}_{xy}(i\Delta t)$	cross-correlation function (normalised cross-covariance function) for time series *x(t)* and *y(t)* at lag $i\Delta t$
$\hat{r}^n_{xy}(i\Delta t)$	cross-correlation function normalised by the large-lag standard error (Sciremammano, 1979)
f_n	Nyquist frequency
ν	degrees of freedom of a time series or estimate
B_e	resolution bandwidth of auto- and cross-spectral estimates
$\chi^2_{\nu,\frac{\alpha}{2}}$	percentile values for the Chi-squared distribution
$F_{2,\nu-2,\alpha}$	percentile values for the F-distribution
$t_{\nu-2,\frac{\alpha}{2}}$	percentile values for the Student-t distribution
$z_{\alpha/2}$	percentile values for the normal distribution

1. INTRODUCTION

Continental shelves form regions of shallow water with an offshore extent that may vary greatly with geographic location. The dynamics of these continental shelf waters are important in that they provide the determining environment for the many biological processes and human activities occurring in these regions.

Much of the ocean biological primary productivity takes place in these shallow waters and many important regional fisheries are found over the continental shelf. The physical environment and variability of these shelf waters place very real constraints on biological productivity and recruitment to the various fisheries. Similarly, human activities such as fishing, shipping, maritime defence, waste disposal, mariculture and especially oil and mineral exploitation, are all operationally constrained by the surrounding continental shelf water environment. A knowledge of the dynamics and the characteristic temporal and spatial scales of shelf water motions is thus essential in determining environmental impacts on fisheries and the operational constraints associated with the many human activities in these regions.

A large number of physical oceanographic phenomena occur on the continental shelf, having temporal scales of minutes to months and spatial scales of metres to thousands of kilometres (Huthnance, 1975, 1981). Although these processes all contribute to the variability of shelf waters, the greatest variability in many shelf regions is due to large-scale, wind-driven motions. This is true for most of the continental shelf waters surrounding southern Africa. Wind stresses over the West and South Coast shelf regions produce energetic fluctuations at subinertial frequencies (for example de Cuevas *et al.*, 1986, Schumann and Brink, 1990; Jury *et al.*, 1990a and Nelson, 1992a,b) with the synoptic or "weather band" variability (2-20 days) being the most energetic.

Experience has shown that, in many cases, these subinertial motions may be adequately described in terms of coastal-trapped wave (CTW) theory (for example Brink, 1987). The aim of this dissertation is to characterise and provide an understanding of the dynamics of

the low frequency variability of sea levels and currents on the southern African continental shelf. This is accomplished both through the analysis of atmospheric pressure and sea level data along the southern African coastline, and analytical and numerical studies of coastal-trapped wave motions over these shelf regions. Historically, coastal-trapped waves in the "long wave" limit (that is, subinertial CTW's having longshore scales that are large relative to cross-shelf scales) have generally been referred to as continental shelf waves (CSW). In this dissertation no such distinction is made and, when used, the term CTW generally refers to subinertial coastal-trapped waves.

CTW motions along the southern African coastline are implicated in the successful recruitment strategies and migration of fish species along the shelf (for example Schumann, 1987 and Boyd *et al.*, 1992) and provide an index of the "quality of upwelling" along the southern African coastline which strongly impacts on the biological productivity of the shelf waters (Jury and Brundrit, 1992; Nelson, 1992a).

These CTW motions also directly affect human activities such as mineral and oil exploitation, waste dispersal and mariculture, as well as coastal protection. A knowledge of the maximum expected current velocities over the shelf is important in providing design criteria for rigs and offshore installations such as those constructed for the Mossgas project. Further, a knowledge of the Lagrangian properties of dominant flows over the continental shelf is necessary to determine the dispersion of tailings from mining activities and to provide oil spill scenarios for offshore oil exploration and production platforms.

CTW motions not only affect activities over the continental shelf but are also important in determining the flushing rates of coastal embayments through the remote forcing of circulation within these embayments (Craig and Holloway, 1991; Holloway *et al.*, 1992). The determination of the flushing of False Bay due to both local and remote forcing is critical to the evaluation of the potential impacts of storm water run-off and sewage outfalls on the recreational potential of False Bay (van Ballegooyen, 1991). Similarly, CTW motions over the continental shelf play a role in determining the input of nutrients and water quality in Saldahna Bay that are so important to the mariculture industry in the

bay (Montiero and Brundrit, 1995). Lastly, the sea level fluctuations associated with CTW motions over the shelf largely determine the nature and severity of extreme sea level events (Searson and Brundrit, 1995).

1.1 Overview of Coastal-Trapped Waves around Southern African

Research into subinertial motions on the continental shelf surrounding Southern Africa has proliferated since the early 1980's. Using limited data sets, attempts have been made to characterise the low frequency response of shelf waters both in terms of sea levels (Brundrit *et al.*, 1984; de Cuevas *et al.*, 1986; Schumann and Brink, 1990; Jury *et al.*, 1990a) and current velocities (Schumann, 1983; Holden, 1986; 1987; Nelson, 1985, 1987; 1989, 1992a,b and Nelson and Polito, 1987 and Schumann and Brink, 1990).

Due to the limited availability and spatial coverage of current meter observations, most analyses of CTW (particularly the earlier ones) involved sea level data only Using tide gauge data, Brundrit (1984) investigated the long-term (seasonal and inter-annual) variability of the sea level along the West Coast. Also using sea level data, de Cuevas *et al.* (1986) isolated the temporal and spatial scales of sea level variability associated with CTW motions on the "event" scale (2 to 20 days) and showed that sea level disturbances travel anti-clockwise around the coast of southern Africa (as is typical of CTW motions in the Southern Hemisphere). Although sea level disturbances are observed to travel along the whole shelf region from Walvis Bay to Durban, de Cuevas *et al.* (1986) noted that they are sometimes limited to the West coast only or to the South Coast only and that the summer and winter responses seem distinct. The phase speeds of sea level propagation were observed to be highly variable. This led the authors to conclude that these sea level disturbances are attributable to forced and not free CTW motions, a conclusion supported by an analysis of wind and current meter observations in the vicinity of the Cape Peninsula (Nelson, 1985). There is, however, tentative evidence in the sea level data of de Cuevas (1985) and Jury *et al.* (1990a) of "remotely forced" shelf wave motions in the southern regions of the West Coast.

More recently Jury *et al.* (1990a) and Schumann and Brink (1990) used sea level data to investigate the forcing and propagation of sea level anomalies along the southern African coastline Jury *et al.* (1990b) used composites of atmospheric forcing and sea levels in their investigation while Schumann and Brink (1990) used statistically more robust techniques as well as theoretical estimates of CTW phase speeds to investigate the forcing and propagation of CTW's. Jury *et al.* (1990a) demonstrate the close relationship that exists between the coastal low and CTW motions and, together with Reason and Jury (1990), provide estimates of the propagation speed of CTW motions and the atmospheric systems that force these CTW motions. Schumann and Brink (1990) calculated theoretical free CTW phase speeds for a number of shelf topographies along the southern African coastline and compared these with the propagation speeds of sea level anomalies and wind systems around the coast of southern Africa. It was found that the trend of the estimated CTW phase speeds agreed with that of the theoretical CTW phase speed estimates and also that the propagation speeds of the wind systems fall in the same range as the estimated CTW phase speeds. This results in a resonance condition between the forcing winds and the first mode free CTW, leading to the large CTW amplitudes observed over the continental shelf of southern Africa.

There has been very little research into CTW motions north of Walvis Bay, a notable exception being the investigation of Hagen (1985) into the mesoscale response of the shelf waters in the northern region of the Namibian continental shelf (latitude 20,5°S). By assuming that the local barotropic shelf dynamics impress their structure upon the baroclinic mass fields, he analysed the local baroclinic structures for evidence of barotropic continental shelf waves. Over the shelf he observed a strong, locally forced barotropic response and identified a 5,6 day wave that he considered to be a second mode barotropic shelf wave

Concurrent with the sea level analyses, the deployment of current meters by the former National Research Institute for Oceanology (NRIO) at the head of the Cape Point valley, and the deployment of current meters on the West Coast by the Sea Fisheries Research Institute (SFRI) and NRIO on the Agulhas Bank, led to the realisation that there is

tremendous current variability on the shelf at time and spatial scales beyond the resolution of previous ship-borne studies. A number of researchers (Holden, 1986, 1987; Nelson, 1985, 1989, 1992a,b; Nelson and Polito, 1987; Schumann, 1983, Schumann and Brink, 1990) proceeded to use current meter data to characterise the low frequency component of this variability. Holden (1986, 1987), using a limited current meter data set obtained off Cape Columbine, identified strong sub-inertial motions having a 5 to 6 day period. (The length of the records precluded rigorous characterisation of the longer period motions.) These 5 to 6 day waves have a roughly estimated phase speed of 2 ms^{-1} to 7 ms^{-1} to the south. He finds a strong correlation between the longshore wind stress and the longshore current velocities and notes the remarkable barotropicity of the response, an observation also made for subinertial currents in the vicinity of the Cape Peninsula (Nelson, 1985), on the Agulhas Bank (Swart, 1987) as well as over the narrow shelf regions along the East Coast (Schumann and Brink, 1990). The current meter data off the Cape Peninsula (Nelson, 1985) display wave-like reversals on a time-scale of 6 to 10 days that are reasonably well correlated with coastal low propagation and/or wind reversals. There is little or no lag between current reversals and changes in the winds, provided that the events do not occur with periods less than 4,5 days.

In an ongoing monitoring program of West Coast shelf currents, Nelson (1987, 1989) and Nelson and Polito (1987) have collected much data from a number of current meter moorings in the Southern Benguela region. The data from some of these moorings show reversals in the longshore currents every 2,9 to 3,7 days. Cross-shore current reversals occur with a period of 2,3 days that differs strongly from the longshore current results, indicating the operation of different physical processes. The data also indicate a 4,6 day variation in the sea levels. The approximate 3 day current reversals are of particular interest as they previously have not been observed in sea level and current meter data despite the observation of distinct 3 day periodicities (Preston-Whyte and Tyson, 1973; Kamstra, 1987) in atmospheric pressure spectra.

Schumann (1983), using both current meter and sea level data, suggested that sub-inertial CTW motions are not a regular feature of the east coast. Tentatively identified events in

this region indicate very low phase speeds of propagation. Schumann (1983) stated that CTW motions on this narrow shelf are expected to be of a baroclinic nature and he suggested that their "upstream" propagation may be precluded by the presence of the strong Agulhas Current close to the coast. A baroclinic event was observed to travel up the coast, but Schumann suggested that it may have had its origin in abnormal flow conditions in the Agulhas Current. Brink (1990) has suggested a mechanism to account for the apparent failure of the CTW to propagate in the Agulhas Current between Port Elizabeth and Durban, however there is not yet consensus on whether CTW's reach Durban with any significant amplitude (see Schumann and Brink, 1990 and Jury *et al.*, 1990a).

Recent current meter data from moorings across the mouth of False Bay indicate the presence of low frequency shelf motions (Potgieter *et al.*, 1987; Nelson *et al.*, 1987 and Wainman *et al.*, 1987) which are expected to have a strong impact on the circulation within the False Bay (van Ballegooyen, 1991). This is undoubtedly the case for other large bays along the southern African coastline.

The above is a brief summary of our present knowledge of sub-inertial motions on the continental shelf regions of southern Africa. Widely varying estimates of phase velocities and periods of motion have been obtained. Besides observations of the remarkable barotropicity of shelf currents, only a few researchers (Schumann, 1983; Nelson, 1985; Nelson and Polito, 1987; Nelson, 1989; Van Foreest and Brundrit, 1985; Schumann and Brink, 1990 and Jury *et al.*, 1990a) have addressed the essential dynamics of CTW motions and their role in determining the circulation of shelf waters surrounding Southern Africa.

1.2 Research Objectives

Despite recent progress in the investigation of CTW motions along the southern African coastline, a number of important questions remain unanswered. Perhaps the most important is how variations in the underlying shelf topography affect the large-scale, low

frequency response of the shelf waters surrounding southern Africa (both directly, through the scattering of CTW wave motions and indirectly in determining the intrinsic CTW response in the different shelf regions)? Further, to adequately characterise the CTW response, it is necessary to determine what constitutes effective forcing for CTW motions in the different shelf regions.

Along with the nature of the underlying shelf topography and atmospheric forcing, the extent of stratification of the shelf waters is an important factor governing the CTW response. Stratification of the water column not only determines the inherent nature of the CTW response but also largely determines the effect that longshore variations in shelf topography have on CTW motions propagating along the continental shelf.

Finally, a knowledge of the longer term changes in the low frequency circulation shelf waters is required because these seasonal and interannual changes often have a large impact on the marine biota (Taunton-Clark and Shannon, 1988 and Shannon *et al.*, 1992) and human activities in these shelf regions

The objective of this dissertation is to provide a characterisation of the low frequency circulation over the continental shelf surrounding southern Africa in terms of CTW theory. In doing so it is intended to:

i) determine the dynamics that govern the CTW response along the coastline of southern Africa and, in particular, determine what constitutes effective forcing in the different shelf regions,

ii) ascertain how important stratification of the water column is in determining the nature of the CTW response in the different shelf regions surrounding southern Africa,

iii) describe how the underlying shelf topography inherently determines the CTW response along the West Coast and further determine the effect that longshore variations in the bottom topography have on CTW propagation and shelf circulation along the west coast of southern Africa,

iv) determine the dominant spatial and temporal scales, and phase speeds of propagation associated with CTW motions along the coastline of southern Africa,

v) document, if any, the seasonal differences in the forcing and propagation of CTW's along the continental shelf surrounding southern Africa, and

vi) if possible, investigate to what extent the low frequency response on the shelf surrounding southern Africa is attributable to remotely forced CTW motions or open ocean forcing.

Considering the paucity of readily available and appropriate data for such a characterisation, the chosen approach is to combine a thorough analysis of long-term adjusted sea level and atmospheric pressure time series with simple analytical and numerical studies of CTW over the continental shelf surrounding southern Africa.

Briefly, the dissertation is structured as follows. First, the background to the investigation and research objectives are detailed in this chapter (chapter 1). Chapters 2, 3 and 4 provide the theoretical framework required for the discussion of CTW motions that follows. The method and results of the data and numerical analyses are reported chapters 5, 6 and 7, while chapter 8 contain the discussion, conclusions and suggestions for future research.

In **Chapter 1**, the importance of CTW motions over the shelf is discussed and a broad background to the proposed investigation is given. The present state of knowledge of CTW's around southern Africa is provided in a brief review of appropriate observations and investigations and finally the research objectives are detailed. A brief review of both free and forced CTW theory follows in **Chapter 2**. The review is not exhaustive as only those aspects of CTW motion relevant to the present investigation are discussed. In **Chapter 3**, the theoretical free CTW response is characterised using dispersion curves calculated for a number of offshore profiles of the bottom topography along the West and South Coast. These offshore profiles of the bottom topography are classified according to the width and depth of the shelf and the steepness of the shelf slope. The nature of the dispersion curves resulting from these classifications of the bottom topography, is

discussed in detail as these dispersion curves are instrumental in characterising the CTW response over the continental shelf and further provide a basis for the discussion of numerical modelling results obtained in Chapter 7. The effects of stratification on the dispersion properties of CTW motions are explicitly considered in this chapter.

The factors governing the CTW response on the west coast are discussed in **Chapter 4**, these being the nature of the shelf topography, atmospheric forcing and the stratification of the water column. Here it is shown that the effects of stratification are generally of secondary importance over the shelf on the west and south coasts of southern Africa. This permits the use of a barotropic model, described in **Chapter 6**, to investigate the generation and propagation of CTW motions along the West Coast of southern Africa. A full description of the numerical properties of the model is provided as this is necessary to enable one to distinguish between actual features of CTW dynamics and artefacts of the numerical modelling methods utilised. Before undertaking the numerical modelling runs, a number of important scales (spatial and temporal) and propagation speeds of atmospheric pressure systems and CTW's are estimated by analysing an 11 year data set of atmospheric pressure and sea level data. The results of this analysis are presented in **Chapter 5**. Besides providing information relevant to the modelling investigation, these analyses also provide information on the nature of the forcing, the extent of the CTW response, the effect of topographic scattering and the influence of open-ocean and remote forcing on the shelf response. The results of the numerical modelling experiments are reported in **Chapter 7** where particular emphasis has been placed on the effect of longshore variations in shelf topography on the CTW response.

Chapter 8 contains a discussion of the theory, data analyses and numerical modelling results contained in Chapters 2 to 7. In particular, the findings of the previous chapters are related to observations of CTW motions on continental shelf surrounding southern Africa and the observation and dynamics of CTW motions on the southern African continental shelf and their importance to regional fisheries and human activities on the continental shelf are commented upon. The dissertation is concluded with suggestions for future research.

2. REVIEW OF COASTAL-TRAPPED WAVE THEORY

The purpose here is to introduce the concept of CTW motions and provide a theoretical framework for the discussion of the results contained in chapters 5 and 7. First, the development of CTW theory over the last few decades is chronicled. A synopsis of the theory of free "long wave" CTW motions in both non-stratified and stratified shelf waters follows and finally the more general theory and models used to investigate forced CTW motions are briefly reviewed

2.1 The Development of CTW Theory

Early analysis of variations in daily sea levels (Shoji, 1961) showed a sea level perturbation to travel south along the east coast and north along the west coast of Japan. Due to the steep shelf along these coasts, the motions were interpreted as being internal Kelvin waves (Yoshida, 1960). At about the same time, Hamon and Hannan (1962) and Hamon (1962) found the relationship between atmospheric pressure and sea level to be less than isostatic along the east coast of Australia, with Hamon (1966) providing clear evidence of sea level propagation along the Australian coast.

These initial observations led to Robinson"s (1964) theory in which he postulated the presence of non-dispersive topographic Rossby waves with frequencies (σ) much less than the local Coriolis parameter (f), and with wavelengths much greater than the shelf width. These waves are trapped over the continental shelf and travel along the coastline with the coast on their left (right) in the southern (northern) hemisphere. Mysak (1968b), in a rudimentary way, extended this theory to include the effects of the slope region, deep ocean stratification and longshore currents. Although numerically different, his results were qualitatively similar to those of Robinson (1964). Mooers and Smith (1968), in searching tide gauge records along the Oregon coast for evidence of CTW's, suggested the presence of both forced and free CTW's. A wave of 0,1 cycles per day (cpd) was observed to move from north to south in sympathy with the atmospheric pressure systems and a much less energetic 0,3 cpd wave was observed to travel from south to north as a free CTW.

Buchwald and Adams (1968) then proceeded to develop a more general theory for CTW's travelling over an exponential model shelf topography. For the scales of

motion considered, they found that the dynamic effect of spatial gradients in the Coriolis parameter is negligible and that the flow associated with CTW motions is essentially non-divergent. Further, they showed the higher wavenumber CTW motions to be highly dispersive and indicated that there existed particular wavenumber motions which have a zero group velocity. Many subsequent investigations of shelf waves considered these wavenumber motions with a zero group velocity to be preferentially generated (for example Cutchin and Smith, 1973; Kubota, 1982). Laboratory experiments (Caldwell *et al.*, 1972) confirmed all the major findings of Buchwald and Adams (1968), in particular, indicating that the assumption of non-divergent flow is justified for the spatial and temporal scales typical of subinertial CTW motions.

The early investigators considered subinertial CTW's to be generated by atmospheric pressure fluctuations (Robinson, 1964; Mysak, 1967). Adams and Buchwald (1969), however, showed the principal generating mechanism to be longshore wind stress. Any previously obtained correlation between sea level and atmospheric pressure was considered by them to be due to the strong correlation between atmospheric pressure and winds.

A major advance in CTW theory occurred with the publication by Gill and Schumann (1974) of their theory of forced barotropic CTW's. They emphasised the role played by the coastal boundary in the dynamics of these subinertial motions over the shelf that has led to the more accurate description of these motions as coastal-trapped waves rather than continental shelf waves. Using boundary layer scaling arguments (that is, the "long wave" assumption), they found that inviscid, subinertial CTW motions are governed by a single wave equation for each mode. Using a moving wind stress field as the forcing, their solutions to the CTW wave equations indicated the presence of both a free and a forced CTW.

All theories had essentially considered only barotropic CTW motions until Gill and Clarke (1974) included the effects of stratification of the water column. Allen (1975) and Wang (1975) simultaneously described the type of CTW motions expected in the presence of significant stratification of the water column. Clarke (1977a) then applied a generalised CTW theory, including both the effects of stratification and topography,

to observations of CTW motions world-wide. Subsequent advances in CTW theory include the determination of the effects of longshore variations in topography (for example, Allen, 1976; Grimshaw, 1977; Huthnance, 1987, Wilkin and Chapman, 1990) and bottom friction (Brink and Allen, 1978; Brink, 1982a) on CTW motions.

Initial applications of CTW theory using only a single mode to describe CTW motions were surprisingly successful (Brink, 1982b, Battisti and Hickey, 1984). Applications that followed used multiple modes to improve the fit to observations (Clarke and van Gorder, 1986). Chapman *et al.* (1988) showed that, in hindcasting currents off northern California, the use of more than three modes resulted in little change in the hindcast, however López and Clarke (1989) state that the use of the above forced CTW method for estimating the alongshore velocities can be in considerable error even when up to seven modes are used. They suggest the use of a "local plus remote" method in which the ocean response can be regarded as the sum of the response due to local wind forcing and that associated with the remotely generated alongshore pressure gradient. In a broader investigation of the low frequency variability on the shelf, Allen and Denbo (1984) used a stochastic approach in a wave-based model to provide some valuable insights into the dynamics of CTW motions, while Brink *et al.*, (1987) developed a more complete model where the many of the restrictive scaling assumptions inherent to previous models were relaxed. This not only results in a more widely applicable model but also allows different physical insights into the dynamics of CTW motions than are provided by the wave-based models.

Since the discovery of CTW motions, many observations of shelf wave motions have taken place (Mysak, 1980a,b; Brink 1991). Initially, observations led to the development of theory, however, rapid theoretical advances have led to the need for carefully planned, extensive field experiments to confirm these theoretical findings. A number of extensive field experiments off the California Coast (CODE), off the south-east Australian coast (ACE), on the West Florida Shelf and on the north-west Australian shelf, have provided substantial data to test the ample and often complex shelf wave theory currently available. Unfortunately such extensive data do not exist for the continental shelf regions surrounding southern Africa and a different approach is indicated for the study CTW's in this region.

2.2 Theory of Free Coastal-Trapped Waves

The aim here is not to provide an extensive review of continental shelf wave theory, since a number of excellent reviews on the topic already exist (for example Le Blond and Mysak, 1977; Allen, 1980; Mysak, 1980a,b and Brink, 1987, 1991). The aim, rather, is to provide a basic insight into the dynamics of sub-inertial CTW motions. Emphasis is placed on barotropic CTW theory and only a cursory consideration is given to the effects of stratification. The reasons for this will become apparent in Chapters 3 and 4.

2.2.1 Barotropic CTW theory

Initially only free CTW's are considered as they form the basis of the forced wave response. Assume a homogeneous layer of water over a variable offshore topography $h(x)$ that does vary in the longshore direction and is bounded by a coastline at $x = 0$ and unbounded in the offshore direction (see Fig 2.1). A left-handed system of axes is used. In such a left-handed system of axes $\frac{\partial h}{\partial x} < 0$ and $f > 0$ (in the Southern Hemisphere).

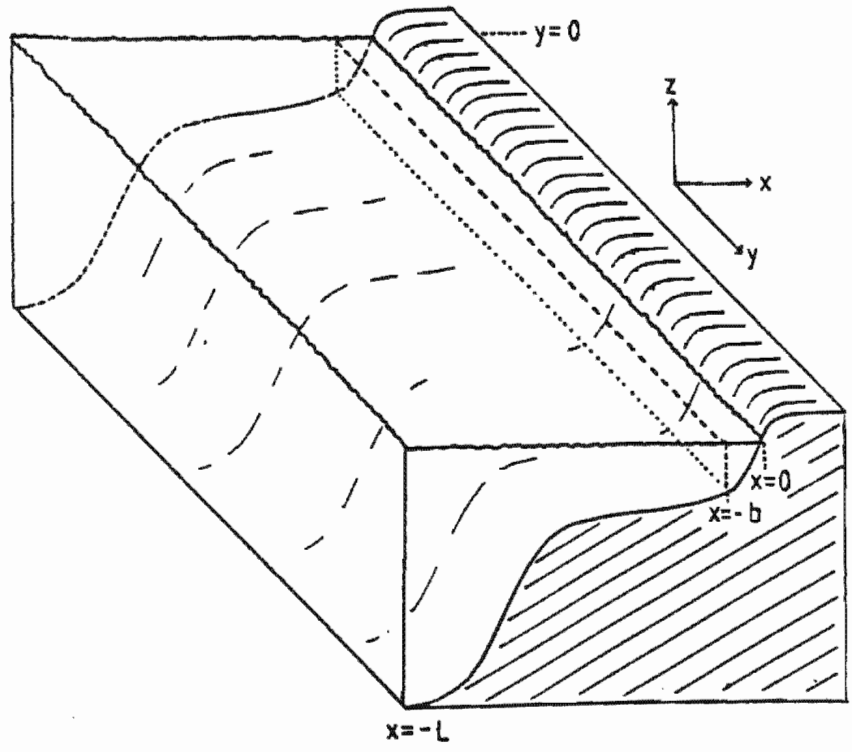

Fig 2.1 The orientation of the continental shelf and the left-handed system of axes used in the description of free barotropic CTW theory in the text.

Barotropic motions over the shelf are assumed to be governed by the inviscid, non-linear, unforced shallow water wave equations (Mysak, 1980a)

$$\frac{\partial u}{\partial t} + u\frac{\partial u}{\partial x} + v\frac{\partial u}{\partial y} - fv = -g\frac{\partial \eta}{\partial x} \tag{2.1a}$$

$$\frac{\partial v}{\partial t} + u\frac{\partial v}{\partial x} + v\frac{\partial v}{\partial y} + fu = -g\frac{\partial \eta}{\partial y} \tag{2.1b}$$

$$\left(\frac{\partial (hu)}{\partial x} + \frac{\partial (hv)}{\partial y}\right) + \frac{\partial \eta}{\partial t} = -\frac{\partial (\eta u)}{\partial x} - \frac{\partial (\eta v)}{\partial y} \tag{2.1c}$$

The notation is standard (see List of Symbols).

For long wave CTW motions, the non-linear terms in the momentum equations are small in comparison to the local acceleration terms (Smith, 1972). This allows the non-linear terms in momentum equations (2.1a and b) to be ignored. Similarly, the non-linear terms on the right-hand side of the continuity equation (2.1c) may be neglected if $\eta \ll h$. This is true everywhere except at the coast where $h \to 0$. This has prompted the use of a "coastal wall" in many studies (Mysak, 1980a). Inviscid, linearised, barotropic, free CTW motions are thus considered to be governed by

$$\frac{\partial u}{\partial t} - fv = -g\frac{\partial \eta}{\partial x} \tag{2.2a}$$

$$\frac{\partial v}{\partial t} + fu = -g\frac{\partial \eta}{\partial y} \tag{2.2b}$$

$$\frac{\partial (hu)}{\partial x} + \frac{\partial (hv)}{\partial y} = -\frac{\partial \eta}{\partial t} \tag{2.2c}$$

where the boundary conditions are such that

i) at the coastal boundary, the cross-shore volume flux is zero, that is

$$hu = 0 \quad \text{at } x = -b \tag{2.2d}$$

where $-b$ is a small distance offshore where $h \neq 0$, and

ii) at the open ocean boundary the motion decays to zero, that is

$$\eta \to 0 \quad \text{as } x \to -\infty \tag{2.2e}$$

The boundary condition (2.2e) is only correct if f is assumed to be effectively constant (that is, the β-effect is negligible) and open ocean forcing is considered to be

negligible. This open ocean boundary condition is justified by the fact that Buchwald and Adams (1968) show that the β-effect dynamics are indeed negligible (see Appendix A) and the effect of open ocean forcing is generally considered to be negligible on mid-latitude shelf regions (for example Wang, 1982; Chapman and Brink, 1987). The velocities may be expressed as

$$\left(\frac{\partial^2}{\partial t^2}+f^2\right)u=-g\left(\frac{\partial^2\eta}{\partial x\partial t}+f\frac{\partial\eta}{\partial y}\right) \tag{2.3a}$$

$$\left(\frac{\partial^2}{\partial t^2}+f^2\right)v=-g\left(\frac{\partial^2\eta}{\partial y\partial t}+f\frac{\partial\eta}{\partial x}\right) \tag{2.3b}$$

and the sea level is determined by solving

$$\left(\frac{\partial^2}{\partial t^2}+f^2\right)\frac{\partial\eta}{\partial t}-g\left[\frac{\partial}{\partial x}\left(h\frac{\partial^2\eta}{\partial x\partial t}\right)+\frac{\partial}{\partial y}\left(h\frac{\partial^2\eta}{\partial y\partial t}\right)\right] + fg\left(\frac{\partial h}{\partial y}\frac{\partial\eta}{\partial x}-\frac{\partial h}{\partial x}\frac{\partial\eta}{\partial y}\right) = 0 \tag{2.4}$$

where it has been assumed that the β-effect dynamics may be ignored.

Further, if it is assumed that the longshore variations in the shelf topography are sufficiently small to be ignored (which avoids the possibility of the coupling of modes), the substitution of a plane wave solution of the form

$$\eta=\sum_{n=0}^{\infty}F_n(x,\ell)\,e^{i(\sigma_n t-\ell y)}$$

into equations (2.4), (2.2d) and (2.2e) results in the following equation governing the dynamics of free CTW's

$$\frac{\partial^2F_n}{\partial x^2}+\frac{1}{h}\frac{\partial h}{\partial x}\frac{\partial F_n}{\partial x}-\left[\frac{f\ell}{\sigma_n h}\frac{\partial h}{\partial x}+\ell^2+\frac{f^2-\sigma_n^2}{gh}\right]F_n=0 \tag{2.5a}$$

with boundary conditions

$$\frac{\partial F_n}{\partial x}=\frac{f\ell}{\sigma_n}F_n \qquad \text{at } x=0 \tag{2.5b}$$

and

$$F_n\to 0 \qquad \text{as } x\to\infty$$

A more practical form of the above boundary condition (Caldwell *et al.*, 1972) is given by

$$\frac{\partial F_n}{\partial x} = \sqrt{\ell^2 + \frac{f^2 - \sigma_n^2}{gH}}\ F_n \qquad \text{at } x = -L \tag{2.5c}$$

where L is some large offshore distance and H is the constant depth at $x = -L$.

Equations (2.5a,b and c) form a Sturm-Liouville problem for a given ℓ and an arbitrary offshore topography, $h(x)$. Solutions to (2.5) consist of eigenvalue pairs (σ_n, ℓ) and eigenvectors $F_n(x, \ell)$ for each mode $n = 0, 1, 2, \ldots\ldots\infty$. A plot of σ_n versus ℓ gives a typical dispersion curve defining the phase properties of the different modal solutions, while a plot of $F_n(x, \ell)$ versus x gives the offshore structure of the amplitude of each mode $n = 0, 1, 2, \ldots\ldots\infty$. Huthnance (1975) has described the full spectrum of solutions to the above set of equations which comprises

i) **"leaky" Poincaré, waves** which are not trapped over the shelf. They occur for frequencies where $\left(\frac{\sigma_n}{f}\right)^2 \geq 1 + \frac{gh\ell^2}{f^2}$,

ii) **barotropic edge waves** with $\left|\frac{\sigma_n}{f}\right| \geq 1$

iii) a **topographically modified Kelvin wave** which decays in the offshore direction with a scale $R_0 = (gH)^{1/2}/f$ (the external Rossby radius of deformation). Due to its large offshore scale, the topographically modified Kelvin wave owes its existence to the presence of the coastal boundary rather than the underlying topography.

iv) **barotropic coastal-trapped waves** with a frequency $\left|\frac{\sigma_n}{f}\right| < 1$

For the scales of motion considered in this investigation, the motion is essentially non-divergent and thus the only subinertial motions of consequence are barotropic CTW motions and Kelvin waves. The CTW's, which rely on the generation of vorticity over the sloping bottom topography for their existence, have the following properties;

i) For each value of ℓ there is an infinite discrete set of frequencies σ_n for each mode n where $\sigma_0 > \sigma_1 > \sigma_2 \ldots$

ii) Associated with each (σ_n, ℓ) is an amplitude function $F_n(x, \ell)$ defining the offshore structure for each mode n where each $F_n(x, \ell)$ has n zero crossings.

iii) At long wavelengths the group velocity (C_g) for each mode n CTW is in the same direction as the phase velocity (C_{ph}). If $\ell \rightarrow 0$, then $C_g \rightarrow C_{ph}$, (that is, the long wavelength CTW motions are non-dispersive).

iv) At short wavelengths ($\ell \rightarrow \infty$), the group velocity of each mode n CTW is such that $C_g = \partial \sigma_n / \partial \ell < 0$. This implies that high wavenumber CTW motions have a group velocity in the opposite direction to their phase velocity and that for each mode there exists an intermediate wavenumber ($\ell = \ell_{crit}$) and a frequency ($\sigma_n = \sigma_{crit}$), where $C_g = \partial \sigma_n / \partial \ell = 0$.

All of the above properties are apparent in an adapted schematic (Fig. 2.2) of the dispersion curves obtained by Huthnance (1975).

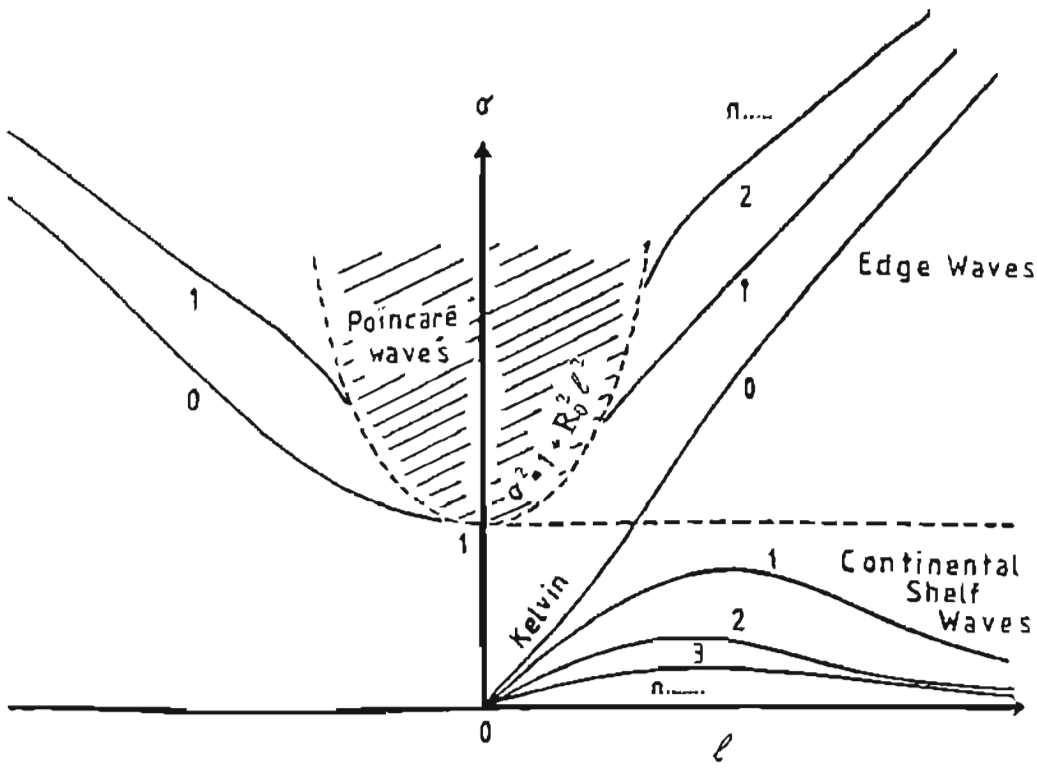

Fig 2.2 General dispersion curves for wave motions that are solutions to Equation (2.6a, b and c) for barotropic motions over the shelf (adopted from Huthnance, 1975)

2.2.2 Energy Relations for Barotropic CTW

Following the method of Shillington (1985), the group velocity ($C_g = \partial\sigma_n/\partial\ell$) is derived from the dispersion relation (2.5a) to give

$$C_g = \left\{\left(2\ell + \frac{f}{\sigma_n h}\frac{\partial h}{\partial x}\right) - \frac{\partial}{\partial \ell}\left[\frac{1}{F_n}\left(\frac{\partial^2 F_n}{\partial x^2} + \frac{1}{h}\frac{\partial h}{\partial x}\frac{\partial F_n}{\partial x}\right)\right]\right\}\left[\frac{f\ell}{\sigma_n{}^2 h}\frac{\partial h}{\partial x} + \frac{2\sigma_n}{gh}\right]^{-1}$$

where equation (2.5a) necessarily places restrictions on $F_n(x, \ell)$ such that C_g is both real and independent of x (the cross-shore axis). The group velocity is however mode dependent.

Manipulation of equations (2.2) result in the energy conservation relation (Gill, 1982, p. 502)

$$\frac{\partial E}{\partial t} + \nabla \cdot \boldsymbol{F} = 0 \qquad (2.6)$$

where $E = \frac{1}{2} h (u^2+v^2) + \frac{1}{2} g\eta^2$ is the energy density,

and $\boldsymbol{F} = (ghu\eta, ghv\eta)$ is the energy flux vector.

We may define $\overline{\boldsymbol{F}} = \boldsymbol{C}_g \overline{E}$, where $\overline{\boldsymbol{F}}$ and $\boldsymbol{C}_g$ are vector quantities, and $\overline{\boldsymbol{F}}$ and $\overline{E}$ are quantities that have been suitably averaged over the shelf domain. A number of other definitions of the mean energy flux exist (Shillington, 1985; Shillington and Brundrit, 1986) where the definition of $\overline{\boldsymbol{F}}$ varies by a non-divergent quantity only, thus it is generally true that

$$\nabla \cdot \overline{\boldsymbol{F}} = \boldsymbol{C}_g \cdot \nabla \overline{E}$$

which implies that

$$\frac{\partial \overline{E}}{\partial t} + \boldsymbol{C}_g \cdot \nabla \overline{E} = 0 \qquad (2.7)$$

The importance of (2.7) is that for negligible alongshore variations in the bottom topography, the mean energy density of inviscid free CTW motions is constrained to travel along the shelf with a group velocity ($\boldsymbol{C}_g$) with no "leakage" of energy to the open ocean. Note, however, that (2.7) is only valid if it is assumed that $\beta = 0$. Grimshaw (1977) and Dorr and Grimshaw (1986) investigated the effect of a non-zero value of β and found that at high latitudes and very low frequencies, barotropic CTW motions "leak" energy off the shelf in the form of topographic Rossby waves. The low

frequency motions of interest off the west coast of southern Africa (having periods of 2-20 days and occurring at latitudes north of 36°S) easily satisfy their criteria for negligible "leakage" of energy off the shelf.

Further discussion of CTW energy relations can be found in Brink (1989) who highlights the importance of energy conservation in the correct application of CTW theory to observations.

2.2.3 CTW Theory for Stratified Waters

The presence of stratification may strongly modify the CTW response, resulting in a number of baroclinic motions depending on the strength of the water column stratification over the shelf. The appropriately scaled equations of motion for CTW's in the presence of significant stratification are not presented here as they are well documented and comprehensively analysed in a number of publications (for example, Clarke and Brink, 1985; Brink and Chapman, 1987; Clarke and van Gorder, 1986 and Brink, 1991).

Early investigations of the influence of stratification on shelf wave motions were undertaken using two-layer models (Mysak, 1968b; Gill and Clarke, 1974; Allen, 1975; Wang, 1975). These studies identified two types of low frequency response, namely

i) internal Kelvin waves modified by the presence of topography, and

ii) barotropic shelf wave motions modified by the presence of stratification.

Although simplistic, the two-layer investigations anticipated many of the findings of more realistic models containing continuous stratification profiles (Wang and Mooers, 1976; Huthnance, 1978). The essential findings of the above studies are:

i) in the absence of a significant coastal wall, the response consists of an infinite discrete sequence of topographic Rossby wave modes (n = 0, 1, 2,...) where the frequency (σ_n) increases with increasing wavenumber and stratification.

ii) the character of the motion is highly dependent on a stratification parameter (Burger number) defined as

$$S^2 = \frac{N^2 H^2}{f^2 X_h^2} = \frac{N^2 \alpha^2}{f^2} \quad \text{or} \quad S^2 = \frac{R_i^2}{X_h^2}$$

where N^2 is the Brunt-Väisälä frequency squared, H is the water depth, X_h is the shelf width, $\alpha = H / X_h$ is the average shelf slope, f is the Coriolis parameter magnitude and R_i is the internal Rossby radius of deformation. This stratification parameter, S, is similar to that defined by Rhines (1970).

iii) For a fixed value of ℓ, an increasing value of S results in an increase in the frequency of each modal response, the increase being more pronounced for higher modes and higher wavenumber motions (see Figure 2.3). Note also that the increase in S may lead to the loss of the high frequency cut-off (σ_{crit}) of each mode observed in barotropic CTW theory. Further, if S increases sufficiently, σ_n may increase until $\sigma_n = f$ (the inertial frequency). Huthnance (1978) showed that this will occur when the ratio $\left|(N/f)\partial h/\partial x\right|$, evaluated at the bottom, exceeds unity. Once $\sigma_n \geq f$ on a dispersion curve, strictly trapped waves no longer exist (that is the CTW are considered to be "leaky") and the group velocity is generally in the same direction as the phase velocity for all wavenumbers. Stratification is thus expected to be important in the vicinity of strong longshore variations in topography, where scattering into higher mode and wavenumber motions occurs. In particular, for the extreme case of the stratification being sufficiently large for the group velocity to be in the same direction as the phase velocity for all wavenumbers, reflection of energy due to topographic scattering theoretically is no longer possible (Wilkin, 1988 as quoted by Brink, 1991).

iv) If $S \rightarrow 0$, the response is barotropic. For intermediate values of S, the motion over the shelf remains barotropic while bottom trapping occurs on the shelf slope. If $S \rightarrow \infty$, the response is essentially that of an internal Kelvin wave. The above result can be summarised by saying that as the value of S increases, the character of the response slowly changes from that of a barotropic shelf wave (containing essentially horizontal motions with vertical nodes in the

modal structure functions), to that of an internal Kelvin wave (where the motion is vertically sheared with horizontal nodes in the modal structure functions).

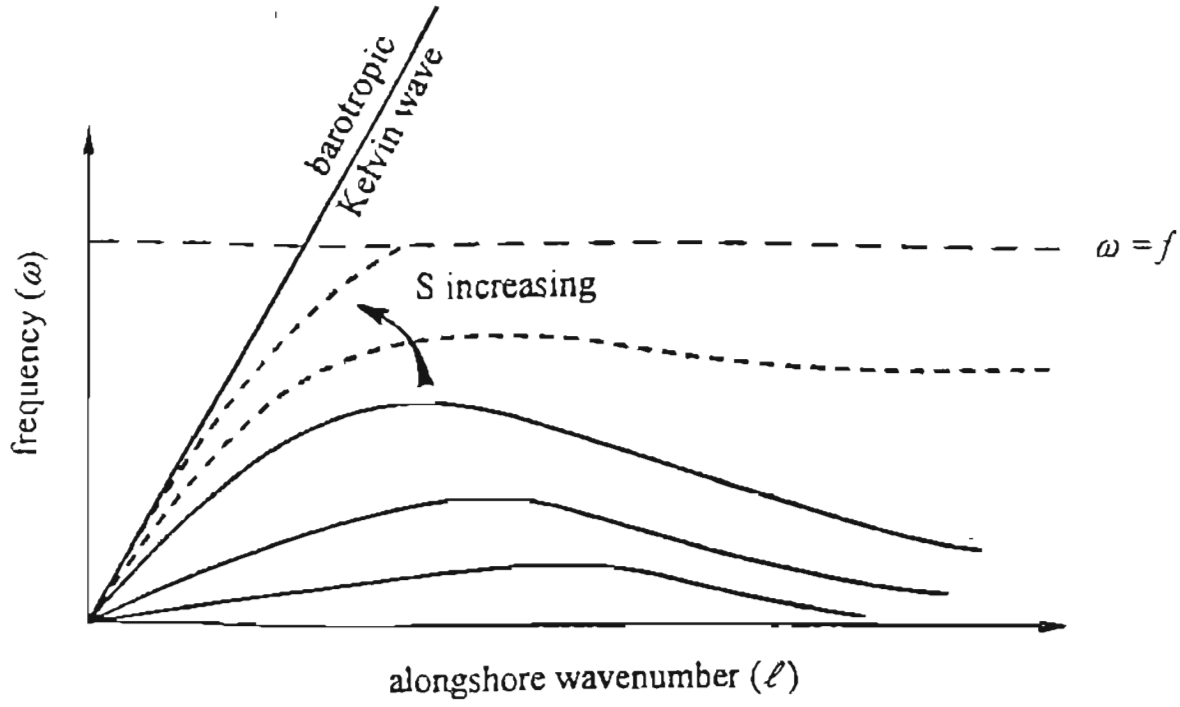

Fig 2.3 Schematic dispersion curves showing how dispersion properties change from those for barotropic CTW motions (solid lines) when stratification is included (dashed lines). (Adapted from Brink, 1991)

Using the same "long wave" approximation as Gill and Schumann (1974), Clarke and Brink (1985) derived the equations governing the interior response of stratified shelf waters to large-scale, low-frequency ("weather band") wind-forcing (2π per few days to 2π per few weeks). Using perturbation expansions they found that

i) the lowest order solution is essentially that obtained from 2.5 (the barotropic equations), provided that

$$S^2 = \frac{N_s^2 \alpha^2}{f^2} \ll 1 \qquad (2.8)$$

where $N_s^2 = \overline{N^2}$ is the shelf-averaged Brunt-Väisälä frequency squared. This implies, that for low frequency ("weather band") forcing, the baroclinic

contribution to the total response is negligible provided that the above relationship (2.8) is true.

ii) If S « 1, not only is the response essentially barotropic but the shelf edge pressure is zero. This implies that if S « 1, the CTW response is totally confined to the shelf.

Thus Clarke and Brink (1985) suggest that if S^2 « 1, the barotropic equations adequately describe the low frequency response of the shelf.

Brink (1982b) gives a useful diagnostic for determining the importance of baroclinic effects, namely the ratio (averaged over a wave period), R_{kp}, between kinetic energy (E_K) and potential energy (E_P) where $R_{kp} = E_K / E_P$. The potential energy is the sum of two components, the first associated with the displacement of the free surface (E_{Pf}) and the second associated with the vertical displacement of water in a stratified ocean (E_{Ps}).

In an unstratified ocean $E_{Ps} = 0$ and E_{Pf} is small compared with E_K (except for the barotropic Kelvin wave) so R_{kp} » 1 for all shelf wave modes. In the rigid-lid limit $R_{kp} \rightarrow \infty$. However, for the opposite limit of Kelvin wave-type behaviour typical of large values of S (large effective stratification), the importance of gravity as a restoring force leads to equipartition of wave energy and $R_{kp} \rightarrow 1$.

Once a specific wave mode has been calculated using the community software of Brink and Chapman (1987), it is possible to determine R_{kp} and thus estimate the importance of baroclinic effects in the CTW response. It is also possible to determine R_{kp} for the total forced response to specific applied wind stress fields. The values appropriate to the first and second mode response at a number of sites around the southern African coastline are tabulated in chapter 4 (Table 2, p49).

2.3 Theory of Forced Coastal-Trapped Waves

In this section it is intended to provide an insight into the basic dynamics of forced CTW's rather than a complete review of the models used to investigate forced CTW's A number of such reviews already exist (for example, Brink, 1991). Although there are many forcing mechanisms responsible for the subinertial variability of shelf waters, it is shown in Chapter 4 that longshore wind stress is the dominant forcing mechanism for subinertial CTW motions over most of the southern African shelf. Consequently, only the forcing of CTW's by propagating wind systems is discussed below.

2.3.1 The Forcing of CTW's by Propagating Wind Systems

The mechanism for the forcing of CTW's is relatively simple. A longshore wind stress causes an onshore (offshore) transport within the surface Ekman layer. In order to conserve mass, a compensating offshore (onshore) transport takes place at greater depth. As this flow crosses isobaths, changes in the local relative vorticity occur due to vortex stretching. This vorticity is expressed largely in terms of alongshore velocity and, in the presence of longshore variability in forcing, gives rise to the propagation of CTW's.

The first formalisation of forced CTW theory was by Gill and Schumann (1974). They show that the inviscid, "long wave" barotropic response to a moving wind stress field, $\tau_w^y(y,t)$, can be expressed as a sum of CTW modes where the amplitude of each mode satisfies a first order wave equation of the form

$$C_n^{-1}\frac{\partial \phi_n}{\partial t} - \frac{\partial \phi_n}{\partial y} = b_n\left(\tau_w^y(y,t)\Big/\rho_0 f\right) \qquad (2.9)$$

where C_n is the phase velocity of the mode n wave. The CTW modes defining the streamfunction $\psi = \sum_{n=0}^{\infty} F_n(x)\,\phi_n(y,t)$ are normalised so that

$$1 = f\int_0^{\infty} \frac{1}{h^2}\frac{\partial h}{\partial x} F_n^{\,2}(x)\,dx$$

It therefore follows that

$$b_n = \int_0^{\infty} \frac{1}{h^2}\frac{\partial h}{\partial x} F_n(x)\,dx$$

and that the velocities can be calculated using

$$v = \frac{1}{h}\frac{\partial \psi}{\partial x} \quad \text{and} \quad u = -\frac{1}{h}\frac{\partial \psi}{\partial y}$$

Gill and Schumann (1974) show that, for each mode, the inviscid response to a moving wind stress field of the form

$$\tau_w^y(y,t) = \tau_w^y\big|_{\max} \cos(\ell + C_f t)$$

consists of a combination of both a free wave and a forced wave. The free wave (having a frequency of ℓC_n) propagates along the shelf at a phase speed, C_n, characteristic of the local shelf topography. The nature of the free wave depends on the history of the forcing at some upstream location and thus may be considered to be remotely forced. The forced wave (having the frequency, ℓC_f, of the forcing) propagates along the shelf at the phase speed of the moving wind stress field. In the absence of bottom friction, the longshore velocity response of the forced wave lags the forcing by a phase angle of $\pi/2$ radians. The combined inviscid response (forced and free wave) for a particular mode has an amplitude proportional to $\left(C_f - C_n\right)^{-1} \tau_w^y\big|_{\max}$. This implies that the amplitude of the total forced response increases with increasing wind stress and a closer matching of the phase speed of the forcing and the free CTW phase speeds characteristic of the underlying shelf topography. When $C_f \approx C_n$, the amplitude of the total inviscid CTW response grows linearly with time and the phase properties of this response are such that the longshore velocity is in phase with the wind-forcing.

The above description of the response is only accurate for an inviscid fluid. Gill and Schumann (1974) included bottom friction in an *ad hoc* manner to show that the free wave is exponentially damped as it travels along the shelf. The first formal analysis of forced CTW's to include bottom friction was provided by Brink and Allen (1978) who considered a linear parameterisation of the bottom friction in a perturbation analysis of the low frequency CTW response. The lowest-order solution for each mode, is again governed by a form of the wave equation (Brink and Allen, 1978; Middleton and Cunningham, 1984)

$$C_n^{-1}\frac{\partial \phi_{0n}}{\partial t} - \frac{\partial \phi_{0n}}{\partial y} + E_0^{1/2} a_{nn} \phi_{0n} = b_n\left(\tau_w^y(y,t)/\rho_0 f\right) \qquad (2.10a)$$

and the second-order response is governed by

$$C_n^{-1}\frac{\partial \phi_{1n}}{\partial t}-\frac{\partial \phi_{1n}}{\partial y}+E_0^{1/2}a_{nn}\phi_{1n}=-\sum_{\substack{m=1\\ m\neq n}}^{\infty}a_{nm}\phi_{0m} \qquad (2.10b)$$

where $E_0 = A_v[2f\,h(0)]^{-1}$ is the Ekman number, and the frictional coupling coefficient is given by

$$a_{nm}=h(0)\int_0^{\infty}\frac{1}{h^2}\frac{\partial F_n(x)}{\partial x}\frac{\partial F_m(x)}{\partial x}\,dx$$

Their solutions to the above equations show that the first order response consists of a forced wave and a time-decaying free wave with a time decay constant $T_f = (C_n E_0^{1/2} a_{nn})^{-1}$. The time-decay constant typically has a value of 2 to 10 days depending on the phase speed of the wave and the magnitude of the friction coefficient. The second order response consists of scattered modes (due to the presence of bottom friction) which impact on the phase properties of the total response. In summary, the net effect of bottom friction is to damp the free wave response, to bring the forced response more into phase with the forcing and set up cross-shelf phase lags such that the nearshore response leads the offshore response. The cross-shelf phase lags can be attributed to the inverse depth dependence of the bottom friction and the more rapid spin-up of flow in the shallower waters. In general, the total response consists of many modes. Where higher modes dominate the response, it is possible for the offshore flow to lead the inshore flow (Simons, 1983). This only will occur where the phase speed of the forcing is well below the phase speed of the first mode free CTW (Brink and Allen, 1983) and this is not expected to be a common occurrence. Using a similar methodology, Brink (1982b) extended the investigation to include the propagation of frictional CTW's in stratified waters. He shows that increasing stratification reduces the effects of bottom friction (due to reduced vertical stresses in the fluid) and results in an increasing phase lag both with distance offshore and increasing depth.

These earlier studies provided a general wave theory for forced CTW's in both homogenous and stratified shelf waters. More recently, Brink(1989) derived the energy conserving forms of these equations for a slowly varying medium and shows that the normalisation of the CTW modes is not arbitrary. The energy conserving

form of the "long wave" equation governing barotropic CTW's in the presence of linear bottom friction is

$$C_n^{-1}\frac{\partial \phi_n}{\partial t}-\frac{\partial \phi_n}{\partial t}+\sum_{m=1}^{\infty}a_{nm}\phi_m=b_n\left(\tau_w^y(y,t)\Big/\rho_0\right) \qquad (2.11)$$

where C_n is the phase velocity of the mode n wave. The CTW modes defining the streamfunction

$$\psi=\sum_{n=0}^{\infty}F_n(x)\ \phi_n(y,t)$$

are normalised so that

$$1=f\int_0^{\infty}\frac{1}{h^2}\frac{\partial h}{\partial x}F_n{}^2(x)\ dx$$

It therefore follows that the frictional coupling coefficient (a_{nn}) is given by

$$a_{nm}=\int_0^{\infty}r\frac{1}{h^2}\frac{\partial F_n(x)}{\partial x}\frac{\partial F_m(x)}{\partial x}\ dx$$

and the wind-forcing coupling coefficient (b_n) is given by

$$b_n=\int_0^{\infty}\frac{1}{h^2}\frac{\partial h}{\partial x}F_n(x)\ dx$$

and the velocities can be calculated using

$$v=\frac{1}{h}\frac{\partial \psi}{\partial x}\quad\text{and}\quad u=-\frac{1}{h}\frac{\partial \psi}{\partial y}$$

Similarly the energy conserving form of the "long wave" equation governing CTW's in the presence of both significant water column stratification and linear bottom friction is

$$C_n^{-1}\frac{\partial \hat{\phi}_n}{\partial t}-\frac{\partial \hat{\phi}_n}{\partial y}+\sum_{m=1}^{\infty}a_{nm}\hat{\phi}_m=b_n\,\tau_w^y(y,t) \qquad (2.12)$$

where C_n is the phase velocity of the mode n wave.

The CTW modes defining the perturbation pressure $p=\sum_{n=0}^{\infty}F_n(x,z)\ \hat{\phi}_n(y,t)$ are normalised so that

$$f\,\delta_{nm}=\int_{-h}^{0}F_n(x,z)\ F_m(x,z)\ dz\Big|_{x=0}+\int_0^{\infty}\frac{\partial h}{\partial x}F_n(x,z)\ F_n(x,z)\ dx\Big|_{z=-h(x)}$$

It therefore follows that

$$a_{nm} = \int_0^\infty \frac{r}{f^2} \frac{\partial F_n(x,-h(x))}{\partial x} \left. \frac{\partial F_m(x,z)}{\partial x} \right|_{z=-h(x)} dx$$

$$f\, b_n = -F_n(0,0)$$

Treating the normalisation correctly as above, accounts for only weak alongshore variability in wave behaviour and cannot account for effects such as wave scattering and Rossby wave radiation into the ocean interior (Brink, 1989). By assuming a slowly varying medium, the alongshore variability in topography, stratification and latitude may be accounted for by local changes in F_n, C_n, b_n and a_{nm}. Lastly, in the limit of weak friction the "long wave" equations (2.11) and (2.12) become uncoupled at the lowest order and a_{nn} can be considered to be the inverse-decay distance (L_f) for free CTW's (Brink, 1990) where

$$L_f = (a_{nn})^{-1} \qquad (2.13)$$

and the frictional decay time, T_f, is given by

$$T_f \approx L_f C_{gn}^{-1} = (a_{nn}\, C_{gn})^{-1} \qquad (2.14)$$

where C_{gn} is the group velocity of the mode n free CTW. In the non-dispersive "long wave" limit, the group velocity is equal to the phase velocity (that is, $C_{gn} = C_n$) and the frictional decay time is given as

$$T_f = L_f C_n^{-1} = (a_{nn}\, C_n)^{-1}$$

These wave-based models provide a powerful conceptual mechanism for understanding the large-scale flow over the continental shelf. Considerable success has been achieved in hindcasting longshore currents and pressures using these wave-based models, however it is not quite clear how many modes need to be included in order to achieve accurate results. For practical reasons many studies have used a maximum of three modes (for example Battisti and Hickey, 1984;, Church *et al.*, 1986 and Chapman, 1987) while more recent studies (Clarke and van Gorder, 1986 and López and Clarke, 1989) have suggested that many more modes are required for an accurate solution. The accurate calculation of the higher modes is computationally expensive. López and Clarke found a solution to this difficulty by noting that for higher modes (C_n small), the alongshore variability (and hence wave

propagation is unimportant) and the general wave equation (2.12) reduces to

$$C_n^{-1} \frac{\partial \bar{\phi}_n}{\partial t} + \sum_{m=1}^{\infty} a_{nm} \bar{\phi}_m \cong b_n \tau_w^y (y,t) \qquad (2.15)$$

They then determine the total solution using a "local plus remote" method where equation (2.12) is used to calculate the "remote forcing" and the "locally forced" information is retrieved from equation (2.15).

Other more sophisticated models based on stochastic principles complement the above wave-based models (for example, Allen and Denbo, 1984; Brink *et al.*, 1987; Chapman *et al.*, 1988). In these stochastic models some of the more restrictive scaling assumptions may be relaxed and different insights into the CTW dynamics are obtained. These results are powerful in that they can readily be compared with observed statistics. One of the most interesting results from these models is that the pressure or alongshore velocity over the shelf should be best correlated with (upstream) non-local winds. This phenomenon has been observed by Schumann and Brink (1990) on the South and East Coasts of southern Africa (see Fig 2.4 below).

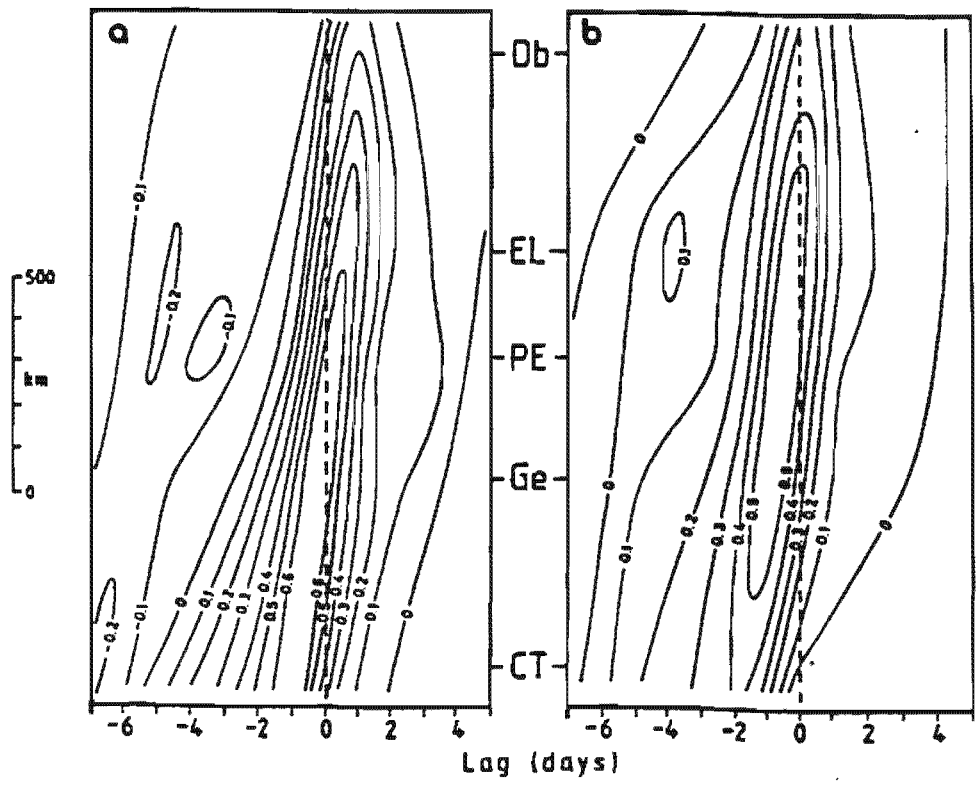

Fig 2.4 Normalised time-lagged cross-correlations between winds at Cape Town, George, Port Elizabeth, East London and Durban, and sea level at a) Port Elizabeth, and b) East London showing the higher correlation of sea levels with the "upstream" wind field. (after Schumann and Brink, 1990)

The models described above all show a reasonable skill in modelling the alongshore velocity and pressure response over the shelf, despite a general underestimation of between 10% to 50% in their magnitude. The models do not provide accurate estimates of densities and cross-shore velocities. This partially can be ascribed to the poor representation of the smaller scales of variation in the alongshore wind stresses. Topographic scattering by alongshore variation in topography which strongly impact on cross-shore velocities and densities further complicate their prediction. Since the observations required to implement these models along the southern African coastline do not exist, the interpretation of the data analyses and modelling studies which follow will be done using the simple wave-based theory.

3. COASTAL-TRAPPED WAVE DISPERSION RELATIONS

Dispersion curves, (plots of σ_n vs ℓ) characterise free CTW motions in terms of their frequency, period, wavelength, group velocity and phase velocity. These properties of the free wave CTW motions determine the essential nature of the forced CTW response over the shelf and therefore are instrumental in discussing both the data analyses in Chapter 5 and the numerical results in Chapter 7.

In general, the dispersion properties of free CTW's are dependent on the stratification of the water column, the strength of the bottom friction and the shape of the offshore profiles of the shelf bottom topography. Stratification effects are shown in Chapter 4 generally to be of secondary importance for most locations along the West and South coasts. Further, the inclusion of a weak bottom friction does not significantly modify the low wavenumber and low mode number structure of the dispersion curves (Webster, 1985). The dispersion properties of free CTW's therefore primarily are determined by the nature of the bottom topography with secondary modifications due to the stratification of the water column and bottom friction should either be of sufficient magnitude.

Dispersion curves have been calculated for eight offshore profiles of bottom topography along the West Coast (see Fig. 3.1) and for three idealised specifications of the stratification of the water column (Fig. 3.5, p41) using both the barotropic dispersion relations (2.5) derived in Chapter 2 and the dispersion relations for a stratified water column (Brink and Chapman, 1987). Certain generalisations can be made concerning the nature of the dispersion curves for the different shelf topographies and for the three idealised specifications of the stratification of the water column.

3.1 Barotropic CTW Dispersion Curves

The barotropic dispersion curves are calculated using the both the "shooting method" as described by Caldwell *et al.* (1972) and the community software (BTCSW program) of Brink and Chapman (1987). The numerical procedures have been tested using the corrected exponential shelf topography of Buchwald and Adams (1968) and in both

(1968), providing confidence in the numerical methods used. Despite the use of slightly different open ocean boundary conditions, the results obtained for barotropic CTW using the "shooting method" are essentially the same as those obtained using the "community software" of Brink and Chapman (1987).

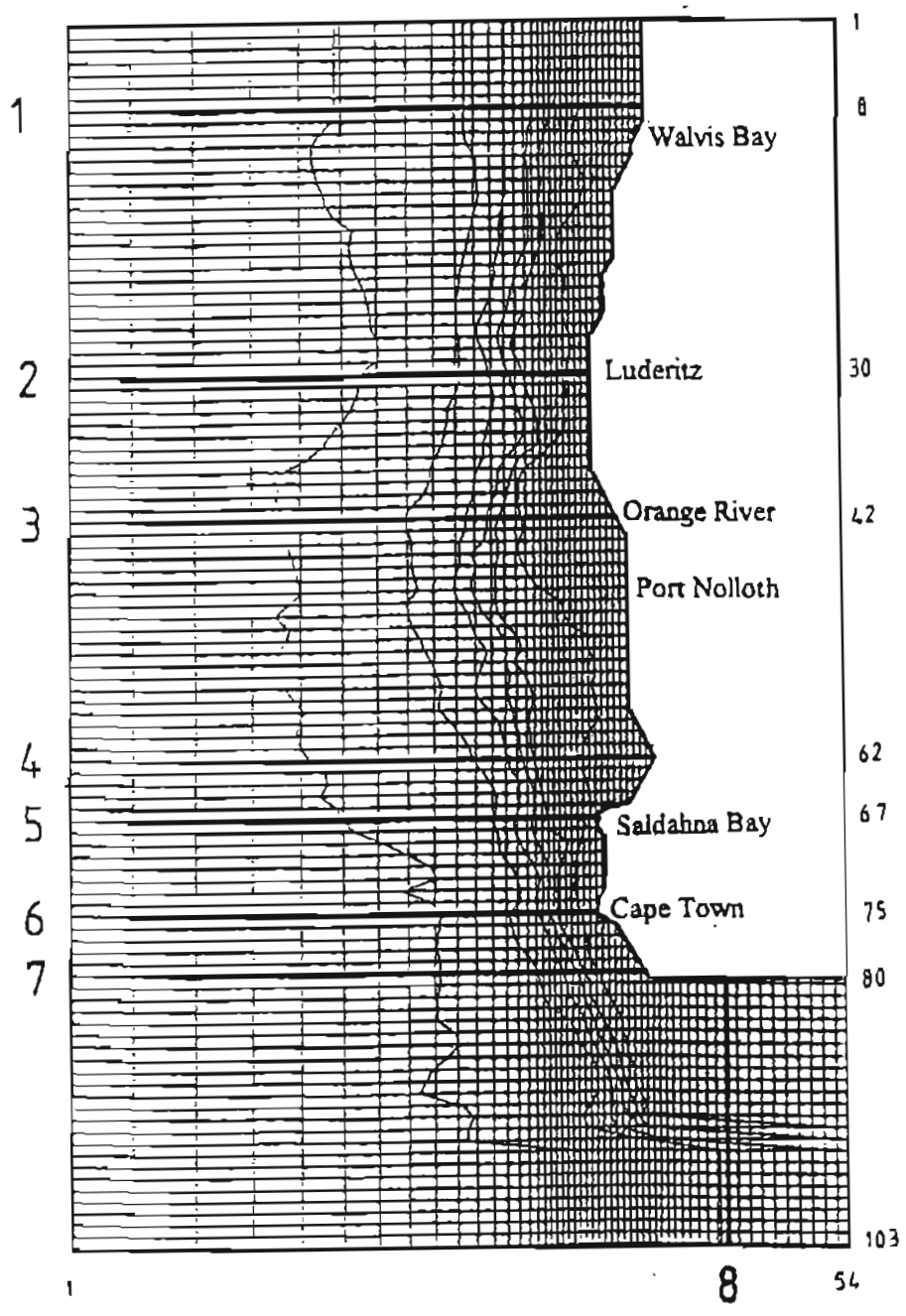

Fig. 3.1 Location of the transects of bottom topography (profiles 1 to 8) for which dispersion curves are calculated.

Since the value of the local Coriolis parameter (f) changes appreciably from north to south over the West Coast, the barotropic dispersion curves are calculated using both a constant value of the Coriolis parameter as used in the numerical model (Fig. 3.2) and local values of the Coriolis parameter at the various longshore locations (Fig. 3.3). Only the first mode of the barotropic dispersion curve for each offshore profile of shelf topography are presented in Fig. 3.2 and Fig. 3.3, since it is the first mode CTW motions that are the most important in determining the shelf water response on the southern African continental shelf (Schumann and Brink, 1990). The slopes of the short lines at the top of the dispersion curves in Fig. 3.2 and Fig. 3.3, denoted "phase velocity of forcing ($m.s^{-1}$)", correspond to a phase speed ($C_{ph} = \sigma / \ell$). These lines serve as a reference, both for the free CTW phase speeds in the dispersion curves as well as for the phase speeds of the moving wind stress fields which generate CTW motions. The significance of these "reference" phase speeds of the wind stress field will be explained in the chapters containing the numerical model results (chapter 7) and the final discussion (chapter 8).

The large differences between the dispersion curves in Fig. 3.2 and Fig. 3.3 are due to the difference between the local Coriolis parameter (see Table 1, pg. 48) and the constant Coriolis parameter as used in the numerical model. The dispersion curves in Fig. 3.2 will therefore be used in discussing the results from the numerical model, while those in Fig. 3.3 are used in discussing observations of CTW's along the coastline of southern Africa.

3.2 The Structural Dependence of Barotropic Dispersion Curves on Bottom Topography

The nature of the dispersion curves is highly dependent on the shape of the offshore profiles of the local bottom topography. The shape of these offshore profiles of shelf topography (Fig. 3.4) are therefore classified according to, a) the width of the shelf, b) the mean slope of the shelf, c) the depth at which the shelf break occurs and d) the "sharpness" of the shelf break.

Profiles 3, 4 and 8 are wide, gently-sloping, shallow shelf regions which have a relatively shallow and sharp shelf break. Profiles 1 and 2 are both relatively strongly

sloping shelf regions of intermediate width with deeper shelf breaks. Lastly, profiles 5, 6 and 7 are narrow, steeply-sloping shelf regions where the shelf break occurs at much greater depths. The dispersion curves (Figs 3.2 and 3.3) may be grouped according to their high wavenumber and low wavenumber characteristics. These groupings correspond closely to the classifications of bottom topography. Dispersion curves of profiles 3, 4 and 8 are characterised by large phase velocities at low wavenumbers, while the dispersion curves of profiles 5, 6 and 7 (especially 6) are characterised by lower phase velocities at low wavenumbers. At high wavenumbers the dispersion curves of profiles 3, 4 and 8 display a strong decrease in frequency with increasing wavenumber, while dispersion curves of profiles 6 and 7 have frequencies which are still slowly increasing at the high wavenumber cut-off of the dispersion curve plots. The relationship between the low and high wavenumber structure of the dispersion curves and the bottom topography may be elucidated through further investigation of the barotropic dispersion relation (2.5) which may be re-written as

$$\frac{\partial}{\partial x}\left(h\frac{\partial F_n}{\partial x}\right) = Q_n F_n \tag{3.1}$$

$$\text{where} \quad Q_n = \frac{f^2 - \sigma_n^2}{g} + h\ell^2 + \frac{f\ell}{\sigma_n}\frac{\partial h}{\partial x} \tag{3.2}$$

A necessary condition for the existence of CTW's over the shelf is that $Q_n < 0$ for some range $-d < x < 0$, where $-d$ is some distance offshore (Schumann, 1973). This ensures the oscillatory nature of the offshore structure function, $F_n(x,\ell)$, typical of CTW motions. It is, however, necessary that $Q_n > 0$ in the range $-\infty < x < -d$ for the motions to be coastally trapped. This condition, $Q_n > 0$, ensures exponential decay of $F_n(x,\ell)$ towards the open ocean. The first term (divergence term) and second term in (3.2) are always positive, the only negative contribution in (3.2) coming from the third term ($\partial h/\partial x < 0$ for the system of axes used). A necessary condition for the existence of CTW motions therefore is

$$\frac{f\ell}{\sigma_n}\left|\frac{\partial h}{\partial x}\right| > h\ell^2 + \frac{f^2 - \sigma_n^2}{g} \tag{3.3}$$

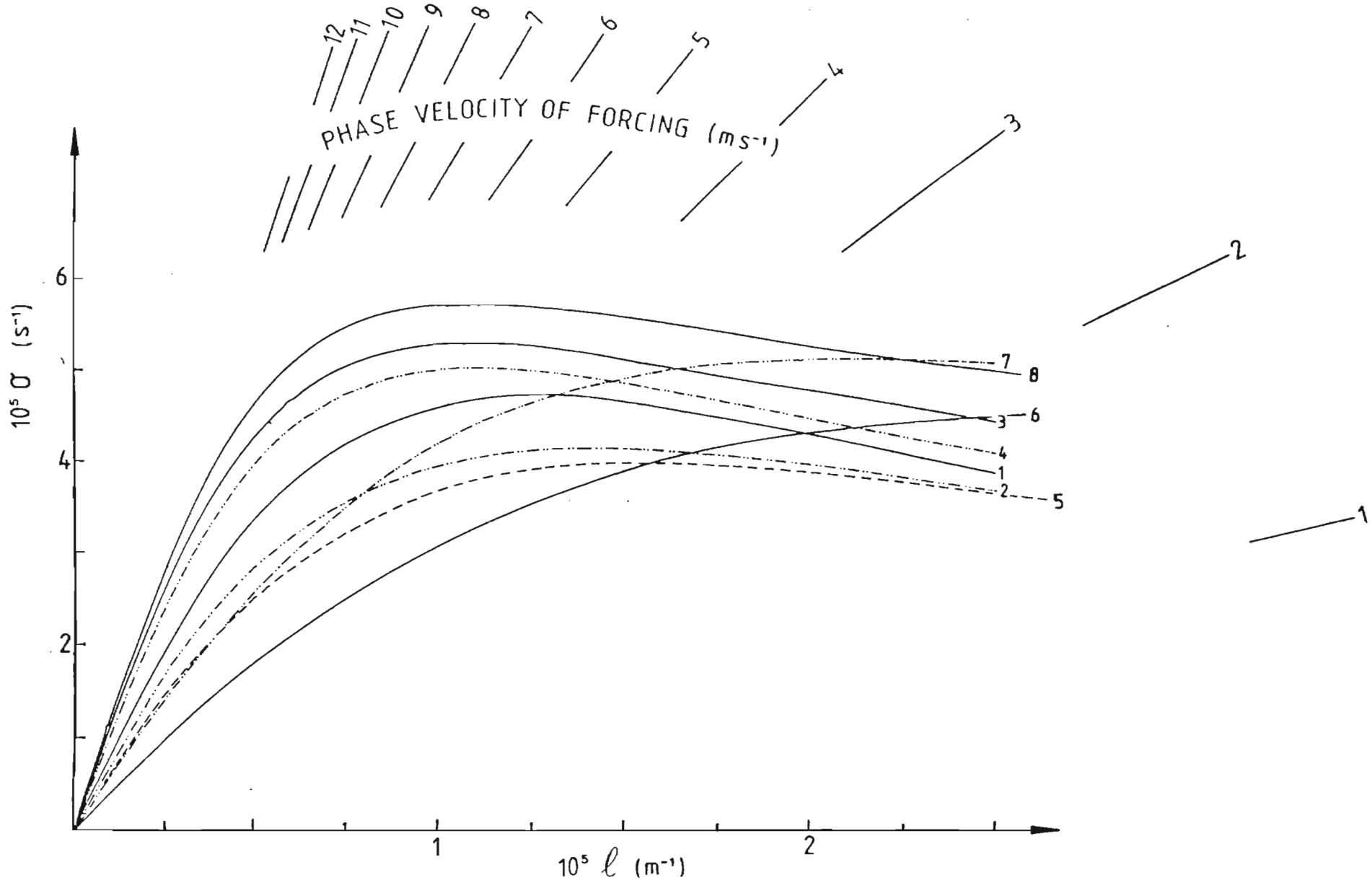

Fig. 3.2 Barotropic dispersion curves (first mode only) for profiles 1 to 8 using the constant value of the Coriolis parameter, $f = 7.272 \times 10^{-5}\ s^{-1}$, as used in the numerical model.

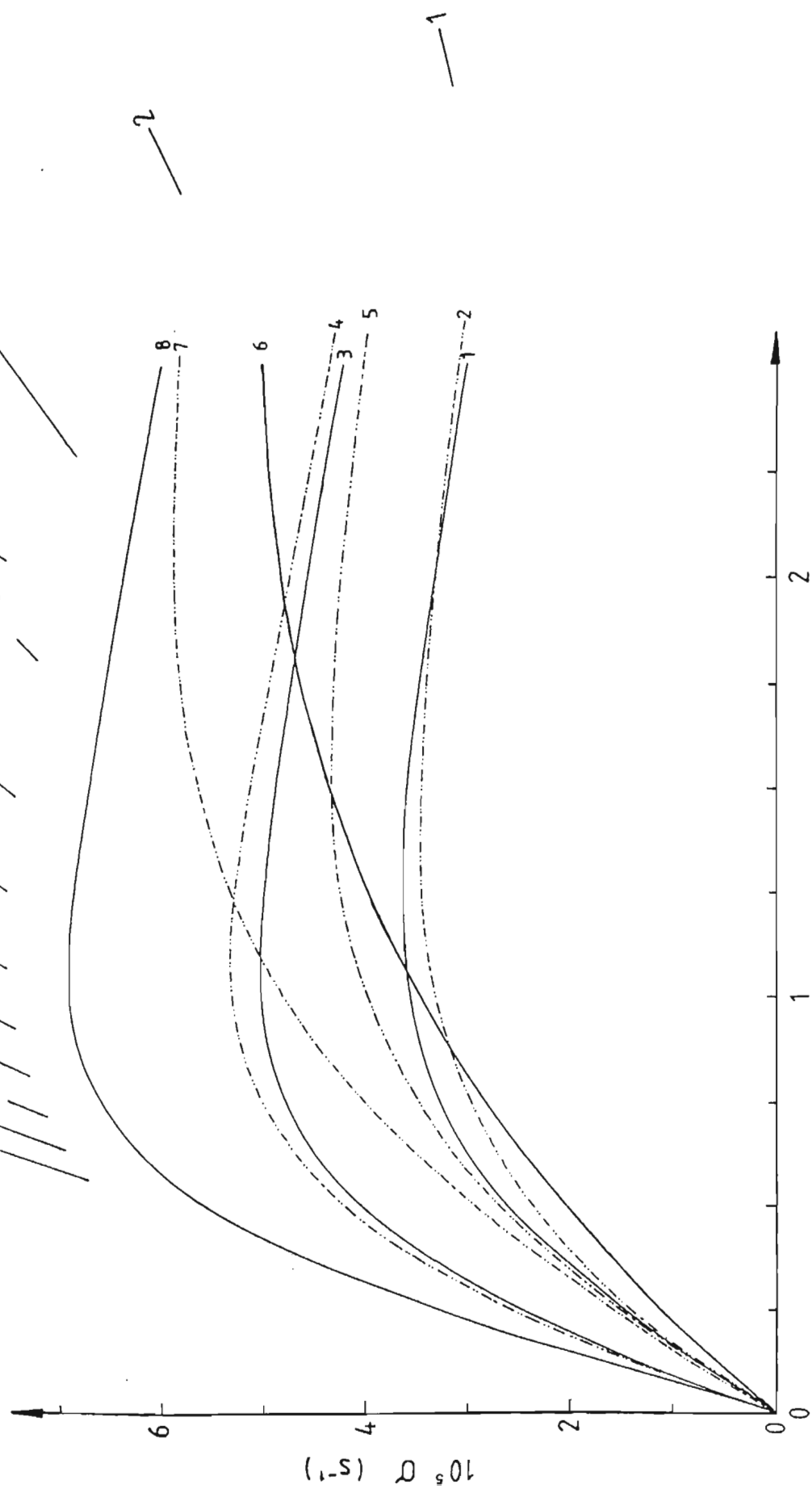

Fig. 3.3 Barotropic dispersion curves (first mode only) for profiles 1 to 8 using a local value of the Coriolis parameter at each location as listed in Table 1.

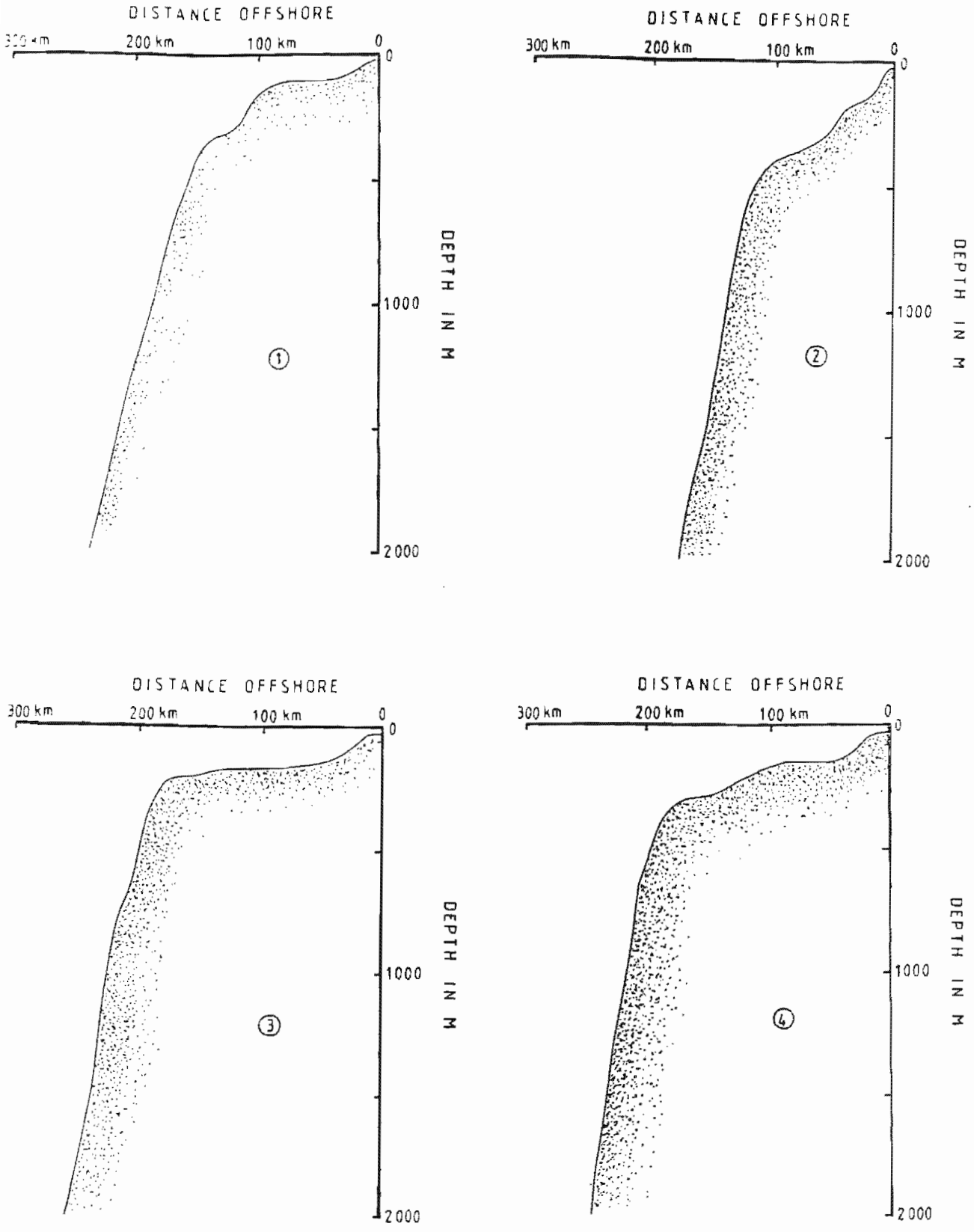

Fig. 3.4 The offshore bottom topography profiles for transects 1 to 4 in Fig. 3.1

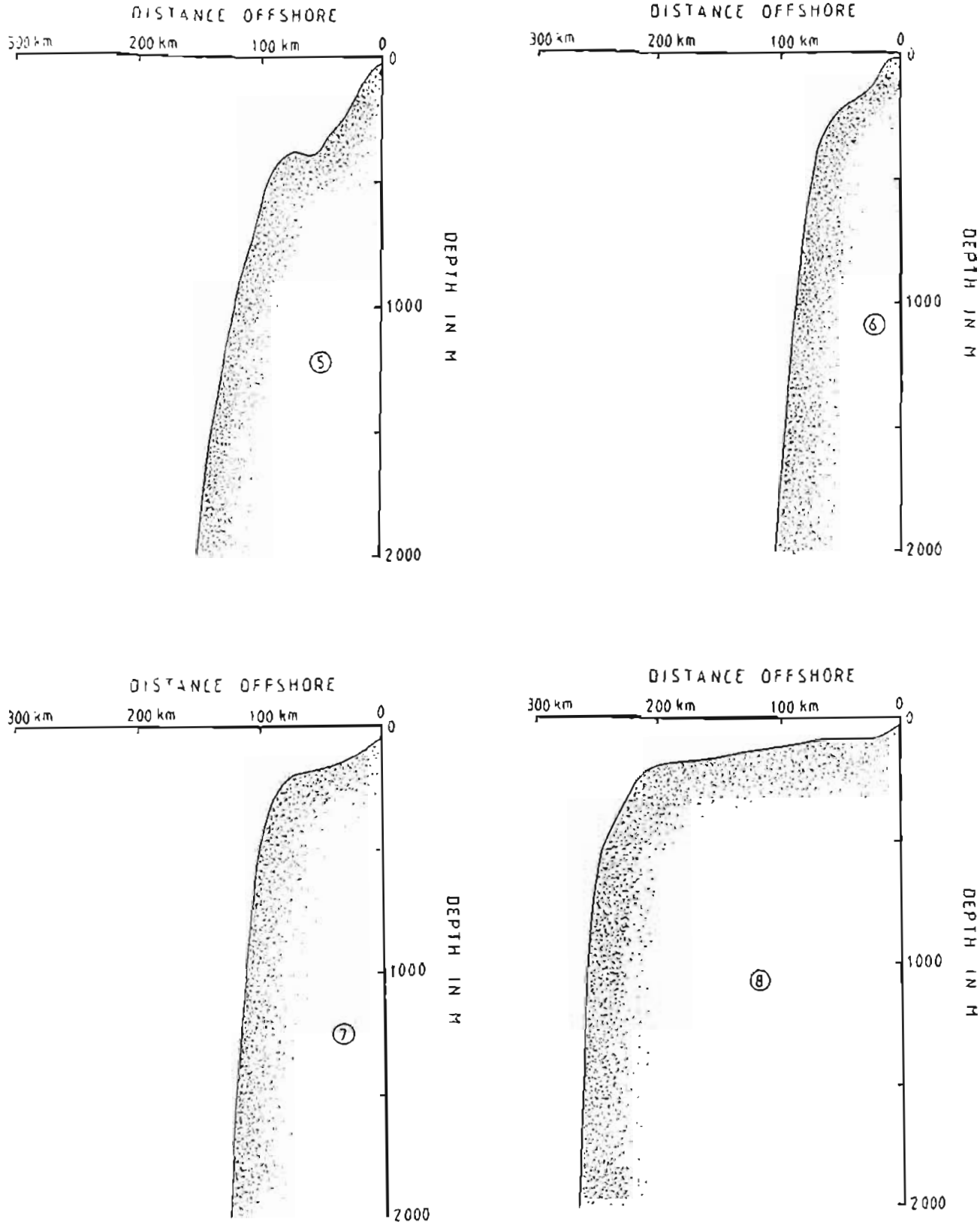

Fig 3.4 (cont.) *The offshore bottom topography profiles for transects 5 to 8 in Fig. 3.1*

For small wavenumber motions, $\ell \rightarrow \delta$ (where δ is a small parameter) and the inequality (3.3) reduces to

$$\left|\frac{\sigma_n}{\ell}\right| < \frac{g}{f}\left|\frac{\partial h}{\partial x}\right|_{\max} \left(1+\mathrm{R}_0{}^2\,\ell^2\right)^{-1}$$

where $\mathrm{R}_0 = gh / f^2$ is the external Rossby radius of deformation and it has been assumed that $\sigma_n \ll f$. Using a binomial expansion this may be approximated as

$$\left|\frac{\sigma_n}{\ell}\right| < \frac{g}{f}\left|\frac{\partial h}{\partial x}\right|_{\max} \left(1-\mathrm{R}_0{}^2\,\ell^2\right)$$

Since $\ell \rightarrow \delta$, the term $\mathrm{R}_0{}^2\ell^2 \ll 1$ and the above condition reduces to

$$\left|\frac{\sigma_n}{\ell}\right| < \frac{g}{f}\left|\frac{\partial h}{\partial x}\right|_{\max} - \left[O\,(h)\right] \text{ correction term} \qquad (3.4)$$

This implies that the low wavenumber structure of the dispersion curve is dependent on the maximum slope of the offshore topography profile $\left|\partial h/\partial x\right|_{\max}$ (i.e. sharpness of the shelf break) with a small O(h) correction. The value of h utilised in the O(h) correction is the depth of the offshore location where $\left|\partial h/\partial x\right|$ assumes its maximum value (that is, the depth of the shelf break). The phase velocities typical of the low wavenumber region of the dispersion curve thus depends on the sharpness of the shelf break as well as the depth at which the shelf break occurs.

The shelf topography of the Agulhas Bank (profile 8) has a both shallow and sharp shelf break, implying high phase velocity, low wavenumber free CTW motions. In profiles 3 and 4, the sharp shelf break occurs at greater depths, resulting in a larger O(h) negative correction in the inequality (3.4). This gives rise to the slightly lower phase velocity, low wavenumber motions for profiles 3 and 4 (see Fig. 3.2). In profiles 5, 6 and 7 the shelf break is not as sharp and occurs at greater depths, leading to the much lower phase velocities of the low wavenumber CTW motions.

For high wavenumber motions, $\ell \rightarrow M$ (where M is a large value), the condition (3.3) may be expressed as

$$\left|\frac{\sigma_n}{\ell}\right| < \frac{f}{h\ell^2}\frac{\partial h}{\partial x}\left(1-\frac{1}{R_0{}^2\,\ell^2}\right)$$

where $[R_0^2 \ell^2]^{-1} \ll 1$, which allows the above condition to be reduced to

$$|\sigma_n| < \frac{f}{h\ell}\frac{\partial h}{\partial x} - \left[O\left(\frac{1}{h}\right)\text{correction}\right] \qquad (3.5)$$

The high wavenumber structure of the dispersion curves therefore is determined by the "effective shelf width", where the "effective shelf width" is a length scale, X_h, defined as $X_h = h\left(\partial h/\partial x\right)^{-1}$. The condition (3.5) may then be expressed as

$$|\sigma_n| < \frac{f}{\ell X_h} - \left[O\left(\frac{1}{h}\right)\text{correction}\right]$$

A small "effective shelf width" (that is where $|\partial h/\partial x|$ is large) implies a slower decrease in the frequency of free CTW motions as $\ell \to \infty$. The dispersion curves for shelf regions having a small "effective shelf width" (profiles 6 and 7), are characterised by slowly decreasing (or even increasing) frequencies as $\ell \to \infty$. It is interesting to note that these are the same type of bottom topography profiles which would result in a larger value of the stratification parameter, S (where the effect of increasing S is to increase the frequency of higher wavenumber motions). Profiles 1, 3 and 4 have a much larger "effective shelf width" resulting in a more rapid decrease in the frequency of the CTW motions as $\ell \to \infty$ (see Fig. 3.2).

Since it is the generation of low wavenumber CTW motions which are of the greatest interest on the West and South coasts, the most important result of the above investigation is that the wide, shallow, gently-sloping shelf topographies (profiles 3, 4 and 8) support much higher phase velocity, long wavelength CTW motions than the narrower, steeply sloping shelf regions (profiles 5, 6 and 7). The maximum possible phase speed of the low wavenumber CTW motions will be shown in Chapters 4 and 7 to largely determine the nature and amplitude of the shelf response to forcing by a moving wind stress field, while the high wavenumber structure of the dispersion curves give an indication of the extent of expected topographic scattering of CTW motions by alongshore variations in the shelf topography. Some of these properties of free CTW's are reflected in analyses of the sea level variability (Chapter 5) and numerical modelling results (Chapter 7) in the different shelf regions.

3.3 CTW Dispersion Curves and the Effects of Stratification

The manner in which CTW dispersion curves are modified in the presence of significant stratification has been briefly discussed in Chapter 2. The modification of CTW dispersion curves by increasing stratification is greatest for higher mode and higher wavenumber motions. Stratification is therefore important in the vicinity of large alongshore variations in bottom topography where scattering into higher mode and higher wavenumber motions is expected to occur. Particularly significant for the interpretation of the modelling results is when the effects of stratification are sufficiently large for the group velocity to be in the same direction as the phase velocity for all wavenumbers. In these circumstances, where there is a loss of the high frequency cut-off (σ_{crit}) typical of each mode in barotropic CTW dispersion curves, the reflection of energy due to topographic scattering theoretically is no longer possible.

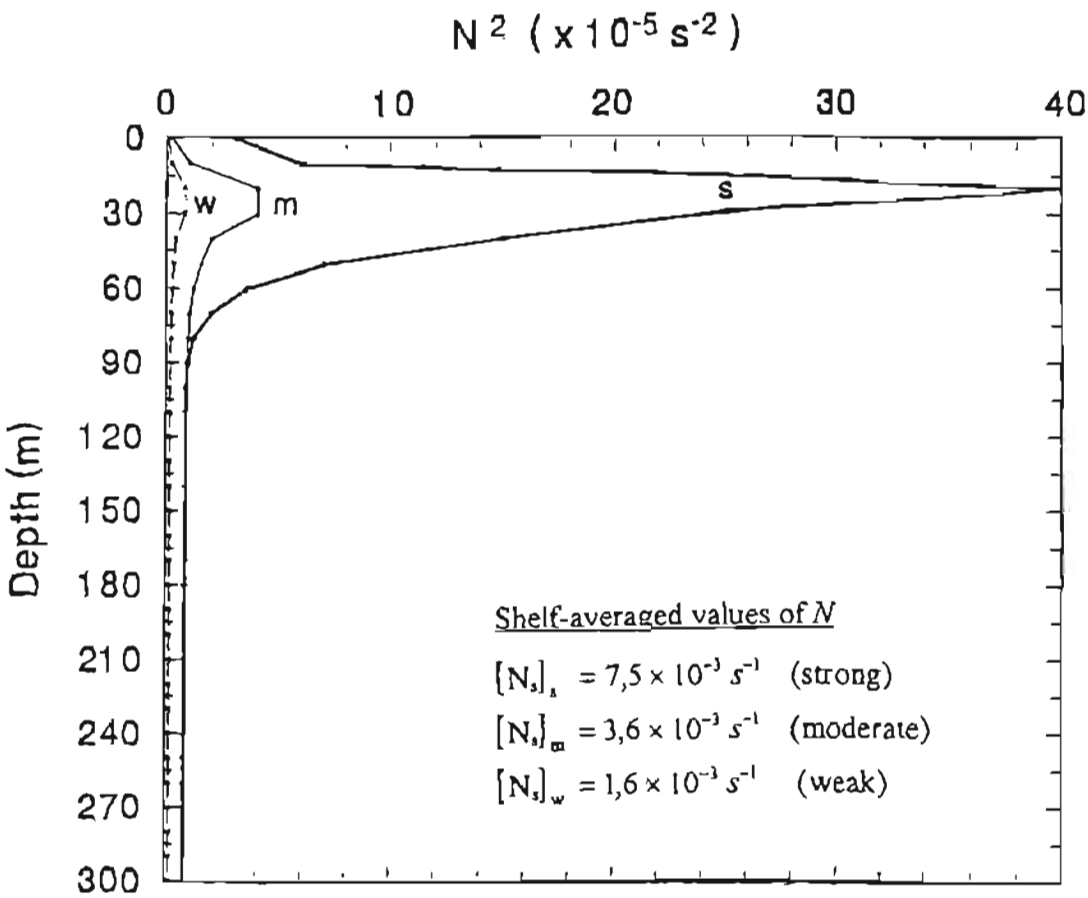

Fig. 3. 5 Three specifications of the Brunt-Väisälä profile used in calculation of free CTW dispersion curves in the presence of stratification.

The effect of stratification on the structure of CTW dispersion curves has been investigated by calculating dispersion curves for three idealised specifications of water column stratification for each of the eight offshore profiles of bottom topography at the transects indicated in Fig. 3.1. The three specifications of water column stratification (given in terms of vertical profiles of Brunt-Väisälä frequency in Fig 3.5) are labelled as strong (s), moderate (m) and weak (w). Strong stratification ($[N_s]_s = 7{,}5 \times 10^{-3}\, s^{-1}$) corresponds to either an extreme situation where quiescent conditions at the less exposed sites on the West Coast lead to the development of a sharp, shallow thermocline or to the highly stratified conditions found on the Agulhas Bank in summer. Moderate stratification ($[N_s]_m = 3{,}6 \times 10^{-3}\, s^{-1}$) is more representative of typical West Coast shelf waters. Weak stratification ($[N_s]_w = 1{,}6 \times 10^{-3}\, s^{-1}$) corresponds to either the situation where upwelling at the more exposed sites along the West Coast results in a more homogenous water column (Boyd, 1987) or to the well-mixed conditions found over the Agulhas Bank in winter. (Note that although the specification of weak stratification is such that the shelf averaged $[N_s]_w$ magnitudes are appropriate, the stratification at depth may be too weak to be realistic.) The first two modes for each offshore topography profile are presented in Figs. B-1 to B-8 in Appendix B. It should be noted here that problems existed with numerical convergence in the algorithm used when determining the dispersion curves for weak stratification over a shelf profile having a "double" shelf break.

There is very little difference between the barotropic CTW dispersion curves and those for weakly stratified waters, however the dispersion curves for moderately and strongly stratified shelf waters are significantly different. Increasing stratification results in a general increase in frequency (and consequently phase and group velocities) in the dispersion curves As expected, the increase is greatest for higher mode and higher wavenumber CTW motions. The effect of changing water column stratification seems to be least for the essentially non-dispersive low wavenumber motions, however the effect on the more dispersive, high wavenumber free CTW motions is substantial. While an increase from weak to strong stratification increases the free CTW phase velocities by only 1,0 to 1,5 $m.s^{-1}$ over the whole wavenumber range (see Fig 15.15a, p119), the group velocities of high wavenumber motions are substantially modified.

curves for these wide, gently-sloping shelf regions (such as the Orange River cone and Agulhas Bank) maintain their high frequency cut-off (σ_{crit}) for realistic specifications of stratification. The only difference is that σ_{crit} is found at higher wavenumbers.

For extreme water column stratification, the increase in frequency in the dispersion curves may be such that the magnitude of the frequencies exceed the inertial frequency. Once this has occurred, the CTW motions are strictly no longer trapped over the shelf (see dispersion curves for profiles 6 and 8).

In general, increased stratification increases both the phase and group velocities of the free CTW's. The implication of increased phase velocities is that the shelf waters will respond more readily to rapidly propagating wind systems. The increased group velocities imply that there will be less *backscattering* of CTW motions due to longshore variations in the bottom topography and consequently increased energy propagation along the shelf. (A necessary consequence is that increasing stratification leads to increased *forward* scattering of incident CTW's (for example, Wilkin and Chapman, 1990)).

The vertical structure of the response changes as stratification of the water column increases and flows that are highly sheared in the vertical or bottom-trapping of motions may occur. The investigation of these changes in the CTW response are discussed in Chapter 4 where the ratio R_{kp} has been calculated for the different sites and specifications of water column stratification.

4. FACTORS GOVERNING THE COASTAL-TRAPPED WAVE RESPONSE IN SOUTHERN AFRICAN SHELF WATERS

The principal factors governing the CTW response over the continental shelf are the water column stratification, longshore variations in bottom topography and the nature of the wind-forcing over the shelf. First, the importance of stratification over the shelf is investigated. This is followed by an investigation of the effect that longshore variations in the shelf topography have on the CTW response. A number of possible forcing mechanisms for CTW's are considered and only longshore wind stress is found to be effective in the forcing of synoptic scale CTW's on the west and south coasts of southern Africa. Consequently, a comprehensive description is provided of the synoptic scale atmospheric systems of southern Africa and their associated marine wind fields. Finally, published observations of CTW's over the continental shelf surrounding southern Africa are briefly reviewed.

4.1 Stratification

In terms of oceanic variables, the shelf region off the West Coast is defined by strong changes in the stratification to the north (Shannon, 1985) and by the influence of the Agulhas waters to the south (Nelson, 1985). Shelf stratification is appreciable beyond these boundaries. Analysis of satellite infra-red imagery (Lutjeharms and Stockton, 1987), indicates the near permanence of upwelled water over a large part of the shelf, implying weaker stratification over the shelf. In particular, Boyd (1987) notes a region of well-mixed shelf waters from 25°S to 27°S where water column stratification is extremely weak. A prominent feature of the West Coast region is the irregular ocean front which is generally located at the shelf edge (Shannon, 1985). The effect of this baroclinic feature on CTW motions is uncertain. Motions as postulated by Bane and Hsueh (1980) may well occur towards the south where the oceanic front is more convoluted, lies closer inshore and is associated with strong flows at the shelf edge (Bang, 1973; Bang and Andrews, 1974 and Nelson, 1985). On the South Coast there is a strong seasonality in the water column stratification (Schumann and Beekman, 1984; Eagle and Orren, 1985). The water column stratification is particularly strong in summer resulting in the development of intense thermoclines over the Agulhas Bank. Since most of the Agulhas Bank is a wide,

gently-sloping shelf region, the strong seasonal changes in water column stratification are not expected to impact significantly on the low frequency CTW dynamics (see Chapter 3 and Table 1 where the stratification parameter for profiles 3 and 8 remain small for all specifications of water column stratification). While the effect of increasing stratification on such a wide, gently-sloping shelf is negligible for low wavenumber CTW's, the effect on higher wavenumber CTW motions and hence topographic scattering may be appreciable (see the dispersion curves for shelf profiles 3 and 8 in Appendix B).

The effect of a longshore currents on CTW dynamics is minimal provided the relative vorticity of the flow is not comparable in magnitude to the local planetary vorticity. On most of the West Coast the magnitude of longshore currents are small in comparison to the long-wave CTW phase speeds. Such weak flows are expected to cause only a small Doppler shift in the modal frequencies of barotropic CTW motions (Brink, 1980). However, in the southern regions of the West Coast where significant baroclinic flows are known to exist, the effect of longshore currents on CTW dynamics may be important (particularly for higher mode and higher wavenumber motions which have small phase velocities). On the South Coast, the CTW response over the shelf generally is not influenced strongly by the Agulhas Current which typically flows along the shelf edge. However, further east towards Port Elizabeth and beyond, the Agulhas Current does impact strongly on the propagation of CTW's. Schumann and Brink (1990) find that the Agulhas Current, although not strong enough to "reverse" the direction of CTW propagation, dramatically enhances the damping of CTW's (see Table 2). They contend that the propagation of CTW's between East London and Durban is strongly inhibited by the Agulhas Current.

The stratification of the continental shelf waters surrounding southern Africa may be roughly parameterised in terms of Brunt-Väisälä frequency as follows:

i) strong stratification (quiescent/sheltered waters) $[N_s]_s \approx 7{,}5 \times 10^{-3}$ to 10^{-2} s^{-1},

ii) moderate stratification $[N_s]_m \approx 3{,}6 \times 10^{-3}$ to 10^{-2} s^{-1}

iii) weak stratification (upwelled/well-mixed waters) $[N_s]_w \approx 1{,}6 \times 10^{-3}$ to 10^{-2} s^{-1}

where N_s is a shelf-averaged Brunt-Väisälä frequency as defined by Clarke and Brink (1985). In Chapter 2 it is stated that the ratio $S = N_s \alpha / f$, is important in characterising the

CTW response to "weather band" wind-forcing. A rough indication of the importance of stratification in the CTW dynamics over the continental shelf surrounding southern Africa is provided by the values of the stratification parameter (S) in Table 1 which have been calculated for a number of shelf profiles along the West Coast (Fig. 4.1) and for the range of shelf-averaged Brunt-Väisälä frequency magnitudes specified above.

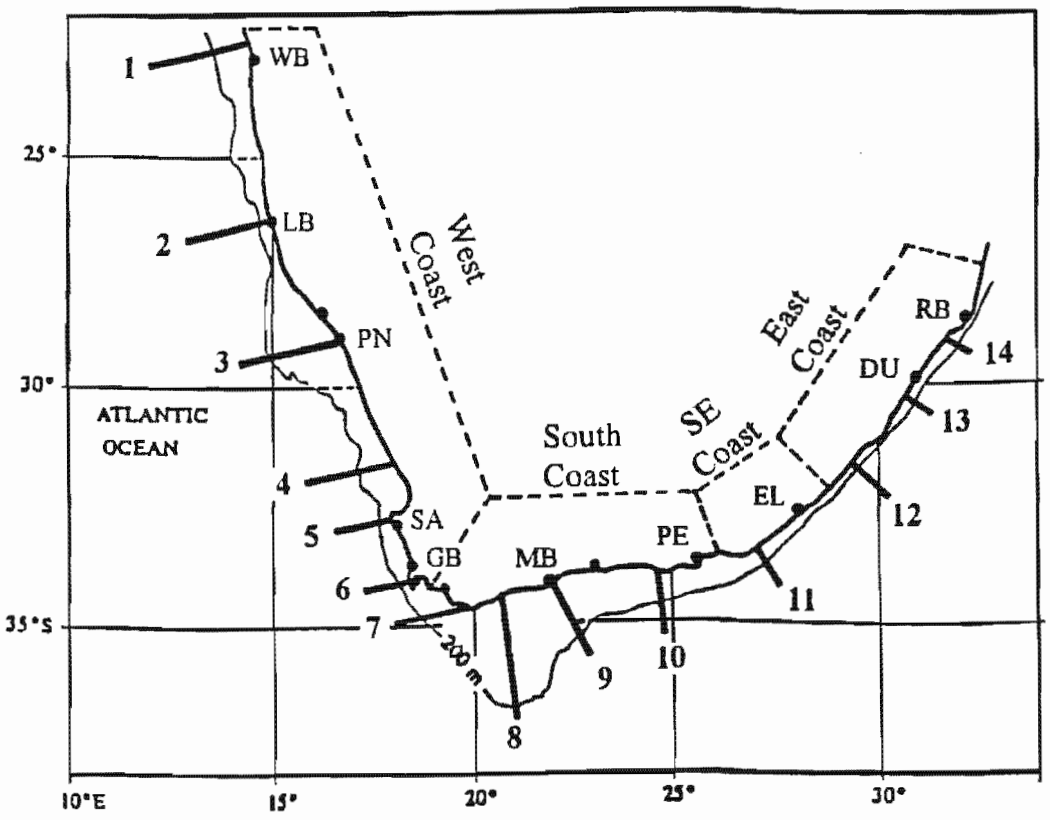

Fig 4.1 The approximate locations of the 14 bottom topography profiles used to determine the parameters listed in Table 1 and Table 2

Generally S « 1 on the West Coast and thus stratification is expected only to be a passive factor in characterising the response over the West Coast shelf. This is also true for the wide shelf regions of the South Coast, however it is not the case for the narrow, steeply-sloping shelf regions of the East Coast. Chapman and Henderschott (1982) have shown that if $S < 0.2$ ($S^2 < 0.04$), the CTW response may be adequately described using the homogeneous shallow water equations. Table 1 shows that this condition generally holds for the water column stratification typically observed along the West Coast and thus, in the numerical investigation in Chapter 7, solutions to the homogenous shallow water equations (see Appendix A) are considered to be representative of the CTW response off

the west coast of southern Africa One should be careful in making the above assumption as larger values of S occur both to the north (where f is small) and to the south (where both $\partial h/\partial x$ and N_s may be large) of the West Coast. Along the South Coast S « 1 and the response is barotropic, however on the East Coast S ≥ 1 and the response is expected to be highly baroclinic. Caution should be exercised in the interpretation of results obtained from the barotropic equations in regions where S ≥ 0.2 and also at the shelf edge where $\partial h/\partial x$ and $\partial^2 h/\partial x^2$ are large and a boundary layer correction to the barotropic response is necessary within a distance of O(S × shelf width) of the shelf edge (Clarke and Brink, 1985).

Bottom Profile Number	Mean Shelf Slope α	Local Coriolis Parameter f_0 (s^{-1})	$\frac{\alpha}{f_0}$ (s)	S for $N_s = 7{,}5 \times 10^{-3}\ s^{-1}$ = $[N_s]_s$	S for $N_s = 3{,}6 \times 10^{-3}\ s^{-1}$ = $[N_s]_m$	S for $N_s = 1{,}6 \times 10^{-3}\ s^{-1}$ = $[N_s]_w$
1	1,7x10^{-3}	5,64x10^{-5}	30,9	0,232	0,111	0,049
2	4,2x10^{-3}	6,25x0^{-5}	66,7	0,500	0,240	0,107
3	1,1x10^{-3}	7,10x0^{-5}	16,1	0,121	0,058	0,026
4	1,8x10^{-3}	7,67x0^{-5}	23,5	0,176	0,085	0,038
5	4,4x10^{-3}	7,91x0^{-5}	56,9	0,427	0,205	0,074
6	3,3x10^{-3}	8,13x10^{-5}	53,8	0,403	0,194	0,070
7	1,7x10^{-3}	8,31x0^{-5}	39,4	0,296	0,142	0,051
8	9.5x10^{-4}	8.78x0^{-5}	10,8	0,081	0,039	0,017
9	1,4x10^{-3}	8,36x0^{-5}	16,6	0,125	0,060	0,027
10	4,0x10^{-3}	8,26x0^{-5}	48,4	0,363	0,174	0,077
11	4,7x10^{-3}	8,12x0^{-5}	57,3	0,430	0,206	0,092
12	13,6x10^{-3}	7,73x0^{-5}	175,9	1,319	0,633	0,281
13	30,6x10^{-3}	7,40x0^{-5}	413,8	3,104	1,490	0,662
14	5,0x10^{-3}	7,18x0^{-5}	69,6	0,518	0,248	0,110

Table 1 Values for the stratification parameter (S) *for a number of offshore bottom topographies along the coastline of southern Africa for 3 different specifications of vertical stratification of the water column* (N_s). *Values of S > 0.2 are underlined.*

Bottom Profile number	mode no	strong stratification $[N_s]_s$			moderate stratification $[N_s]_m$			weak stratification $[N_s]_w$			barotropic no mean flow		
		C_{ph} ($m.s^{-1}$)	R_{kp}	T_f (days)	C_{ph} ($m.s^{-1}$)	R_{kp}	T_f (days)	C_{ph} ($m.s^{-1}$)	R_{kp}	T_f (days)	C_{ph} ($m.s^{-1}$)	R_{kp}	T_f (days)
1	1	7,7	17.4	3,9	7,7	11,8	4,1	7,2	32,3	3,7	7,0	-	3,5
	2	3,97	9,2	5,5	3,6	6,3	6,3	3,1	24,2	6,5	3,8		6,5
2	1	7,5	17,9	8,2	7,6	9,8	8,8	6,9	34,0	7,8	6,6	-	7,5
	2	3,8	11,2	9,8	3,3	5,9	15,0	2,8	25,1	14,9	2,6		14,4
3	1	12,1	18,8	4,2	12,0	16,0	4,2	11,8	24,6	4,1	11,6	-	4,1
	2	6,7	23,7	12,1	5,8	14,4	18,4	5,4	30,6	18,9	5,0		21,6
4	1	12,1	18,5	4,6	12,0	15,1	4,7	11,6	24,1	4,6	11,4	-	4,4
	2	6,5	31,5	10,3	5,5	18,1	17,2	5,2	57,6	17,5	4,8		18,3
5	1	8,5	19,8	9,6	8,2	11,7	9,6	7,6	36,8	8,8	7,2	-	8,4
	2	4,5	24,1	12,6	3,8	14,5	20,6	3,6	49,1	18,9	3,2		19,4
6	1	6,1	16,4	7,8	5,8	7,8	7,3	5,2	25,2	6,1	4,9	-	5,5
	2	3,9	19,6	5,5	3,4	10,9	9,6	3,1	36,3	8,2	2,8		9,7
7	1	7,7	23,2	5,0	7,6	13,4	5,0	7,1	36,3	4,6	7,0	-	4,5
	2	5,1	26,3	7,3	4,2	13,9	14,3	4,0	44,7	14,7	3,6		20,2
8	1	14,3	10,4	2,8	14,2	10,2	2,9	14,2	11,6	2,8	14,0	-	2,8
	2	2,7	7,63	4,3	2,8	4,9	4,6	2,4	18,8	3,3	2,3		3,0
					Stratified			barotropic with mean flow			barotropic no mean flow		
9	1				10,0	11,9	5,0	-	-	-	9,3	-	4,6
	2				5,5	-	-	-	-	-	4,8	-	-
10	1				7,5	8,6	4,8	-	-	-	6,4	-	4,2
	2				3,7	-	-	-	-	-	2,7	-	-
11	1				4,2	4,3	5,3	2,2	-	1,8	2,8	-	3,0
	2				2,4	-	-	-	-	-	1,4	-	-
12	1				3,4	4,3	19,5	1,6	-	3,5	2,2	-	27,3
	2				2,1	-	-	-	-	-	1,0	-	-
13	1				2,7	2,1	18,9	0,7	-	3,8	1,3	-	17,5
	2				1,0	-	-	-	-	-	0,7	-	-
14	1				5,0	8,0	10,7	-	-	-	3,9	-	10,3
	2				2,5	-	-	-	-	-	1,7	-	-

Table 2 Values of C_{ph} (phase velocities), R_{kp} (the ratio of kinetic to potential energy) and T_f (the e-folding frictional decay time in days) for a number of offshore bottom topographies along the southern African continental shelf for different specifications of vertical stratification of the water column. The data for Profiles 9 to 14 have been obtained from Schumann and Brink (1990). All of the above parameters are calculated for the "long wave" non-dispersive limit for free CTW's

A more robust analysis of the baroclinicity of the response is possible using the software of Brink and Chapman (1987) which outputs values of R_{kp} (the kinetic/potential energy ratio). The significance of these ratios has been discussed in Chapter 2. In a nutshell, if $R_{kp} \rightarrow \infty$ then the motion is barotropic, however if $R_{kp} \rightarrow 1$ the CTW response is highly baroclinic. The R_{kp} values have been calculated for 8 offshore profiles of bottom topography (profiles 1 to 8) and three specifications of water column stratification (Table 2). Also tabulated are values of the frictional decay time (T_f) and the local phase velocities (C_{ph})of the free CTW's at these locations. Results are tabulated for both first and second mode free CTW's. Similar parameters, extracted from tables published by Schumann and Brink (1990), have been tabulated for other sites around the coast (profiles 9 to 14). Comparison of their values for the West Coast and the parameters calculated for profiles 1 to 4, indicate that their results for a stratified water column correspond to the specification of "moderate" stratification used in this dissertation.

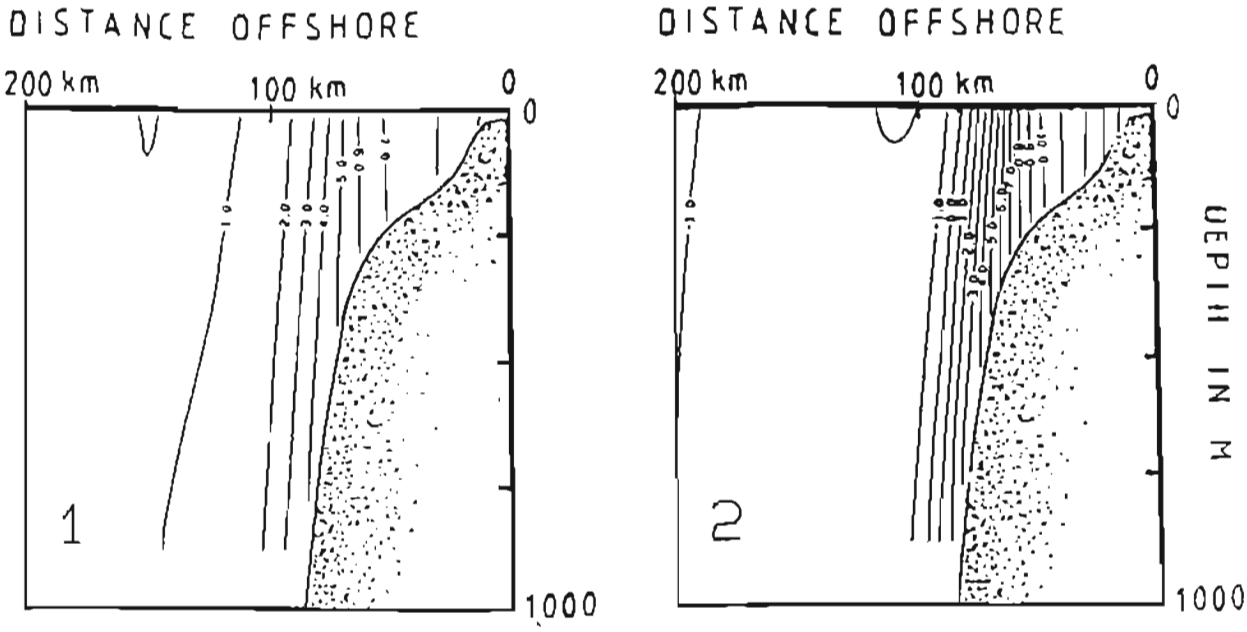

Fig 4.2 The first and second mode free CTW alongshore velocity response for strong stratification over a narrow, steeply-sloping shelf region (profile 6)

In general, $R_{kp} < 8$ on the West Coast, a finding also made by Schumann and Brink (1990). The smallest values of R_{kp} on the West Coast occur off Lüderitz (profile 2) and Cape Columbine (profile 6), however for even the strongest specifications of stratification over the steepest shelf regions along the West Coast, the first and second mode responses over the shelf display very little vertical shear in longshore velocities (fig 4.2). On the wide

shelf region to the south (Agulhas Bank) the R_{kp} values indicate a barotropic response while further eastwards beyond Port Elizabeth the response is strongly baroclinic. Moving anticlockwise around the coast of southern Africa, the CTW response changes from being barotropic along the West Coast to increasingly baroclinic in the southern Benguela and the transition zone from the West to South Coast, strongly barotropic over the wide Agulhas Bank and finally changing to a strongly baroclinic response northeast of Port Elizabeth.

In those narrow shelf regions where the response is expected to be significantly baroclinic, the first mode free CTW phase speeds are greatly reduced, while over the wide, gently-sloping shelf regions the first mode phase speeds are large. The difference between the phase speeds of the first and second mode free CTW's is greatest for the wide, gently-sloping shelf regions, while over a strongly-sloping shelf region this difference is quite small (see Fig. 15.15a, p119). The frictional decay times (T_f) suggest that there is a large disparity in frictional damping between the first and second mode CTW's, however there seems to be very little difference between the respective frictional decay distances (L_f). In the absence of a mean flow, L_f ranges from 2000 km to 6000 km for all first and second mode CTW's. The higher the mode number the smaller are the L_f values, implying that the damping of CTW's is greatest for the higher mode CTW's. Conversely, these frictional decay distances increase with increasing stratification, suggesting that free CTW's are able to travel further in the presence of increased water column stratification. Schumann and Brink (1990) calculated the free CTW modes for the East Coast region in the presence of the Agulhas Current. The impact of such a strong flow on the frictional decay times and distances is dramatic, decreasing these scales by nearly an order of magnitude.

In conclusion, the vertical motion of the isopycnals often observed over the shelf is not necessarily indicative of baroclinic control on the CTW response, but rather is a movement of the isopycnals in sympathy with the strong barotropic motions over the shelf. The importance of these vertical movements of the thermocline in modulating local upwelling at sites along the West Coast has been discussed by Nelson (1992b) and Jury and Brundrit (1992).

4.2 Longshore Variations in the Coastline and Bottom Topography

Early studies of the effect of longshore variations in the coastline and bottom topography on CTW propagation considered barotropic CTW propagation over shelf topography having longshore variations that are small in comparison to the shelf width (for example, Allen, 1976 and Grimshaw, 1977). These studies were followed by investigations of the effect of bottom irregularities (Brink 1980), small topographic features (Chao *et al.*, 1979) and more abrupt alongshore changes in topography (Middleton and Wright, 1988) on the propagation of barotropic CTW's along the shelf. The effects of longshore variations in topography on barotropic CTW's has been succinctly reviewed by Huthnance (1987). Recently, the analyses have been extended to investigate CTW wave propagation along shelf regions characterised both by significant alongshore variations in bottom topography and substantial water column stratification (Wilkin and Chapman, 1990).

4.2.1 Longshore Variations in the Coastline

Clarke (1977b) concludes that variations in the coastline result in no major modification of the propagation characteristics of "long-wave" barotropic CTW motions with Killworth (1978) explaining that the effect of a changing coastline is simply to move the response such that it follows the coastline.

Grimshaw (1977) and Allen (1976), using perturbation analyses, show that the effect of coastline variations on "long-wave" barotropic CTW's is not nearly as great as the effect of longshore changes in the topography. This suggests that the effects of variations in the coastline generally may be ignored when investigating CTW propagation around southern Africa. One should, however, be cautious in making this assumption because radical changes in the coastline (such as occur at Cape Columbine) are accompanied by large changes in the bottom topography which are expected to strongly modify the CTW response.

4.2.2 Longshore Changes in the Bottom Topography

The effects of longshore variations in the bottom topography on free and forced CTW propagation along a continental shelf are elucidated through both a scale analysis of the

equations of motion governing the barotropic CTW response over the shelf, and a brief review of the relevant literature.

A scaling analysis pertinent to "long-wave" barotropic CTW motions is presented in Appendix A. Two possible "long-wave" CTW responses over a shelf with longshore variations in bottom topography exist, namely

i) a strong response to strong longshore topographic control where the typical scales involved are $X/Y \approx U/V \approx X_h/Y_h \approx \delta$, and

ii) a strong response to weak longshore topographic control where the typical scales involved are $X/Y \approx U/V \approx \delta$ and $X_h/Y_h \approx \delta^2$.

These are the familiar "boundary layer" scales used in most investigations of barotropic CTW motions. For the above scales of motion (see Appendix A)

i) the longshore velocities are in geostrophic balance with the cross-shore gradient in sea level,

ii) cross-shelf wind/bottom stresses and cross-shelf wind/bottom stress curl do not play a significant role in the first order CTW dynamics,

iii) the response is essentially non-divergent,

iv) atmospheric pressure forcing is not considered to be a first order effect, and

v) where the alongshore gradients in the topography are small (that is, $X_h/Y_h \approx \delta^2$), their role in the first order dynamics of CTW's is negligible.

Consider the situation where there is a particularly strong variation in the longshore topography ($X_h/Y_h \approx 1$). Under these circumstances the cross-shore and longshore response are expected to develop similar length scales, that is, $X/Y \approx 1$. At these scales ($X/Y \approx 1$), the cross-shore wind stress and cross-shore bottom stresses are significant and cannot be ignored. For the long time scales normally considered in subinertial CTW dynamics ($fT \approx 1/\delta$), the time-dependent terms in the equations of motion governing the CTW response are very small, suggesting the development of quasi-steady flows which follow the bottom topography (see Allen, 1976). Similarly, on shorter time-scales ($fT \approx 1$), the response is expected to consist of higher frequency, small scale motions where $X/Y \approx 1$. Under these circumstances all terms in the equations of motion are of

similar magnitude and no simplifications can be made to the equations (A.4 to A.6 in Appendix A) which govern the barotropic CTW response over the shelf. Note that for the scales $X/Y \approx 1$, the scaling arguments of Clarke and Brink (1985) are no longer valid. Their criterion for a barotropic response may no longer hold and a significantly baroclinic response may occur even in regions where $S \ll 1$. Wang (1980) has noted that "long wave" CTW energy may be scattered into baroclinic motions in the vicinity of sharp changes in the shelf topography.

The above scale analysis provides a simple overview of the effects of longshore variations on the barotropic CTW dynamics. More detailed investigations of the effects of longshore variations in bottom topography on the propagation of CTW's are briefly reviewed below.

Topographic Scattering of Barotropic CTW's

In general, it is expected that where significant longshore variations in the bottom topography are encountered, the incident CTW's are scattered into other CTW modes both propagating and evanescent. This often leads to the observation of incoherent longshore and cross-shore velocities in the vicinity of large changes in the shelf topography.

Allen (1976) investigated barotropic CTW propagation over shelf topography where the amplitude of the longshore topographic variations is small in comparison to the shelf width. He showed that under the "long-wave" approximation, barotropic CTW's could be scattered into other forward propagating modes by small alongshore variations in the shelf topography. Where the "long-wave" approximation is not made, CTW energy can be scattered into both forward and backward propagating modes. In general, as the incident CTW passes over large changes in the bottom topography, the energy of the wave is partially scattered into higher wavenumber and higher mode motions. These in turn are extremely susceptible to scattering and frictional damping.

Higher mode and wavenumber motions have a cross-shelf energy distribution which is concentrated further offshore than the lowest mode CTW's. It is therefore expected that where there are substantial longshore variations in topography (and thus scattering into higher mode and wavenumber motions), the energy in the shelf response will be

concentrated further offshore. The higher modes CTW's also have larger cross-shore transports than the lower mode CTW's. Consequently, where topographic scattering into higher modes occurs, the transmitted CTW response may look like the lower modes in alongshore transport and the higher modes in the cross-shore transport. Thus topographic scattering may lead to large amplitude, incoherent alongshore and cross-shore transports in the vicinity substantial alongshore changes in shelf topography.

Allen (1976) has shown that the amount of scattering of the incident long wave depends on the ratio of the longshore CTW response scale to the scale of the topography feature. If this ratio is large, the loss of energy due to scattering is small, whereas a small ratio leads to substantial topographic scattering of CTW's (especially the higher mode CTW's). Chao *et al.* (1979) largely confirm the above findings and shows that for small isolated topographic features, the incident CTW is scattered preferentially into the higher mode and shorter wavelength CTW motions. This results in the general cascade of energy into smaller scale motions as barotropic CTW's pass over extensive topographic irregularities

Wang (1980) provides a very clear insight into the scattering of free barotropic CTW's by observing the modification and scattering of a single mode incident CTW by a canyon, a ridge and converging/diverging isobaths. The canyon and ridge topographies both backscatter a large proportion of the incoming CTW energy which implies that substantial canyons or ridges can effectively block "long wave" CTW motions propagating along a shelf, resulting in strong, localised disturbances in their immediate vicinity. Little backscattering occurs for Wang's specifications of convergent or divergent depth contours, unless the incident CTW frequency exceeds the maximum possible frequency of all transmitted modes, in which case total reflection of the incident CTW occurs. He also shows that propagation of CTW's over converging (diverging) depth contours, leads to a decrease (increase) in the phase and group velocity of the transmitted wave and energy conservation considerations (see Chapter 2) require that the transmitted wave amplitude is greater (less) than the incident wave.

Wang's (1980) observation of minimal topographic scattering for convergence/divergence of depth contours when the longshore topographic scale is of the order of the shelf width or greater, is supported by the more general findings of others. Hsueh (1980) states that

variations in shelf width over large alongshore distances (that is, where the "long wave" approximation is valid) will not scatter barotropic CTW's if the topography varies in a "shelf-similar" manner. Hsueh (1980) defines a "shelf-similar" topography as one where the distance from each isobath to the coast remains a fixed fraction of the local shelf width. Davis (1983) showed that the restrictive "long wave" approximation need not be made in investigating CTW propagation over of "shelf-similar" topographies. Using conformal mapping arguments he demonstrates that any shelf topography can be mapped to one of constant width in the new co-ordinate system, and that the equations of motion governing the propagation of barotropic CTW's are invariant under the new mapping. He further shows that if the logarithm of the depth satisfies Laplace's equation then the shelf maps to a shelf of constant width with parallel isobaths, a topography which will not result in topographic scattering. This property forms the basis of Hsueh's definition of "shelf-similar" topographies. The above findings only are valid in the barotropic limit. With the introduction of stratification, the equations of motion governing CTW propagation are no longer invariant under conformal transformations and topographic scattering may occur over "shelf-similar" topographies. In a more general analysis Webster (1987) studied the scattering of barotropic CTW over a "shelf similar" topography as defined by Hsueh (1980). Webster confirms the previous observation that significant topographic scattering of CTW's only occurs where the spatial scales associated with longshore variations in shelf topography are less than the shelf width. He further shows that extent of topographic scattering depends not only on the strength of interaction between the incident CTW and the topographic variations, but also on the degree of interference within the scattered modes.

Middleton and Wright (1988) investigated barotropic CTW propagation over an abrupt jump in depth and found that

i) the transmission of a wave past a longshore jump in the topography decreases with increasing jump size,

ii) a longshore topographic jump acts to pass (retard) incident modes which have cross-shelf scales that are larger (smaller) that those of the change in topography,

iii) the ratio of the incident CTW energy to the CTW energy transmitted past the topographic jump is greatest for frequencies $\sigma \ll \sigma_{crit}$ and the transmission of energy

past the jump in topography monotonically decreases to zero as the frequency of the incident wave increases to $\sigma = \sigma_{crit}$ and lastly,

iv) most of the incident CTW energy is scattered in to the gravest mode and thus the longshore topographic variations tend to act to low pass filter incident CTW's in both the frequency and wavenumber domain, an observation first made by Webster (1987).

The above findings suggest that where a very abrupt feature (such as a peninsula) is encountered, the incoming barotropic CTW's may be almost totally reflected as short waves with a negative group velocity. Davis (1981) confirms this almost total reflection of incident barotropic CTW's by abrupt changes in longshore topography, a result which is simply an extreme case of the general findings of Wang (1980).

Lastly, Brink (1980) indicates that small random changes in the topography result in strong scattering of free waves with frequencies corresponding to $C_g = \partial \sigma_n / \partial \ell = 0$. The dissipation of the propagating incident wave due to the small random variations in the topography is considered to be of the same order or greater than that due to bottom friction alone. He also notes that mean longshore flow in the direction of CTW propagation reduced the damping of the propagating CTW due to topographic scattering by extensive bottom irregularities.

Topographic Scattering of CTW's in Stratified Shelf Waters

The above results for barotropic CTW's are strictly only applicable in a homogenous ocean. Shelf waters, to a greater or lesser extent, are stratified and the effects of water column stratification on topographic scattering of CTW's need to be elucidated. Increasing stratification of the water column increases the frequency in the free CTW dispersion curves, ultimately resulting in the loss of the high-frequency cut-off typically found in barotropic CTW dispersion curves (see Appendix B). When this occurs, theoretically, no CTW wave motions capable of transporting energy in a backwards direction exist and back-scattering of CTW wave energy by longshore changes in the topography is no longer possible.

The qualitative nature of CTW propagation over abrupt increases in shelf width ("shelf-similar" topographies where little or no backscattering occurs) is not likely to be changed by the introduction of stratification, while the results for CTW propagation over abrupt changes in depth (where backscattering is typically strong) are expected to be substantially modified by the introduction of stratification unless the stratification is extremely weak. Brink (1986) has demonstrated that topographic scattering is not necessarily reduced by the introduction of stratification of the water column. He shows that the presence of stratification may or may not enhance the scattering of a first mode CTW by bottom irregularities, a concept which is counter-intuitive to the idea that stratification of the water column may to some extent "insulate" the CTW response from the effects of bottom variations.

Wilkin and Chapman (1990) used a numerical model to investigate the effect of stratification on the scattering of CTW's. They show that the amount of scattering of incident CTW is proportional to a topographic "warp" factor which estimates the extent to which the topography departs from "shelf-similarity" (that is, the severity of the topographic variations). Little or no scattering occurs for topographic variations which are "shelf-similar" (small topographic "warp" factor) while scattering is substantial for regions which are not " "shelf-similar" (large topographic "warp" factor). While *backscattering* may be eliminated or greatly reduced by increasing stratification of the water column, the *forward scattering* induced by "nonshelf-similar" topographic variations of necessity increases with increasing water column stratification. Once again this is a concept that is counter-intuitive to the idea that stratification of the water column may "insulate" the CTW response from the effects of bottom variations. As is the case for barotropic CTW's, in the immediate vicinity of the scattering region the scattered-wave-induced currents vary substantially over small spatial scales, there is a marked intensification of flow in this region and rapid changes in phase are observed. The topographic scattering seems to be equal in magnitude both for transitions from a wide to a narrow shelf and *vice versa*, however on narrowing shelves the influence of scattering can extend upstream into the region of uniform topography even when no freely propagating backscattered waves exist. Johnson (1991) provides an elegant analysis of CTW's having frequencies less than a "profile" frequency of ($f \times S$). He notes that very

strong stratification ($S > 1$) over the shelf suppresses topographic scattering at all subinertial frequencies while at intermediate values of the stratification parameter ($S \leq 1$), all energy is scattered forwards.

Given

i) the fact that the CTW dispersion curves presented in Appendix B do not in general lose there high frequency cut-off for specifications of the water column stratification typically observed on the West and South Coast, and
ii) the statement of Wilkin and Chapman (1990) that forward scattering increases with increasing stratification,

the topographic scattering of CTW is expected to be substantial for the water column stratification observed along the West and South Coasts.

Very few analytical studies have been devoted to the investigation of longshore variations in shelf topography on the *forced* CTW response. Allen (1976) and Grimshaw (1977) both use perturbation analyses to investigate the effect of longshore changes in the topography on the forced barotropic response over a shelf in terms of CTW's. They conclude that forcing on a long time scale results in the development of nearly steady-state flow in the vicinity of large changes in the topography. These flows tends to follow the local bottom topography. The scale analysis in Appendix A confirms this behaviour.

In summary, the effect of longshore variations in topography on both free and forced CTW's is that

i) the CTW energy transmission along the shelf may be greatly reduced due to topographic scattering. The topographic scattering of longer wavelength, low frequency CTW's is less that that of shorter wavelength, higher frequency CTW's,
ii) most of the forward scattered (transmitted) energy is scattered into the gravest mode CTW's and thus longshore topographic variations tend to act to low pass filter incident CTW's in both the frequency and wavenumber domain,
iii) very strong, localised disturbances are expected to be generated (especially further offshore) in the vicinity of large changes in the bottom topography,
iv) topographic scattering may lead to an incoherence between the cross-shore and longshore transports in the vicinity of large changes in the bottom topography,

v) the introduction of stratification at magnitudes typically observed along the West and South Coasts is not expected to *qualitatively* change the nature of the results obtained for the topographic scattering of barotropic CTW's by significant longshore variations in the shelf topography, and

vi) the forcing of CTW's on a long time scale results in a quasi-steady flow in the vicinity of large alongshore changes in the bottom topography.

The above discussion suggests that the strongly varying bottom topography of the West Coast is an especially hostile environment for free CTW propagation if not for the propagation of a forced CTW's. This is especially the case for the higher frequency, shorter wavelength free CTW's. The dissipation of locally forced CTW's is generally less evident due to the continual energy input by the wind which, to a large extent, masks the energy losses due to topographic scattering of the forced CTW response.

Given the importance of the topographic scattering of CTW's, features of note along the West Coast (Fig 4.3) are:

i) the narrow shelf region off Lüderitz and narrow shelf region to the south of the West Coast where two granite outcrops (Cape Columbine and Cape Point) constrict the shelf. Also of importance in the narrow shelf region off Cape Columbine is the presence of a substantial submarine canyon, the Cape Canyon.

ii) the rapid widening of the shelf south of Chamais Bay (27° 55'S; 15° 40'E), the wide, shallow Orange River cone and the rapidly narrowing shelf region south of the Orange River cone. These are shelf topographies which are not "shelf-similar".

iii) the rapid change in coastline and bottom topography forming the Cape Columbine peninsula.

Other significant topographic features along the coastline of southern Africa are:

i) the very wide, gently-sloping shelf (Agulhas Bank) on the South Coast.

ii) the substantial ridge (upon which the shallow Alphard Banks are located) extending seawards across the Agulhas Bank between Cape Agulhas and Mossel Bay.

iii) the rapid narrowing of the continental shelf to the eastwards beyond Port Elizabeth.

In most of the above cases, the changes in the bottom topography of the shelf cannot be considered to be "shelf similar" and substantial topographic scattering is likely to occur.

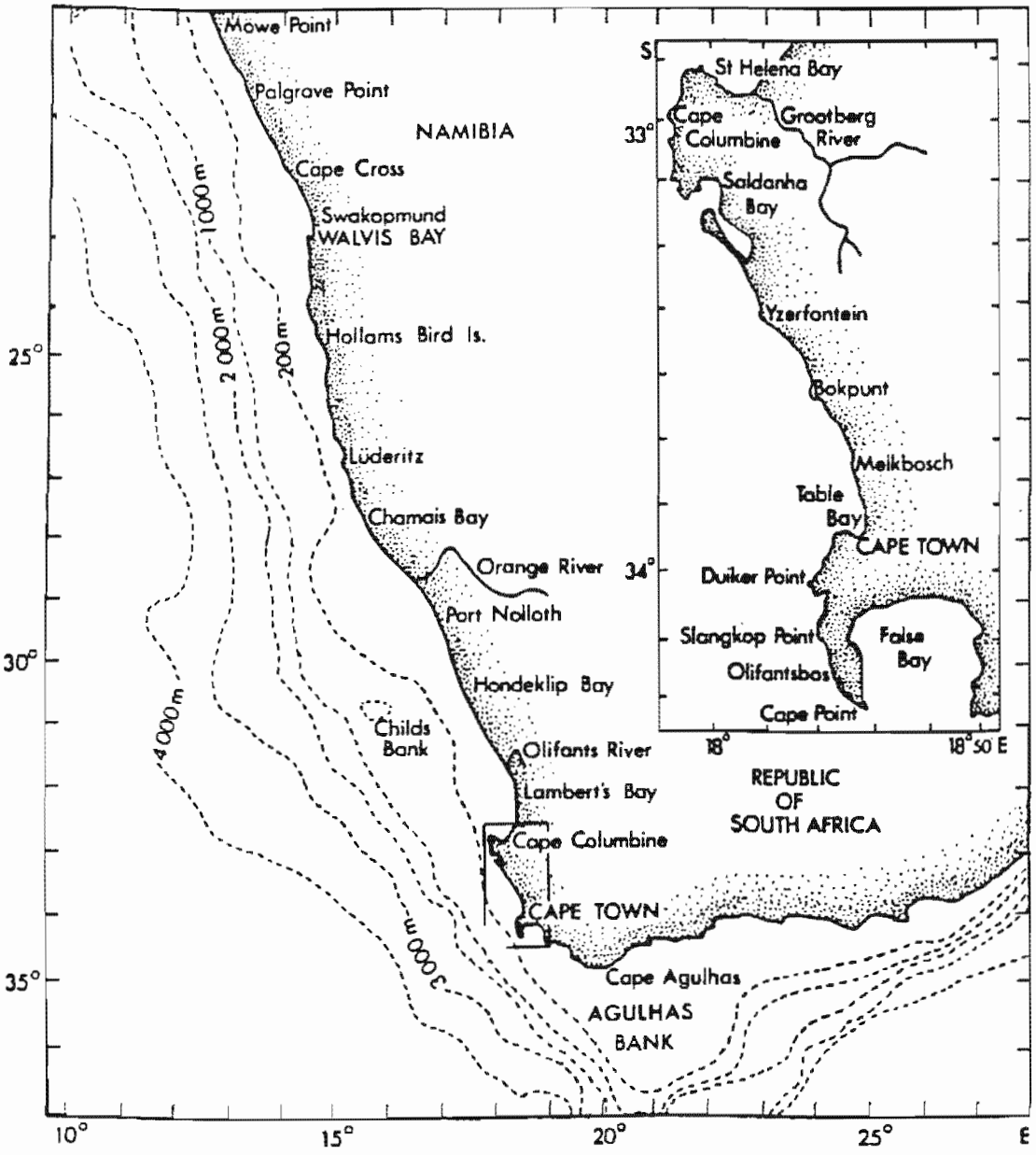

Fig 4.3 Map of the West and South Coast of southern Africa indicating the nature of the shelf topography and the location of place names used in the text. (adapted from Nelson, 1989).

4.3 The Generation and Dissipation of CTW's in Southern African Shelf Waters

A knowledge of the nature of the forcing, the CTW response and the manner in which CTW's decay is important in understanding the subinertial dynamics of the continental shelf of southern Africa. In this section, the longshore winds are shown to be the dominant forcing mechanism for subinertial CTW motions along the West and South Coasts of southern Africa. Consequently, the marine wind fields along the southern African coastline are described in some detail. Finally, published observations of CTW's in southern African shelf waters are briefly reviewed to provide the necessary framework for the discussion contained in Chapter 8.

4.3.1 The Dominant Forcing Mechanisms for CTW's

Atmospheric pressure variations, alongshore and cross-shore wind stresses, wind stress curl, tides and deep ocean forcing all have the potential to generate CTW motions over the continental shelf. Scale analyses however suggest that alongshore wind stress is generally the dominant forcing mechanism for "long wave" CTW motions over the continental shelf. Below, all possible mechanisms for the forcing CTW's along the southern African coastline are considered and the alongshore wind stress is found to be the dominant forcing mechanism for CTW's on the west and south coasts of southern Africa.

Tidal forcing of subinertial CTW's is only possible at higher latitudes (polewards of 30°) where the local inertial frequency exceeds the frequency of the diurnal tide. Cartwright (1969) reported unusually strong diurnal currents over the shelf in the Hebrides which he considered to be due to shelf wave motions. More recently, the application of CTW theory in several higher latitude locations has indicated that the diurnal tide includes a barotropic Kelvin wave (which dominates the sea level variability but has weak associated currents) and a lowest mode subinertial CTW (associated with strong current fluctuations). It has been suggested that the subinertial CTW is excited by irregularities in the bottom topography (Crawford and Thomson, 1984; Daifuku and Beardsley, 1983), however Flather (1988) has observed the direct forcing of CTW by tidal currents through a channel (Juan de Fuca Strait). Although most of the shelf waters of southern Africa lie south of 30°S, semi-diurnal tides predominate and tidal forcing of CTW motions is only really a possibility in the south where the Agulhas Bank is at its widest and the maximum possible

frequency of free barotropic CTW motions (period ≈ 25.9 hours as shown in the dispersion curves) is both less than the local inertial frequency (period ≈ 20 hrs) and approaches diurnal frequencies (periods ≈ 24 hrs). If the effects of stratification are included the maximum frequencies in the free CTW dispersion curves increase and tidal forcing of CTW motions could be more widespread (for example, the dispersion properties of free CTW's characteristic of the bottom profiles 6 and 7 off Cape Town).

Deep ocean forcing of CTW motions is a distinct possibility in a region like southern Africa where the deep-ocean circulation is characterised by extreme variability. There is evidence of an open ocean influence on shelf circulation in current meter data from the West Coast (Nelson, 1989) and Duncombe Rae *et al.* (1992) have described the interaction of Agulhas eddies with the shelf waters off the West Coast. Similarly, the Natal Pulse of the Agulhas Current has been observed to dominate the inshore circulation along the narrow shelf of the East Coast (Lutjeharms and Roberts, 1988; Lutjeharms and Connell, 1989). In the time series analyses in Chapter 5, the effect of the Natal Pulse is clearly reflected in sea level observations along the East coast. Theoretical studies (Chapman and Brink, 1987; Kelly and Chapman, 1988), however indicate that for open ocean forcing (western boundary currents and eddies), the shelf response is nearly always barotropic and occurs at frequencies and wavenumbers near free CTW resonances. The shelf response decreases rapidly with decreasing frequency of the open ocean forcing (as friction dominates over the entire shelf at these low frequencies) with significant response only occurring for higher frequency open-ocean forcing. Louis (1989) observed short wavelength trapped oscillations off the New South Wales coast of Australia at these higher frequencies (periods of 3 to 5 days). Further, the penetration of forcing onto the shelf is more effective for steep rather than gently-sloping continental shelf slopes and for surface intensified forcing (Wright, 1986; Kelly and Chapman, 1988). Thus steeply-sloping, narrow shelf regions are seemingly more strongly affected by open ocean forcing due to the closer proximity of the coast rather than the nature of the bottom topography. Since open ocean forcing generally has a low frequency nature which leads to a weak shelf response, it is not considered to be a significant forcing mechanisms for low frequency CTW motions over the continental shelf off the west coast of southern Africa. The East Coast region, where the narrow shelf and higher frequency open-ocean forcing is

conducive to the forcing of CTW motions over the shelf and shelf slope, is specifically excluded from the investigations using the numerical model (see Chapter 7).

Inverse estuary forcing or CTW generation by a coastal flux, as reported by Weaver (1987) and Middleton (1988), is not a possibility along the southern African coastline, however *remotely forced oscillations* entering the region of interest from the north on the West Coast may be important (Nelson, 1992a) and are discussed later in the dissertation.

Barometric pressure can be a significant source of sea level variability, particularly in mid- and high latitude locations (Gill and Niiler, 1973, Ponte, 1993). The atmospheric pressure response of the ocean is generally considered to be isostatic and atmospheric pressure fluctuations are not considered to be an effective forcing mechanism for CTW motions. In analyses of CTW-induced sea level variability, the atmospheric pressure-driven signals in sea level are usually removed from the raw sea level data using the inverse barometer (IB) approximation (e.g. Pugh, 1987; Ponte *et al.*, 1991)

$$\eta_{IB} = \frac{1}{\rho_s g}\left(p_{mean} - p_o\right) \qquad (4.1)$$

where ρ_s is the surface density, g the acceleration due to gravity, p_{mean} is a representative atmospheric pressure mean for the sea level records being analysed, p_o is the atmospheric pressure at the site where the sea level are recorded and η_{IB} is the isostatic sea level response to the atmospheric pressure at sea level. This approximation translates into an approximate -1 cm change of sea level height for every 1 hPa increase in atmospheric pressure. The IB approximation implies that the η_{IB} signal acts to balance the applied barometric pressure gradients and thus is considered to have no dynamical significance. The IB approximation holds for most temporal and spatial scales in both a homogenous and stratified ocean (Wunsch, 1972; Ponte *et al.* 1991; Ponte, 1992), however there are important dynamical responses on small spatial and short time scales (Philander, 1978) resulting in, for example, edge wave motions (Shillington, 1985; Shillington and van Foreest, 1986).

The scaling arguments in appendix A suggest that for the scales of motion considered in CTW studies, atmospheric pressure forcing is negligible in comparison to wind-forcing of CTW motions. This is confirmed by analyses by Gill (1982) and Schumann (1973). The

inviscid shallow water equations may be written in such a manner that all the forcing terms in the momentum equations are transferred to the continuity equation (p 339-340, Gill, 1982). Here the forcing terms normally present in the momentum equations appear in the continuity equation as a time-dependent constraint on the flow in the inviscid interior. Written in this manner, the equations governing the motion in an inviscid interior are

$$\frac{\partial u_p}{\partial t} - f v_p = -g\frac{\partial \eta'}{\partial x}$$

$$\frac{\partial v_p}{\partial t} + f u_p = -g\frac{\partial \eta'}{\partial y}$$

$$\frac{\partial \eta'}{\partial t} + \left(\frac{\partial (h u_p)}{\partial x} + \frac{\partial (h v_p)}{\partial y}\right) = \frac{\partial \eta^F}{\partial t}$$

where η' is the pressure-adjusted sea level, u_p and v_p are the velocity components due to pressure components within the fluid and $\eta^F = \eta^E + \eta^a$ where η^E and η^a are the "equivalent" sea level contributions due to wind stress and atmospheric forcing, respectively. The ratio η^E / η^a determines the relative importance of local atmospheric pressure and wind-forcing and for scales typical of subinertial CTW motions, $\eta^E / \eta^a \sim 10^2$. Similarly, Schumann (1973) defined a ratio that compares the wind-forced response with the pressure-forced response.

$$\text{wind forced response : pressure forced response} = \frac{\tau_w}{\rho h}\frac{\partial h}{\partial x} \Big/ f\frac{\partial \eta^a}{\partial t}$$

which also assumes a value of approximately 10^2. The analysis of Schumann (1973) is superior in that it emphasises the fact that CTW's depend on the generation of vorticity by the movement of water over the sloping shelf topography for their existence and he also stresses the necessity of the coastal boundary condition for the forcing to be effective. Atmospheric pressure forcing is therefore clearly secondary to wind-forcing in the generation of subinertial CTW motions. Note however, that wide, gently-sloping shelf regions (such as the Orange River cone and the Agulhas Bank) are more susceptible to the forcing of higher frequency and wavenumber motions by atmospheric pressure fluctuations.

Scaling arguments in Appendix A also show that *cross-shore wind stresses* are generally not efficient in generating subinertial CTW's. Cross-shore wind stresses only are

important where the response develops cross-shore and longshore spatial scales of similar magnitude which typically develop in the presence of strong alongshore variations in the bottom topography and for higher frequency motions. Similarly, forcing due to *the wind stress curl* is negligible (Adams and Buchwald, 1969; Schumann, 1973), provided that the offshore scale of variations in the longshore wind and the alongshore scale of variations in the cross-shore wind greatly exceed the spatial scales of the CTW response (typically given by the shelf width). Near headlands, where this is rarely true, wind stress curl forcing becomes important and Ekman dynamics predominate resulting in significant upwelling. Similarly, Ekman dynamics may become important over very wide shelf regions such as the Agulhas Bank and the Orange River cone.

Cross-shore wind stresses and wind stress curl are expected not to be important for the generation of large -scale CTW motions over the West Coast shelf regions. For the purposes of this investigation, only *longshore wind stresses* are used as forcing terms in the numerical studies, however the spatial and temporal scales associated with the marine winds around southern Africa are taken into account in the interpretation of these modelling results and the results from the data analyses in Chapter 5. A brief overview of the winds field over the continental shelf regions of southern Africa follows.

4.3.2 The synoptic scale atmospheric systems of southern Africa and their associated marine wind fields

West Coast of Southern Africa

The winds along the West Coast are predominantly south or south-easterly with strong cyclonic wind stress curl over the shelf region except in mid-winter when the wind stress curl is anticyclonic in the southern regions (Bakun and Nelson, 1991). It is the perturbations to these mean winds which are important in the generation of CTW's. The large-scale atmospheric controls on these perturbations are discussed by Jury et al. (1990a) and Nelson (1992b). The prevailing winds on the West Coast are determined by three macroscale atmospheric features;

i) the South Atlantic high pressure system,

ii) the pressure field over the adjacent subcontinent and

iii) the mid-latitude cyclones traversing the southern regions,

as well as a less extensive, but more important atmospheric circulation, the coastal low which is observed to move anti-clockwise around the coastline of southern Africa (Nelson and Hutchings, 1983; Hunter, 1987, Reason and Jury, 1990). The wind fields, associated with the above large and smaller scale synoptic systems, are implicated in the generation of CTW motions along the West Coast. In particular, perturbations (sudden strengthening, relaxation or reversals) of the predominant south or south-easterly alongshore winds associated with the South Atlantic High, are efficacious in generating CTW motions along the West Coast and similar rapid changes or reversals in wind direction drive CTW motions along the South and East Coast.

The surface winds associated with the South Atlantic High are guided by the coastline of the adjacent subcontinent. Although the coastline of the West Coast north of Cape Columbine consists of mostly sand-dunes and a weakly sloping topography landwards, the desert-like nature of this region causes it to act as a thermal barrier to cross-shore winds near the surface, leading to the winds along this coast being predominantly south to south-easterly. Further, minor modification of the nearshore winds occurs due to the land-sea breezes which are common over the whole coast north of Cape Columbine (Jackson, 1947). As noted above, these cross-shore winds are not important to the forcing of subinertial CTW motions in the absence of substantial longshore variations in the shelf topography. However, the substantial coastal topography in the southern regions can lead to rapid variation and acceleration of the local winds and forcing by wind stress curl is significant, leading to the formation of local upwelling cells (Nelson, 1981, 1985, 1992b).

A comprehensive description of the temporal and spatial scales characteristic of the wind field over the continental shelf requires a knowledge of how the easterly-moving mid-latitude cyclones and the southerly-moving coastal lows interact with the larger scale South Atlantic High. The south to south-easterly surface winds associated with the South Atlantic High are modulated by both easterly-moving cyclones and southerly-moving coastal lows. The synoptic sequence which leads to this modulation of the winds on the West Coast has been described by Nelson and Hutchings (1983) with Reason and Jury (1990) providing a more comprehensive description of the forcing and propagation of coastal lows around southern Africa.

The development of the coastal low on the West Coast begins with the ridging of the South Atlantic High to the south of the continent or over the continent. As this anti-cyclone ridges eastwards, offshore flow at the plateau level (easterlies) extends down the West Coast resulting in the generation of the coastal low (generally just to the north or in the vicinity of Lüderitz). On occasion, the anticyclonic ridge strengthens or remains stationary south of the continent (Jury *et al.*, 1990a). The coastal low which develops to the north then remains stationary or even moves northwards. In general, however, the coastal low moves southwards down the West Coast reaching Cape Town in about two to three days. Towards the southern regions, the coastal low acts as a "leader front" to mid-latitude cyclones approaching from the west. After the passing of the coastal low and the first cold front, either the South Atlantic High again ridges to the south of the continent or a succession of mid-latitude cyclones follow the initial cold front and its associated coastal low. If the South Atlantic High immediately ridges in behind the coastal low and cold front, the slackening off or reversal of the S/SE winds is of shorter duration. If, however, a succession of cyclones follow the initial cold front and coastal low, extended periods of NW to SW winds may occur in the southern regions.

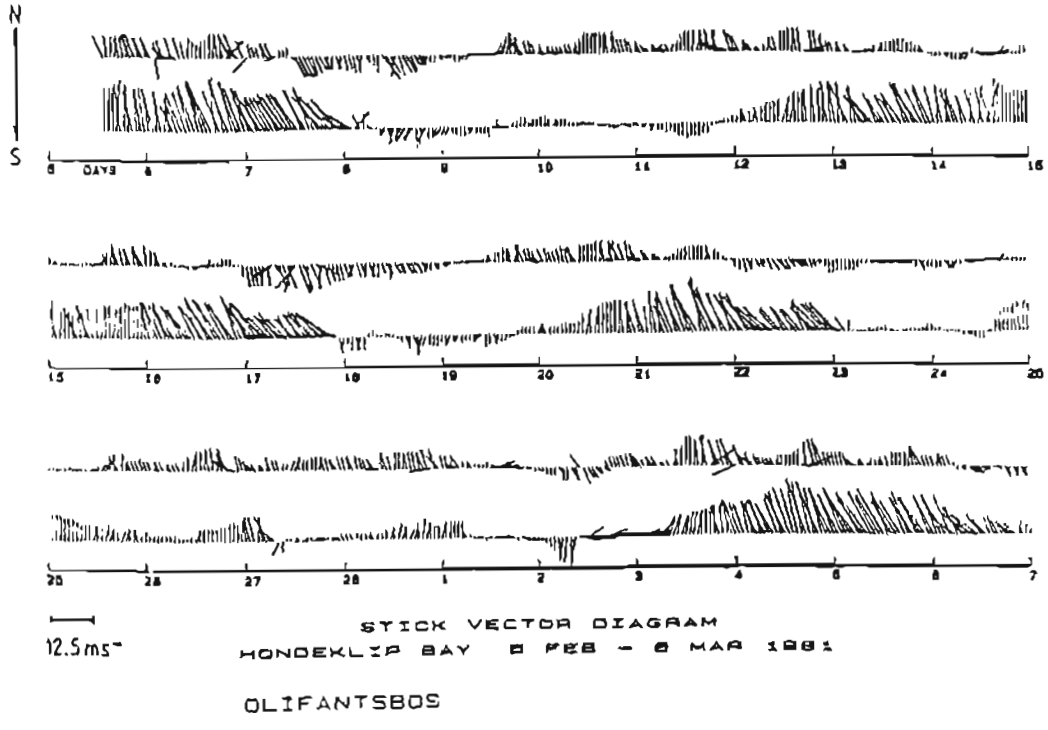

Fig 4.4 Wind vectors at Hondeklip Bay (30°19'S; 17°16,5'E) and Olifantsbos (34°16,5'S; 18°23'E) showing how the S/SE winds reverse or slacken due to the propagation of frontal systems past these sites (after Walker, 1984)

The above sequence of events, associated with the ridging of the South Atlantic High, results in a modulation of the winds on the West Coast with a period of roughly 4,5 to 12 days. Estimates of the cyclicity of the coastal low as indicated by spectral analysis of pressure records are typically 6 days (Preston-Whyte and Tyson, 1973; Kamstra, 1987, Coastal Low Workshop, 1984). Walker (1984) has provided tentative evidence of a seasonal variability in the periodicity of this cycle of events, her data suggesting a mean periodicity of 6 days in spring and summer which lengthens to approximately 10 days in winter and autumn. An example of the winds observed at two coastal sites on the West Coast (Walker, 1984) is given in Figure 4.4 which emphasises the cyclical nature of the wind events at West Coast sites.

In the northern regions of the West Coast, it is easier to see the effect that the coastal low has on the predominant S/SE winds. As the coastal low approaches a site along the coast, the S/SE winds intensify (Jury *et al*, 1990b). On passing, the coastal low causes a sudden abatement or reversal of the wind. These changes or reversals in the S/SE winds due to the passing coastal low are generally of shorter duration in these northern regions than are the changes or reversals in the S/SE winds in the more southerly regions which are also strongly affected by the trailing mid-latitude cyclones. Consequently, the effect of these coastal lows on the surface wind field is best seen to the north or in the south during summer when the modulation of the S/SE winds by the easterly-moving mid-latitude cyclones is usually weakest.

The mid-latitude cyclone frontal systems are observed to modify the winds as far north as the Orange River, with an intensity increasing southwards towards Cape Point. In summer the effect of these frontal systems on the West Coast is usually but not necessarily weak, resulting in a periodic slackening or abatement of the S/SE winds to the south. In winter the effects are generally more pronounced, in extreme cases resulting in NW to SW gales in the southern regions. Thus it is difficult (especially in winter) to distinguish between the effect of the coastal low and the cyclones that follow in the southern regions. In general, the coastal low is responsible for the sharp changes or reversals in the wind field, while the one or more cyclones which may follow, determine the duration of this change in the wind field in the southerly regions.

Estimates of the phase speed with which the coastal lows propagate southwards along the West Coast, are typically 6.0 to 7.0 $m.s^{-1}$ (Reason and Jury, 1990). However, these phase speeds are considered to be highly variable, ranging from 4 to 10 $m.s^{-1}$ (Walker, 1984) with observations suggesting a possibly even greater range in phase speeds (De Cuevas, 1985, Schumann, 1989). Wind data from an offshore site suggest that the offshore scale of coastal lows are much smaller (Hunter, pers. comm.) than the typical offshore scales (internal Rossby radius) of 200 to 300 km suggested by the theoretical models of Gill (1977) and Ahn and Gill (1981). In their model, Reason and Jury (1990) use 137 km as a typical offshore scale for the coastal low which compares well with the approximately 100 km suggested in the West Coast oil rig data reported by Hunter (1987). Using the wind data of Walker (1984), the longshore extent of these changes or reversals in the wind is very roughly estimated to be 600 km or more. Unlike other regions where coastally trapped atmospheric circulations occur, the appearance of the coastal low is not seasonal off southern African coasts. These coastal lows, forced by upper level offshore flow, occur at all times of the year and can be considered to be a climatological phenomenon of the region (Reason and Jury, 1990).

South Coast of Southern Africa

Both the easterly-moving cyclones and coastal lows strongly affect the ocean circulation over the continental shelf (Agulhas Bank) to the south of Africa. Reason and Jury (1990) show that the coastal lows formed on the West Coast, propagate past Cape Town, rapidly traverse the Agulhas Bank and dissipate in the region of Durban. The higher periodicity (4.4 days) of these events on the South Coast (Hunter, 1987), suggest that some of the coastal low events observed in this region are specific to the South Coast. This distinction has been noted by Schumann (1989) and Estie (1984) who states that "the West Coast low and the South Coast and Southeast Coast low are generally separate systems". The continuity in the propagation of the coastal low from the West Coast, is most obvious in summer when the effects of the mid-latitude cyclones are further offshore. Particularly rapid switches in wind direction and very strong wind conditions ("southwest buster") are associated with the passing of coastal lows along the South Coast (Hunter, 1987, Jury *et al*, 1990b) with the strongest southwest buster conditions occurring near Port Elizabeth.

On the South Coast as well as the East Coast, the propagation of the coastal low and its lifespan are strongly influenced by the intensity and proximity of the trailing mid-latitude cyclone. At times the trailing mid-latitude cyclone may overtake the coastal low as it propagates along the South Coast and the coastal low is dissipated within the front of the trailing cyclone. At other times the coastal low and the front of the trailing cyclone remain distinct as they propagate along the South and East Coasts. When the mid-latitude cyclone is relatively weak or lies far to the south of the landmass (summer mode), the low is able to propagate more rapidly along the South Coast (Reason and Jury, 1990). Schumann (1989) and Jury *et al.* (1990b) find that the propagation of atmospheric systems seems to be slower on the South Coast than on either the West Coast or Southeast Coast. Schumann (1989) also finds the wind associated with the propagating winds systems to be the weakest along the South Coast, strengthening towards Port Elizabeth and then decreasing as the coastal low moves northwards up the East Coast.

In looking at three specific case studies Jury *et al.* (1990b) find that the trapped waves in the atmosphere start to move slowly southwards down the West Coast, accelerating to reach speeds of 6 to 10 $m.s^{-1}$ near Alexander Bay. The coastal lows then seem to slow between Cape Town and George and then accelerate rapidly in the vicinity of Cape St Francis (just west of Port Elizabeth) to speeds of over 20 $m.s^{-1}$. In the vicinity of Durban the coastal low propagation is observed to slow to 4 to 10 $m.s^{-1}$ and either disperse or move out to sea. Jury *et al* (1990b) attribute the slowing of the coastal low propagation near Cape Town to the sharp change in coastal topography and the rapid acceleration of the coastal low off the Southeast Coast to the influence of the Agulhas Current. Schumann (1989) and Schumann and Brink (1990) have used statistically more robust techniques on pressure and wind time series. Using autocorrelation techniques they find the wind systems to propagate along the South Coast at approximately 7.4 $m.s^{-1}$ while the atmospheric pressure systems propagate at approximately 19 $m.s^{-1}$. Hunter (1987) estimates the phase speed of propagation of the coastal lows along the South Coast to be a highly variable 7 to 25 $m.s^{-1}$, while Preston-Whyte and Tyson (1973) estimated a 6,5 $m.s^{-1}$ propagation speed of coastal lows from atmospheric pressure data. Using phase and coherency estimates Schumann and Brink (1990) tabulated the propagation velocities of wind systems for the different period peaks in coherency between sites. Their phase speed

estimates for the South Coast reflect the high degree of variability observed by others but nevertheless seem to be lower than those on the East Coast.

The above highly idealised characterisation of the wind fields enables one to develop some idea of the nature of the wind-forcing responsible for subinertial CTW motions on the West and South Coast shelf. A more comprehensive account of the large scale synoptic atmospheric pressure systems and their associated winds is available in publications by Hunter (1987), De Cuevas (1985), Jury and Brundrit (1992), Nelson (1992a) and Nelson and Hutchings (1983), while Reason and Jury (1990) and a report on the Coastal Low Workshop (1984) specifically deal with the coastal low phenomenon in more detail. It is, however, immediately apparent that the lack of knowledge of the synoptic-scale wind fields over the shelf (especially their spatial scales) is the weakest link in any study of subinertial CTW motions along the southern African coastline.

Nelson (1992a) shows that even if one has wind observations from coastal sites, they are generally not representative of the wind field over the shelf as the land-sea boundary introduces thermal and orographic noise into the coastal wind times series in a relatively narrow strip along the coastline. Schumann (1989) also cautions against the use of coastal winds in CTW studies. Nelson suggests that winds derived from offshore pressure gradients assuming geostrophy would be more representative of the marine wind field that forces CTW motions and further suggests that pressure spectra are better estimators of synoptic wind variations. However, without more detailed information of the offshore gradient of pressure the pressure spectrum is not an accurate estimator of wind speed and principally yields only frequency information. Further, the use of pressure time series to investigate to investigate the propagation of wind systems along the coast is not ideal as Schumann (1989) has shown that the phase speeds of propagation of air pressure systems and wind systems are remarkably different. The propagation of wind systems (7,4 $m.s^{-1}$) along the coastline is observed to be substantially slower that the air pressure systems (19 $m.s^{-1}$) which have a periodicity of 3 to 9 days. A certain ambiguity in phase speeds of propagation is expected on the South Coast where strong cyclones follow and sometimes overtake the coastal low.

The above uncertainties and the lack of knowledge of the wind field over the shelf is unfortunate as Thomson and Middleton (1985), Chapman (1987) and López-Mariscal and Clarke (1993) have all shown that the nature of the CTW response is particularly sensitive to the detail of the wind-forcing.

4.3.3 The Relationship Between Wind Stress Fields and CTW motions over the southern African continental shelf.

A number of researchers using observations of primarily pressure adjusted sea level data (with a more limited use of current meter data), have noted the presence of coastally trapped motions along the continental shelf regions of southern Africa and have attempted to characterise their behaviour (Brundrit et al., 1984; de Cuevas *et al.*, 1986; Holden, 1987). Only recently have studies dealt in any detail with CTW generation and propagation along the continental shelf (Jury *et al*, 1990a,b; Schumann, 1983, 1989; Schumann and Brink, 1990; Brink, 1990, Nelson, 1989; Nelson, 1992a,b). Schumann (1983, 1989) and Schumann and Brink (1990) investigate the generation of these CTW's in a holistic manner by looking at the temporal and spatial structures of the observed wind stress fields and relating them to the expected spatial and temporal structures of CTW motions over the continental shelf region. Jury *et al.* (1990a) and Nelson (1992a) use a broader brush approach by looking at the large scale atmospheric controls on CTW's, while Jury *et al.* (1990b) are quite specific in investigating primarily coastal lows as a forcing mechanism for CTW's by using composites of selected coastal low weather sequences.

Jury *et al.* (1990b), through analysis of composites of the hourly values of pressure adjusted sea level at a number of sites along the coast, have described certain characteristics of the sea level variation along the southern African continental shelf. The composite wave in the sea levels moved anti-clockwise around the coast with an mean speed of 430 km.day^{-1} or about 5 m.s^{-1}. The assumption of a weekly weather cycle results in the rather large estimate of 3000 km for the CTW wavelength. The phase speed of the CTW vary along the coast with speeds of 200 km.day^{-1} (2.3 m.s^{-1}) just south of Walvis Bay, over 1000 km.day^{-1} (11,6 m.s^{-1}) north of Cape Town, slowing to just over 700 km.day^{-1} (8,1m.s^{-1}) east of Cape Town and continuing to decelerate to 300 km.day^{-1}

(3,5m.s^{-1}) near Port Elizabeth and finally decreasing to less than 100 km.day^{-1} (1,2 m.s^{-1}) south of Durban. In the region from approximately Port Nolloth to Cape Town the simple wavelike propagation of CTW's seems to be interrupted, with a more complicated structure occurring in this region. A similar discontinuity between Port Nolloth and Cape Town is apparent in a limited period of space-time contours of pressure-adjusted sea level reported by Schumann and Brink (1990) who also noted that the propagation of CTW's is often not continuous between Port Nolloth and Cape Town. Jury *et al.* (1990b) tentatively suggest that this may be due to changes in the shelf width or possibly a consequence of a general reduction of southerly winds known to occur at approximately 33°S.

Further, the pressure-adjusted sea level composites show the shelf wave to progress as far as Durban, albeit with reduced amplitude and a much reduced phase speed. This is in direct contrast with the results of Schumann (1983) and Schumann and Brink (1990) who show the propagation of the shelf wave to be severely inhibited between East London and Durban. Their data show that in only one or possibly two cases could the shelf wave be considered to progress as far as Durban with any meaningful amplitude.

Jury *et al.* (1990b) demonstrate a strong relationship between the coastal low synoptic sequence and the shelf wave response over the shelf. Their overlays of selected composites of pressure adjusted sea level and alongshore winds show the trough of the shelf wave to precede the wind reversal associated with the coastal low synoptic sequence by approximately 36 hours while the crest of the shelf wave follows the wind reversal by about 12 hours. Towards Durban the coastal low is seen in the above composite to outrun the shelf wave and dissipate to the north of Durban where the synoptic forcing for the coastal low withdraws and the topographic constraint recedes. Interestingly, from Alexander Bay southwards towards Cape Town, the composites show the shelf waves to coincide or even precede the atmospheric forcing. A similar observation is made by De Cuevas (1985) who found the sea level response to lead the local wind forcing at Gansbaai.

In summary, the results of Jury *et al.* (1990) show that for their *subjectively selected* data set, shelf wave motions are predominantly locally forced by the synoptic winds

associated with the propagation of coastal lows. This does not preclude other synoptic weather sequences, not selected in their data set, from playing a role in the generation of CTW motions. Further, one should be cautious in unequivocally accepting the other more detailed relationships between the shelf wave motions and coastal lows from these limited analyses. The methods employed, while instructive and possibly more appropriate than other spectral analysis techniques in looking at the propagation of "events", is subjective (in the selection of events to provide the composites) and not statistically robust.

Schumann and Brink (1990), using a statistically more robust approach, have investigated the propagation of CTW's using pressure-adjusted sea levels as well as current meter records at East London. They calculated the phase speeds of propagation of pressure-adjusted sea levels, atmospheric pressures and winds using both cross-spectral and cross-correlation techniques. While their analysis concentrated on CTW propagation along the South and East Coasts of southern Africa, they did note more limited CTW activity along the West Coast and suggested that this may be due to the nature of the forcing and the underlying shelf topography along the West Coast. Their estimates of sea level propagation speeds along the South Coast (from coherence and phase spectra) display a good deal of scatter, varying from 4,4 to 5 $m.s^{-1}$ on the western Agulhas Bank, 5 to 9 $m.s^{-1}$ on the central Agulhas Bank and decreasing to 2.5 $m.s^{-1}$ on the eastern Agulhas Bank where the shelf narrows and the influence of the Agulhas Current becomes significant. These estimated phase speeds follow the general trend of their calculated theoretical free CTW phase speeds, however the estimated phase speeds (< 6.5 $m.s^{-1}$) are less than the theoretical free wave speeds (8 $m.s^{-1}$) of even barotropic CTW's. A possible explanation for this is the presence of higher mode (slower) CTW's which decrease the theoretical phase speeds expected. There is excellent agreement between the theoretical free CTW phase speeds (8 $m.s^{-1}$) and the phase speeds (7,5 $m.s^{-1}$) estimated from the maximum correlation between alongshore winds and pressure-adjusted sea levels in time lagged cross-correlation plots. This suggests that the response is predominantly a first mode CTW response. Schumann and Brink (1990) do however caution that analyses of only coastal sea levels could fail to detect higher mode CTW's which do not contribute greatly to coastal sea level fluctuations.

Although a number of current meter analyses have been undertaken where CTW motions have been investigated (for example Holden, 1987; Schumann and Brink, 1990; Nelson, 1989, 1992a,b), the lack of spatial and temporal coverage has resulted in CTW propagation analyses at present being limited to the use of pressure-adjusted sea level data.

4.3.4 Local and Remote Forcing of CTW motions

As noted previously (in Chapter 2), any observed CTW signal is generally a combination of a remotely-forced and locally wind-driven response. In the case of CTW motions along the southern African coastline it is difficult to discern between the two components as both locally and remotely forced CTW motions propagate around the coastline in the same direction. The importance of the interaction between remotely forced CTW's and local upwelling has been noted by both Nelson (1992a) and Jury and Brundrit (1992). CTW's can travel several hundreds or even thousands of kilometres (in the case of low frequency, low wavenumber CTW's) from remote sites to the area of interest and in doing so, influence the upwelling dynamics in a local upwelling cell by imposing time-dependant boundary conditions on arrival.

Jury *et al.*, (1990a) show that it is only the longer pulsing events which result in significant changes in environment variables such as temperature and nutrients, with the shorter (approximately 5 day or less) period events displaying a reduced sea level response, reduced current meter reversals and very little signal in other environmental variables. These observations are consistent with the results of a numerical study of stratified shelf currents (Johnson, 1982) which indicate that that significant changes in the temperature field require long periods of upwelling favourable winds, whereas the longshore currents react more quickly to changes in the wind stress.

The ultimate control of the CTW response on the West Coast by the modal patterns in the upper air (Rossby waves) of the southern hemisphere has been commented upon by Jury *et al.* (1990a), Nelson (1992a,b) and Jury and Brundrit (1992). Jury and Brundrit (1992) suggest that under a scenario of rapid pulsing consistent with the short wavelength or multi-mode Rossby waves, the South Atlantic High may not bud-off and

the interaction between the coastal low and the CTW's on the West Coast is disrupted which decreases the amplitude of the environmental changes in the Benguela ecosystem. Slower, near monthly, pulsing intervals dominated by single-mode Rossby wave patterns results in larger amplitude environmental changes. These slower events are clearly visible in the low pass atmospheric and pressure-adjusted sea level data of 1985, particularly at the southern sites (see Fig 5.6a,b and c in Chapter 5).

The situation is undoubtedly more complicated (Nelson, 1992a,b) and if the combined CTW/upwelling response is to be estimated at a site, sophisticated modelling methods requiring extensive wind data along the West Coast need to be applied. In Chapter 5 observations are made of low frequency forcing originating to the north of Walvis Bay as well as low frequency open-ocean forcing at other sites which also need to be considered in such a model. López and Clarke (1989) and Zamudio and López (1994) suggest the use of a "local plus remote" method in which the ocean response can be regarded as the sum of the response due to local wind forcing and the alongshore pressure gradient.

5. ANALYSIS OF CTW MOTIONS USING SEA LEVEL

In the absence of readily available and appropriate current meter data, pressure-adjusted sea levels are frequently used to investigate CTW motions (for example, Denbo and Allen, 1984 and de Cuevas *et al.*, 1986). Here an eleven year record of sea level and atmospheric pressure data (1980 to 1990) is used to investigate both the forcing and propagation of sea level anomalies associated with CTW motions along the southern African coastline.

5.1 Description and Pre-processing of Time Series Data

The raw sea level data, measured by tide gauges at a number of sites in Namibia and South Africa (see Fig. 5.1 and Table 3), are described by de Cuevas (1985) and Searson (1994). These sea level data (hourly values running from 00:00B to 23:00B) have been obtained from the South African Navy Hydrographic Office and have undergone preliminary processing by the Sea Level Research Group at the University of Cape Town. The raw sea level time series have a large number of small (generally < 6 hour) gaps in the data. Most of these data gaps have been removed using interactive interpolation software.

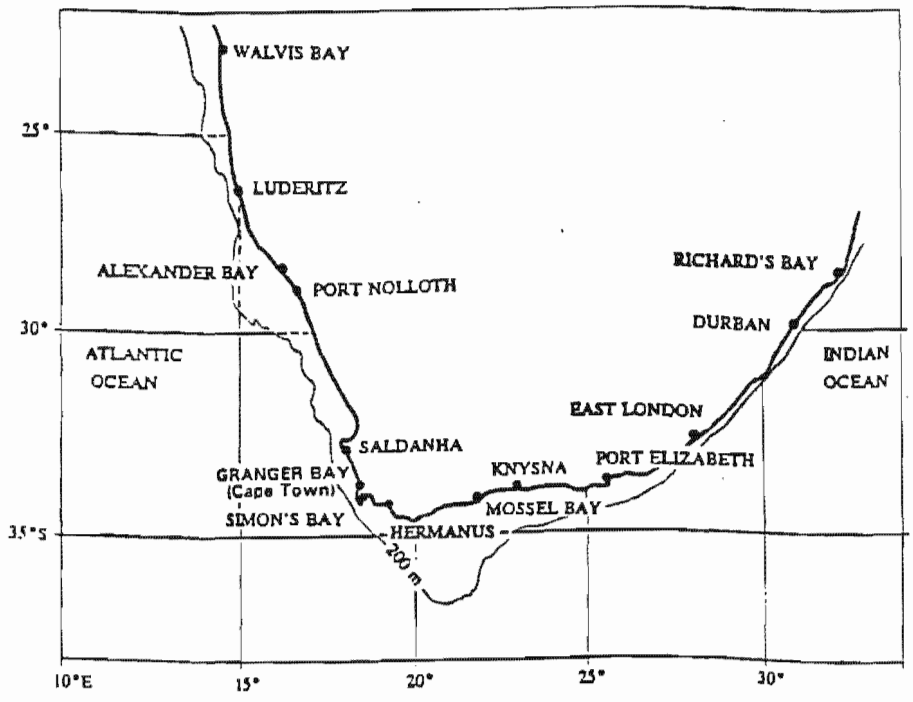

Fig. 5.1 Map of southern Africa showing the tide guage sites (after Searson, 1994)

To remove the assumed static (non-dynamic) effect of atmospheric pressure on the sea level, the raw sea level data are adjusted for atmospheric pressure effects (see Chapter 4 for the detail of the pressure adjustment). The raw atmospheric pressure data (obtained from the Maritime Weather Office of the South African Weather Bureau) have a nominal resolution of 6 to 12 hours (08:00B, 14:00B and 20:00B) and have been adjusted to obtain atmospheric pressures at sea level. Gaps in these pressure data are filled by linear interpolation only if the data gap is no greater than 12 hours. The hourly values, used in the pressure-adjustment of the hourly raw sea level data, are obtained by further interpolation of these atmospheric pressure data. The inverse barometer pressure adjustment of sea level is implemented as a pressure correction factor of approximately 0.994 cm for every 1 hPa increase of atmospheric pressure above the assumed mean atmospheric pressure of 1014 hPa.

Tide gauge site	Lat	Long	Longshore position (km)	Unadjusted sea level mean	Pres-adjusted sea level mean	Atmospheric Pressure Recording Site	Mean atmospheric pressure
Walvis Bay (WB)	22° 56' S	14° 30' E	0	92.84 cm	91.02 cm	Pelican Point (PP)	1014.15 hPa
Lüderitz (LB)	26° 39'S	15° 09'E	418	74.57 cm	75.67 cm	Diaz Point (DP)	1015.83 hPa
Port Nolloth (PN)	29° 15' S	16° 52'E	753	90.11 cm	90.89 cm	Port Nolloth (PN)	1014.77 hPa
Saldahna Bay (SA)	33° 05'S	18° 00'E	1193	106.46 cm	109.35 cm	Langebaan (LA)	1016.74 hPa
Granger Bay (GB)	33° 54'S	18° 25'E	1291	104.84 cm	107.97 cm	Cape Town (CT)	1017.01 hPa
Simon's Bay (SB)	34° 12'S	18° 25'E	1360	108.83 cm	110.58 cm	Cape Point (CP)	1015.96 hPa
Mossel Bay (MB)	34° 11'S	22° 09'E	1731	112.05 cm	115.35 cm	Cape St. Blaize (CB)	1017.05 hPa
Knysna (KN)	34° 05'S	23° 04'E	1817	118.37 cm	121.25 cm	Cape St Francis (CF)	1017.33 hPa
Port Elizabeth (PE)	33° 58'S	25° 38'E	2053	116.27 cm	118.75 cm	Port Elizabeth (PE)	1017.08 hPa
East London (EL)	33° 02'S	27° 57'E	2292	115.57 cm	118.90 cm	East London (EL)	1017.21 hPa
Durban (DU)	29° 53'S	31° 03'E	2750	110.09 cm	112.51 cm	Durban (DU)	1016.40 hPa
Richard's Bay (RB)	28° 48'S	32° 06'E	2907	107.60 cm	109.54 cm	Richard's Bay (RB)	1017.03 hPa

Table 3 Sites where sea levels are measured and the corresponding sites from which atmospheric pressure data are obtained for the inverse barometer pressure-adjustment of the sea level data

5.2 Filtering of Time Series Data

The temporal scales of interest in the pressure-adjusted sea level and atmospheric pressure at sea level data are those of the synoptic-scale events having periodicities of 2 to 20 days. The data are filtered to remove those components having frequencies greater than the inertial frequency (i.e. periods of approximately 1 day) which include the major semi-diurnal tides (periods of 11.8 hours to 13.2 hours), diurnal tides (periods from 21.6 hours to 26.9 hours) and inertial oscillations. The inertial period varies from approximately 30 hours at the northernmost site (Walvis Bay) to approximately 21 hours at the southernmost sites (Simon's Bay and Mossel Bay). Depending on the nature of the analysis, the low frequency signals excluded from the different data sets are a long-term mean or linear trend, interannual and/or seasonal sea level variations. (A potentially significant longer term signal not removed from the data is the lunar fortnightly tidal component which has a period of approximately 328 hours.)

Since there are many gaps in the pressure-adjusted sea level data, all filters utilised are constrained to have as narrow a bandwidth as possible to avoid excessive data loss. The filters also require a sharp amplitude cut-off near the half power point and, since the tidal signal is much larger than the sea level residuals of interest, it is important that the filters effectively remove all diurnal and semi-diurnal tidal components in the data. This is less important for the inertial period oscillations which are not as strongly reflected in sea levels as they are in horizontal currents.

Three filtered data sets have been obtained from each of the raw sea level, the pressure-adjusted sea level and the sea level atmospheric pressure time series. For each of these time series, the filtered data comprise a low pass time series (periods > 18,5 days), a subinertial time series (periods > 40 hours) and a synoptic-scale time series (band passed data containing signals with periods of approximately 2 to 18 days)

The **low pass** time series are obtained using a cosine-lanczos filter (241 unique weights) with an effective high frequency cut-off (quarter power point) of 18,5 days (see Fig. 5.2a). This filter is the best compromise between the requirement of a

minimum bandwidth and a sharp high frequency cut-off. The low pass data sets are labelled (and henceforth referred to) as LLP (low pass atmospheric pressure), LLC (low pass pressure-adjusted sea level) and LLR (low pass raw sea level).

The **subinertial** time series are obtained using a cosine-lanczos filter having 97 unique weights and a high frequency cut-off (quarter power point) of 40 hours (see Fig. 5-2b). The resulting subinertial time series are labelled (and henceforth referred to) as CLP (subinertial atmospheric pressure data), CLC (subinertial pressure-adjusted sea level) and CLR (subinertial raw sea levels). Two other filters often used are the Doodson "tide-killer" (as used on these data by de Cuevas, 1985 and Searson, 1994) and the PL64 filter as described in the CODE I (1983) and CODE II (1985) data reports. The Doodson "tide-killer", having only 19 unique weights, leads to minimal data loss when filtering data containing numerous data gaps, however this filter does not have a sharp high frequency cut-off (see Fig 5-2c). This results in strong damping of higher frequency signals (in particular, the signals having a 2,5 to 3 day periodicity which are known to exist in the sea level and atmospheric data). This and other undesirable high frequency properties (see Fig 5-2d) make the use of the Doodson "tide-killer" inappropriate for the present analysis. The PL64 filter, having a limited bandwidth (65 unique weights), also results in minimal data loss when processing time series containing numerous gaps. Despite the apparently suitable amplitude response properties of PL64 (Fig 5-2e), this filter does not effectively remove all tidal components. Spectral analysis of PL64-filtered sea level time series indicate the existence of significant energy at periods of approximately 26 hours in the sea level data. This reflects the inability of the PL64 filter to remove the O1 (25.82 hour) and Q1 (26.87 hour) tidal components from the raw sea level time series.

The **synoptic-scale** (approximately 2 to 20 day band-pass) time series are obtained by subtracting the low pass time series from the subinertial time series. The amplitude properties of such band-pass filtering process is given in Fig 5-2f. These band-pass data sets are labelled (and henceforth referred to) as BPP (band-pass atmospheric pressure), BPC (band-pass pressure-adjusted sea level) and BPR (band-pass raw sea level). Griffin and Middleton (1991) used a similar bandpass filter (20d to 40 hours) to exclude longer period signals which they attributed to open ocean forcing.

A long-term (eleven year) mean was removed from all of the above filtered data sets during the filtering process. This effectively removes any biases due differences in instrument calibration between atmospheric pressure sites and uncertainties in the sea level datum at the tide guage sites, but does not remove any changes in sea level datum that may have occurred at a particular site during the eleven years.

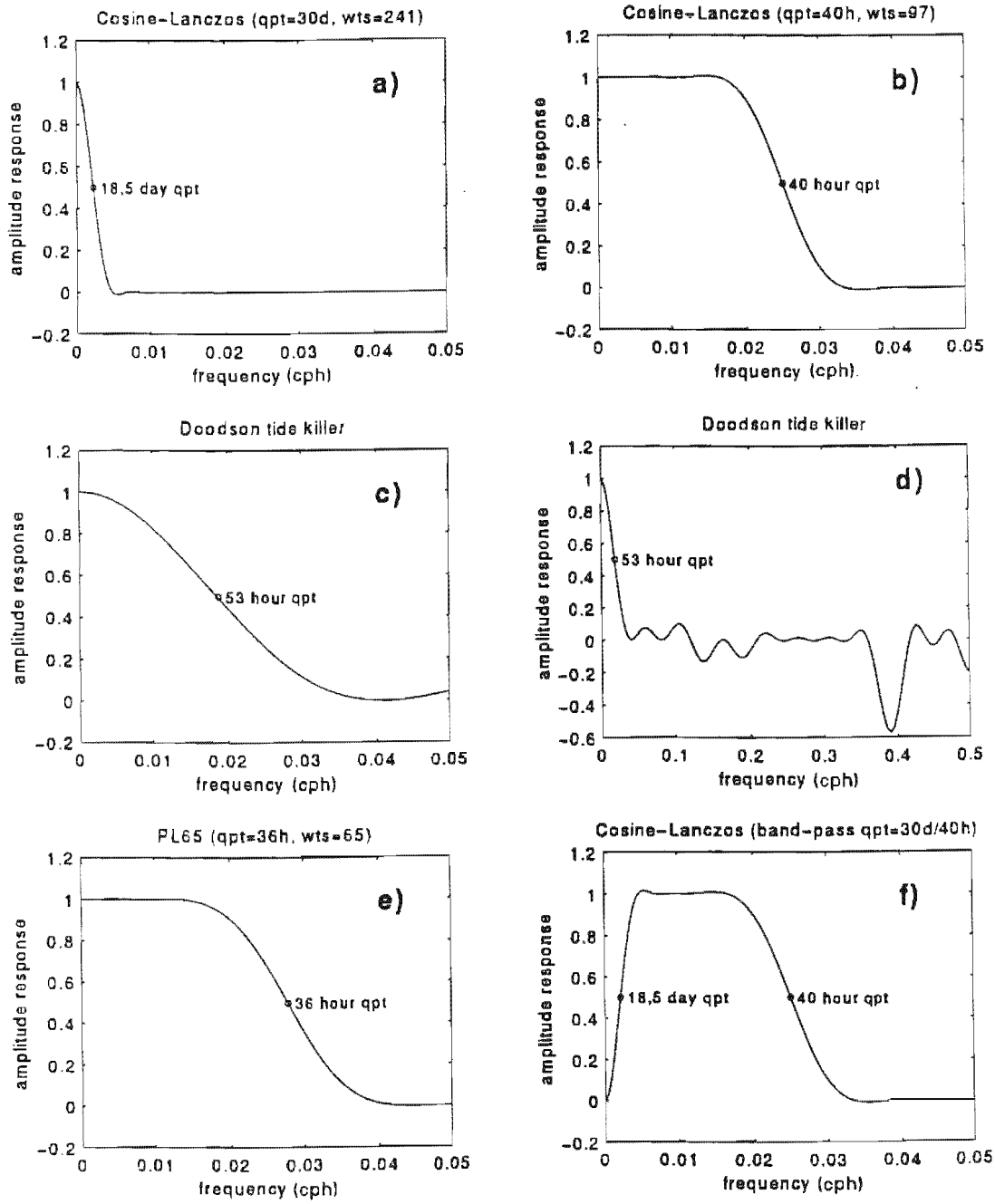

Fig. 5.2 Amplitude response versus frequency in cycles per hour (cph) for:
a) low low pass cosine-lanczos filter (18,5 day quarter power point, 241 weights),
b) low pass cosine-lanczos filter (40 hours quarter power point, 97 weights),
c) Doodson tide-killer,
d) Doodson tide killer (extended frequency scale)
e) PL64 filter (36 hour quarter power point, 67 weights), and
f) band pass filter (18,5 day and 40 hours quarter power points).

5.3 Preliminary Analysis of Atmospheric Pressure and Sea Level Time Series

Each time series is split into annual subsets. To facilitate seasonal analyses, the annual data sets comprise of data extending from 1 December to 30 November the following year. For example the 1985 time series consists of data from 1 December 1984 to 30 November 1985 which encompasses all four seasons, namely summer (1 December 1984 to 28/29 February 1985), autumn (1 March 1985 to 31 May 1985), winter (1 June 1985 to 31 August 1985) and spring (1 September to 30 November 1985). Note that for these time series the sixth month now refers to May rather than June as would normally be expected. Due to the many gaps in the time series and the consequent limited spatial data coverage (Figs 5.3 to 5.5), the analyses that follow are limited to the 1982, 1984, 1985 and 1986 time series. Emphasis is placed on the 1985 times series which is the most complete.

5.3.1 Atmospheric Pressure at Sea Level

The low frequency atmospheric pressure data (LLP in Fig 5-6a) contains a strong seasonal as well as an approximate 22 to 25 day signal at all sites. The lowest atmospheric pressures at sea level are recorded in summer and the highest in winter.

The magnitude of the seasonal signal in atmospheric pressures is approximately 10 hPa at all sites along the southern African coastline, while the amplitude of the synoptic-scale or "weather band" pressure fluctuations (CBP) increases southwards from less than 10 hPa at Walvis Bay to approximately 15 hPa to 20 hPa at the South and East Coast sites. The seasonal atmospheric pressure signal is greater than the synoptic-scale variability in atmospheric pressures at the northern sites along the West Coast, however from Port Nolloth southwards as well as along the South and East coasts, the magnitude as the synoptic-scale atmospheric pressure variations generally exceeds that of the seasonal pressure signal. At the northern East Coast sites the magnitudes of the synoptic and seasonal pressure fluctuations are approximately equal. A knowledge of the relative magnitude of these signals in the pressure data is important as they give an idea of the magnitude of the "inverse barometer" adjustments to the raw sea level data and the size of the potential errors should the raw rather than the pressure-adjusted sea level data be used in CTW analyses that follow.

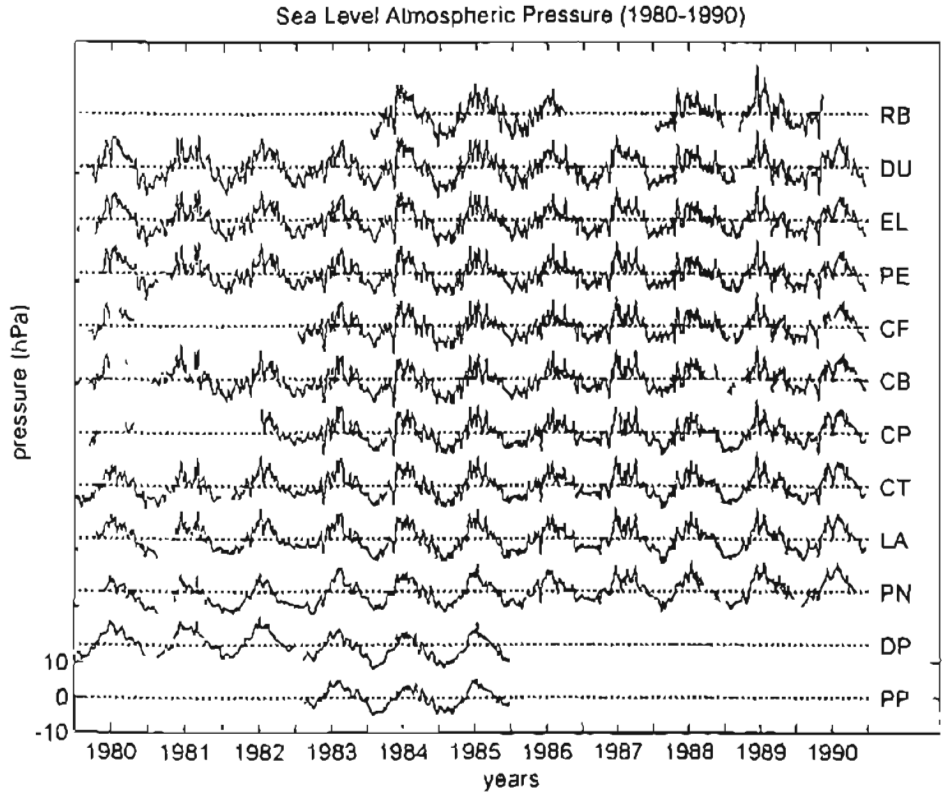

Fig. 5.3a Low pass (periods greater than 18,5 day) atmospheric pressure data at sea level for 12 selected sites along the southern African coastline.

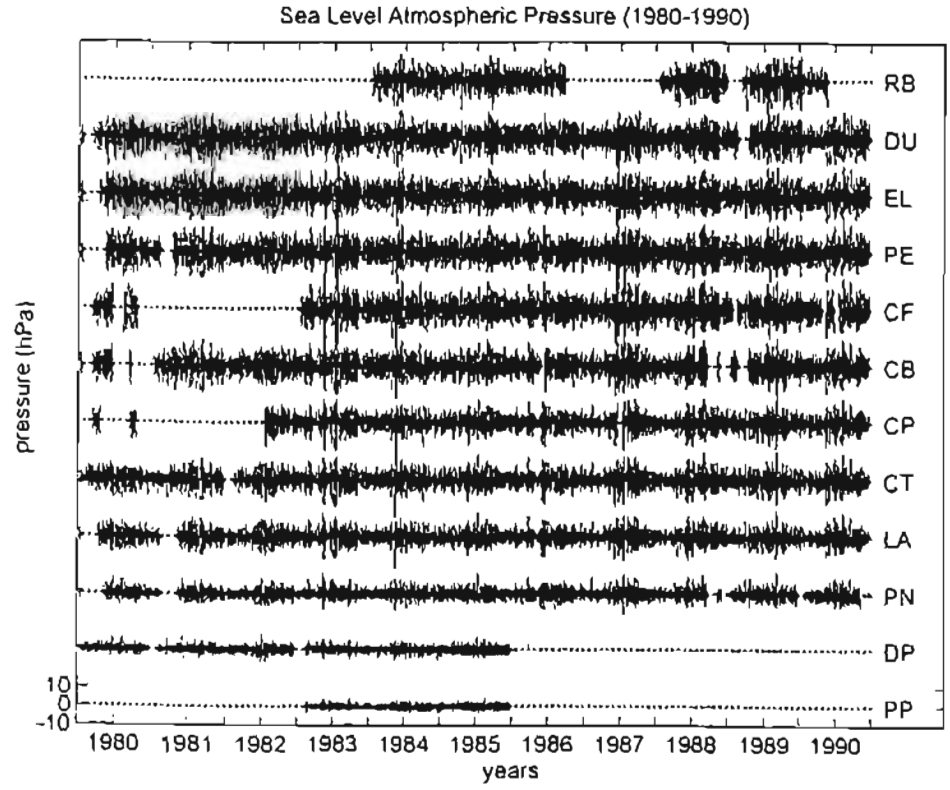

Fig. 5.3b Band pass (2 to 18,5 day) atmospheric pressure data at sea level for 12 selected sites along the southern African coastline.

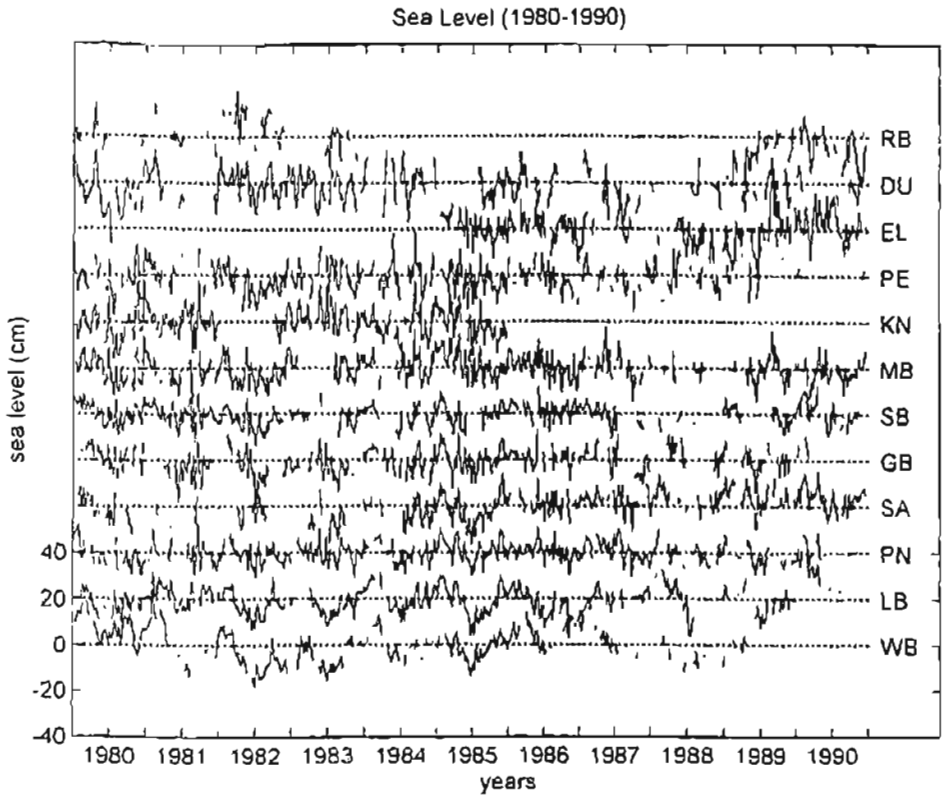

Fig. 5.4a Low pass (periods greater than 18,5 days) raw sea level data for 12 selected sites along the southern African coastline.

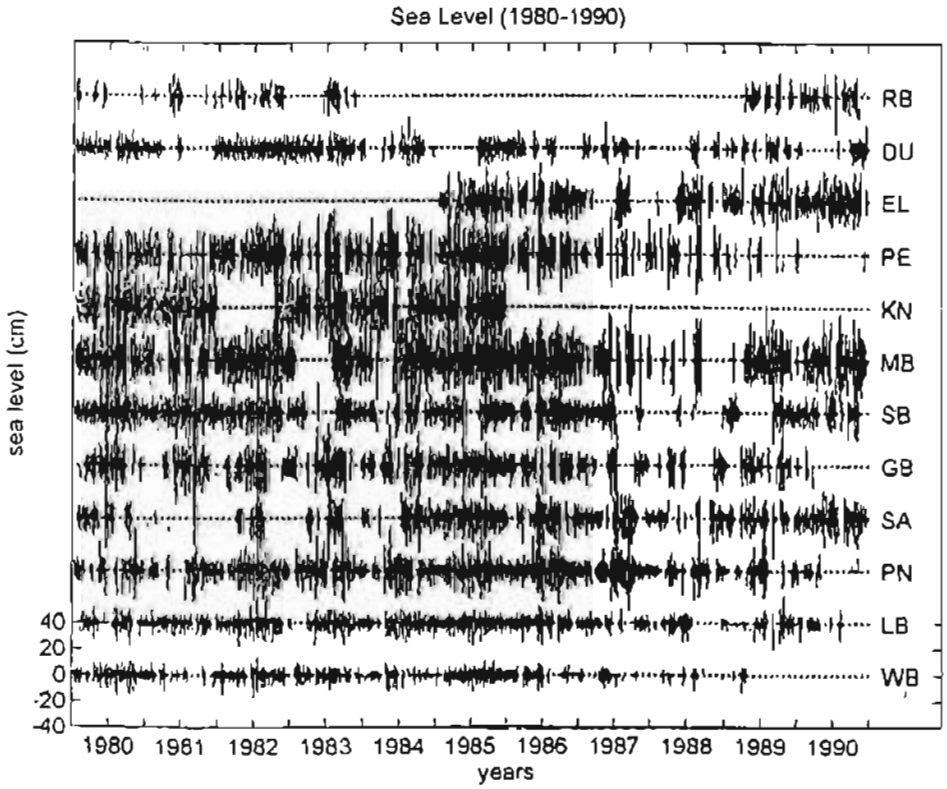

Fig. 5.4b Band pass (2 to 18,5 day) raw sea level data at sea level for 12 selected sites along the southern African coastline.

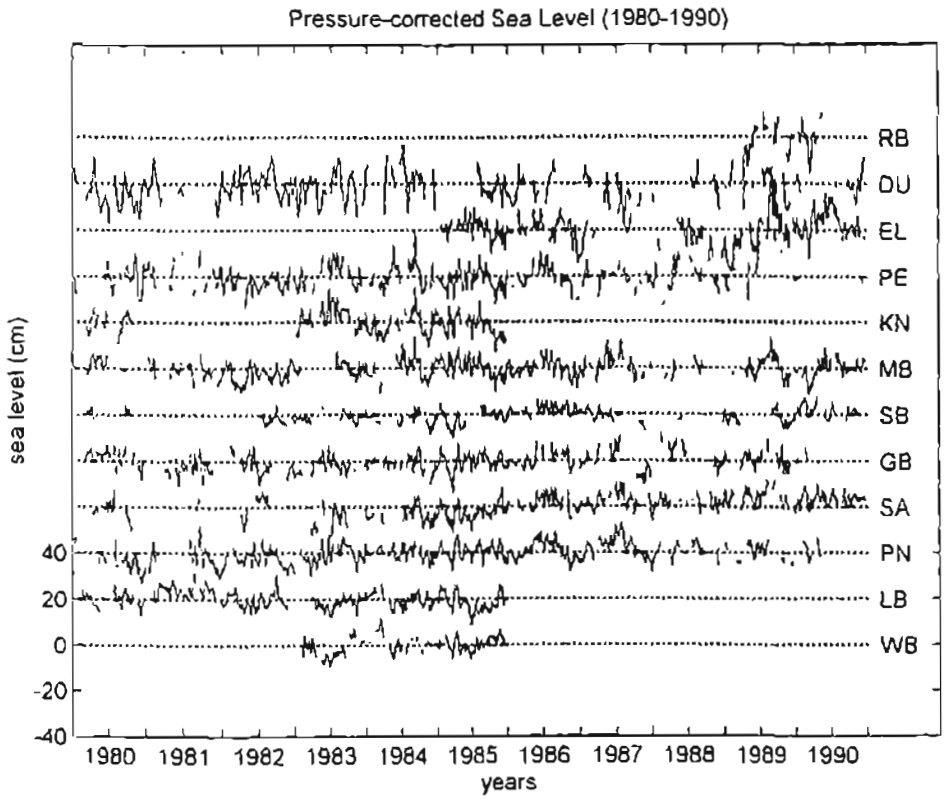

Fig. 5.5a Low pass (periods greater than 18,5 days) pressure-adjusted sea level data for 12 selected sites along the southern African coastline.

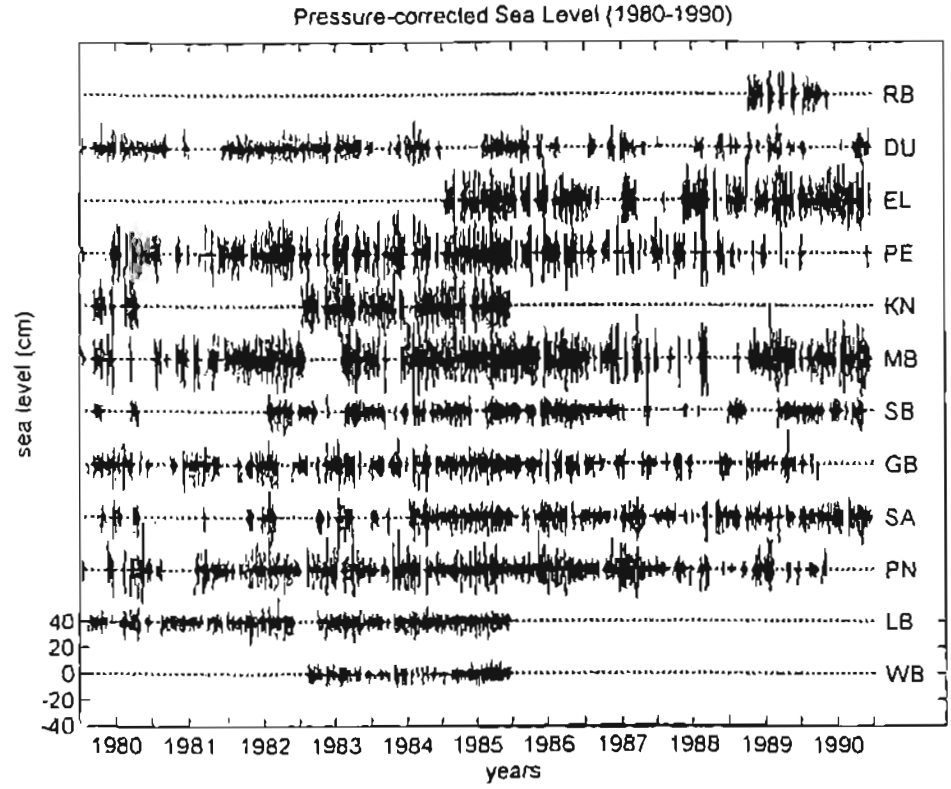

Fig. 5.5b Band pass (2 to 18,5 day) pressure-adjusted sea level data for 12 selected sites along the southern African coastline.

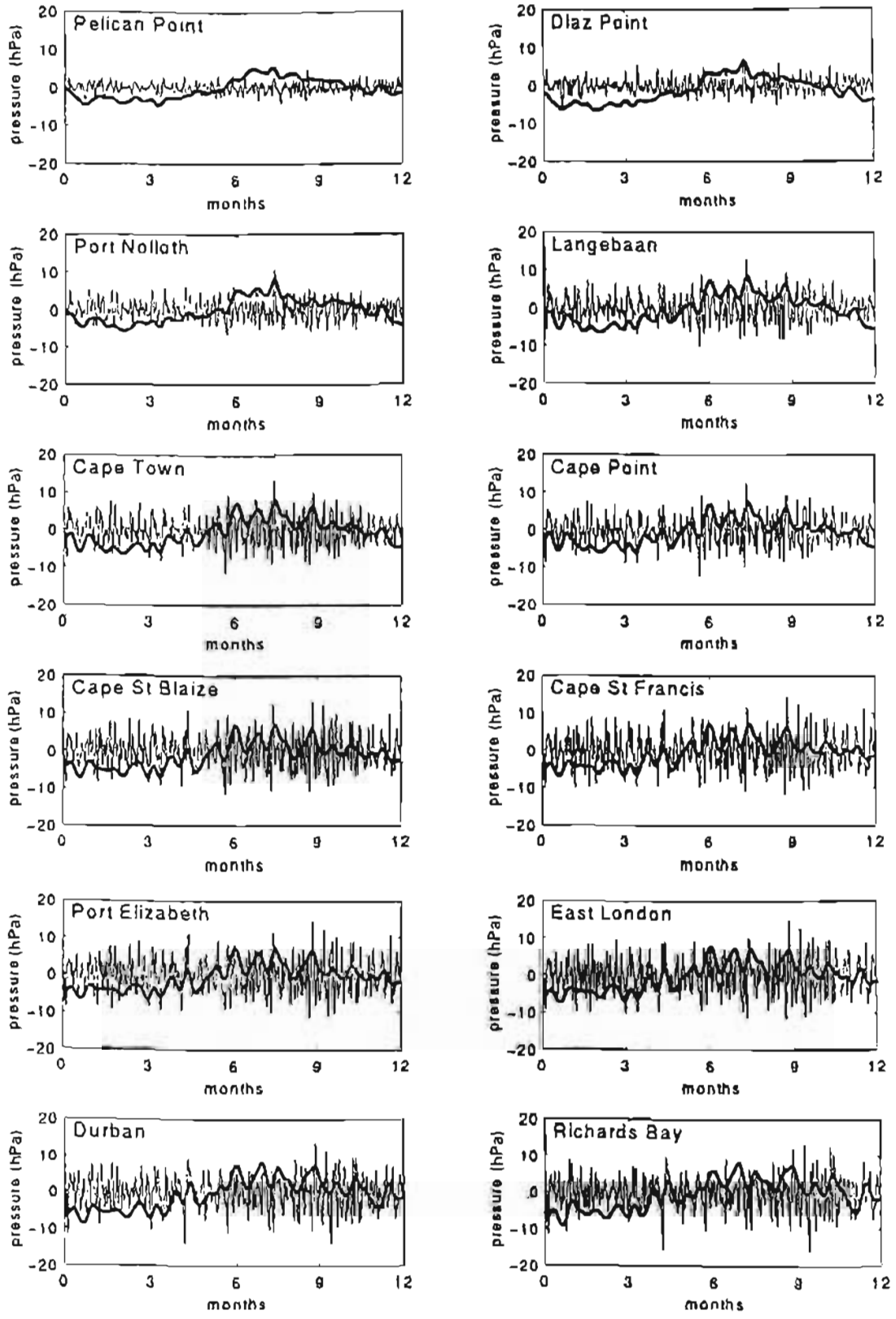

Fig. 5.6a Sea level atmospheric pressure time series at twelve sites for 1985. The bold line represents the LLP data and the lighter more variable lines represent the synoptic (band-passed) atmospheric pressure variations (BPP data).

Histograms of the distribution of the three atmospheric pressure time series (LLP, CLP and BPP) show the data to be normally distributed except for the low frequency (LLP) time series which has large data gaps and appears to have a bimodal distribution. Further, it is interesting to note that during 1985 there is a general increase of 6 hPa in the atmospheric pressure at the West Coast sites and an approximate 7 hPa increase in atmospheric pressure at the South and East Coast sites.

5.3.2 Sea Level

The magnitude of the seasonal signal in the raw sea level data is greatest at the northern sites on the West coast, decreasing southwards from Walvis Bay (10 - 15 cm) to Simon's Bay where the seasonal fluctuations in the LLR time series are largely indiscernible amongst the other low frequency fluctuations (Fig. 5.6b). Along the South and Southeast Coasts the low frequency fluctuations (mainly of a 22 to 25 day period) are of sufficient magnitude to mask any seasonal signal present. This is particularly true of the more erratic low frequency fluctuations in sea level at Durban.

The seasonal fluctuations in sea level (LLR) exceed the magnitude of the synoptic sea level variations (BPR) at Walvis Bay and Lüderitz Bay (Fig. 5.6b), however from Port Nolloth southwards, as well as along the South and East coasts, the magnitude of the synoptic-scale sea level variability (40 to 50 cm) exceeds that of the low frequency variability. An exception is the Durban site where the 1982 data indicate a substantially reduced synoptic variability and consequently low frequency sea level fluctuations predominate.

The long-term secular trend in the 1985 atmospheric pressure data is clearly reflected in the raw sea level time series. The general 6 hPa increase in atmospheric pressure along the west coast in 1985 is concurrent with an approximate 4 to 10 cm decrease in raw sea level along the west coast, while the approximately 7 hPa increase in atmospheric pressure along the south and east coast during 1985 is concurrent with an approximately 14 to 25 cm drop in raw sea level. Where the data from other years (1982, 1984 and 1986) are sufficient to determine such a secular trend in raw sea levels, no significant upwards or downwards trend is observed.

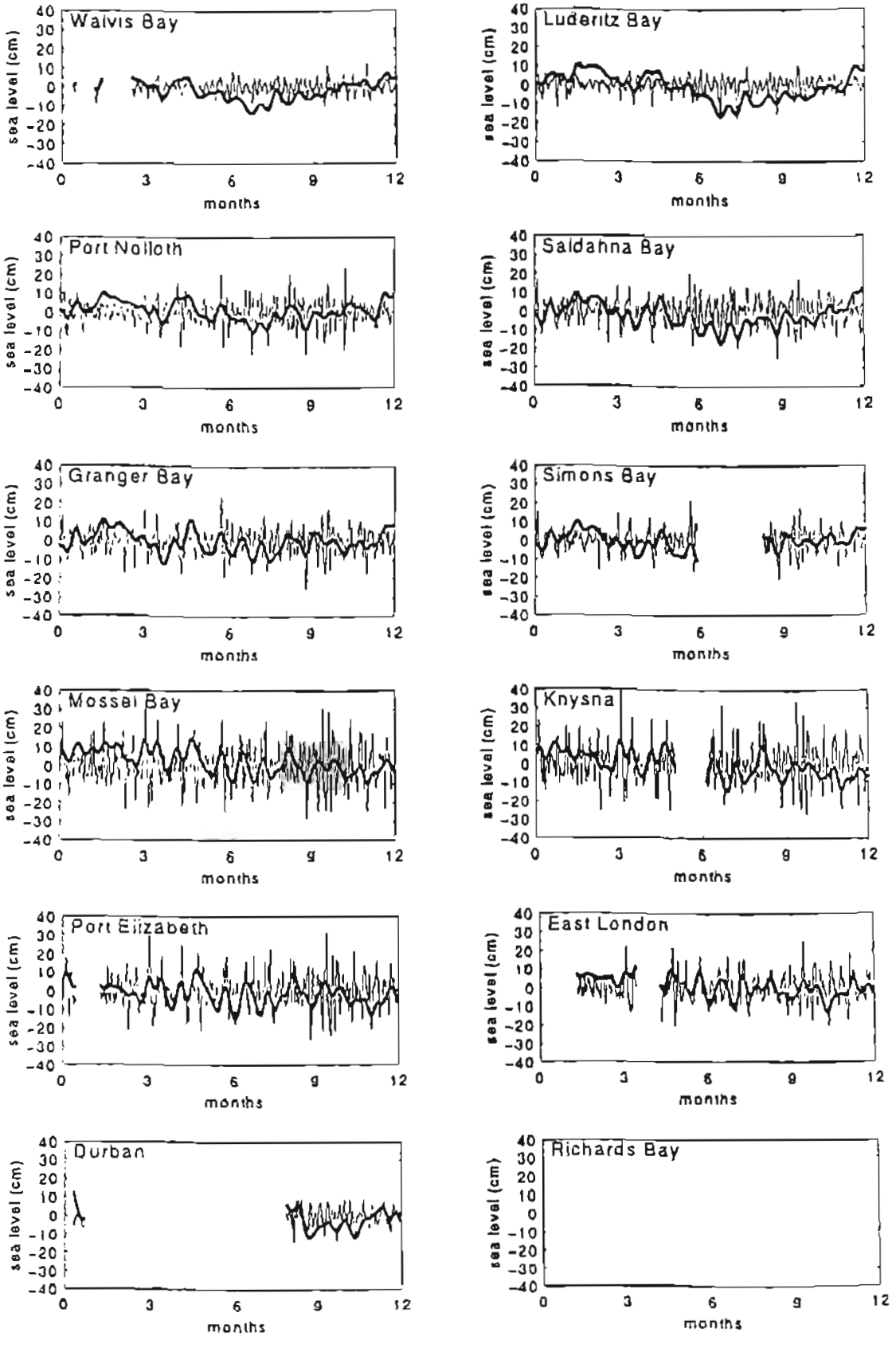

Fig. 5 6b Raw sea level for 1985 at twelve sites along the southern Africa coast. The bold line represents the LLR data and the lighter more variable lines represent thesynoptic-scale (band-passed) raw sea level variations (BPR).

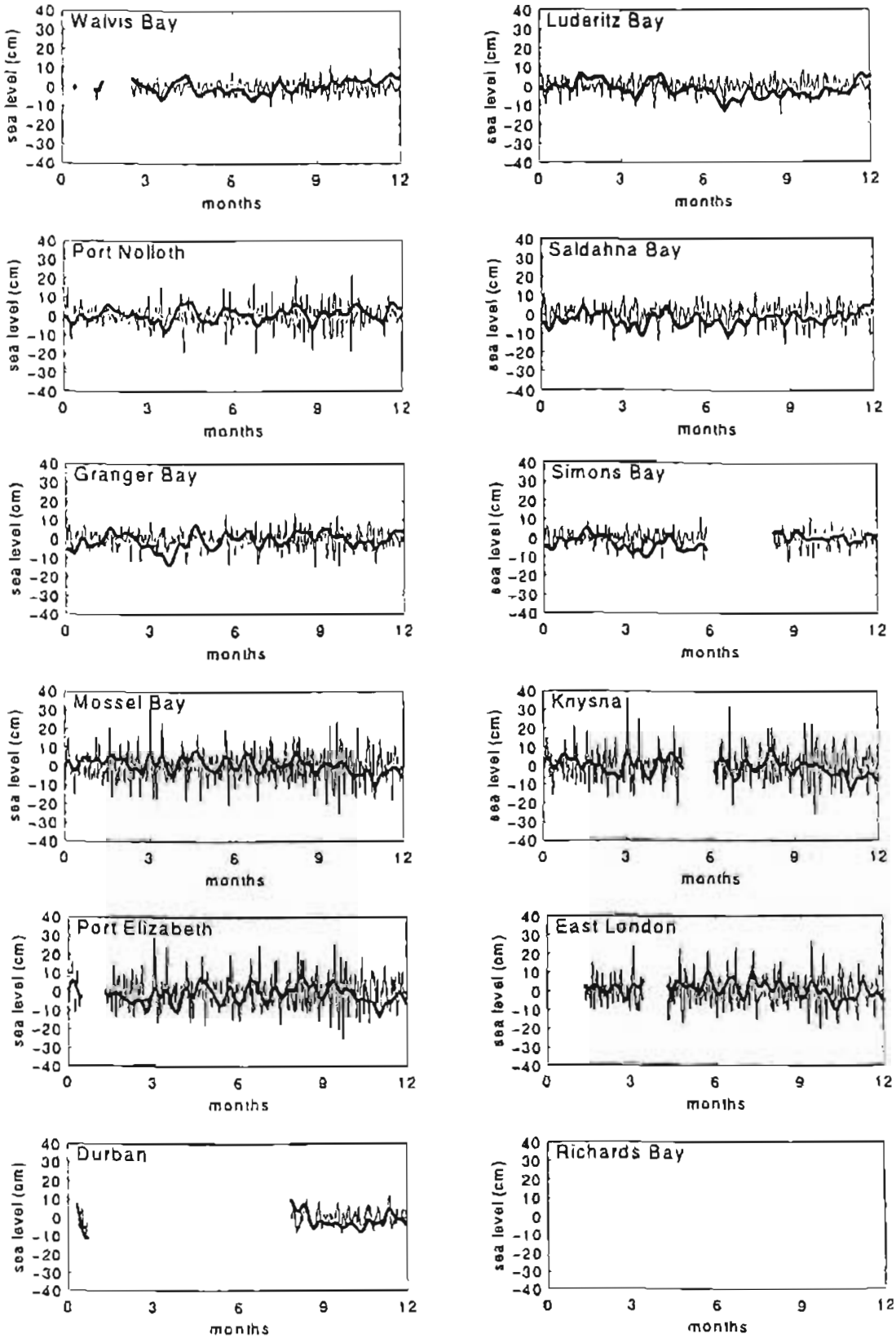

Fig. 5.6c Pressure-adjusted sea level for 1985 at twelve sites along the southern Africa coast. The bold line represents the LLC data and the lighter more variable lines represent thesynoptic-scale (band-passed) raw sea level variations (BPC).

In contrast to the raw (unadjusted) sea level data, there is little or no evidence of either the seasonal or longer term secular trend in the pressure-adjusted sea level data (Fig. 5.6c). This implies that a large proportion of the seasonality and longer term trends in the raw sea level data are due to an inverse barometer response to atmospheric pressure fluctuations rather than dynamic signals in the ocean circulation. Assuming an inverse barometer response, the upwards trend in atmospheric pressure accounts for some 70% (30% to 50%) or more of the longer term decrease in observed raw sea levels on the West (South) Coast. The small seasonal signal of 2 cm to 9 cm in the pressure-adjusted monthly sea level data reported by Brundrit *et al.* (1984) and de Cuevas (1985) cannot be readily distinguished from the relatively much larger amplitude low frequency variations in pressure-adjusted sea level (LLC) observed at all sites along the coast in the 1982 and 1985 data.

The range of fluctuations and variance of the pressure-adjusted sea level data (LLC, BPC and CLC) are substantially less than those of the raw sea level data (LLR, BPR and CLR). This has been previously noted in an analysis of pressure-adjusted monthly mean sea level data by Brundrit (1984). The decrease in the energy (especially at low frequencies), brought about by pressure-adjusting the raw sea level data is reflected in the power spectra of the sea levels at all of the tide guage sites (not shown).

In summary, the low frequency signal in these pressure-adjusted sea level data greatly exceed that of the synoptic-scale sea level fluctuations at the northern sites along the West coast. From Port Nolloth southwards, as well as along the South and East coasts, the synoptic-scale sea level fluctuations exceed the low frequency variability in sea levels. An exception, however, are the sea levels at Durban which display a reduced synoptic-scale variability and large amplitude low frequency variability in pressure-adjusted sea levels

5.4 Synoptic Variability in Atmospheric Pressure and Sea Level

In the sections which follow, the synoptic variability in atmospheric pressure and sea level is analysed using space-time contour plots, auto- and cross-spectral analysis and auto- and cross-correlation analysis. The theory and detail of these analysis techniques are given in Appendix C.

Space-time contours of synoptic-scale, pressure-adjusted sea levels provide a preliminary description of the general nature, extent, and seasonal and spatial variability in the sea level response to synoptic atmospheric forcing. Autospectra are used to identify the most common frequencies present in the sea level response at the different sites, while the cross-spectra, coherency and phase plots provide a measure of the coherence in sea level (and thus common CTW dynamics) between sites as well as robust estimates of the phase speeds of CTW motions along the southern African coastline.

Spectral analysis techniques are designed to analyse data containing strongly periodic signals (providing robust estimates in the frequency domain), however the sea levels associated with CTW motions along the coastline of southern Africa are at best quasi-periodic and can better be described as "events". This suggests the analysis of sea levels in the time domain using cross-correlation techniques to obtain estimates of the mean phase speed of propagation of sea level "events" along the southern African coastline and the longshore changes in these phase speeds. Although these cross-correlation techniques have the advantage of requiring shorter time series, they provide less robust estimates of phase speed than the spectral analysis techniques described above.

Given that the synoptic-scale variability of pressure-adjusted sea levels is considered to reflect CTW activity over the shelf, space-time contour plots of the band-passed 1985 pressure-adjusted sea levels from Walvis Bay to Durban are used broadly to characterise the CTW response of the shelf regions of southern Africa (see Fig. 5.7). Sea level atmospheric pressures have been similarly contoured but are not presented.

Fig 5.7 indicates that pressure-adjusted sea level "events" (CTW's) propagate anticlockwise around southern Africa. These sea level events generally develop in the vicinity of Lüderitz, rapidly increase in amplitude in the vicinity of Port Nolloth, propagate around the Cape of Good Hope, attain a maximum amplitude between Mossel Bay and Port Elizabeth and finally are strongly attenuated between East London and Durban. The pressure-adjusted sea level contours for summer 1985 indicate the presence of two distinct regimes, one on the West Coast and the other on

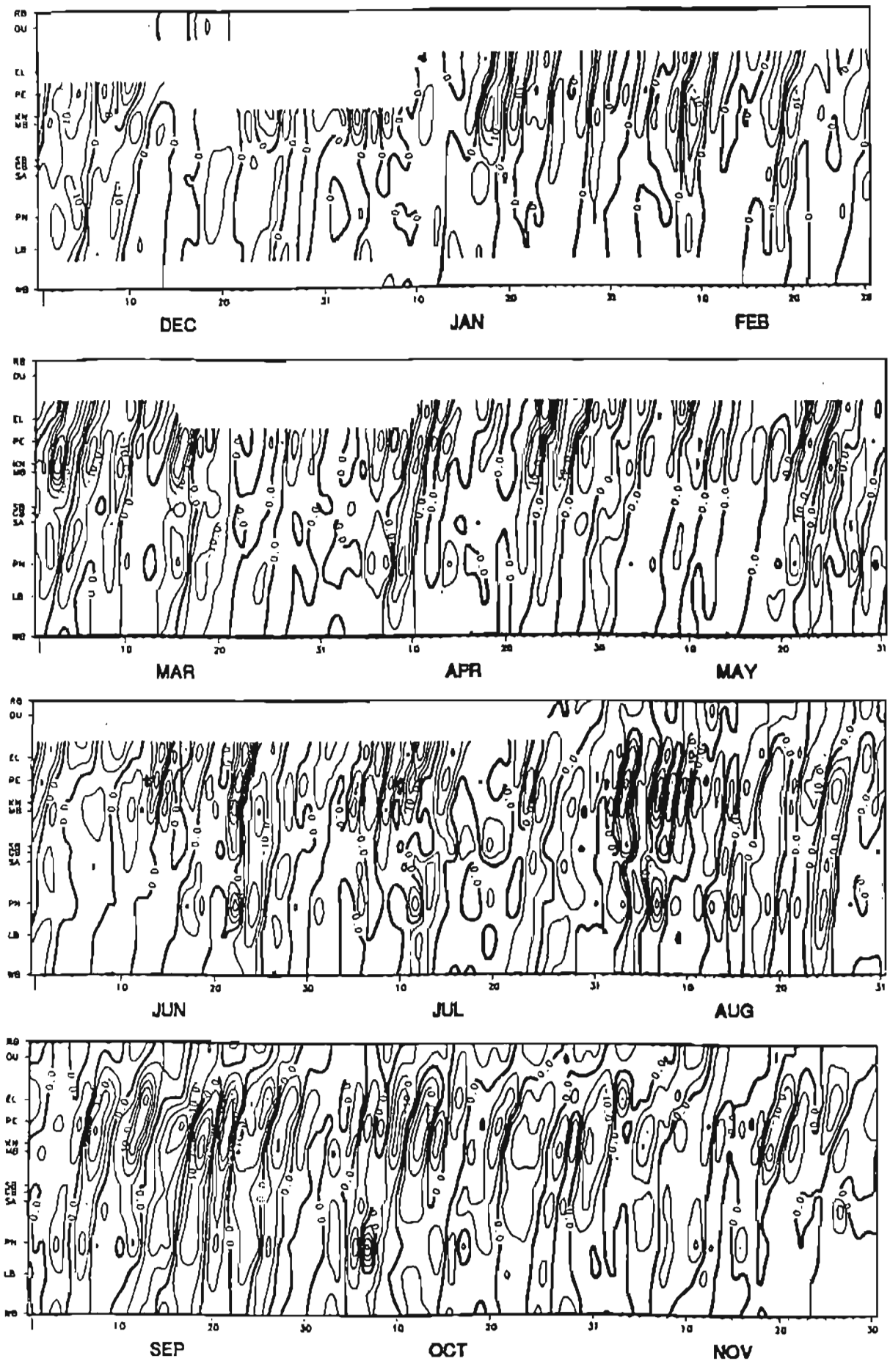

Fig. 5.7 Space-time contours of 1985 pressure-adjusted sea levels from Walvis Bay to Durban.

the South and East Coasts. On only rare occasions is there clear continuity in the sea level "events" observed in summer on the West and South Coasts. In general the space-time contours of pressure-adjusted sea level indicate a reduced sea level variability on the West Coast in summer, mostly of a lower frequency nature. On the South Coast, the summertime sea level variations are more energetic and of a higher frequency. In autumn there is increased sea level variability on the West Coast with slightly more continuity between the West and South Coast, while in winter and spring the amplitude of the sea level variability in the 0,01 to 0,02 cpd range increases dramatically, especially in late winter and early spring. During this period (especially in spring), there is an increased frequency of events and a substantial increase in continuity between the sea level events observed on the West and South Coasts. Of note, however, is the absence of energetic fluctuations in the 0,01 to 0,02 cpd range in late winter and early spring of 1984, a year characterised by anomalous oceanographic conditions over the West Coast shelf (Shannon *et al.*, 1987). In 1984, the strong sea level variability characteristic of late winter and early spring occurred at lower frequencies (< 0,01 cpd) than normal.

Further observations can be made regarding the nature and extent of CTW activity over the southern African shelf using the space-time contours of pressure-adjusted sea level.

i) The West Coast sea level variability is characteristically of a lower frequency than that observed on the South and East Coasts.

ii) The amplitude of the sea level variability on the West Coast is greatest at Port Nolloth which lies on a wide shelf region (the Orange River cone) and a number of the higher frequency sea level "events" on the West Coast are observed to have a significant amplitude only at Port Nolloth. A similar maximum in sea level variability is observed on the South Coast between Mossel Bay and Port Elizabeth.

iii) The lack of continuity of sea level "events" along the coastline of southern Africa reported by others (for example Schumann and Brink, 1990) is indicative of a rapidly changing amplitude of sea level events at the different sites along the coast rather than a clear indication that the sea level event does not propagate along the coastline. The often reported "lack of continuity" in

sea level events between Port Nolloth and Granger Bay on the West Coast and between East London and Durban (for example , Schumann and Brink, 1990) is clearly observed in the pressure-adjusted sea level contours (Fig 5.7) and is discussed in more detail in the analyses that follow.

iv) The phase speed of propagation of sea level events along the coast are quite variable. This observation led de Cuevas *et al.* (1986) to conclude that the CTW's around southern Africa are directly forced by local synoptic weather systems. It is difficult to estimate the phase speed of the propagation of these sea level events between coastal sites using only the space-time contours of pressure-adjusted sea level in Fig. 5.7. Estimates obtained using more robust statistical techniques are reported in section 5.4.2. The space-time contours do however indicate that the phase speed of propagation of sea level events around the coastline of southern Africa decreases rapidly between East London and Durban as does the amplitude of the sea level event.

Most of the above observations are dealt with more comprehensively in the statistical analyses that follow.

5.4.1 Temporal Variability of Atmospheric Pressure and Sea Level

A number of researchers have commented of the importance of the nature of the temporal variability of the West Coast shelf waters to the biological productivity in this region (for example, Jury and Brundrit, 1992; Nelson, 1992a) and various suggestions have been made as to the optimum periodicity of the environmental fluctuations required to maximise the trophic efficiency of such an ecosystem. The temporal variability of CTW motions also has important implications for other human activities over the shelf (see chapter 1). Since the synoptic-scale variability of pressure-adjusted sea levels is considered to reflect the CTW activity, these data are used to provide the frequency characteristics of CTW motions over the shelf regions of southern Africa.

It has been noted by a number of researchers (for example, Jury et al, 1990a; Nelson, 1992a) that the atmospheric systems forcing CTW's and the CTW's themselves are quasi-periodic. For this reason, spectral analysis of pressure-adjusted sea levels analysis has been only partially successful in describing the temporal characteristics of

both propagating atmospheric pressure systems and their associated CTW motions (de Cuevas, 1985; Schumann, 1989; Schumann and Brink, 1990). Recognising this quasi-periodicity of atmospheric pressure and sea level variability, a *time-lagged spectral analysis* has been undertaken for the 1982, 1984, 1985 and 1986 subinertial time series using the MATLAB *specgram* routine. *Specgram* computes the (Hanning) windowed discrete-time Fourier transform of the time series using a sliding data window. There is a large confidence interval associated with these unsmoothed spectral estimates, nevertheless the estimates seem sufficiently robust to provide information on the temporal variability in the spectral properties of the time series. In Fig. 5.8, the logarithm of the unsmoothed spectral estimates for a) atmospheric pressure and b) pressure-adjusted sea level for 1985 have been contoured as a function of both time and frequency. These time-lagged power spectra confirm that the variability in the atmospheric pressure and pressure-adjusted sea level is at best quasi-periodic which explains the difficulties encountered using conventional smoothed power spectra to identify dominant frequencies in the data.

There is an ubiquitous 22 to 25 day signal in both the atmospheric pressures and pressure adjusted sea levels that is not resolved using spectral analysis techniques (as the times series are too short to provide adequate resolution at these low frequencies). This signal, which is particularly strong at the southern sites and in winter, can be attributed to the Rossby wave mode 4 pattern in the atmosphere (Jury, pers comm.).

The atmospheric pressure spectra (Fig. 5.8a) indicate that energy of a specific frequency typically persists for approximately 25 to 50 days, with the energy at lower frequencies (< 0.1 cpd and mainly observed in winter) having a greater persistence. There is a strong burst of low frequency (0.03 cpd) energy in the atmospheric pressure time series at all sites in May, June and July 1985. At the northernmost West Coast sites there is very little energy at higher frequencies. The energy at these higher frequencies is only significant from Saldahna Bay southwards and increases along the South Coast to reach a maximum in the region between Cape St Francis and East London. Of particular interest is the burst of 0,1 cpd to 0,2 cpd energy that persisted for approximately 30 to 40 days on the South Coast in both September 1985 and September 1986. In 1984 the September burst of energy occurred in a lower

frequency range (0,01 to 0,1 cpd), implying greater pertubations to environmental parameters (Jury and Brundrit, 1992) in the southern Benguela.

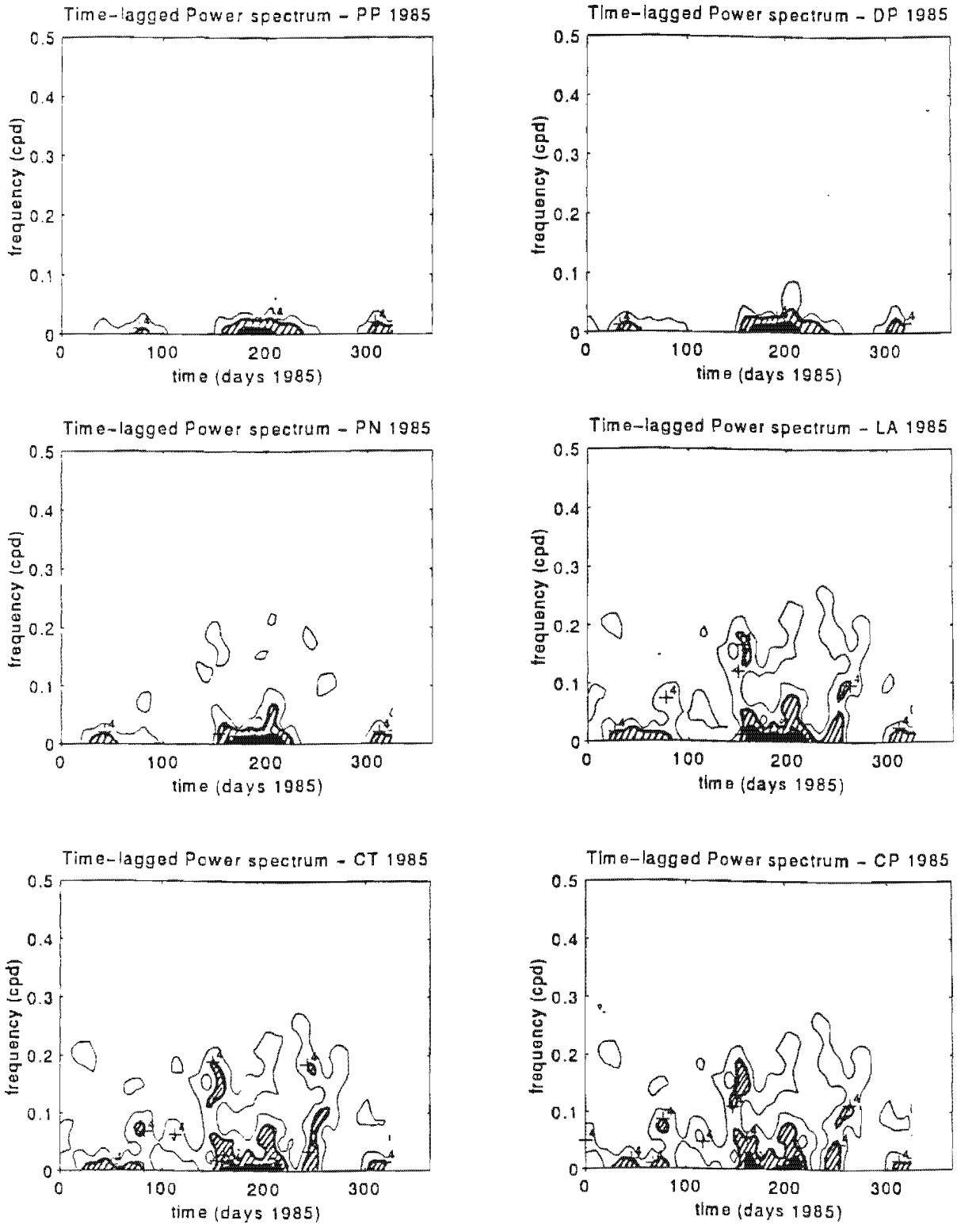

Fig 5.8a) Time-lagged power spectra of atmospheric pressures at 12 sites along the southern African coastline in 1985. The contours are the logarithm of the power spectral estimates (in hPa^2.day). Values > 4 are shaded with a dashed line while values > 4.5 are indicated using a solid shading.

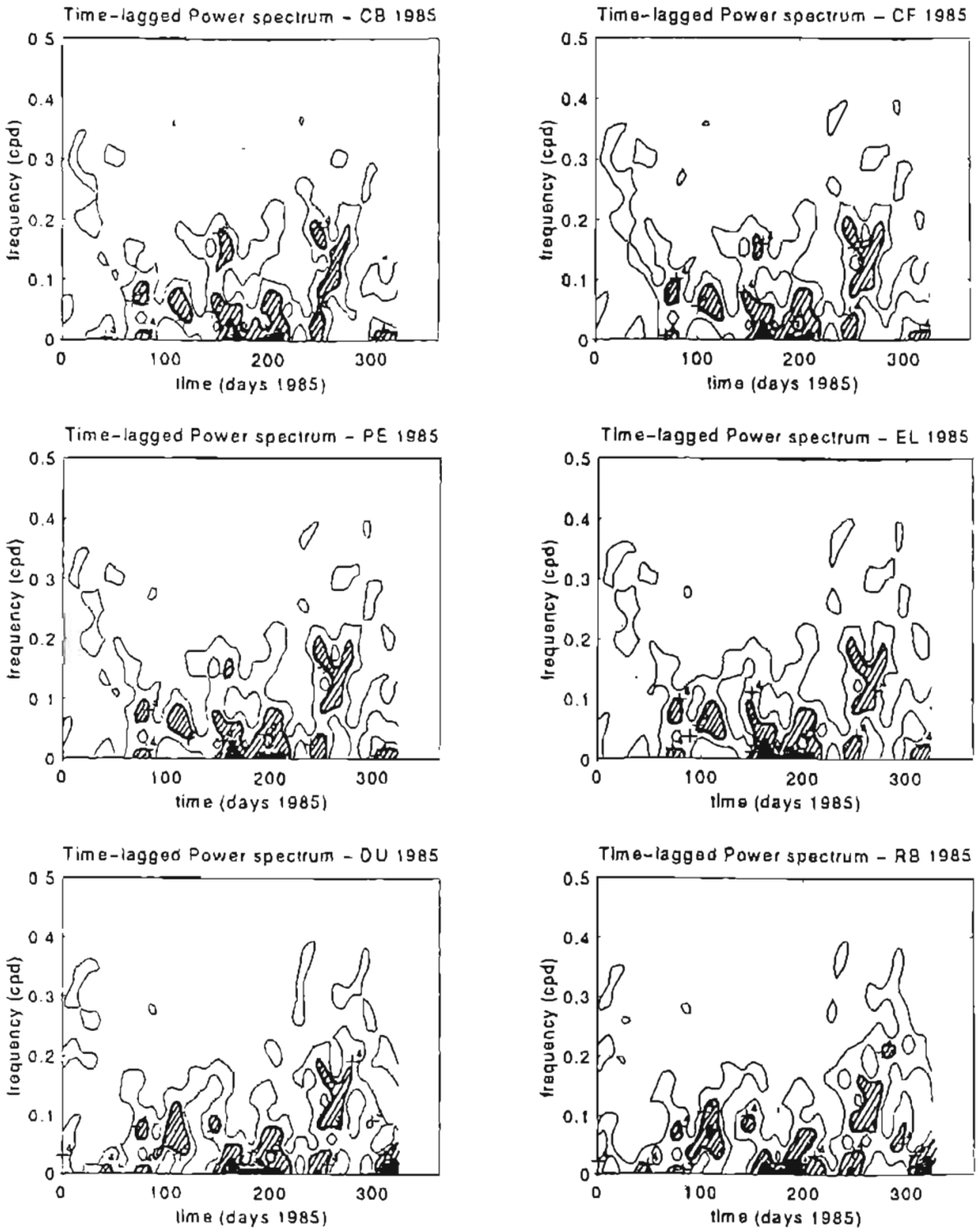

Fig 5.8a) (cont) Time-lagged power spectra of atmospheric pressures at 12 sites along the southern African coastline in 1985. The contours are the logarithm of the power spectral estimates (in hPa^2.day). Values > 4 are shaded with a dashed line while values > 4.5 are indicated using a solid shading.

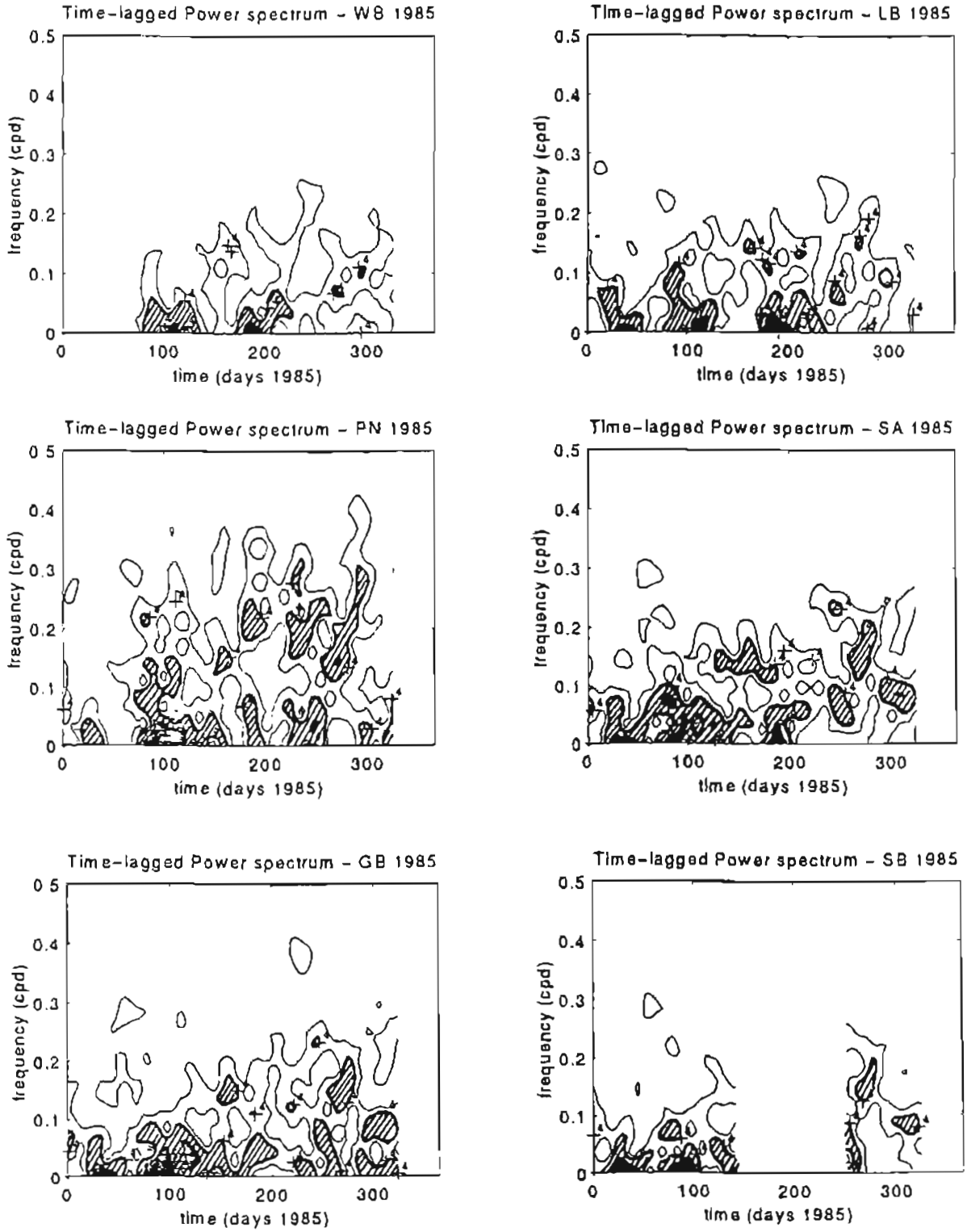

Fig 5.8b) Time-lagged power spectra of pressure-adjusted sea level at 12 sites along the southern African coastline in 1985. The contours are the logarithm of the power spectral estimates (in cm^2.day). Values > 4 are shaded with a dashed line while values > 4.5 are indicated using a solid shading.

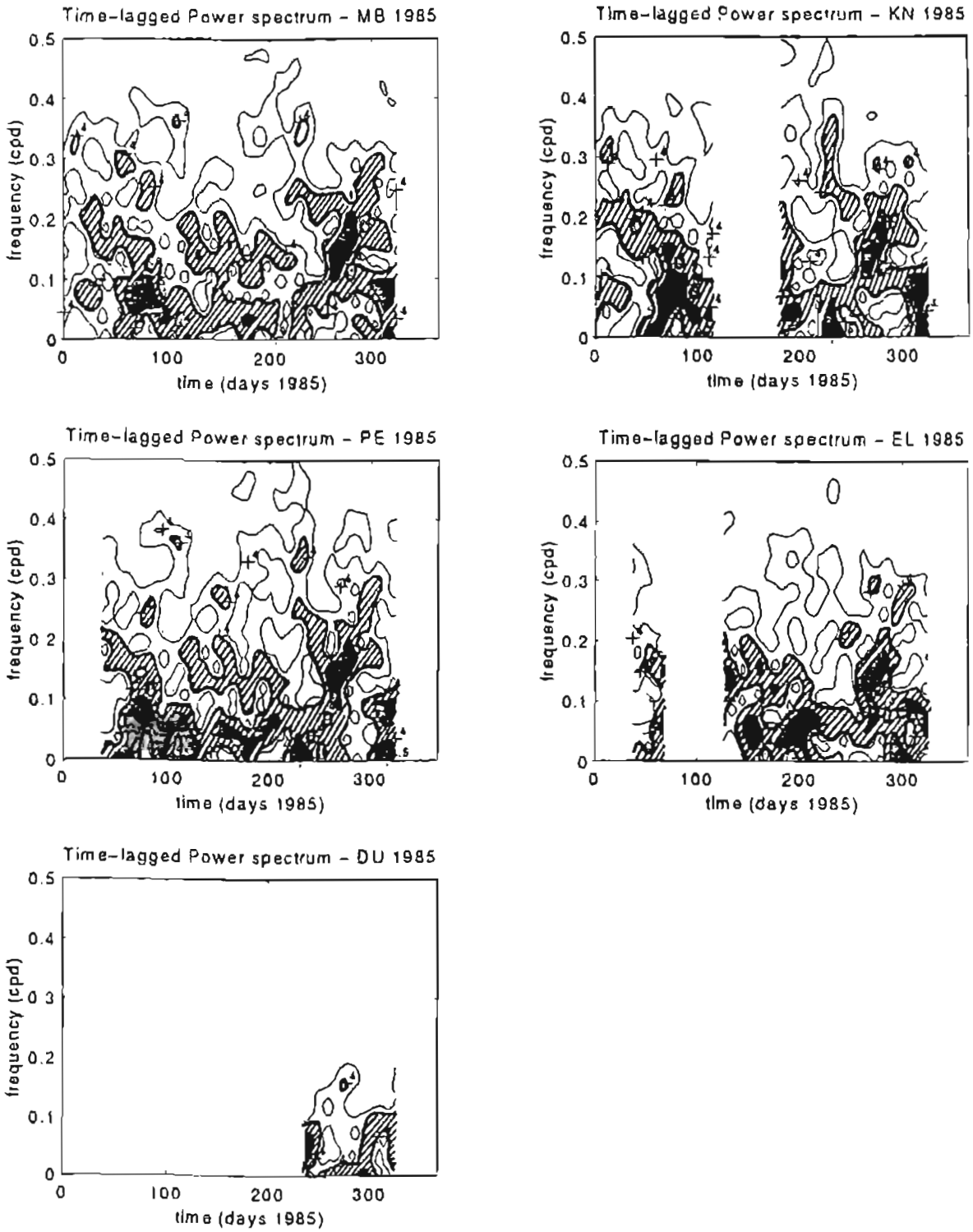

Fig 5 8b) (cont) Time-lagged power spectra of pressure-adjusted sea level at 12 sites along the southern African coastline in 1985. The contours are the logarithm of the power spectral estimates (in cm^2.day). Values > 4 are shaded with a dashed line while values > 4.5 are indicated using a solid shading.

The time-lagged power spectra of 1985 sea levels Fig. 5.8b) display somewhat different characteristics to those of the 1985 atmospheric pressures. The low frequency energy observed in the atmospheric pressure spectra is not evident in the spectra of pressure-adjusted sea levels, however it is clearly visible in unadjusted sea level spectra. This indicates that there is very little energy in forced CTW motions (pressure-adjusted sea levels) at these low frequencies and that this low frequency energy in the unadjusted sea levels is largely indicative of an inverse barometer response to low frequency variations in atmospheric pressure. In general there is substantially greater energy at higher frequencies in the pressure-adjusted sea level data at sites situated on wide, gently-sloping shelf regions (e.g. Port Nolloth, Mossel Bay and Knysna)

The burst of energy (0,01 cpd to 0,02 cpd in 1985 and 1986, < 0,01 cpd in 1984) observed in atmospheric pressures in early September is also present in the spectra of pressure-adjusted sea levels. Of further interest is the low frequency energy observed in mid March 1985 at the northern sites (day 105 in Fig. 5.8b). This observation of low frequency variability is discussed in more detail in section 5.4.4.

As with the atmospheric pressures, the energy at particular frequencies in the pressure-adjusted sea levels persists for 25 to 50 days and even longer on some occasions. This is consistent with the findings of Jury *et al.*, (1990), Nelson (1992) and Jury and Brundrit (1992). Considering the quasi-periodic nature of the above time series it is unlikely that one will be able to identify dominant frequencies in the atmospheric pressure and pressure-adjusted sea level time series or document seasonal changes in the spectral properties of the atmospheric and sea level time series.

To facilitate the identification of particular frequencies, the *smoothed power spectral estimates* (see Appendix C) are calculated using data windows each containing 40 days of data This choice obviously places a rather severe limitation on the low frequency resolution of the estimates (since B_e = 0.025 cpd). The power spectra of atmospheric pressure at sea level have been calculated for the full year and for summer/autumn 1985 and winter/spring 1985 (Fig. 5.9) Typically, the energy at all frequencies increases from a minimum at Walvis Bay on the West Coast to a maximum in the

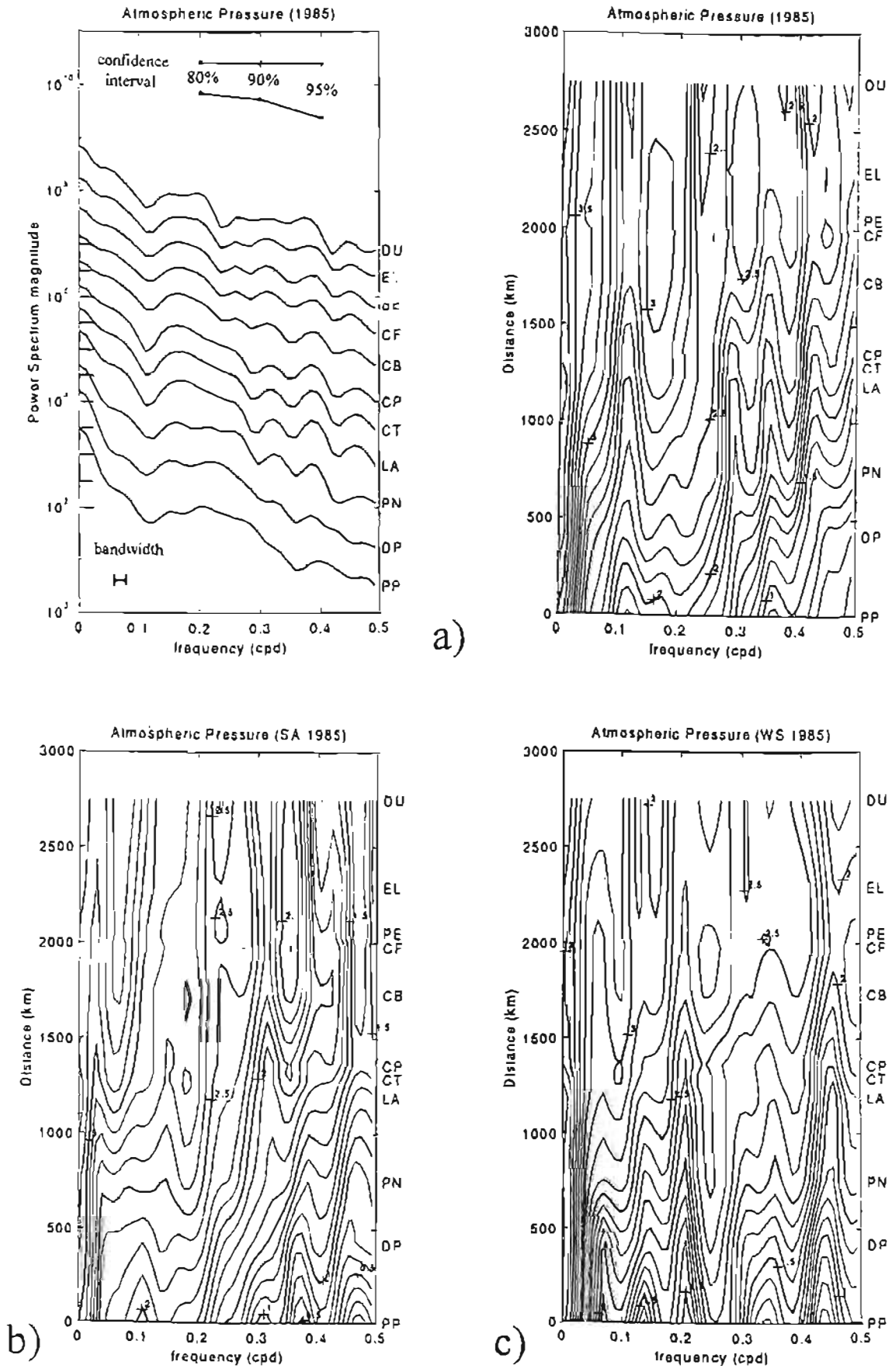

Fig 5.9 Power spectral estimates (in hPa^2.day) of sea level atmospheric pressures at various sites along the coast for a) the whole year of 1985, b) summer/autumn 1985 and c) winter/spring 1985 at all sites along the coast. The contours are the logarithm of the power spectral estimates. The bandwidth and confidence intervals indicated are valid for all spectra.

vicinity of Port Elizabeth/East London on the South Coast and from a minimum in summer/autumn to a maximum in winter/spring (especially at higher frequencies). At low frequencies the energy is comparable for all sites along the coast (with slight maxima on the West Coast and the northern regions of the East Coast), while at higher frequencies the energy increases rapidly upon moving anti-clockwise around the coast. The energy at periods less than 3 days is only significant from Langebaan (Saldahna Bay) southwards and peaks in the vicinity of Port Elizabeth.

Energy peaks in atmospheric pressure data for 1982, 1984, 1985 and 1986 are observed at periods of 50 days, 13 to 15 days, 10 days, 6 to 7 days, 5 days, 3 days and 2,7 days. The most common energy peaks in atmospheric pressure data are those at periods of 10 days (mainly winter), approximately 6 days (all year round, particularly on the south coast), 3 days (occurring mostly in winter and generally restricted to the South Coast) and 2,5 to 2,7 days (restricted to the South Coast). These results support those of Walker (1984) who found a general 6 day cyclicity in the coastal lows in spring and summer lengthening to 10 days in autumn and winter.

A similar analysis of pressure-adjusted sea levels (Fig. 5.10) shows the same broad features as the atmospheric pressure spectra. On moving anticlockwise around the coast from Walvis Bay to Durban there is a slow increase in energy at lower frequencies (< 0.15 cpd), however this is not the case for higher frequencies ($> 0,15$ cpd). Instead there are two high frequency energy maxima, namely at Port Nolloth and between Mossel Bay and Port Elizabeth. These energy maxima are consistent with the notion that shelf waters in these wider shelf regions respond more readily and energetically to rapid changes in the wind stress fields and consequently serve as geographic origins for CTW motions.

A second more striking feature of the pressure-adjusted sea level spectra is the strong decrease in energy at all but the lowest frequencies at the southern sites along the West Coast (that is, Saldahna Bay and Granger Bay). The decrease in higher frequency energy at Saldahna Bay could be due to the fact that such an enclosed embayment acts as a low pass filter to shelf variability, however a similar decrease in higher frequency energy at Granger Bay suggests that some other process is responsible for this

observation. Other possibilities are that the winds forcing CTW's weaken in this region, that wind-forcing is not effective over this shelf region or even that the CTW motions change from being predominantly barotropic (with a large sea level signal) to baroclinic (with a reduced sea level signal). However, more likely is that these observations are due to the dissipative effects of large longshore variations in bottom topography on the CTW propagation. The strong decrease in energy (especially at higher frequencies) at these sites is consistent with the notion that large alongshore variations in bottom topography scatter incident CTW's and thus tend to act as a low pass filter in both the frequency and wavenumber domain for forward scattered CTW's (Webster, 1987; Middleton and Wright, 1988). A similar decrease in high frequency energy is observed at East London and Durban where low frequency variability is dominant. This strong damping of higher frequency motions has been attributed to enhanced frictional damping of CTW's due to the presence of the Agulhas Current in this region (Brink, 1990). The increased low frequency energy at these locations is also attributable to the influence of the Agulhas Current rather than to wind-forced CTW motions.

Energy peaks in pressure-adjusted sea level for 1982, 1984, 1985 and 1986 are typically observed at periods of 25 to 30 days, 14 days, 10 days, 7 to 8 days, 4,5 days, 3 days and 2,3 days. This compares well with the results of de Cuevas *et al.* (1986) and Schumann and Brink (1990) who analysed pressure-adjusted sea level data and results of Holden (1987) and Nelson (1989) who analysed current meter data. The most common energy peaks in the pressure-adjusted sea level data are those at periods of 10 days (mainly winter), 4 to 4,5 days and 3 days (occurring mostly in winter and largely restricted to the South Coast). These results are consistent with those of Krause and Radok (1976) who found marked peaks in sea level at periods of about 4.5 to 10 days, with the largest amplitude sea level variability occurring in September (as quoted by Schumann and Brink, 1990). Despite the fact that the time series are at best quasi-stationary and that consequently one cannot confidently define frequencies or periods at which energy peaks occur in the time series, most analyses of pressure-adjusted sea levels along the southern Africa coastline indicate that broad peaks exist in the pressure-adjusted sea level autospectra at periods of approximately 10 days and 3 days.

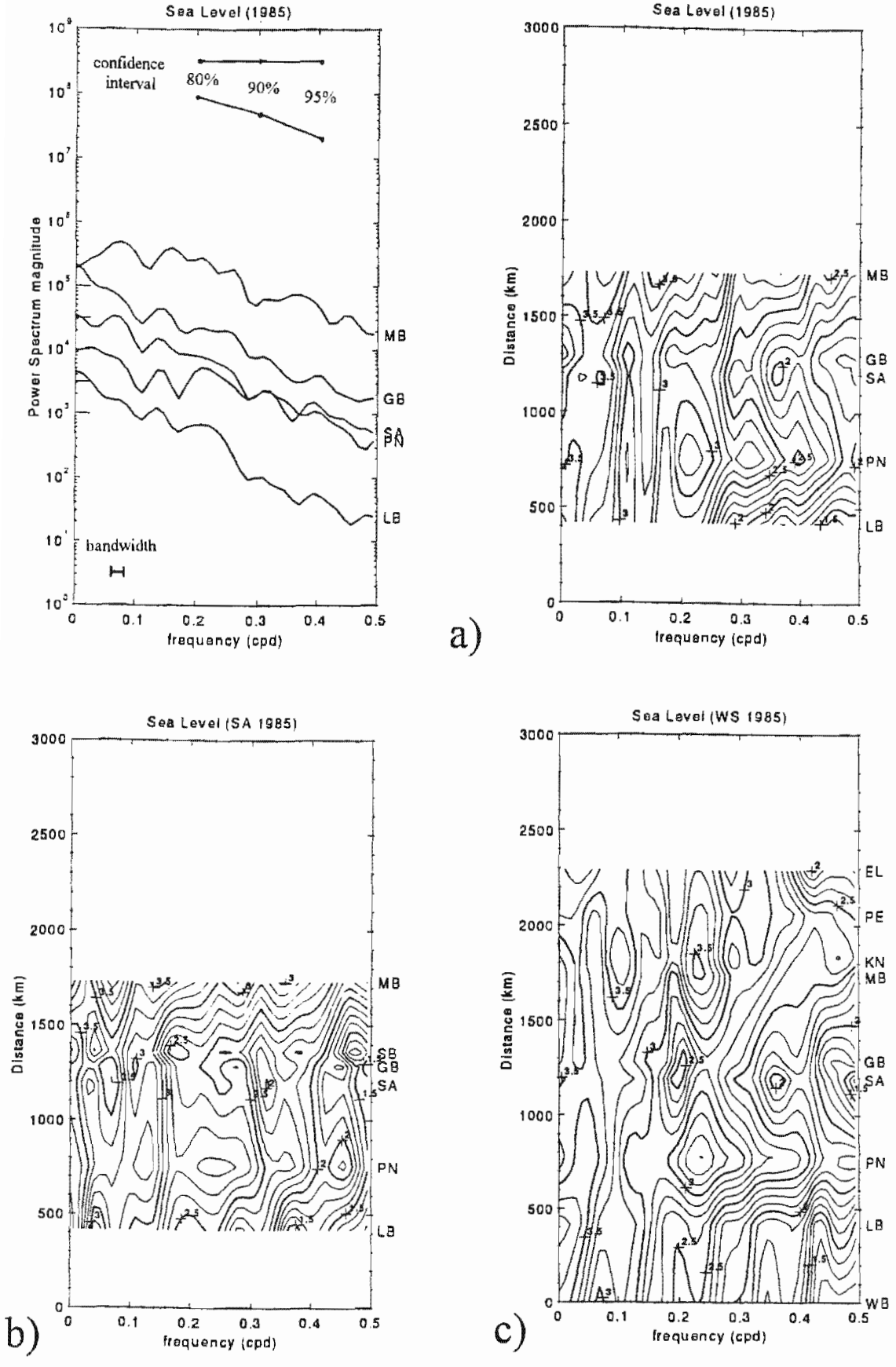

Fig 5.10 Power spectral estimates in (cm^2.day) of pressure-adjusted sea level at various sites along the coast for a) the whole year of 1985, b) summer/autumn 1985 and c) winter/spring 1985 at all sites along the coast. The contours are the logarithm of the power spectral estimates. The bandwidth and confidence intervals indicated are valid for all spectra.

Since the periods of interest in the time series are such that it is not possible to obtain robust spectral estimates for shorter time series, the seasonal changes in the spectral properties of the time series have not been investigated. However, comparison of the summer/autumn and winter/spring periods indicate that the winter/spring sea level variability exceeds that of summer/autumn at all sites along the coast. The results of de Cuevas (1985) give no distinct indication of seasonality. Similarly, here it is not possible to identify dominant frequencies in the summer/autumn and winter/spring data.

5.4.2 The Spatial Extent and Phase Velocities of CTW's around Southern Africa

Coherence analyses of the atmospheric pressures and sea levels may be used to isolate significant variability at common frequencies at the various observation sites along the coastline and in so doing provides an indication of common dynamics at the different sites. A coherence analysis of 1985 atmospheric pressure data indicates a high degree of coherence between all sites along the coast of southern Africa. The frequency ranges containing the highest coherence in atmospheric pressure between sites and the propagation velocity of events in these frequency bands, are listed in Table 4. A similar analysis of pressure-adjusted sea level indicates a high degree of coherence between *adjacent* sites along the coastline. This high coherence between adjacent sites is largely attributable to the close proximity of the sites to one another. To determine at which frequencies there is significant coherence at all sites along the coastline, the coherence has been calculated between all sites and a number of reference sites. The reference sites that have been used are Port Nolloth, Granger Bay, Mossel Bay, East London and Port Elizabeth. The results are largely similar for all reference sites used, therefore only the results obtained using Granger Bay as a reference site are presented (Fig 5.11a,b,c). All coherences greater than 0,7 are more than 95% significant.

In summer (Fig. 5.11b) there are a number of frequencies at which there is a high degree of coherence in pressure-adjusted sea levels along most of the coastline of southern Africa, while in winter (Fig 5.11c) there are two broad frequency ranges for which there is a high coherence. These frequency ranges and the associated propagation velocities are listed in Table 4.

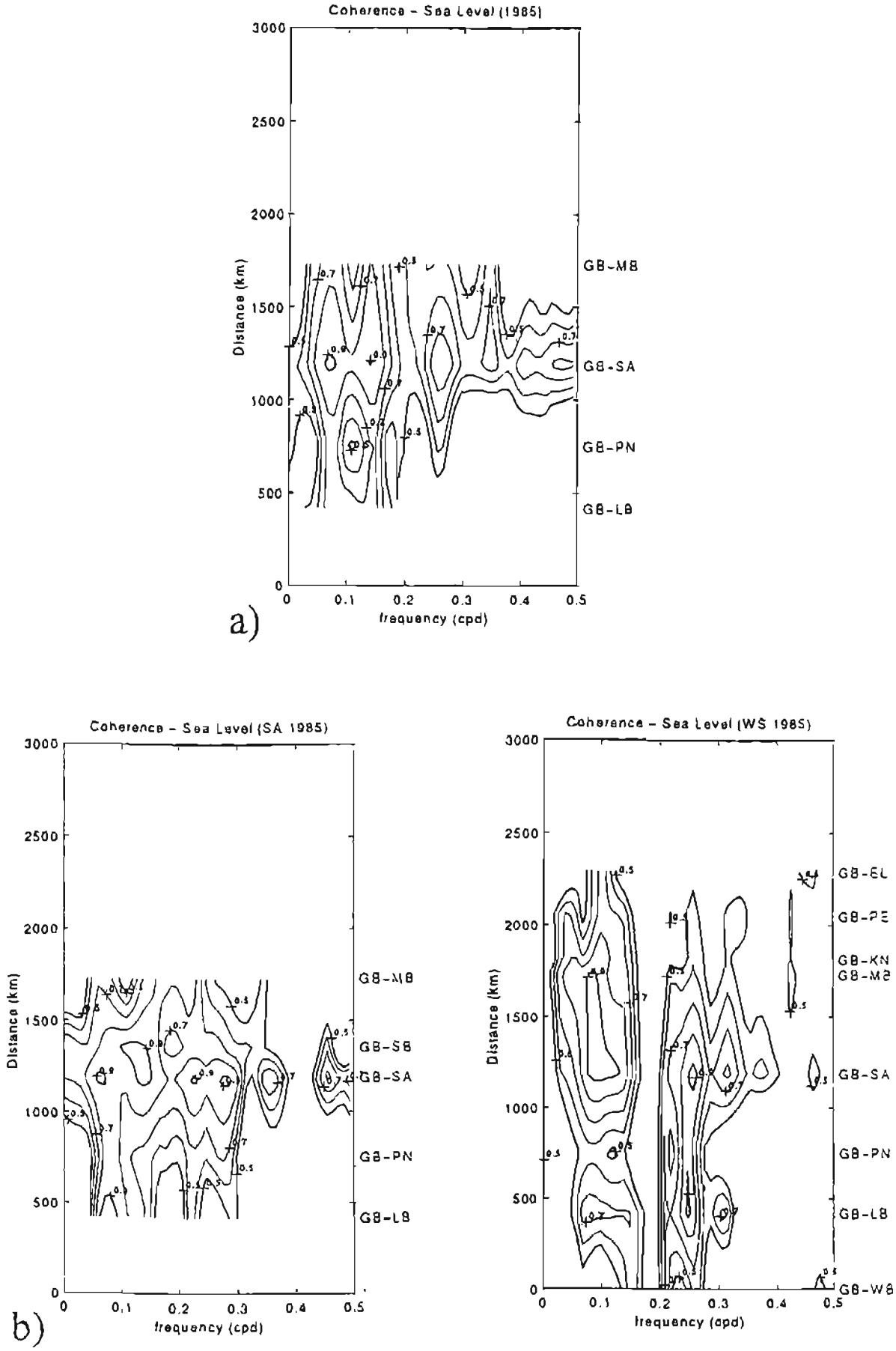

Fig. 5.11 Longshore coherence in sea level at various sites along the southern African coastline relative to Granger Bay for a) the whole year of 1985, b) summer/autumn 1985 and c) winter/spring 1985.

The following observations can be made regarding the alongshore coherence in pressure-adjusted sea level:

i) The alongshore coherence is greatest for lower frequencies and there is very little coherence between sites at frequencies above 0,3 cpd.

ii) There is reduced low frequency and very little high frequency coherence in pressure-adjusted sea levels between Port Nolloth and the southern West Coast sites of Saldahna Bay and Granger Bay, however there is a high coherence between Port Nolloth and Lüderitz Bay to the north. (These data are not shown). This is indicative of the higher frequency motions generated at the northern West Coast sites being attenuated before reaching the southern sites on the West Coast. This could be ascribed to the topographic scattering of CTW's by the large alongshore variation in bottom topography on the West Coast.

iii) The frequency characteristics of the coherence between sites along the coast not only changes from season to season but also from year to year (see Fig 5.11d,e).

iv) Lastly, coherence analyses of 1982 pressure-adjusted sea levels along the coastline (Fig 5.11d) indicate a high degree of coherence (even at higher frequencies) between the South Coast sites and Durban. This suggest that there is continuity in CTW motions between the South and East Coast sites albeit at large time lags and vastly reduced amplitudes.

The propagation velocities derived from the coherence analyses, despite being highly variable, compare reasonably well with the theoretical estimates for free CTW motions (Table 4). Schumann and Brink (1990), however, found that their estimates of propagation velocities (derived from coherence analyses) were substantially smaller than theoretical estimates for free CTW's.

A puzzling feature of the propagation velocities listed in Table 4 is that the propagation velocities tend to increase with increasing frequency. A similar observation can be made for the results in Table 2 of Schumann and Brink (1990). It is not known why this should be the case, however contours (Fig 5.16) and cross-correlation analyses of low frequency pressure-adjusted sea levels confirm that the low frequency sea level variability (periods > 18,5 days) propagates more slowly along the coastline that the higher frequency variability (periods of 2 to 20 days).

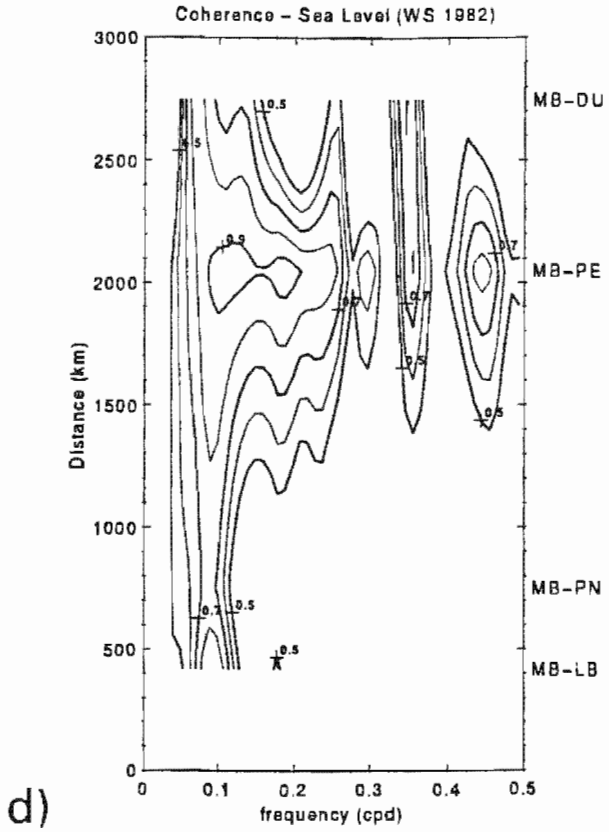

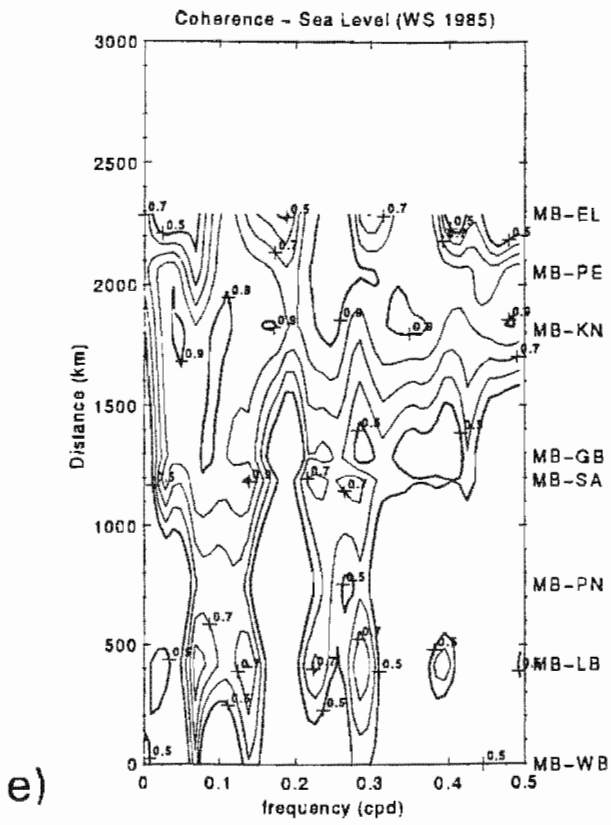

Fig. 5.11 (cont) Longshore coherence in sea level at various sites along the southern African coastline relative to Mossel Bay for d) the winter/spring 1982 and e) winter/spring 1985.

	Atmospheric Pressure Summer/Autumn 1985			Atmospheric Pressure Winter/Spring 1985		
	frequency (cpd) 0.045 - 0.055 period (days) 22.2 - 18.2	frequency (cpd) 0.185 - 0.190 period (days) 5.4 - 5.3	frequency (cpd) 0.325 - 0.350 period (days) 3.1 - 2.9	frequency (cpd) 0.100 - 0.115 period (days) 10.0 - 8.7	frequency (cpd) 0.165 - 0.175 period (days) 6.1 - 5.7	frequency (cpd) 0.390 to 0.400 period (days) 2.6 - 2.5
PP to -DP	no coherence	infinite	22.0 to 22.5	6.5 to 7	13.5 to 21.0	> 40
DP to -PN	no coherence	18.5 to 19.5	18.0 to 35.0	5.5 to 7.0	14.0 to 21.0	9.0 to 10.0
PN to -LA	no coherence	14.0 to 15.0	23 0 35.0	6.0 to 6.5	29.0 to 40.0	14.5 to 16.0
LA to -CT	2.5 to 3.0	14.0 to 15.0	19.0 to 25.0	5 0 to 5.5	13.0 to 14.0	13.0 to 14.0
PN to CT	11.0 to 18.0	13.5 to 15.0	25.0 to 35.0	5.5 to 6.0	23.0 to 25.5	15.5 to 17.0
CT to CP	2.5 to 3.0	7.0 to 7.5	18.0 to 24.0	3.5 to 4 0	10.0 to 10.5	10.0 to 10.5
CT to CB	4.5 to 5.0	17.0 to 17.5	23.0 to 26.5	9.0 to 9.5	31.0 to 33	21.0 to 22.0
CB to CF	5.0 to 6.0	15 5 to 16.0	22.0 to 29.0	14.0 to 16.0	31.0 to 38.0	17.5 to 18.0
CB to PE	5.0 to 7.5	17.0 to 18.0	21.5 to 31.0	15.0 to 18.0	33.0 to 40.0	19.0 to 20.0
PE to EL	7.0 to 8.5	31.0 to 33.0	27.0 to 30.0	17.0 to 19.0	21.0 to 23.5	30.0 to 30.5
EL to DU	6.5 to 7.5	15.5 to 16.0	15.5 to 23.0	11.0 to 11.5	19.0 to 20.0	22.0 to 23.0
DU to RB	8.0 to 30.0	11.0 to 13.0	9.0 to 11.0	8.0 to 9.0	6.5 to 8.0	13.5 to 14.0

	1985 Sea Level Summer/Autumn			1985 Sea Level Winter/Spring			1982 Sea Level Winter/Spring	
	frequency (cpd) 0.070 - 0.080 period (days) 22.2 - 18.2	frequency (cpd) 0.225 - 0.250 period (days) 4.4 - 4.0	frequency (cpd) 0.280 - 0.300 period (days) 3.6 - 3.3	frequency (cpd) 0.070 - 1.300 period (days) 14.3 - 7.7	frequency (cpd) 0.230 - 0.245 period (days) 4.3 - 4.1		frequency (cpd) 0.075 0.110 period (days) 13.3 - 9.1	frequency (cpd) 0.350-0.370 period (days) 2.9 - 2.7
WB to LB	-	-	-	-5.0 to 10.0	25.0 to 30.0	WB to LB	-	
LB to PN	3.0 to 3.5	8.0 to 12.5	6.5 to 7.0	2.5 to 4.0	22.5 to 23.5	LB to PN	4.0 to 9.0	no cohere
PN to SA	< 0	9.5 to 11 0	10.5 to 12.0	< -10.0	13.0 to 13.5	PN to SA	no cohere	no cohere
SA to GB	4.0 to 4.5	5.5 to 6.0	4.0 to 5.0	8.0 to 14 0	9.0 to 13.0	PN to MB	7 0 to 8.0	no cohere
PN to GB	< 0	9.0 to 9.5	10.0 to 10.5	infinite	12.0 to 12.5	MB to PE	2 5 to 3.5	7.5 to 9.0
GB to SB	3.5 to 4.0	3.5 to 4.0	2.5 to 3.5	-	-	MB to DU	2.0 to 2.5	15.0 to 16.0
GB to MB	7 5 to 8.5	7.5 to 8.0	8.0 to 8 5	5.5 to 15.0	9.0 to 10.0	PE to DU-		
MB to KN	-	-	-	1.0 to 1.5	infinite	-		
MB to PE	-	-	-	2.5 to 3.0	8.0 to 8 5	-		
PE to EL	-	-	-	2.0 to 3.5	4 5 to 5.5	-		

Table 4 Estimated propagation velocities of atmospheric pressure and sea level events between sites along the southern African coastline as estimated from coherence analyses. The velocities are reported in $m.s^{-1}$ with a resolution of 0.5 $m.s^{-1}$. The range in velocities reported is due to the width of each specified frequency range rather than due to the confidence interval of the estimates.

Since the propagation of CTW's along the southern African coastline generally occurs as events rather than a periodic waves, the use of cross-correlations to investigate CTW propagation is perhaps more appropriate than spectral analysis. Cross-correlation have been calculated between adjacent sites and also between all sites and particular reference sites. The same reference sites have been used as in the coherence analyses. To avoid spurious correlations, only the band-pass data have been used in the cross-correlation analyses as the low frequency components of the input time series lead to artificially high correlations between time series. Further, the methods of Davis (1976) and Sciremammano (1979) have been used where the dominant time scales and the different lengths of the time series are taken into account when determining the correlations. The method of Davis presents the correlations in a standard manner, however the significance of the estimates is determined using a reduced number of degrees of freedom (see Appendix C). In the method of Sciremammano (1979), the correlations are normalised by their large lag standard errors which not only gives the strength of the correlation (after taking account of autocorrelation of time series, time series length, dominant time scales, etc.) but also directly provides a statistic which determines the significance of the cross-correlation estimate. Note that, while standard correlations assume a value of between -1 and 1, the normalised correlations have values ranging from -5 to 10.

The time lag in hours of the maximum normalised correlation between times series has been used to estimate the time lags and propagation velocities of CTW's between sites. This is possible because the maximum normalised correlation (Sciremammano, 1979) is by definition also the most significant correlation. In general, the maximum correlation occurs at the same lag as the maximum normalised correlation and there is very little qualitative difference in the correlation fields.

To determine the extent and phase velocity of coherent sea level propagation along the coastline, the 1985 pressure-adjusted sea level at Granger Bay has been cross-correlated with pressure-adjusted sea levels at all sites along the coast. The contours for winter and spring are presented in Fig 5.12. (The data coverage in summer and autumn are inadequate to provide sufficient information along most of the coastline.)

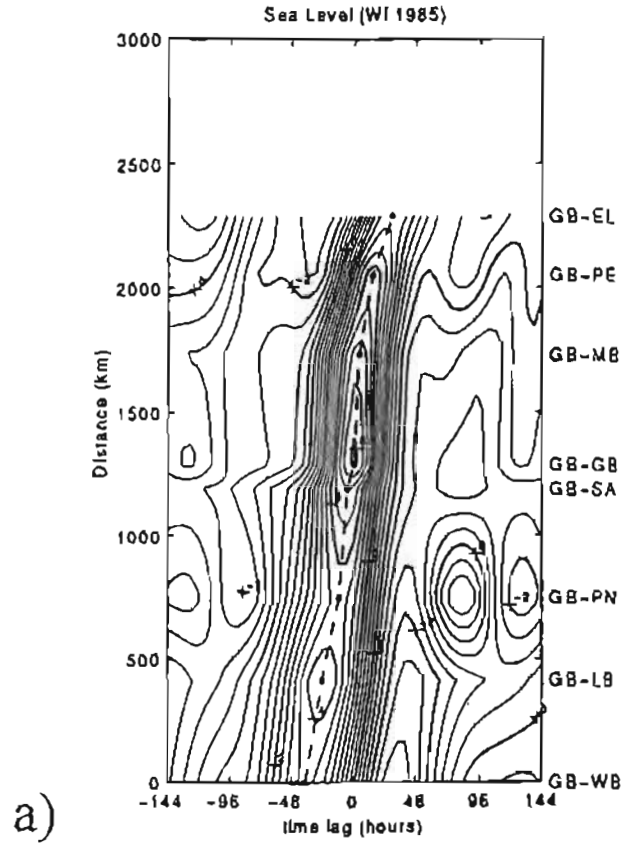

Fig 5.12 Normalised cross-correlation contours between the pressure-adjusted sea level all sites along the southern African coastline and that at Granger Bay for a) winter 1985 and b) spring 1985.

Two noticeable features in Fig 5.12 are the reduced correlation in pressure-adjusted sea levels between Granger Bay and Port Nolloth (in winter), and the significant correlation between the pressure-adjusted sea levels at Durban and those at Granger Bay. Between Granger Bay and Durban the normalised correlations are > 3 (significance > 99%). The magnitude of the standard correlation between Granger Bay and Durban exceeds 0,5. Figure 5.12 and other cross-correlation information indicate a clear continuity in CTW activity between the south coast sites and Durban, however the propagation between East London and Durban is very slow and the amplitude of the sea level event reaching Durban is greatly reduced. Further correlation data for 1985 indicate a distinct difference between CTW propagation on the West and South Coasts in both summer and winter. No such distinction is apparent in the autumn and spring of 1985.

In the absence of appropriate wind data, the propagation velocity of atmospheric pressure systems may be considered to represent the propagation velocities of the wind fields that generate CTW's. The limitations of such an approach are discussed in detail in Chapter 4. Of particular concern is the fact that Schumann (1989) found that the atmospheric pressure systems propagate much more rapidly along the South Coast than the associated wind fields which generate CTW's.

The propagation velocities of atmospheric pressure systems along the southern African coastline in 1982 and 1985 (as estimated from cross-correlation analyses) are presented in Fig 5.13. The coastal low develops in the vicinity of Walvis Bay and Lüderitz Bay, consequently the high estimates of the propagation velocities between these two sites most probably represents shifts in the large scale pressure fields rather than the southwards propagation of the coastal low. The propagation velocity of atmospheric pressure systems (coastal lows) along the West Coast varies from 10 $m.s^{-1}$ to 15 $m\,s^{-1}$, increases rapidly along the south coast and typically reaches a maximum between Port Elizabeth and East London. Jury *et al.* (1990a,b) have commented upon this acceleration of the weather systems in the vicinity of Port Elizabeth and ascribe this acceleration to the influence of the warm Agulhas Current on the overlying atmosphere. The propagation velocities of these atmospheric pressure systems decrease rapidly towards Durban (see Fig 5.13).

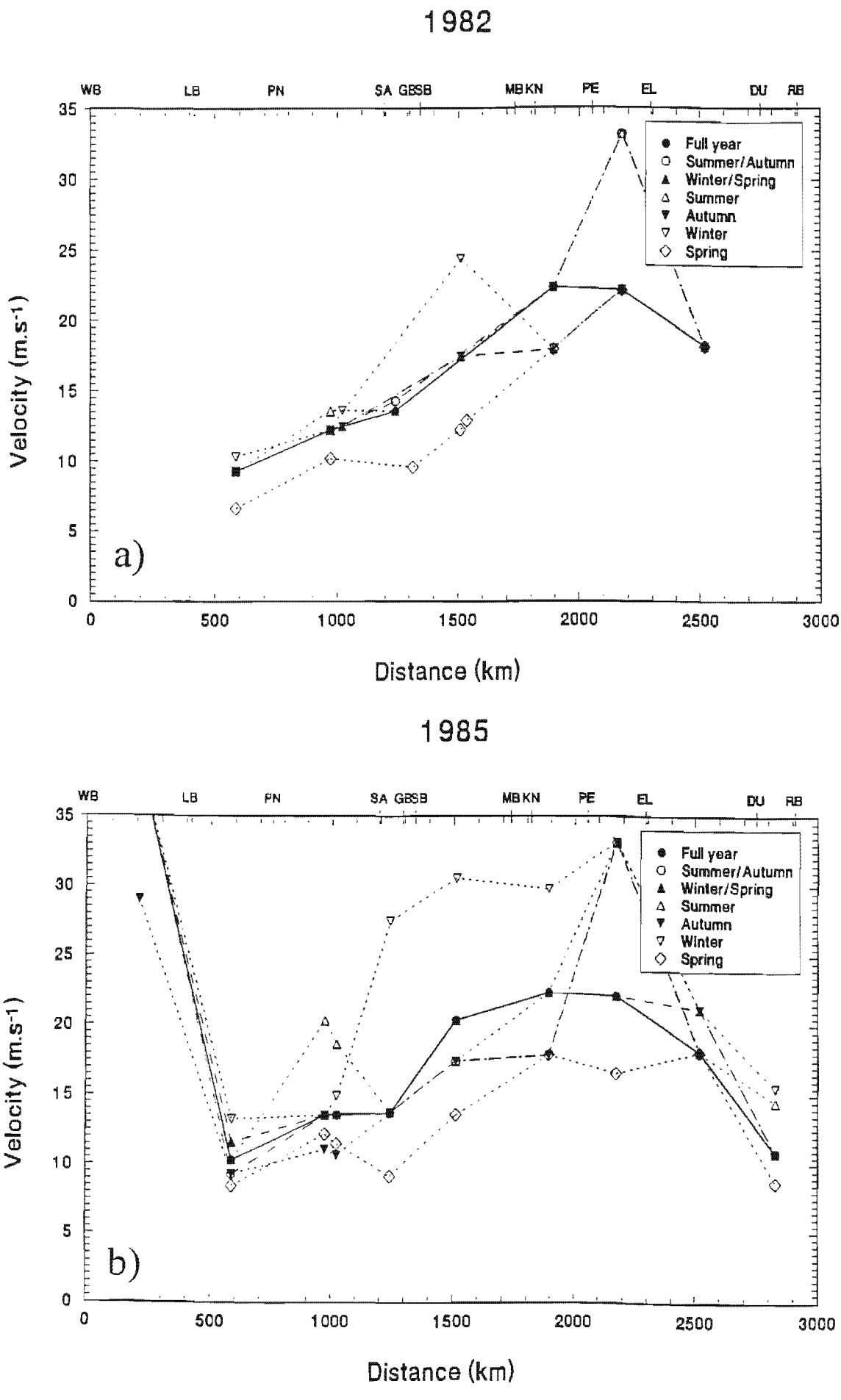

Fig 5.13 The propagation velocities of atmospheric pressure systems along the southern African coastline (estimated from cross-correlation analyses) for a) 1982 and b) 1985.

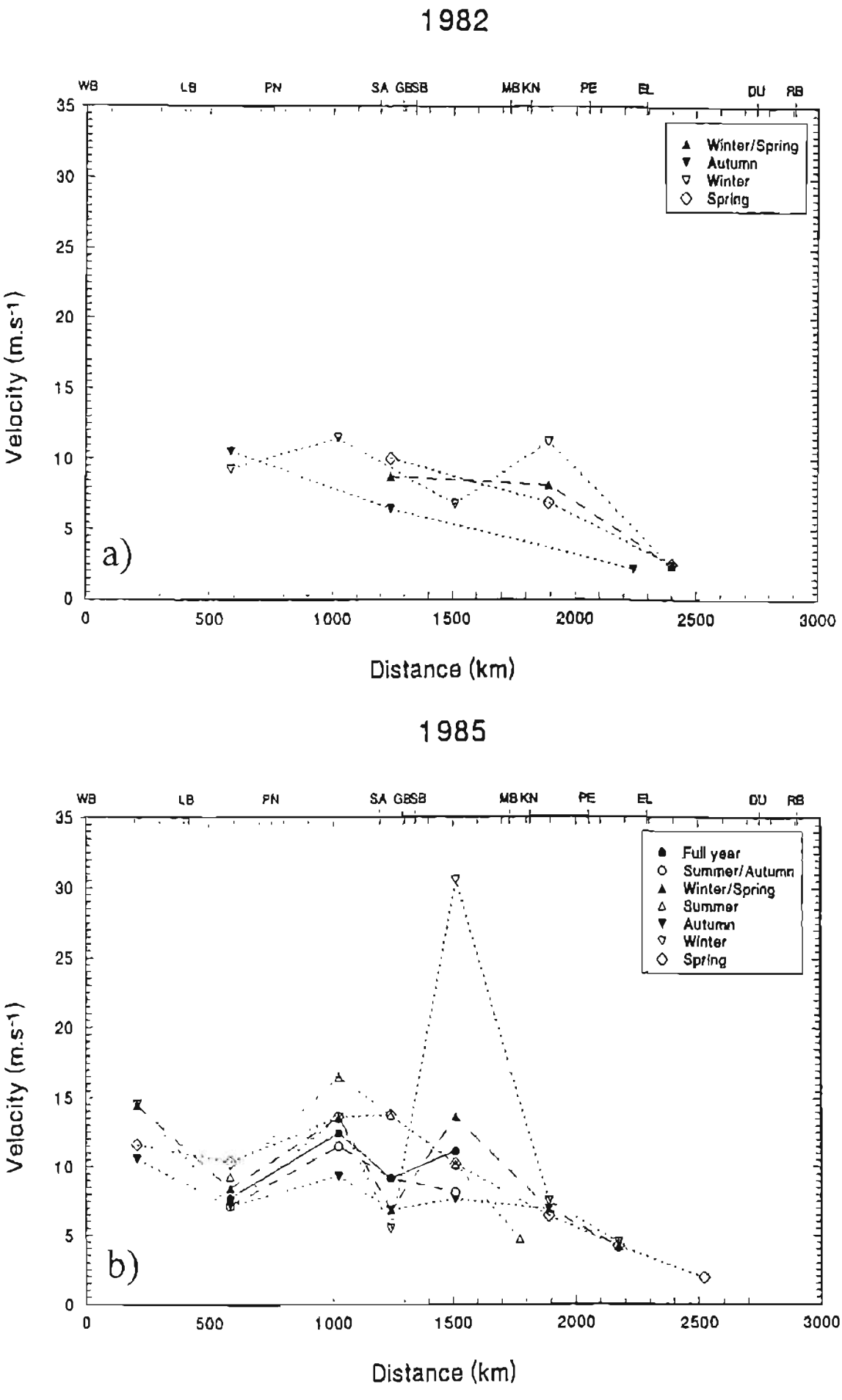

Fig 5.14 The propagation velocities of pressure-adjusted sea level events (CTW's) along the southern African coastline (estimated from cross-correlation analyses) for a) 1982 and b) 1985.

Similarly, the propagation velocities of sea level events along the southern African coastline in 1982 and 1985 (as estimated from cross-correlation analyses) are presented in Fig 5.14. The sea level events typically propagate along the West and South coast at 7 $m.s^{-1}$ to 15 $m.s^{-1}$, slowing dramatically to approximately 2,5 $m.s^{-1}$ as they propagate beyond Port Elizabeth towards Durban. This reduced propagation velocity beyond Port Elizabeth is not unexpected as the theoretical propagation velocities for free CTW's are small on the narrow East Coast, especially if the influence of the opposing Agulhas Current is taken into account (Table 2, p49). Similarly, the estimated propagation velocities of the CTW events qualitatively reflect the theoretical propagation velocities of free CTW's along other sections of the southern African coastline (see Fig 5.15a). Of particular interest is the sharp increase in propagation velocities between Port Nolloth and Granger Bay. The estimates of propagation velocities between Port Nolloth and Saldahna Bay (not shown) are even larger. This observation is consistent with the notion that only the lower frequency (higher phase velocity) components of the CTW's propagate between Port Nolloth and Granger Bay, the higher frequency (lower phase velocity) components of the CTW's being topographically scattered by the large alongshore variations in topography in this region.

5.4.3 Wind-Forcing of CTW's around Southern Africa

If one assumes that the propagation velocities of the atmospheric pressure systems reflect the propagation velocities of the wind systems along the southern African coastline, cross-correlations between atmospheric pressure and pressure-adjusted sea levels will provide information on the forcing of CTW's around southern Africa. Although such an assumption is known to be incorrect for the South Coast (Schumann, 1989), cross-correlations between atmospheric pressure and pressure-adjusted sea levels are nevertheless informative.

The propagation velocities of atmospheric pressure systems (Fig 5.13) and pressure-adjusted sea levels (Fig 5.14) suggest that a resonance condition between the wind associated with the atmospheric weather systems and the ocean should only exist along the West Coast where the propagation velocities of the atmospheric pressure systems are similar to the theoretical free CTW phase velocities. On the South Coast the

propagation velocities of the atmospheric pressure systems greatly exceed the theoretical free CTW phase velocities. This suggests that the winds associated with the atmospheric weather systems propagate too rapidly along the south coast to be able to generate a strong sea level response. However, observations indicate that the amplitude of the sea level events reaches a maximum between Mossel Bay and Port Elizabeth, implying that there is effective forcing of CTW motions over most of the Agulhas Bank. This can only occur if the wind systems travel more slowly over the Agulhas Bank (i.e. at approximately the same velocity as free CTW's) than do the atmospheric pressure systems. The observations are therefore consistent with the results of Schumann and Brink who state that the wind systems propagate more slowly along the South Coast (7,5 $m.s^{-1}$) than the atmospheric pressure systems and consequently provide a particularly efficacious forcing mechanism for CTW's over the Agulhas Bank.

Space-time cross-correlations between alongshore winds and sea level (see Schumann and Brink, 1990) are expected to have a maximum correlation along a line having the same slope as the theoretical free CTW phase velocity Schumann and Brink (1990) find that on the South Coast the slope of the maximum correlation (7,5 $m.s^{-1}$) closely matches the theoretical free CTW phase velocities for the South Coast (8,0 $m.s^{-1}$). A similar analysis along the West Coast is not possible due to a lack of suitable wind data. The slope of a line of maximum correlation between 1985 atmospheric pressure and pressure-adjusted sea levels (not shown) varies between 6 $m.s^{-1}$ and 9 $m.s^{-1}$ on the West Coast and 9 $m.s^{-1}$ and 19 $m.s^{-1}$ on the South Coast.

A cross-correlation between the atmospheric pressure and sea level at sites along the coastline indicate that the atmospheric pressure minimum associated with the coastal low on the West Coast and the coastal low or mid-latitude cyclones on the South Coast leads the sea level maximum associated with CTW's in these regions. The atmospheric pressure minimum leads the pressure-adjusted sea level maximum by between 24 hours and 40 hours on the West Coast and by between 24 hours and 30 hours on the South Coast. On the Southeast and East Coast, the atmospheric pressure lead increases rapidly as the propagation of the sea level maximum associated with the CTW's slows and the atmospheric pressure systems accelerate over the

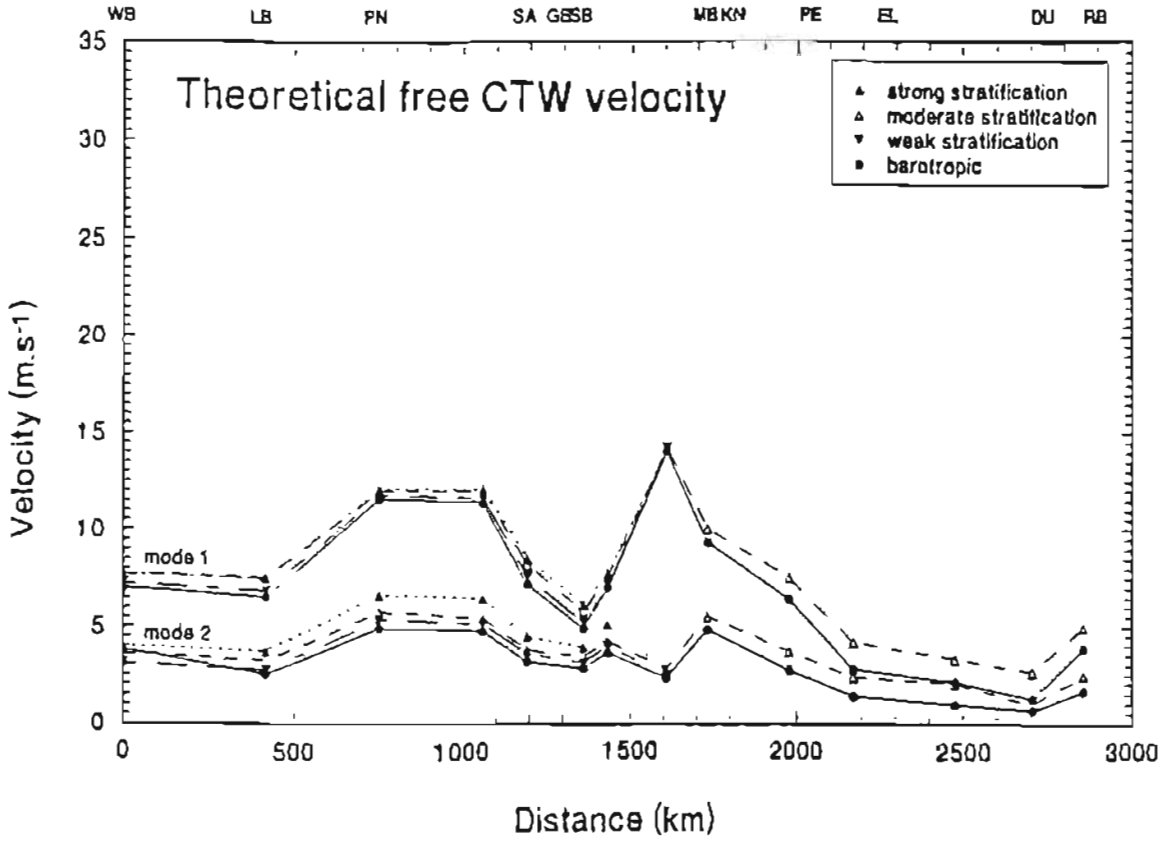

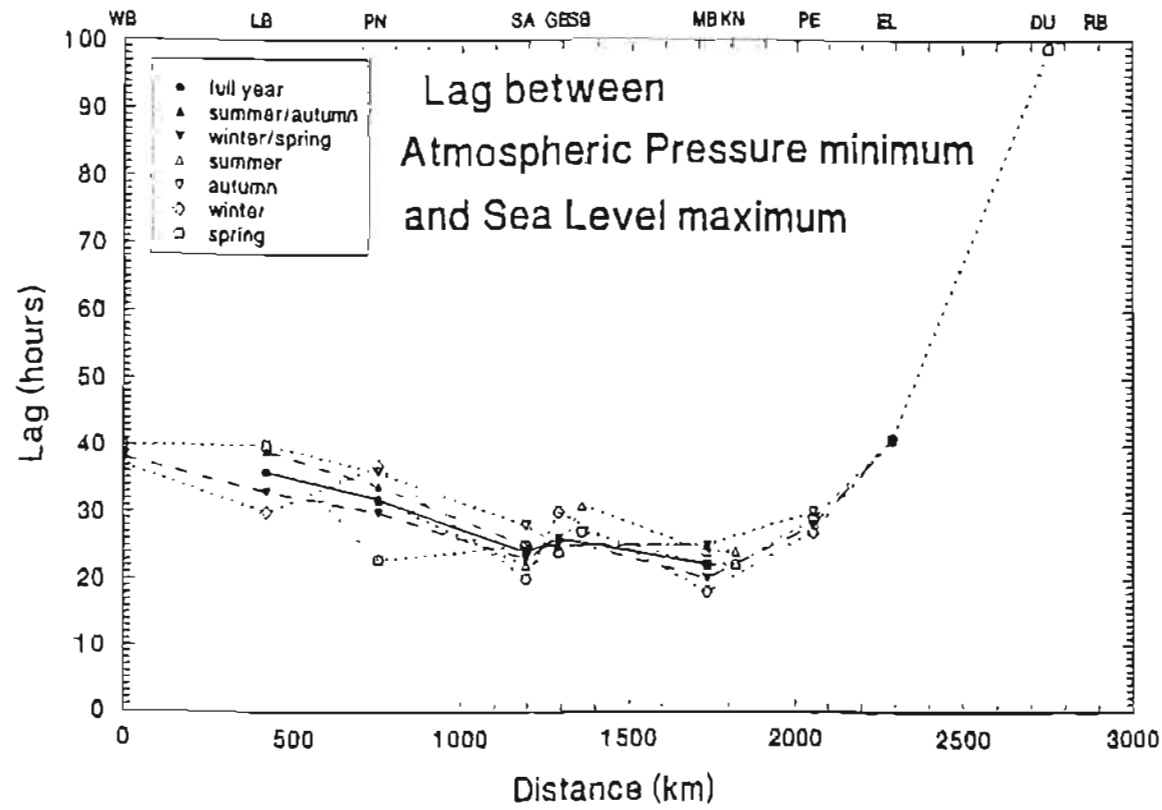

Fig 15.15 a) Theoretical first and second mode free CTW velocities for the shelf region surrounding southern Africa, and
b) the time lag between the atmospheric pressures minimum associated with the coastal low or mid-latitude cyclones and the pressure-adjusted sea level maximum associated with CTW propagation.

Agulhas Current. The results in Fig 5.15b seem to indicate that the atmospheric weather systems and their associated winds start to "outrun" the sea level anomalies associated with CTW's in the ocean in the vicinity of Port Elizabeth. One can therefore tentatively assume that only free CTW activity occurs between East London and Durban. Further, the uniformity of phase velocity estimates for the propagation of sea level events along the East Coast and their qualitative agreement with theoretical estimates of free CTW propagation velocities for the East Coast, is consistent with the CTW motions in this region being free rather than forced CTW motions.

The relative minimum in the lag between the atmospheric pressure minimum and the sea level maximum on the South Coast (Fig 15.5b) can be ascribed to the fact that the atmospheric pressure minimum on the South Coast is often associated with the mid-latitude cyclone that trails the coastal low rather than the coastal low itself. Thus the reduced lag between the atmospheric pressure minimum and the sea level maximum on the South Coast.

5.4.4 Remote Forcing of CTW's around Southern Africa

Analysis of sea level data indicates that not all CTW activity on the shelf surrounding southern Africa is directly forced by wind. In particular, low frequency CTW motions may originate from the shelf regions north of Walvis Bay or may occur anywhere along the shelf due to open ocean forcing. While there is no evidence of interaction between shelf water on the West Coast and open-ocean rings (as documented by Duncombe Rae *et al.*, 1992), contours of low frequency variations in the 1985 pressure-adjusted sea levels provide evidence of remotely forced sea level variability both over the West Coast and East Coast shelf regions.

A strong low frequency signal with a periodicity of approximately 40 days is observed in the pressure-adjusted sea levels along the southern African coastline for the period March 1985 to May 1985 (see Fig. 5.8b, p100) These sea level fluctuations are unusual in that there is no concomitant low frequency variability in atmospheric pressures (and presumably winds) during this period. Further, the pressure-adjusted sea level fluctuations of approximately 10 cm to 15 cm at Walvis Bay are unusually large for this location and can therefore be assumed to have their origin to the north of

Walvis Bay, possibly originating near the equator. These "remotely forced" CTW motions persist for a few months and are observed to propagate at least as far as East London at velocities of between 1,6 $m.s^{-1}$ and 2,7 $m.s^{-1}$ (Fig 5.16).

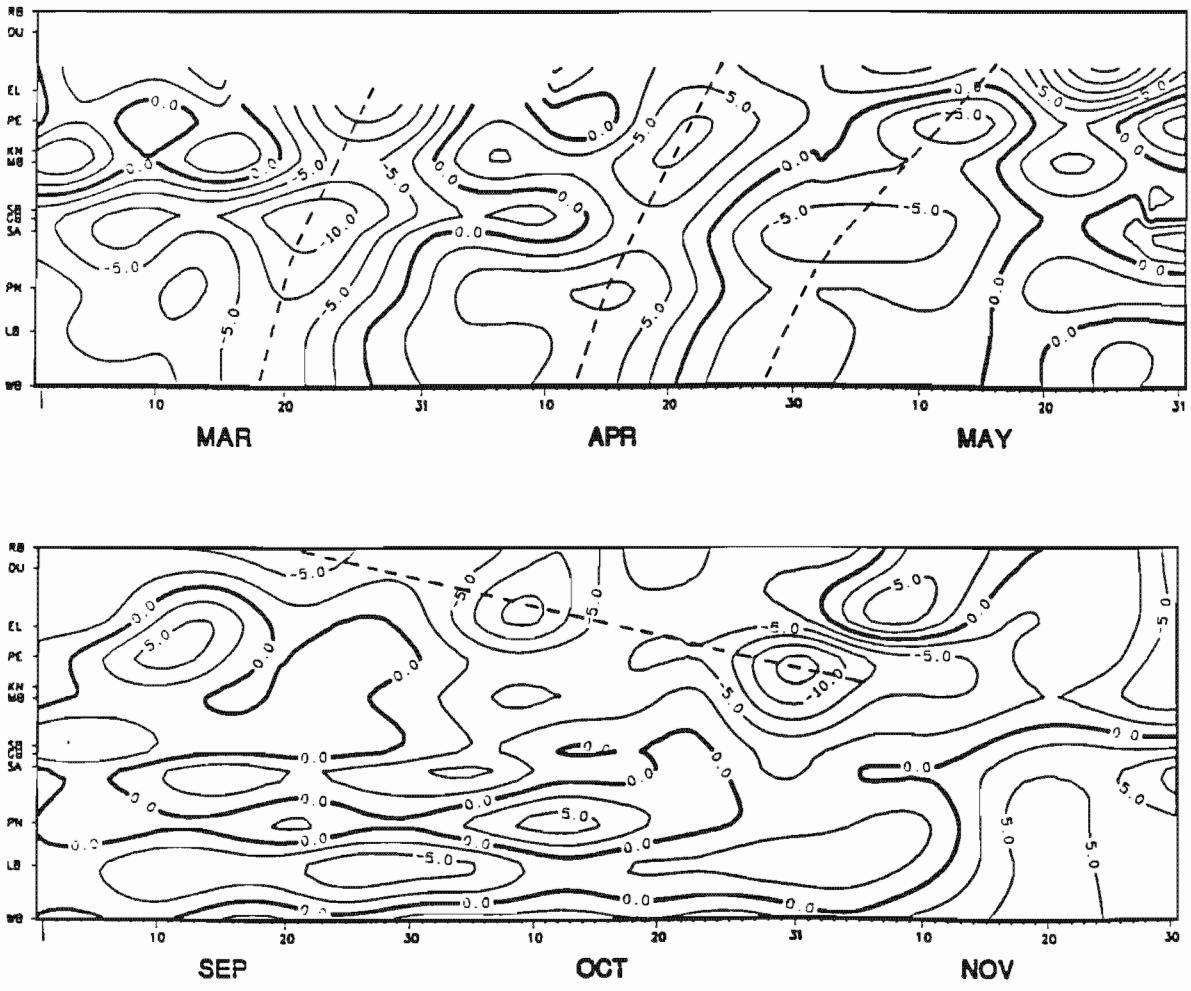

Fig. 5.16 Contours of the low frequency variability in the 1985 pressure-adjusted sea levels over the southern African shelf.

Large amplitude sea level variability is also observed on the East Coast in spring 1985. Sea level fluctuations of approximately 5 cm to 15 cm are observed at Durban, increasing to 10 cm at East London and almost 15 cm at Port Elizabeth. Unlike the CTW motions described above, the sea level anomaly propagates clockwise along the coastline from Durban to Port Elizabeth at approximately 20 $cm.s^{-1}$. Current meter data and satellite infra-red imagery indicate that this sea level signal is related to the progression of a Natal Pulse (a large perturbation in the Agulhas Current) along the East Coast. Associated with the Natal Pulse are strong reversals of the currents over

the shelf (Lutjeharms and Connell, 1989). Although these shelf currents cannot be considered to be forced CTW motions, the influence of the Natal Pulse gives an indication the extent to which open-ocean forcing can modify shelf circulation. There is ample (albeit less dramatic) evidence of such open-ocean forcing of shelf circulation along the East Coast and the strong low frequency variability observed at the East Coast sites can largely be attributed to such open-ocean forcing of shelf waters.

The open-ocean or remotely forced shelf variability described above is not as predictable as wind-forced CTW activity. In particular the remotely forced CTW activity originating north of Walvis Bay may modulate the environmental variability over much of the shelf region of southern Africa in a somewhat less predictable manner than the locally wind-forced CTW activity. (It should be noted however that remotely forced fluctuations originating equatorwards of the region of interest may be in principle be hindcast given the appropriate data.)

Although the use of wind and current meter data are most appropriate for characterising CTW activity along the southern African coastline, very little such data is available. Atmospheric pressure and sea level data have been used due to their availability and more extensive temporal and spatial coverage, however these data are only able to provide a limited characterisation of CTW activity over the continental shelf of southern Africa. Given these limitations, further characterisation of CTW's along the southern African coastline can only be accomplished through theoretical and modelling studies. In the chapters that follow a numerical model is developed and used to investigate the forcing and propagation of CTW's along the West Coast of southern Africa.

6. THE BAROTROPIC CTW NUMERICAL MODEL

In Chapter 7 the homogenous, shallow water wave equations are solved numerically to investigate the barotropic CTW response off the West Coast. Great care should be taken when interpreting these modelling results because the set of discretised equations used in the numerical model have certain properties which differ from those of the continuum equations. The smaller spatial and temporal scales are often inadequately resolved in the computational grid and at the boundaries of a numerical model. The consequence is numerical dispersion and the introduction of noise into the numerical domain.

Through careful design of the numerical model it is possible to minimise (but not totally remove) the impacts of numerical dispersion and computational noise which may severely degrade the accuracy of the numerical solutions. This requires an appropriate choice of finite difference scheme and computational grid, and suitably formulated boundary conditions. The chosen numerical model and associated computational grid, offshore/coastal/cross-shelf boundary conditions, surface and bottom boundary conditions and the numerical model diagnostics are described and discussed in this chapter.

6.1 The Continuum Equations

While the full primitive equations of motion are required to model the total (combined barotropic and baroclinic) response of shelf waters to atmospheric forcing on all temporal and spatial scales, the scaling arguments in previous chapters indicate that the *low-frequency* response of shelf waters to *synoptic-scale* atmospheric forcing primarily comprises large-scale, wind-forced, *barotropic* motions. In stating the above it is assumed that

a) $\frac{\eta}{H} \ll 1$,

b) atmospheric pressure forcing is negligible,

c) the spatial scales of interest are sufficiently large to preclude non-linear effects,

i.e. $\frac{U}{fX} \ll 1$, $\frac{V}{fY} \ll 1$,

d) the characteristic spatial scales of the bottom topography are much greater in the longshore direction than in the cross-shore direction (boundary layer scaling), i.e. $\frac{X}{Y} \approx \frac{U}{V} \ll 1$ and,

e) that the stratification parameter (Burger number) is everywhere small ($S \ll 1$).

Under the above assumptions, the expected predominantly low-frequency, barotropic response of shelf waters to synoptic-scale forcing can successfully be modelled using the homogenous, linear shallow water wave equations.

Boundary layer scaling arguments indicate that the low-frequency barotropic response over a shelf having little or no longshore variation in the bottom topography, is essentially non-divergent (see appendix A). Assuming non-divergence, it is possible to implement a "rigid lid" boundary condition at the sea surface and consequently introduce a streamfunction. This allows the shallow water equations to be reduced to a single vorticity equation (for example Mysak, 1980a). The use of such **vorticity-streamfunction** equations in a numerical model is computationally efficient as the assumption of a "rigid lid" boundary condition at the sea surface "filters out" a large class of fast-moving waves (gravity-inertia waves) that would normally severely restrict the magnitude of the time step required to ensure numerical stability in an explicit numerical model. However, a numerical model based on the vorticity-streamfunction equations is restrictive in that, a) surface gravity waves which allow for rapid flow adjustments in the model are "filtered out", and b) the vorticity-streamfunction equations do not explicitly provide information on the sea level response associated with low-frequency barotropic motions over the shelf.

The homogenous **shallow water wave equations**, although computationally more expensive to solve, do allow for surface divergence and thus a more general response. Further, solutions to the shallow water wave equations both include surface gravity waves (which allow for rapid flow adjustments) and provide information on the sea level response associated with CTW's. For these reasons the shallow water wave equations have been chosen as a basis for the numerical model used in chapter 7 to investigate the low-frequency barotropic response over a realistic shelf topography.

However, should the water column stratification be so large that the stratification parameter nears or exceeds unity ($S \geq 1$) or should the alongshore variations in topography be extreme, the effects of stratification within the water column become significant and it is necessary to revert to the full set of equations of motion where variable densities are explicitly considered.

Since it is intended to model the low frequency barotropic response over a shelf which has significant (but not excessive) alongshore variation in the bottom topography and where the stratification parameter is small ($S \ll 1$), it is appropriate to use the homogenous, linear shallow water wave equations as the basis of such a numerical model. Further, the β-effect and non-linear effects are assumed to be negligible and the equations of motions used (the homogenous, linear, f-plane shallow water wave equations) are as follows

$$\frac{\partial u}{\partial t} - fv = -g\frac{\partial \eta}{\partial x} + \frac{1}{\rho h}\left[\tau_w^x - \tau_b^x\right] \tag{6.1}$$

$$\frac{\partial v}{\partial t} + fu = -g\frac{\partial \eta}{\partial y} + \frac{1}{\rho h}\left[\tau_w^y - \tau_b^y\right] \tag{6.2}$$

$$\frac{\partial \eta}{\partial t} = -\left(\frac{\partial (hu)}{\partial x} + \frac{\partial (hv)}{\partial y}\right) \tag{6.3}$$

where $f = 2\Omega \sin\theta_0$, $\tau_b^x = \rho r u$ and $\tau_b^y = \rho r v$ and u and v are the cross-shore and longshore velocities, respectively. To ease the development of the FORTRAN code for the numerical model, the shallow water wave equations have been implemented after re-writing them in terms of vertically integrated transports U and V, namely

$$\frac{\partial U}{\partial t} - fV = -gh\frac{\partial \eta}{\partial x} + \frac{1}{\rho}\left[\tau_w^x - \tau_b^x\right]$$

$$\frac{\partial V}{\partial t} + fU = -gh\frac{\partial \eta}{\partial y} + \frac{1}{\rho}\left[\tau_w^y - \tau_b^y\right]$$

$$\frac{\partial \eta}{\partial t} = -\left(\frac{\partial U}{\partial x} + \frac{\partial V}{\partial y}\right)$$

where $f = 2\Omega \sin\theta_0$, $\tau_b^x = \frac{\rho r U}{h}$ and $\tau_b^y = \frac{\rho r V}{h}$ and $U = hu$ and $V = hv$ are the cross-shore and alongshore vertically integrated transports.

6.2 The Finite-Difference Numerical Scheme and the Computational Grid

The combination of an Arakawa-C (Richardson) finite difference grid having a non-uniform spatial specification (Batteen and Han, 1981) and an Euler forward-backward finite difference scheme (Martinssen *et al.*, 1979) is the most accurate and computationally efficient combination possible for the numerical investigation which follows. The rationale behind the choice of the above combination is given in section 6.3 and in Appendix D where the Arakawa-C finite difference grid and Euler forward-backward finite difference numerical scheme are described in detail and the numerical properties of the chosen combination are discussed.

6.2.1. The Computational Grid

The shallow water wave equations (equations A.1 to A.3 in Appendix A) permit two distinct types of motion (Mesinger and Arakawa, 1976), namely low-frequency quasi-geostrophic and quasi-nondivergent flow, and high and low frequency gravity-inertia waves. Since these gravity-inertia waves are important to adjustment processes in large-scale motions, it is essential to represent these waves as accurately as possible within the numerical grid. An overview of grid meshes by Haltiner and Williams (1980) specifies a number of staggered grids that are most efficient in the finite difference numerical modelling of mesoscale processes. (A staggered grid is one in which the different variables are not spatially coincident) The most suitable of these staggered grids for the mesoscale modelling undertaken here is the Arakawa-C (Richardson) grid (Batteen and Han, 1981; Foreman, 1987). When combined with a suitable finite difference numerical scheme (in this case the Euler forward-backward numerical scheme), the Arakawa-C grid has the most favourable phase and group velocity properties (see 6.3 Stability and Dispersion Properties of the Numerical Scheme) and also suppresses the two-grid interval noise common to many other more complicated finite difference numerical scheme and grid combinations (Engedahl, 1992). In addition to a staggered grid, a non-uniform spatial specification of variables in the offshore direction has been chosen (Fig. 6.1). This further reduces memory storage and computation time requirements. The numerical stability of the Euler forward-backward finite difference scheme used, is dependent on the relationship between the time step Δt, grid spacings Δx (offshore) and Δy (alongshore), and the

depth, h. For this reason, the non-uniform, offshore grid spacing (Δx) is loosely related to the water depth (h). Roughly speaking, the greater the underlying water depth , the greater is the magnitude of the offshore grid spacing required to ensure computational stability in the explicit finite difference scheme used. The spatial relationship between the variables on the Arakawa-C grid is illustrated in Fig 6.1.

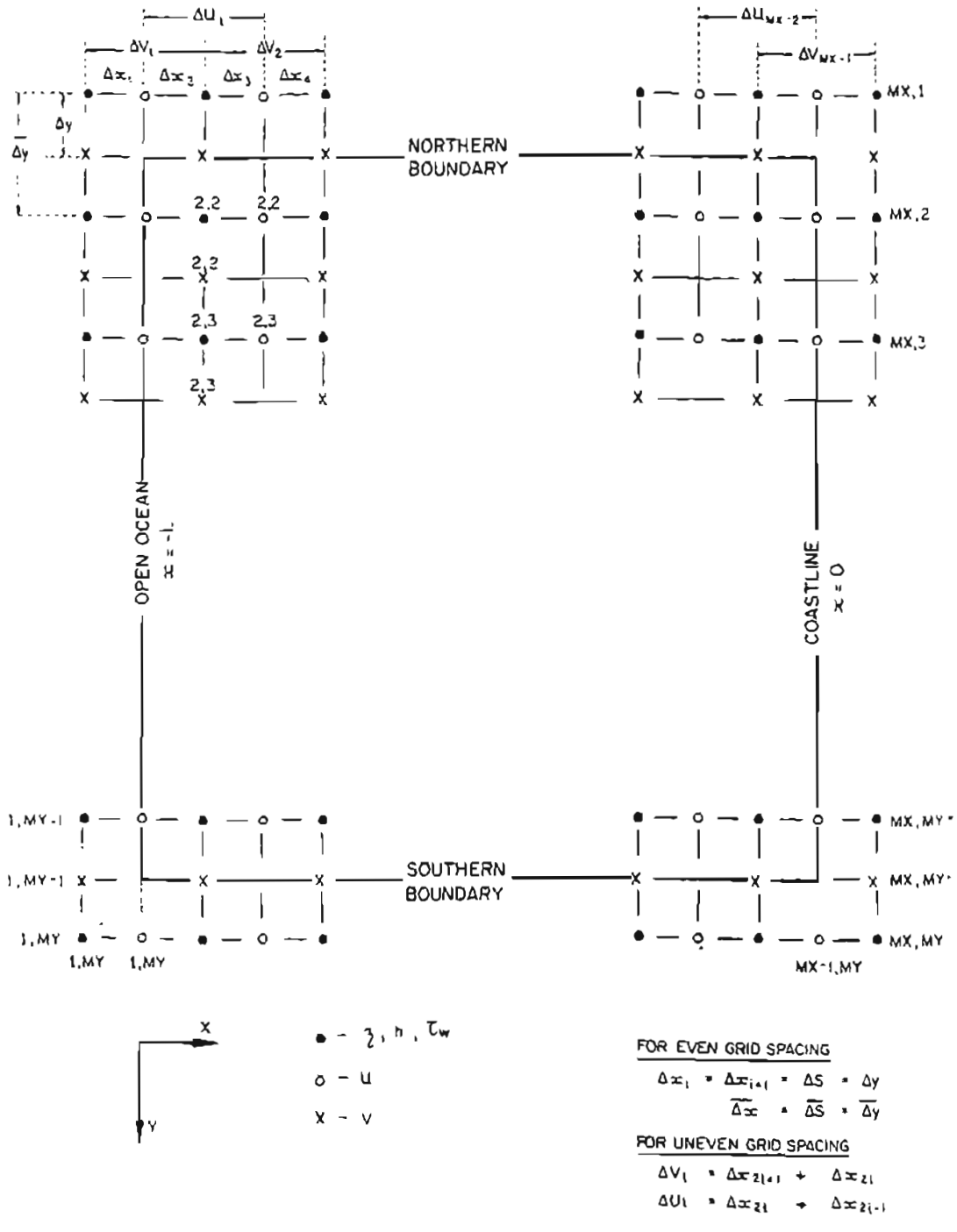

Fig 6.1 The Arakawa-C grid used in the numerical model

6.2.2. The Euler Forward-Backward Finite Difference Scheme

The choice of the Euler forward-backward scheme is closely allied to fact that the Arakawa-C grid is used (see Appendix C for details of the finite difference numerical scheme). The Euler forward-backward scheme is semi-implicit finite difference scheme, although the fields $(\eta, U, V)_{i,j}^{n+1}$ are obtained in an explicit manner. In the absence of advection (non-linear) terms and for a constant depth, this finite difference scheme is $O(\Delta x^2)$ accurate in space and $O(\Delta t^2)$ accurate in time. Being essentially a two-level scheme, computational modes are avoided so there is no computational overhead required to remove spurious computational modes. When uneven grid spacings are used, the finite difference scheme becomes considerably more complicated (see Appendix C) and the finite difference scheme is then only $O(\Delta x_i - \Delta x_{i-1})$ accurate. However, one can specify the uneven grid spacings such that $O(\Delta x_i - \Delta x_{i-1}) \approx O(\Delta x^2)$ and thus maintain the second order spatial accuracy of the numerical scheme.

6.3 Stability and Dispersion Properties of the Numerical Scheme

6.3.1 Requirements for Numerical Stability

The stability properties of the semi-implicit Euler Forward-backward finite difference scheme are outlined in Appendix C. For a finite difference grid where the cross-shore and alongshore spacings are not equal (i.e. $\Delta x \neq \Delta y$), the stability criterion, the Courant-Friederich-Lewy (CFL) condition is

$$\frac{\overline{\Delta x}}{\Delta t} \geq \sqrt{gh\left[\left(\frac{\overline{\Delta x}}{\overline{\Delta y}}\right)^2 + 1\right]} \qquad or \qquad \frac{\overline{\Delta y}}{\Delta t} \geq \sqrt{gh\left[\left(\frac{\overline{\Delta y}}{\overline{\Delta x}}\right)^2 + 1\right]}$$

and $\Delta t \leq 2/f$

where $\overline{\Delta x} = 2\Delta x$, $\overline{\Delta y} = 2\Delta y$ are the distances between two variables of the same type within the grid in the cross-shore and alongshore direction, respectively. When the grid spacings are equal (i.e. $\overline{\Delta x} = 2\Delta x$, $\overline{\Delta y} = 2\Delta y$) then the stability criteria reduce to

$$\frac{\overline{\Delta x}}{\Delta t} \geq \sqrt{2\,gh} \qquad or \qquad \frac{\overline{\Delta y}}{\Delta t} \geq \sqrt{2\,gh}$$

and $\Delta t \leq 2/f$

Provided that the CFL condition is satisfied, the numerical scheme is neutral (errors are not amplified). If bottom friction is included, the scheme becomes a slightly damping scheme (see Appendix C), where the magnitude of the damping depends linearly on the amplitude of the friction. With the largest allowable time step, the maximum phase speed possible of a wave in the grid is a factor of $\sqrt{2}$ larger than the barotropic gravity wave speed, enabling the scheme to adequately model even the fastest gravity waves.

If the mismatch in magnitude of $\overline{\Delta x}$ *and* $\overline{\Delta y}$ is not too great (i.e. $\overline{\Delta x}/\overline{\Delta y} \approx O(1)$), then time step (Δt) is not unduly restricted compared to the case of an evenly spaced grid. Further, the CFL condition for the staggered grid is twice as restrictive as that for a standard grid (where all the variables are coincident on the mesh). However, the finite difference scheme on the staggered grid is more accurate in space. Since errors (in accuracy and phase properties) in finite difference schemes are almost entirely due to the spatial discretization (Foreman, 1987), the required doubling of the number of time steps seems a small price to pay for increased accuracy in the spatial domain.

For the spacing used in the grid (Δx = 5 km, Δy = 10 km), a time step of Δt = 60 seconds is adequate to ensure stability of the numerical scheme. Where a realistic bottom topography is used, the fine mesh overlies deep water in the southern regions of the model. Here a more restrictive time step of Δt = 45 seconds is required.

6.3.2 Numerical Dispersion

The dispersion properties of external gravity waves in the discretized equations differ from those in the continuum equations. This difference in the phase behaviour of the external gravity waves in the finite difference numerical scheme and the continuum equations is due to numerical dispersion. The numerical dispersion inherent to the Euler forward-backward scheme is discussed in Appendix C, where it is shown to be dependent on the spatial arrangement of the variables, the magnitude of the spatial increments (Δx and Δy), and the time increment (Δt). Thus the alongshore grid increment has here been kept at a constant value of Δy = 10 km ($\overline{\Delta y}$ = 20 km) to ensure that the alongshore dispersion properties of the scheme do not change.

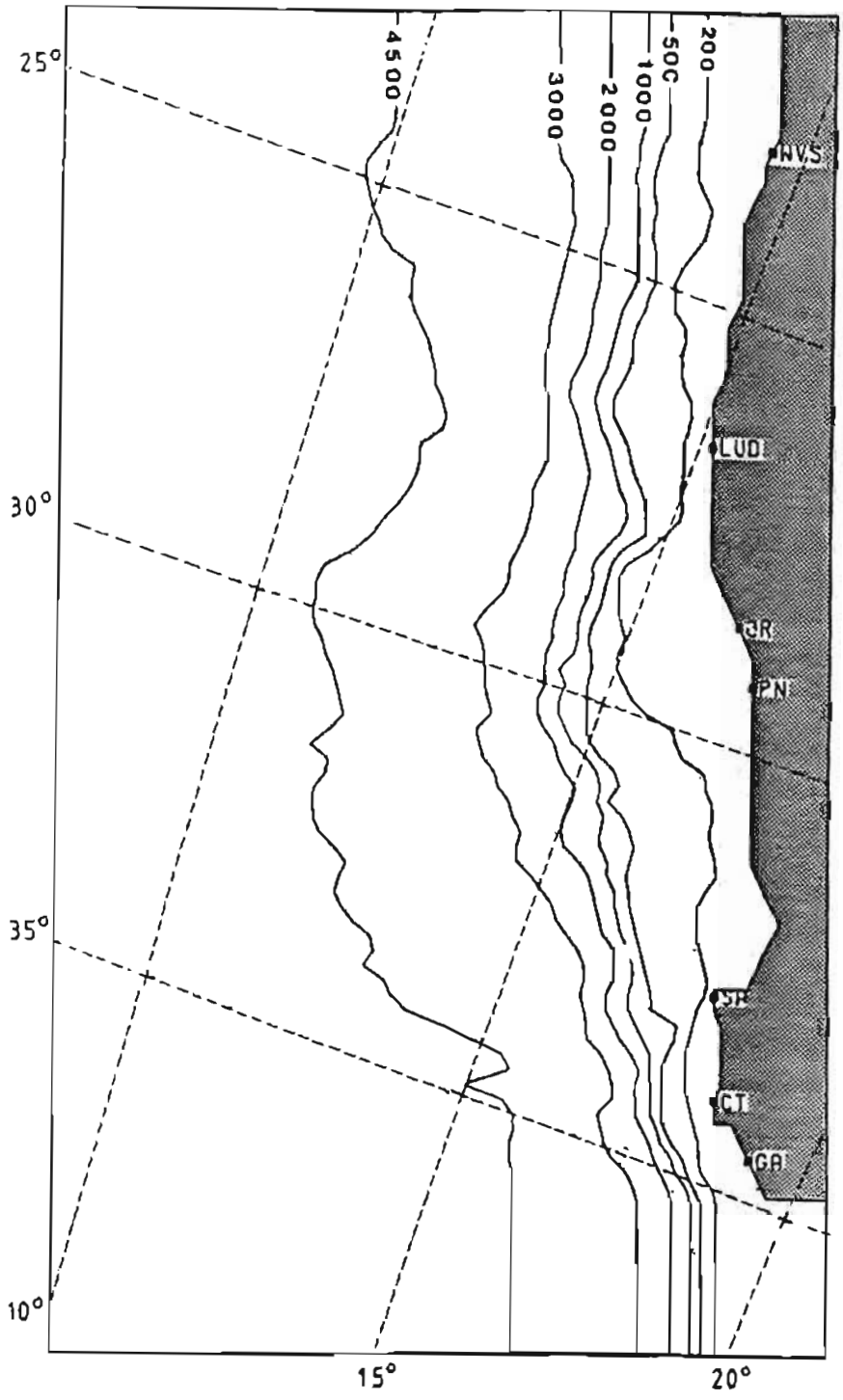

Fig 6.2 The orientation of the bottom topography and coastline used in the numerical model

The relative phase errors that occur due to numerical dispersion are small for all but the shortest resolvable wavelengths, $\lambda_x = 4\Delta x$ and $\lambda_y = 4\Delta y$ (i.e. the phase speed of waves in the numerical model compare well with those in the continuum equations for all but the shortest resolvable wavelengths). The shortest resolvable wavelengths have a zero group velocity in the numerical domain (Mesinger and Arakawa, 1976;

Foreman, 1987) and thus can lead to trapping of energy at specific locations in the numerical domain where these shortest resolvable wavelength motions are excited. This can unfortunately lead to problems at open boundaries where inferior open boundary conditions can introduce "noise" at these short wavelengths.

In this investigation, $\Delta x \geq 5$ km and $\Delta y = 10$ km and the shortest resolvable wavelengths in the cross-shore direction are $\lambda_x \geq 20$ km and in the alongshore direction are $\lambda_y = 40$ km. It is important to be aware of these phase properties when interpreting the outputs from the numerical model, especially where topographic scattering results in the presence of higher mode, shorter wavelength CTW motions.

6.4 The Bottom Topography in the Numerical Model

The bottom topography has been digitized from a chart by Dingle *et al.* (1977), rotated clockwise through 20° and scaled to account for the fact that the bottom topograpghy has been derived from a Mercator projection (Fig. 6.2). These digitized depth values were then interpolated onto the staggered grid mesh (Fig. 7.1b, p140).

6.5 The Boundary Conditions in the Numerical Model

The boundary conditions used in the numerical model are essentially a barotropic form of those utilised by Clarke and Brink (1985).

6.5.1 The Coastal Boundary Condition

The boundary condition applied at the coastline is simply that there is no cross-shelf volume transport at the coast

$$h(0)u = 0 \qquad \text{at} \quad x = 0$$

where $h(0)$ is the depth at the coastline. However, singularities can occur if $h(0) = 0$ at the coastline (Mysak, 1980a), therefore in the model the coastal boundary condition is applied at a small distance ($-b$) from the coastline i.e.

$$h(-b)u = 0 \quad or \quad U(-b) = 0 \qquad \text{at} \quad x = -b$$

where $h(-b)$ is the depth at a small offshore distance, $-b$, from the coast and $U(-b)$ is the cross-shelf volume flux at this location.

Mitchum and Clarke (1986a) show that, even for the more general equations required for stratified shelf waters, no significant error is introduced by assuming such a boundary condition. To exclude the highly turbulent inner shelf, they assume a "coastal wall" at a water depth which is three times the scale thickness of the turbulent (Ekman) boundary layer. Because the wind still excites motions within this nearshore region, ideally a (often small) correction proportional to the alongshore wind stress must be added to the "coastal sea level" to achieve the desired accuracy when applying CTW theory to observations (Mitchum and Clarke, 1986b). Here the correction is assumed to be negligible and a "coastal wall" is assumed to exist at $h(-b) = 25$ m. The coastal boundary condition (zero flux through the coastal boundary) is implemented numerically as

$$U_{i,j} = 0 \quad \text{for a straight coastline}$$

or

$$U_{i,j} = V_{i+n,j} = 0 \quad \text{for an irregular coastline}$$

where i,j are the coastal boundary mesh points in the numerical grid and $n = 0$ or $n = 1$, depending on the changes in the coastline.

Spurious short wavelength oscillations may occur along such a boundary for a very coarse resolution of the coastline. The criterion given by Pederson (1986) suggests that for the resolution in the present model, these oscillations should be of negligible amplitude. This is found to be true as the numerical results show no signs of these spurious oscillations along the coastline.

6.5.2 The Open Ocean Boundary Condition

The ideal open ocean boundary condition is

$$\eta \rightarrow 0 \qquad as \quad x \rightarrow \infty$$

which may be substituted by a more practical form (Brink, 1982b), namely an open ocean boundary condition applied at some large offshore distance, $x = -L$.

$$\frac{\partial u}{\partial x} = 0 \qquad at \quad x = -L$$

If we assume that the depth is constant at $x = -L$, this condition may be expressed in vertically integrated velocities as

$$\frac{\partial U}{\partial x} = 0 \qquad at \quad x = -L$$

This is boundary condition is applied in the numerical model as

$$U_1 = U_2 \text{ at the open ocean boundary}$$

There is no significant difference between the derived CTW dispersion properties in chapter 3 when either of the above two open ocean boundary conditions are used. Further, the numerical model is implemented in such a manner that the open ocean boundary is far away from the region of interest and thus is not expected to impact on the numerical results over the shelf.

6.5.3 The Cross-shelf Boundary Conditions

The application of suitable boundary conditions at the cross-shelf open boundaries is crucial to the numerical investigation. The open boundary conditions must allow disturbances to pass freely through the boundaries without modifying the interior solution of the truncated numerical domain. These open boundaries are potentially the "weakest link" in the numerical model and their effect on the interior solution needs to be understood to ensure that the results of the numerical model are correctly interpreted. For this reason an extensive survey of open boundary conditions was undertaken and two open boundary conditions were identified as being the most appropriate to apply in the numerical model, namely a modified Miller and Thorpe (1981) OBC and the Camerlengo and O'Brien OBC (see Appendix D for detail).

To test the OBC's, numerical experiments are undertaken for an idealised shelf topography where a continental shelf wave motion is input at the northern boundary of the computational domain. The results are as follows;

a) the two versions of the advective radiation (MT OBC) condition, as defined by Miller and Thorpe (1981), are found to be suitable for handling short wavelength oscillations arriving at the open boundary, but result in substantial reflections at the boundary for long, slow-moving CTW motions. Fig. 6.3a, a "snapshot" of the sea level field after 96 hours of simulation using the MT (version 1) OBC, shows evidence of strong reflections at the southern boundary.

b) the Camerlengo and O'Brien (1980) version of the above open boundary condition (CO OBC) performed well for slow-moving, small amplitude CTW

motions. This OBC also performs well in situations where forcing is present on the boundary. Fig. 6.3b, a "snapshot" of the sea level field after 96 hours of simulation, shows little or no evidence of modification of the interior flow near the boundaries when this OBC is used.

The Camerlengo and O'Brien (1980) version of the OBC is therefore used in the numerical model since it seems to cope well with dispersive waves in both the forced and unforced situations. For large-scale, slowly varying motions it is difficult to obtain a phase speed estimate (C_{est}) for a wave leaving the truncated domain by using only a few interior mesh points near the boundary. This poor resolution at the boundary results in poor estimates of C_{est} in the Miller and Thorpe OBC's.

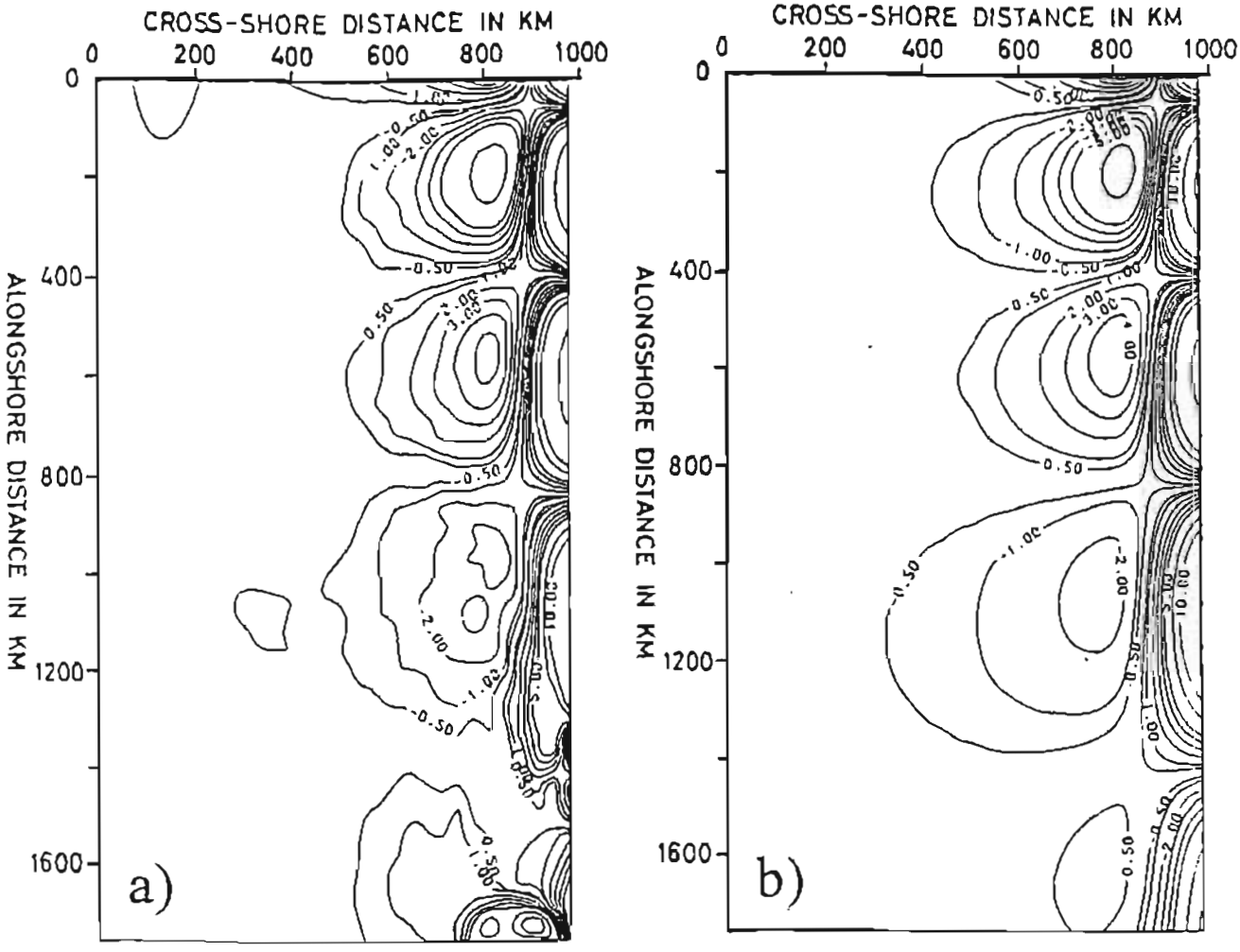

Fig 6.3 "Snapshot" of the sea level at time t = 96 hours where in a) the Miller and Thorpe OBC has been used showing that substantial and unwanted reflection occur at the southern boundary, and in b) the Camerlengo and O'Brien OBC has been used and shows almost perfect transmission of the wave through the southern boundary.

The Camerlengo and O'Brien OBC has a fixed estimate for the phase speed of the outgoing wave, given by $C_{est} = \Delta y/\Delta t$. This fixed estimate enables the OBC to perform well for slow-moving, small amplitude CTW motions. Since $C_{est} = \Delta y/\Delta t$, the fastest possible phase speed in the grid, the variables on the boundary are able to respond very rapidly to changes in the interior variables. This is most probably why the Camerlengo and O'Brien OBC performs so well when forcing occurs on or near the boundary.

6.5.4 The Bottom Friction Formulation

The relation of bottom stress to velocities in the logarithmic bottom boundary layer is commonly expressed as a quadratic with a drag coefficient, C_d (Heaps, 1978). This quadratic formulation for the bottom friction has been used in a number of numerical investigations (for example Beardsley and Haidvogel, 1981; Blumberg and Kantha, 1985). In CTW studies, however, the use of a linearised version is common (for example, Clarke and Brink, 1985). The linear form is given by

$$\left(\tau_b^x, \tau_b^y\right) = \left(\rho r u, \rho r v\right) \quad \text{(in terms of velocities } u,v\text{)}$$

or $$\left(\tau_b^x, \tau_b^y\right) = \left(\frac{\rho r U}{h}, \frac{\rho r V}{h}\right) \quad \text{(in terms of vertically integrated velocities } U,V\text{)}$$

where $r = C_d \mid V_{rms} \mid$, and V_{rms} represents the current velocity at the top of the bottom boundary layer. The value of V_{rms} is typically 0,1 to 0,15 $m.s^{-1}$.

This linearisation has some justification for low-frequency flows (Rooth, 1972; Csanady, 1976). Values of the friction parameter, r, used in numerical studies range between 10^{-4} and 5×10^{-4} $m.s^{-1}$. Typically the value of the friction parameter used in earlier numerical and analytical studies of CTW motions has been a constant of $r = 2,5 \times 10^{-4}$ $m.s^{-1}$. This value is used in the present model, however the choice of a constant friction parameter is not strictly correct as the magnitude of the friction parameter changes in the cross-shelf direction due to the action of high frequency gravity waves (Grant and Madsen, 1979, 1986). The value of r typically increases towards the coastline and is generally larger in the nearshore regions (shallow waters) than the value used in the present numerical model (Clarke and Brink, 1985). Schumann and Brink (1990) used a constant value of $r = 5 \times 10^{-4}$ $m.s^{-1}$ in their analysis of CTW motions around the southern African coastline. One should not be too

concerned with the uncertainty in the magnitude of the bottom friction since Chapman (1987) has shown that the accurate parameterisation of the wind field is far more important in determining the nature of the response.

6.5.5 Specification of the Wind Stress Forcing in the Numerical Model

Highly idealised wind stress fields are used in the model. The wind stress is specified directly and does not depend on any relationship between wind speed and wind stress. The applied alongshore wind stress in the model varies from 0 to 0.12 $N.m^{-2}$, which roughly corresponds to a 0 $m.s^{-1}$ to 8 $m.s^{-1}$ wind. Cross-shore wind stresses are not effective in generating long-wave CTW motions and are assumed to be zero in the numerical model. The different specifications of wind stress used in the numerical model are described in more detail in the Results in chapter 7.

6.6 Diagnostics of the Numerical Model

Graphic outputs from the model provide the essential details of the solutions. The form of these graphic diagnostics are:

i) a **"snapshot"** of the entire grid of variables at a specified time, providing an instantaneous picture of the sea level contours (Fig. 6.3) or their associated velocity vectors (Fig. 7.4b, p145).

ii) **"space-time" contours** showing the evolution of the sea level and velocity component amplitudes with time. These contour plots are produced for both longshore and cross-shore transects. In the "longshore space-time" contour plots, the space axis (abscissa) runs from north to south along the continental shelf at a specified distance offshore. Fig. 6.4a shows a three-dimensional plot of the bottom topography off the west coast. Fig. 6.4b shows the longshore transect along which the variables are referred to as the "shelf-edge" response and Fig. 6.4c shows the longshore transect in which the variables are referred to as the "nearshore" response. The variables along a further longshore transect which follows the coastline, are referred to as the "coastal" response. The ordinate in the "longshore space-time" contour plots is elapsed time in hours.

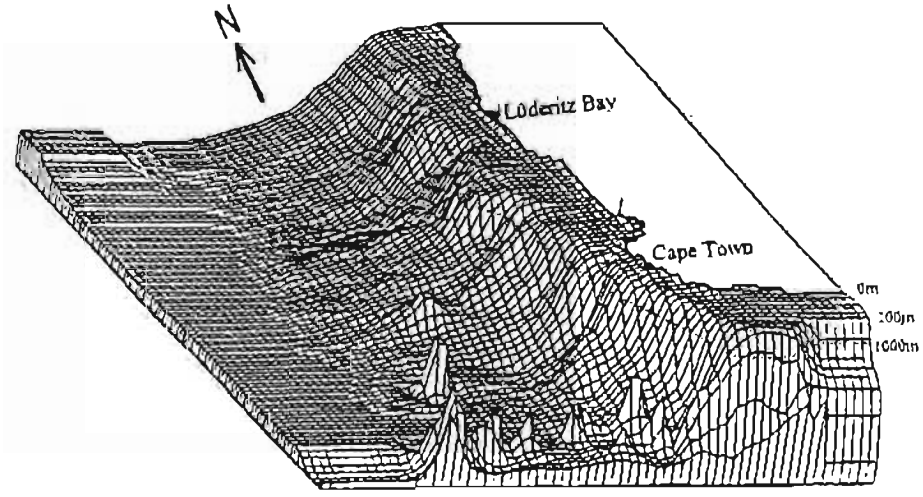

Fig. 6.4a A 3-dimensional view of the digitized bottom topography used in the numerical model

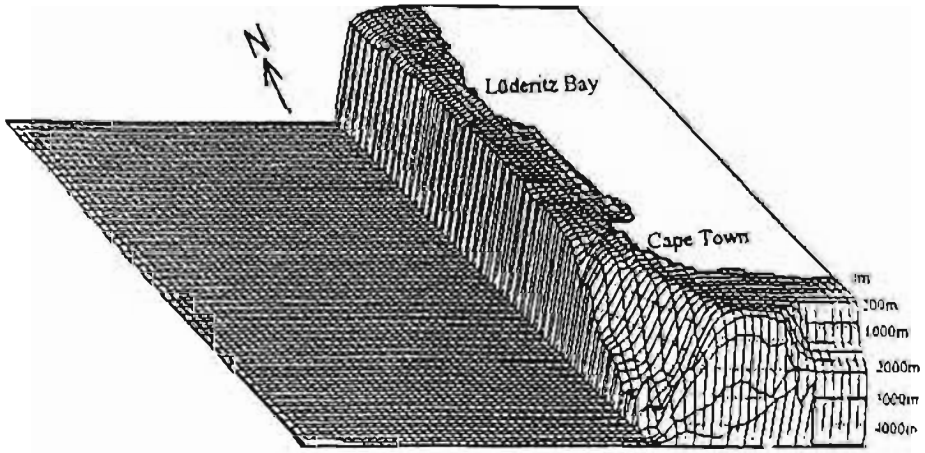

Fig. 6.4b A transect of Fig 6.4a at a fixed distance offshore. Variables along this transect are referred to as the shelf-edge response

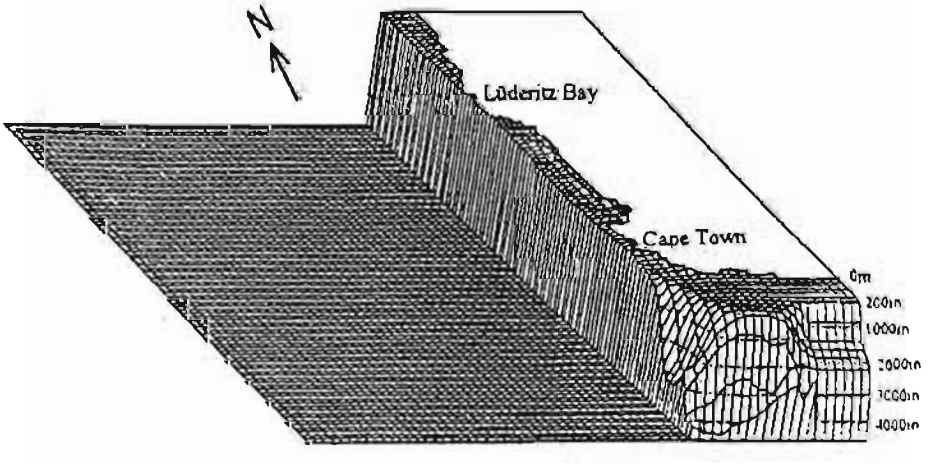

Fig. 6.4c A transect of Fig 6.4a at a fixed distance offshore. Variables along this transect are referred to as the nearshore response

These contour plots, consisting of a series of ridges and troughs, indicate the progressive nature of CTW motions (Fig. 7.2, p141) and may be interpreted as follows:

a) the inverse of the slope of a particular ridge (or trough) gives the phase velocity (C_{ph}) of the CTW.

b) the inverse of the slope of a particular contour (say the maximum amplitude contour) gives the group velocity (C_g) of the wave.

c) the length of a transect through the ridge (or trough) at a fixed time gives half the wavelength of the wave.

d) a transect through the ridge (or trough) at a fixed longshore distance gives one half of the wave period.

e) a transect along the axis of a ridge gives the rate of growth or decay of the response. However, for CTW motions which are highly dispersive, this is only true for a limited time as the energy of the dispersive CTW motions travel at the group velocity which is generally less than the phase velocity.

iii) an energy diagnostic where the total cross-shelf integrated energy (E_{TOT}) at a given cross-shore transect is plotted against elapsed time in hours where E_{TOT} is given by (Chapman, 1985)

$$E_{TOT} = \frac{1}{L} \int_{-L}^{0} \tfrac{1}{2} \left[h \left(U^2 + V^2 \right) + g \eta^2 \right] dx$$

which is approximated in a regularly spaced numerical grid as

$$E_{TOT}(j = 60) = \sum_{i=1}^{MX-2} \tfrac{1}{2} \left[\tilde{h}_{i,j} \left(U_{i,j}^{\,2} + \tilde{\tilde{V}}_{i,j}^{\,2} \right) + g \tilde{\eta}_{i,j}^{\,2} \right]$$

where $\tilde{h}_{i,j} = \left(h_{i+1,j} + h_{i,j} \right) / 2$, $\tilde{\eta}_{i,j} = \left(\eta_{i+1,j} + \eta_{i,j} \right) / 2$,

$\tilde{\tilde{v}}_{i,j} = \left(v_{i+1,j} + v_{i,j} + v_{i+1,j-1} + v_{i,j-1} \right) / 4$

This diagnostic is arbitrary and is used to investigate the energy travelling along the shelf at a transect at j = 60 (y = 1180 km). The longshore evolution of the energy in a CTW with time is thus given by a plot of E_{TOT} versus elapsed time, t (Fig. 7.4d, p146).

7. THE NUMERICAL MODEL RESULTS

A number of numerical experiments have been carried out using the barotropic CTW model described in Chapter 6. These numerical experiments provide an insight into the nature of CTW motions over both an idealised bottom topography and the real bottom topography of the continental shelf off the west coast of Southern Africa. First, the propagation of free CTW's along the continental shelf is investigated. This is followed by an investigation of the forced response along the continental shelf where both an idealised and a more realistic wind-forcing has been used.

The two different shelf topographies used in these numerical experiments are:

i) a "idealised" shelf topography where there is assumed to be no longshore variation in the bottom topography. The bottom topography off Walvis Bay (offshore profile 1) constitutes the idealised shelf (Fig. 7.1a).

ii) a "real" shelf topography, which consists of the accurately digitised bottom topography of the continental shelf off the west coast of southern Africa (Fig. 7.1b).

The numerical investigation is structured as follows:

i) Initially a number of test runs (Section 7.1) are carried out to determine if the model provides the expected response in a number of standard situations. These test runs also have been used to eliminate programming errors and test the open boundary conditions (Fig. 6.3, p134)

ii) Secondly, the nature of the free wave response on both an idealised and the real shelf topography is investigated (numerical experiments 1 to 6 in Section 7.2). Particular emphasis is placed on the topographic scattering of the free wave as it propagates along the shelf.

iii) Thirdly, the forced response due to idealised wind-forcing is investigated. Initially only the forced response over an idealised topography is considered (numerical experiments 7 to 11 in Section 7.3). The investigation is then extended to include the forced response over the real West Coast shelf topography (numerical experiments 12 and 13 in Section 7.4). The idealised

forcing consists of a longshore band of wind stress which is allowed to propagate southwards along the shelf at various speeds.

iv) Finally, a more realistic wind field is used to determine the nature of the forced response over both the idealised and real shelf topographies (numerical experiments 14 and 15 in Section 7.5).

The results from the above numerical investigations along with the analysis of the sea level data, provide the basis of the discussion in Chapter 8.

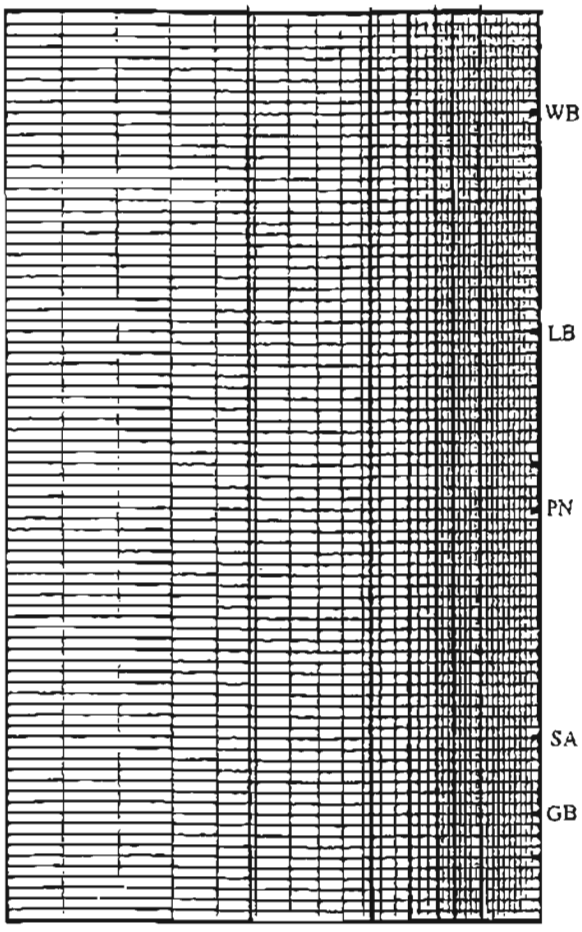

Fig 7.1a A plan view of the idealised shelf topography and finite difference grid used in the model. The depth contours are given in metres.

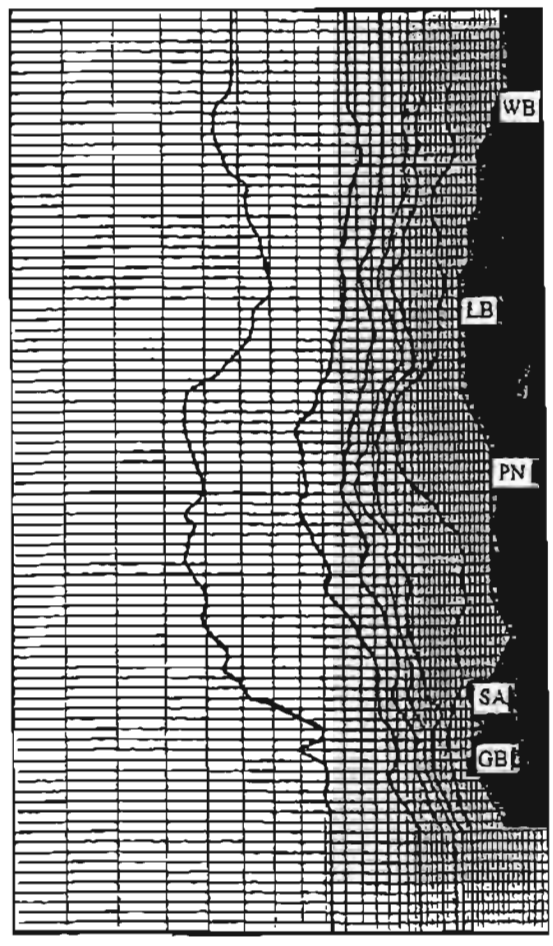

Fig. 7.1b A plan view of the real shelf topography and finite difference grid used in the model. The depth contours are given in metres.

7.1 Initial Testing of the Numerical Model

A number of test runs have been carried out to determine if the model provides the expected results for a number of standard situations. The results from only one series of test runs are described below.

An initial sea surface displacement having a "$\sin^2 y$" longshore dependence and a linear decay in the offshore direction, was input into the model. This test has been used by a number of authors to check the performance of their numerical models (for example Beardsley and Haidvogel, 1981; Shillington, 1985). The initial sea surface "mound" splits into two signals, one moving northwards and the other, slightly larger amplitude signal, moving southwards (Fig. 7.2). These two sea level signals are quantifiable as edge waves (Shillington, 1985) which propagate north and south, respectively, at typical edge wave phase velocities. The dispersive nature of the edge waves ($C_g \ll C_{ph}$) is apparent in Fig. 7.2. The expected phase velocity difference (Mysak, 1968a) between the two edge waves cannot be resolved in the numerical output.

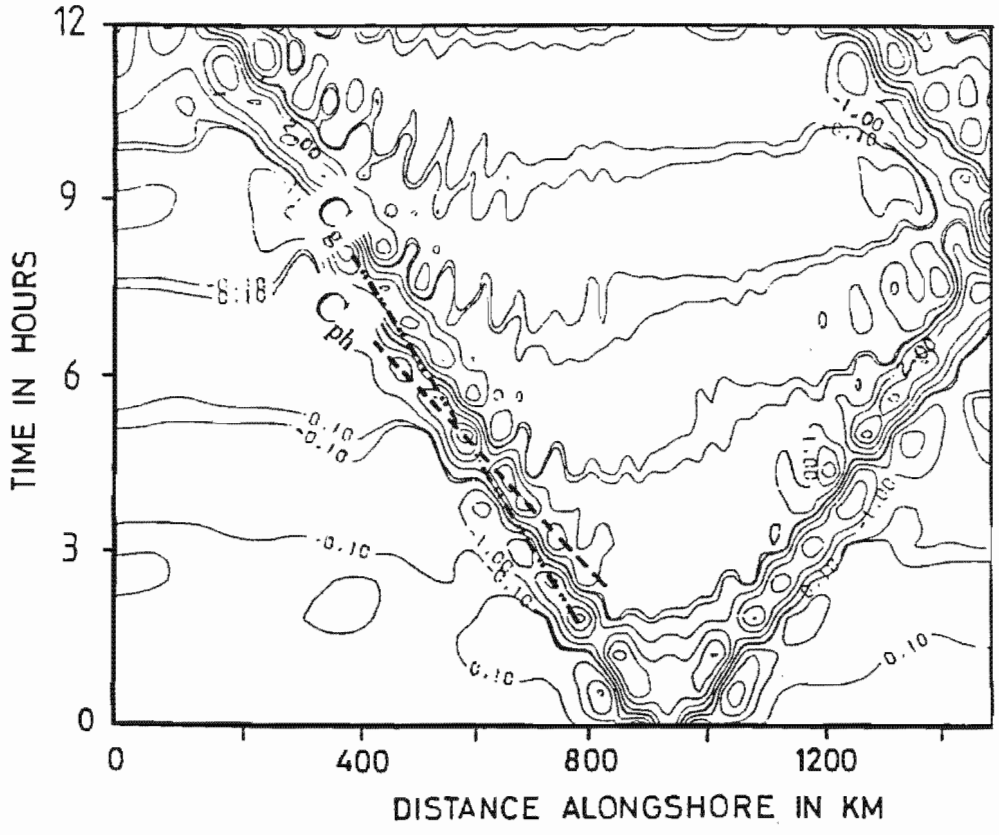

Fig. 7.2 Longshore "space-time" contours of the sea level response (in cm) resulting from the input of a sea level "mound" as described in the text. The dashed line denoted C_{ph} gives the phase velocity of the northward propagating edge wave while the dashed line denoted C_g gives the group velocity of the edge wave.

An experiment where a sea surface "mound" with a larger alongshore scale (more typical of CTW's) is input into the model shows the same behaviour. The only difference observed, is that the "mound" splits into longer wavelength edge waves and a stationary oscillation develops at the coast at the site of the sea level "mound" input. The above are expected results, providing confidence in the numerical model output.

It was during these initial tests the poor performance of the cross-shelf open boundary condition (OBC) was noted. This prompted an extensive survey of OBC's and the ultimate choice of the Camerlengo and O'Brien OBC.

7.2 Free CTW Propagation over an Idealised Shelf Topography and the West Coast Shelf Topography

The nature of the free CTW response is investigated in numerical experiments 1 to 6. The diagnostic of total energy in a cross-shelf transect at a longshore site to the south of the domain, is used in describing the dispersive nature of the free wave as well as quantify the topographic scattering and frictional dissipation of the free CTW as it propagates southwards along the shelf. Waves having offshore modal structures, $F_1(x,k)$, typical of the first mode CTW for profile 1, are input at the northern boundary of the model. These inputs represent free waves travelling from north to south in the numerical model domain. The two free wave inputs used at the northern boundary are,

i) a highly dispersive free wave (wave input I) for which there is limited energy transmission along the shelf. The free CTW properties of input I are

$\sigma = 4.71 \times 10^{-5}$ (frequency)
$\lambda_\ell = 510.5$ km (wavelength)
$C_{ph} \approx 3.83$ m.s^{-1} (phase velocity)
$C_g \approx 0$ (group velocity)

ii) a less dispersive, longer wavelength free wave (wave input II) where the transmission of energy along the shelf is greater since the group and phase velocities are similar in magnitude (that is, C_g and C_{ph}). The free CTW properties of wave input II are

$\sigma = 3.45 \times 10^{-5}$ (frequency)
$\lambda_\ell = 1\ 225$ km (wavelength)
$C_{ph} \approx 6.73$ m.s^{-1} (phase velocity)
$C_g \approx 4.5$ (group velocity)

The frequency and wavenumber characteristics of these two wave inputs (I and II) are shown in the first mode (n=1) dispersion curve in Fig. 7.3.

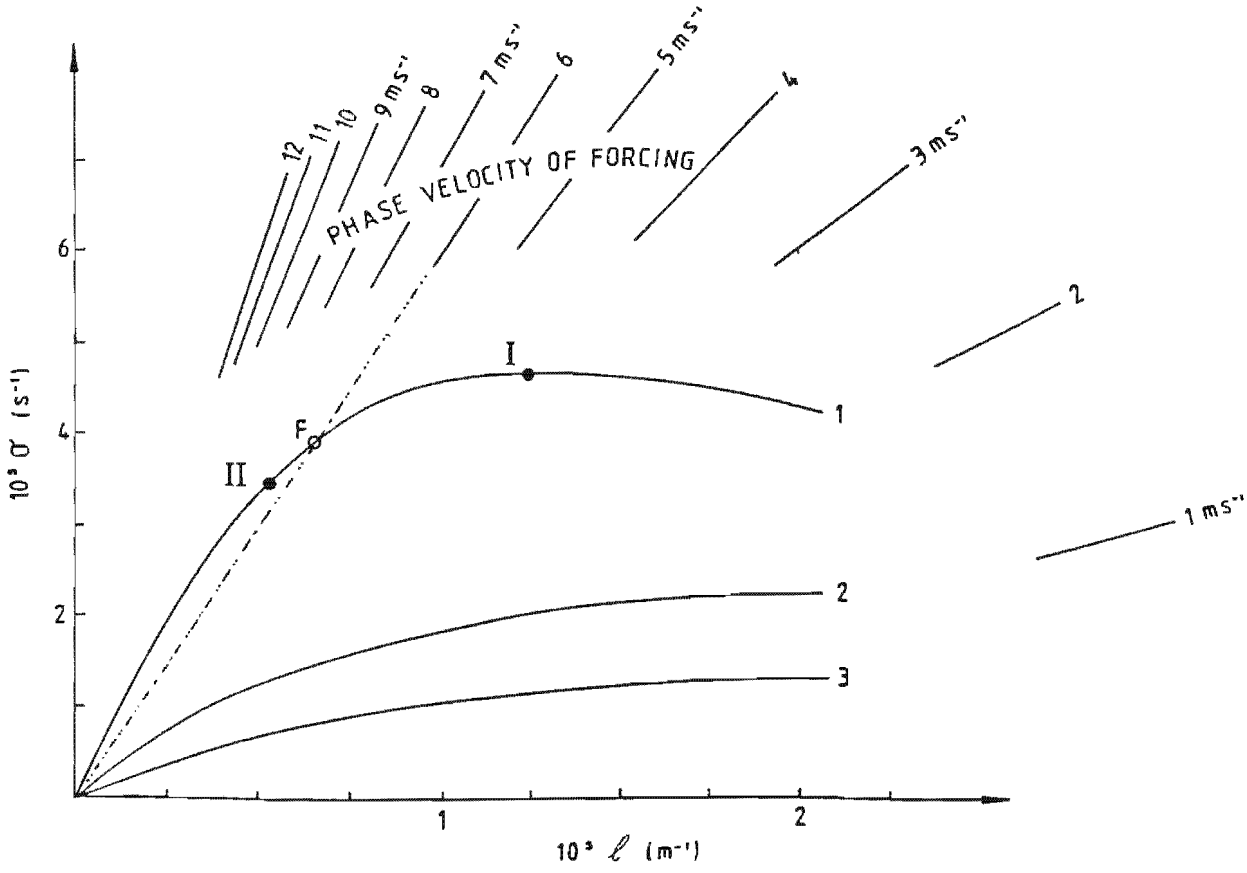

Fig. 7.3 The dispersion curve characteristic of the idealised bottom topography. The frequency wave-number (σ, ℓ) characteristics of the two free wave inputs (I) and (II) are marked on the first mode dispersion curve. The point denoted (F) gives the expected (σ, ℓ) characteristics of a CTW generated by a band of wind stress propagating along the shelf at a phase velocity of 6 m.s^{-1}.

In experiment 1, the general characteristics of inviscid, barotropic free wave propagation along the idealised shelf topography are described. Weak bottom friction is then included in experiment 2 to quantify the frictional decay of the free wave amplitude. Two similar experiments (numerical experiments 3 and 4) are carried out using the real shelf topography to determine the extent of the topographic scattering of free CTW's due to alongshore changes in the topography. The highly dispersive wave input (I) is used in experiments 1 through to 4, while the less dispersive wave input (II) is used in numerical experiments 5 and 6 to determine to what extent the results of experiments 1 to 4 hold for less dispersive free CTW's.

Numerical experiment 1 - (idealised shelf topography, no bottom friction)

The free wave input (I) is used at the northern boundary. The amplitude of the input wave is increased linearly over one wave period and thereafter remains constant at 40 cm. (The free CTW input in numerical experiments 1 through to 6 are all introduced in this manner at the northern boundary.) In this experiment bottom friction is ignored (that is, $r = 0$), allowing the properties of inviscid, barotropic, free CTW's over an idealised shelf topography to be described.

As expected, the results in Fig. 7.4a and Fig. 7.4b show the free wave to be strongly trapped over the shelf, the longshore velocity response (v) being much larger than the cross-shore velocity response (u). The sea level and longshore velocities are in phase while the cross-shore velocities lag by $\pi/2$ radians as is expected

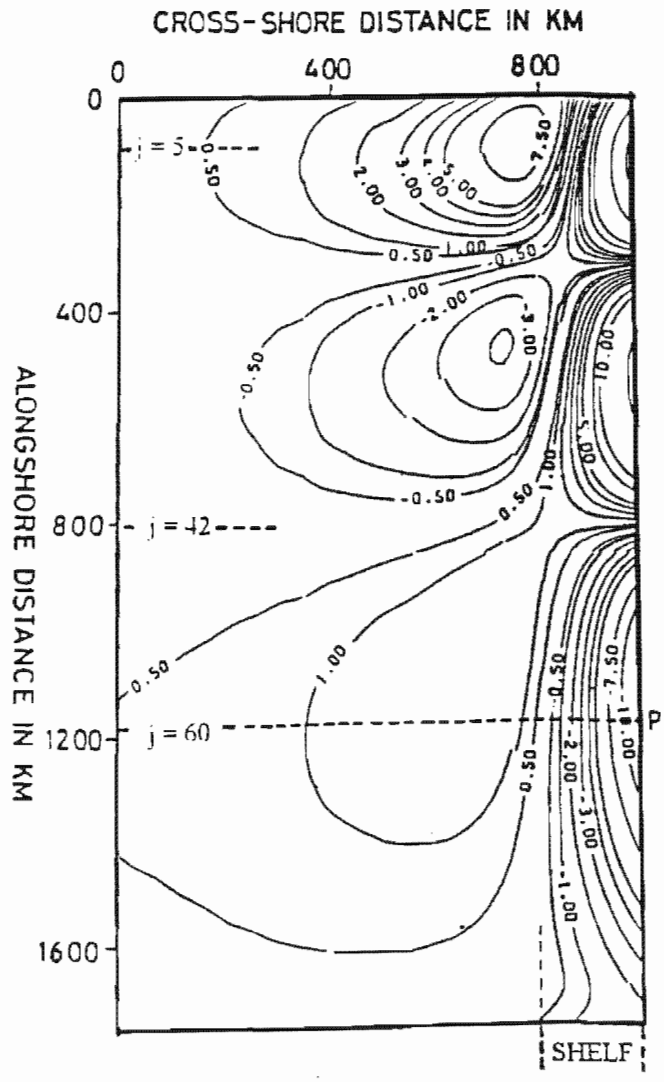

Fig. 7.4a "Snapshot" of the sea level at time t = 72 hours. The dashed line at j = 60 gives the location of the cross-shore transect in which the total energy at a particular time is calculated. The contours are given in cm. [numerical experiment 1]

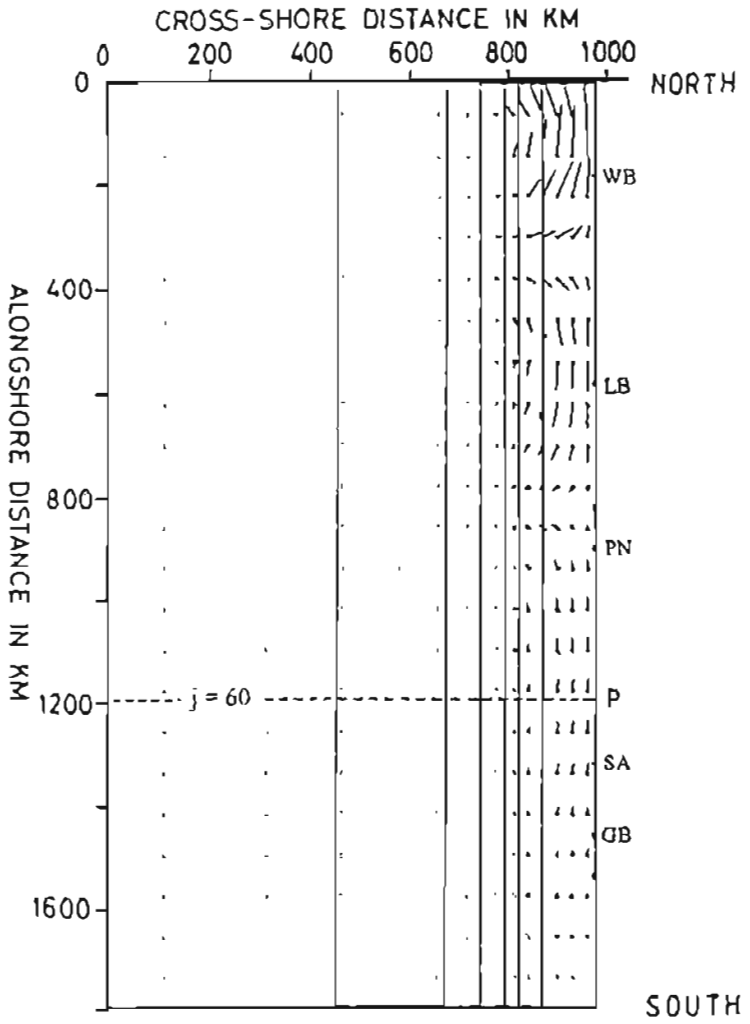

Fig. 7.4b "Snapshot" of the velocity vector field at time t = 72 hours. The maximum amplitude of the velocity vectors are approximately 60 cm.s^{-1}. [numerical experiment 1]

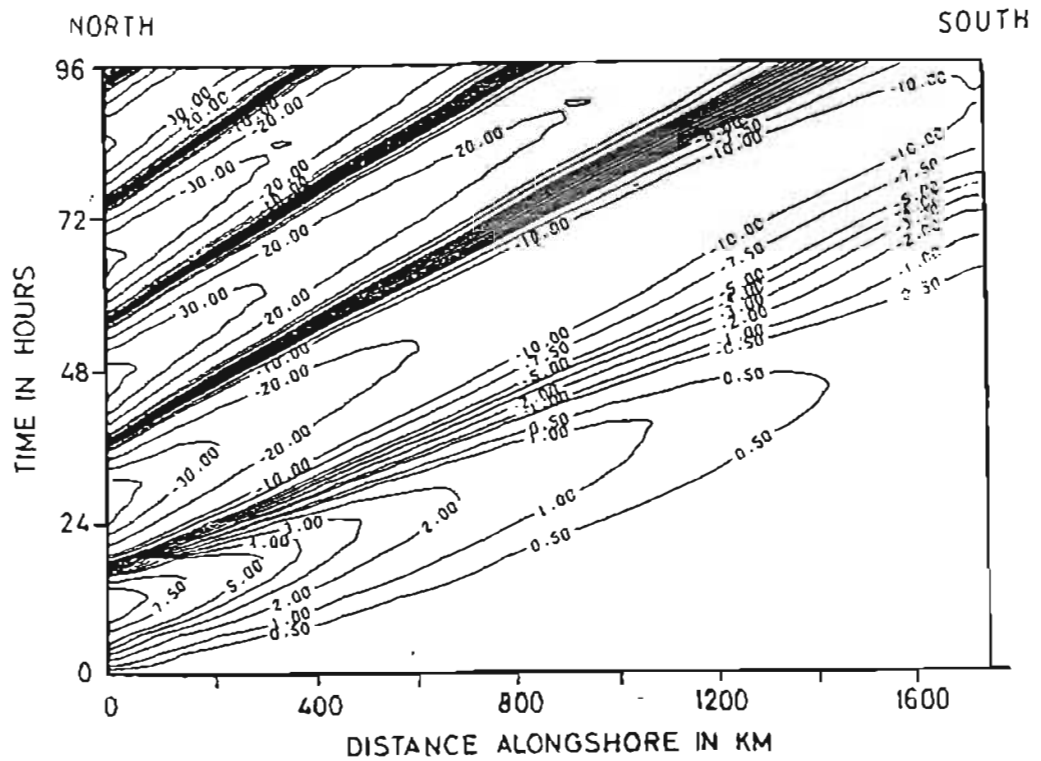

Fig. 7.4c Longshore "space-time" contours of the nearshore sea levels associated with the free wave input (A). [numerical experiment 1].

The strongly dispersive nature of the input wave is apparent in the "snapshots" of the sea level (Fig. 7.4a), in the velocity vector field (Fig. 7.4b) and in the longshore "space-time" plot of sea level (Fig. 7.4c). The wave dimensions expand in the longshore direction and the amplitude of the input free wave rapidly decreases downstream due to the strong dispersion inherent to the input wave (I) where $C_g \ll C_{ph}$.

A plot of the total energy in the cross-shore transect at the longshore location j = 60 (y ≈ 1200 km) indicates an energy peak (denoted "P") at time t = 72 hours (Figure 7.4d). This peak corresponds to the peak (denoted "P") in the amplitudes of longshore velocity (Fig. 7.4b) and sea level (Fig. 7.4a). The energy in barotropic CTW's is mostly kinetic energy ($R_{kp} \gg 1$), thus most of the energy in this peak is due to the longshore velocity maximum at j = 60. The labels in all of the energy versus time plots in this chapter refer to the total cross-shore integrated CTW energy (denoted A), the cross-shore integrated CTW energy in only the shallow shelf waters (denoted B), and the cross-shore integrated CTW energy both over the shelf break and in deeper waters (denoted C).

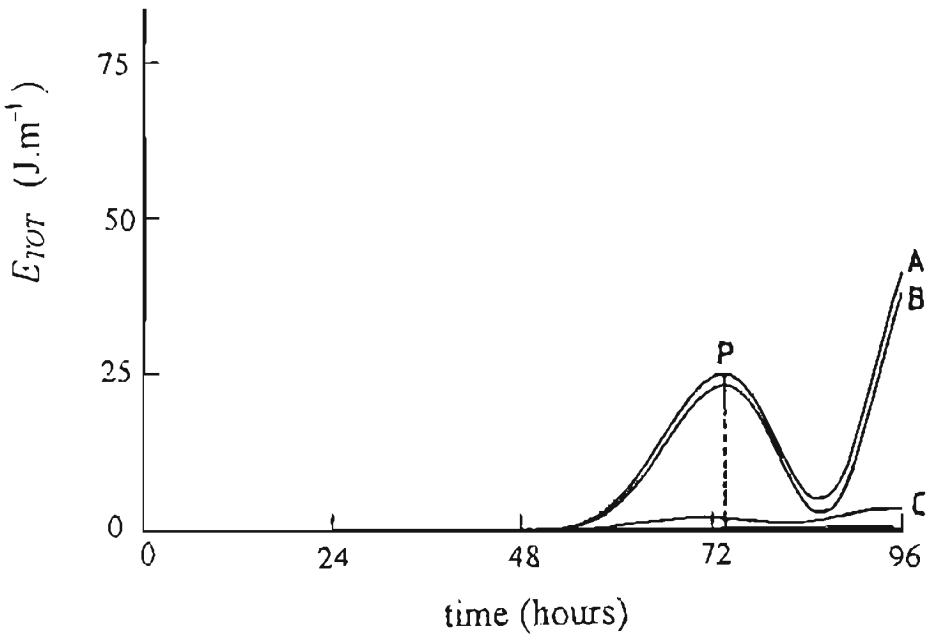

Fig. 7.4d Plot of the total energy at a transect at j = 60 versus time (E_{TOT} vs t). The labels refer to the total cross-shore integrated CTW energy (denoted A), the cross-shore integrated CTW energy in only the shallow shelf waters (denoted B), and the cross-shore integrated CTW energy both over the shelf break and in deeper waters (denoted C). [numerical experiment 1]

Numerical experiment 2 (idealised shelf topography with bottom friction)

Wave input (I) is again used at the northern boundary in this model run where bottom friction has been included ($r = 2{,}5 \times 10^{-4}$ m.s^{-1}). The numerical output indicates that the sea level amplitudes are significantly reduced due to the inclusion of bottom friction effects (compare Fig. 7.4c and Fig 7.5a). The longshore velocities in the nearshore zone lead the shelf-edge longshore velocities by a small phase angle due to the enhanced bottom friction in the nearshore zone. This small nearshore phase lead is not apparent in either the sea levels or the cross-shore velocities.

A plot of the total energy in a cross-shore transect at $j = 60$, shows a strong decrease in the free wave energy reaching this transect (Fig. 7.5b) due to the dissipation of the free wave by bottom friction.

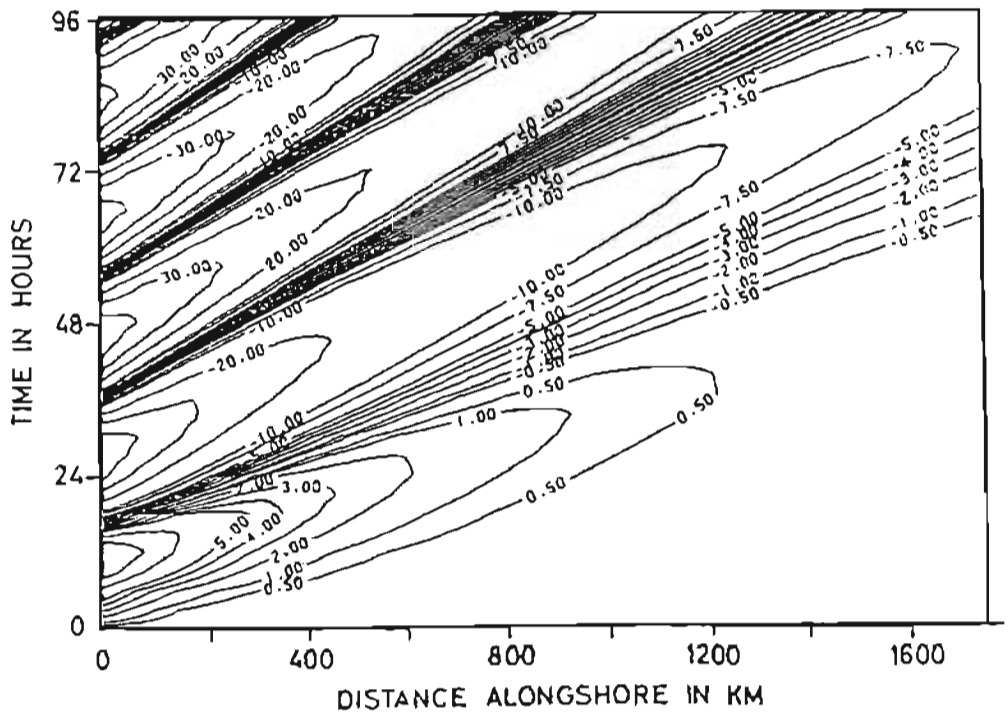

Fig. 7.5a Longshore "space-time" contours of the nearshore sea levels associated with the free wave input (A) [numerical experiment 2].

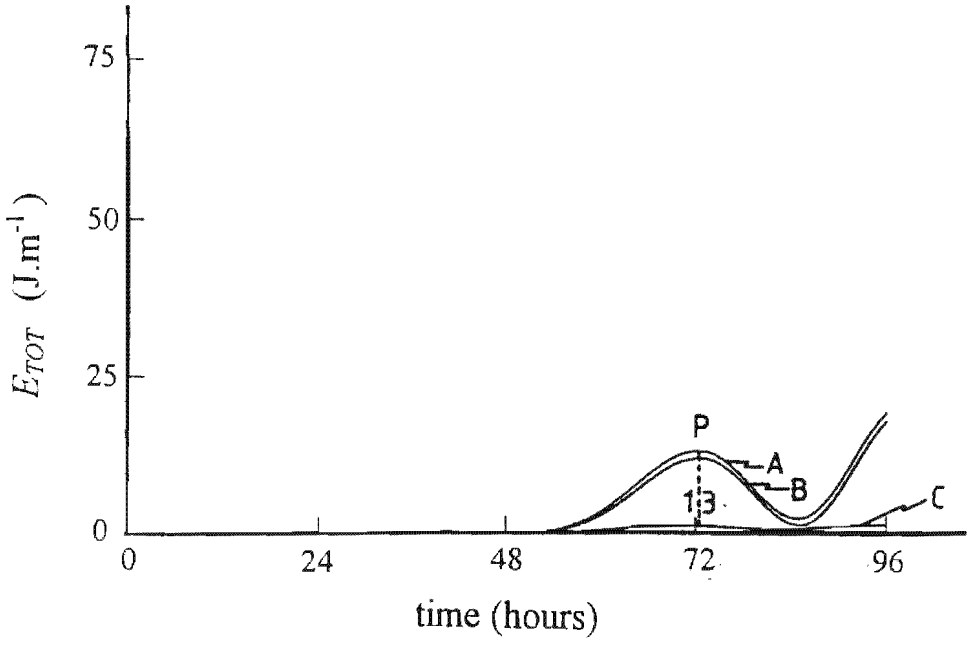

Fig. 7.5b Plot of the total energy at a transect at j = 60 versus time (E_{TOT} vs t). The labels refer to the total cross-shore integrated CTW energy (denoted A), the cross-shore integrated CTW energy in only the shallow shelf waters (denoted B), and the cross-shore integrated CTW energy both over the shelf break and in deeper waters (denoted C). [numerical experiment 2]

In contrast to numerical experiments 1 and 2 where a "idealised" shelf topography is used, a "real" shelf topography is introduced in numerical experiments 3 and 4 to determine the effects of longshore changes in the bottom topography.

Numerical experiment 3 (real shelf topography, no bottom friction)

Here free wave input (I) is used in a numerical experiment utilising the real bottom topography to investigate the effects of longshore changes in the bottom topography in the absence of bottom friction (that is, r = 0).

The longshore "space-time" plots (Figs 7.6a, b, c and d) indicate a less coherent response due to the effects of longshore variations in the bottom topography. The nearshore sea levels (Fig. 7.6a) and longshore velocities (Fig. 7.6b) remain fairly coherent, while the cross-shore velocities (Figs 7.6c and d) are less coherent and develop much shorter scales of motion. The cross-shore velocities are particularly sensitive to large changes in the bottom topography, leading to a lack of coherence

between the longshore and cross-shore velocities in the vicinity of large changes in the bottom topography

A feature of both the nearshore (Fig 7.6c) and shelf-edge (Fig. 7.6d) cross-shore velocities are the strong, quasi-steady, onshore/offshore flows that develop in response to the topographic scattering of the free wave in regions of large alongshore variation in shelf topography. These quasi-steady cross-shore velocities, observed just south of Lüderitz Bay and in the vicinity of Hondeklip Bay (see Fig. 7.6e), are the quasi-steady flows alluded to by Allen (1976) and suggested by the scaling arguments in Appendix A.

Although quantitative measurements are not possible, the longshore "space-time" plots (Figs 7.6a, b, c, and d) and "snapshots" of the sea level at different times (Figs 7.6f,g) indicate how the propagation characteristics of the input CTW changes as it propagates southwards over a changing bottom topography. The frequency of the free CTW remains constant as it propagates along the shelf, however both its wavelength and phase velocity change. At location L1 in Figs. 7.6a and 7.6b, the phase velocity of the free CTW increases from approximately 3,7 m s^{-1} to approximately 8,8 m.s^{-1} and simultaneously the wavelength of the free CTW approximately doubles

These changes in the modelled free CTW phase velocity are consistent with those indicated by the theoretical free CTW dispersions curves (Fig. 3.2, p35). Thus the results for a free CTW's moving over a varying topography in the model agree qualitatively with analytical studies which state that "the frequency of the free wave remains fixed while the phase velocity and wavelength adjust to values typical of the local shelf topography".

The situation is different in the vicinity of large alongshore changes in the shelf topography where the incident CTW is topographically scattering into high wavenumber CTW motions characterised by small scale, large amplitude cross-shelf flows at the shelf edge.

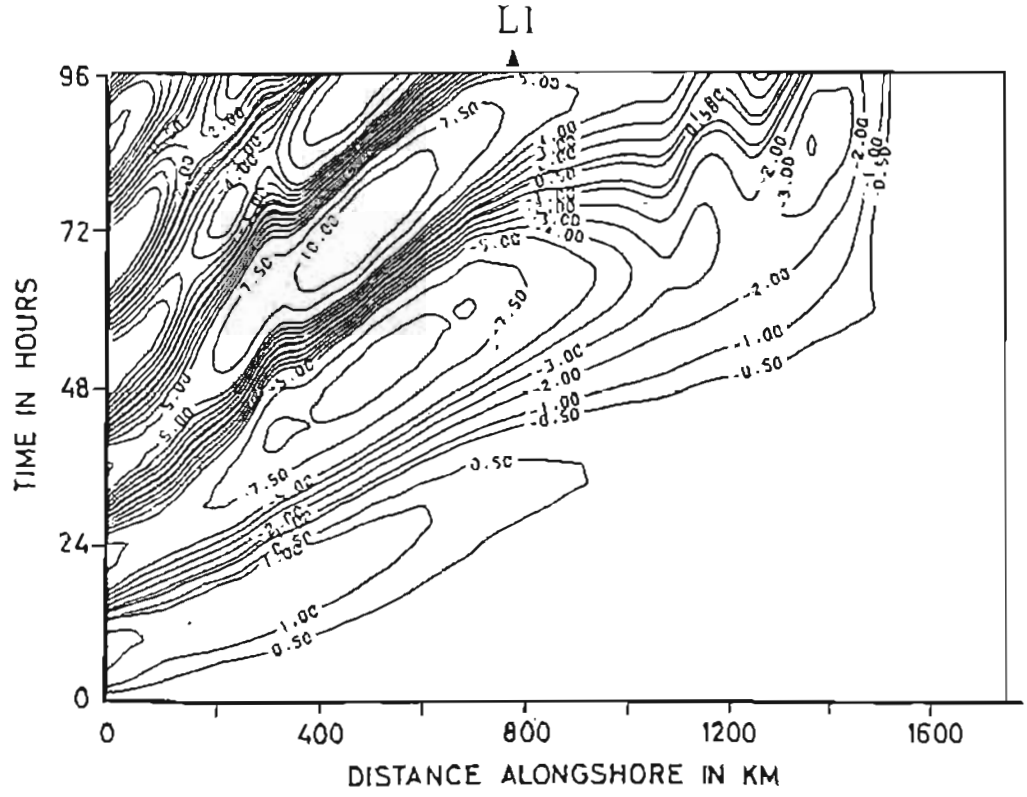

Fig. 7.6a Longshore "space-time" contours of the nearshore sea level as input wave (1) propagates over a realistic bottom topography. [numerical experiment 3]

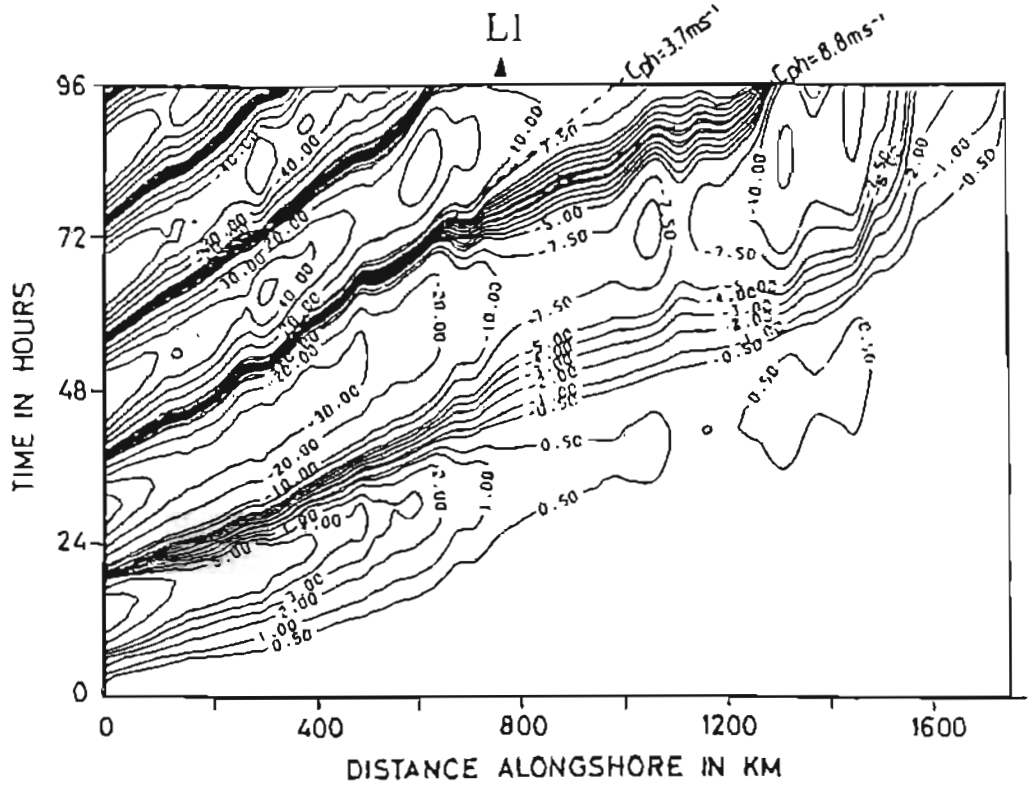

Fig. 7.6b Longshore "space-time" contours of the (nearshore) longshore velocity response indicating how the phase velocities change over a realistic bottom topography. [numerical experiment 3]

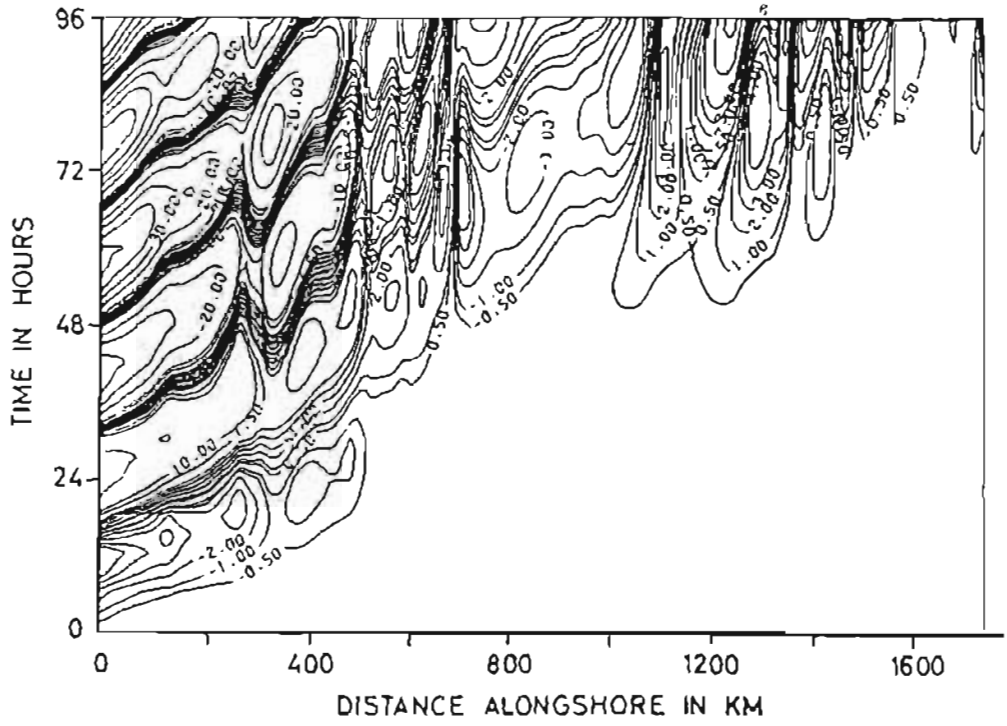

Fig. 7.6c Longshore "space-time plots of the cross-shore velocities in the nearshore region. [numerical experiment 3]

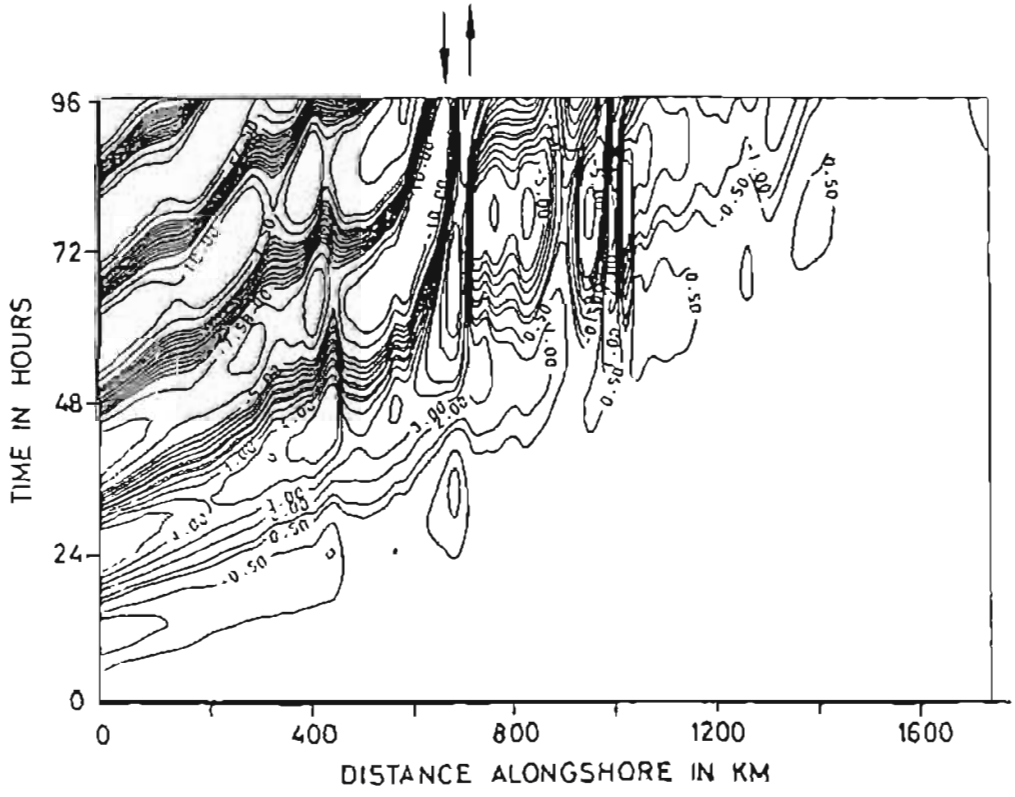

Fig. 7.6d Longshore "space-time plots of the cross-shore velocities at the shelf edge. [numerical experiment 3]

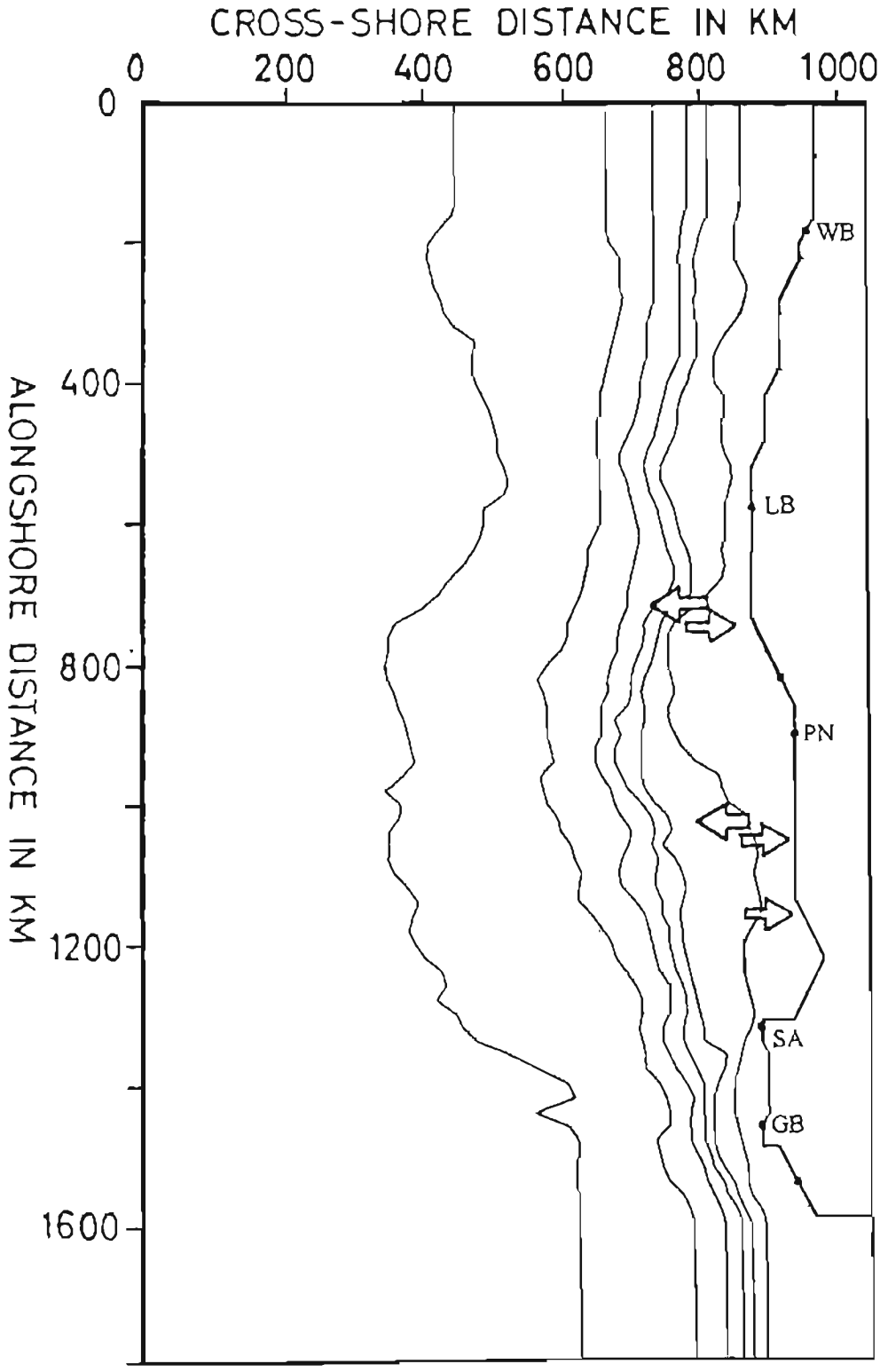

Fig 7.6e Plan view of the shelf topography indicating the location of the strong quasi-stationary onshore/offshore flows which develop as the free wave propagates along the shelf. [numerical experiment 3]

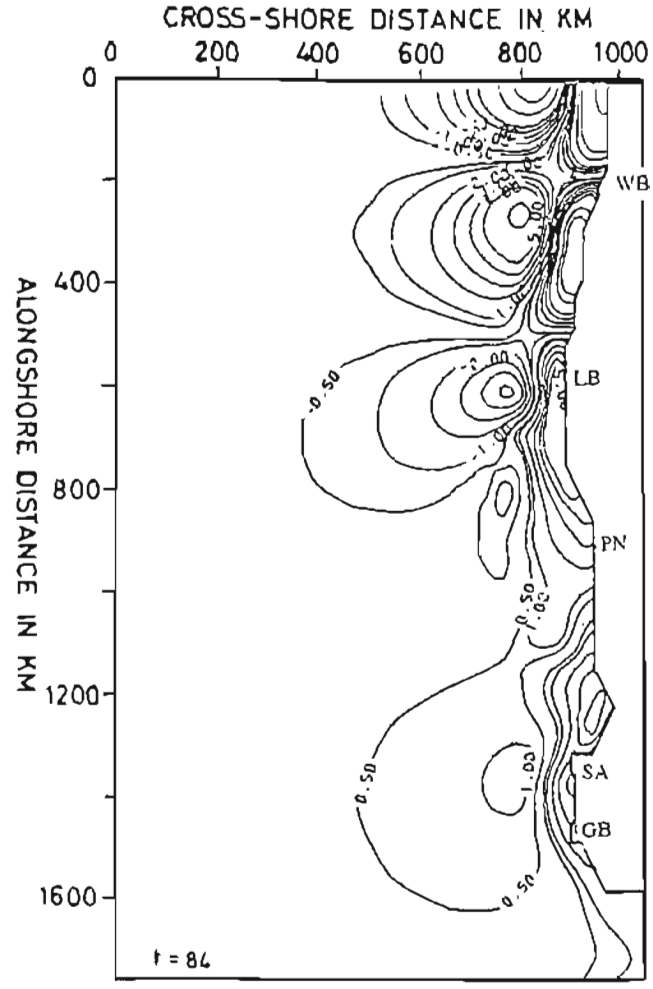

Fig. 7.6f Snapshot of the sea level at time, t = 84 hours. [numerical experiment 3].

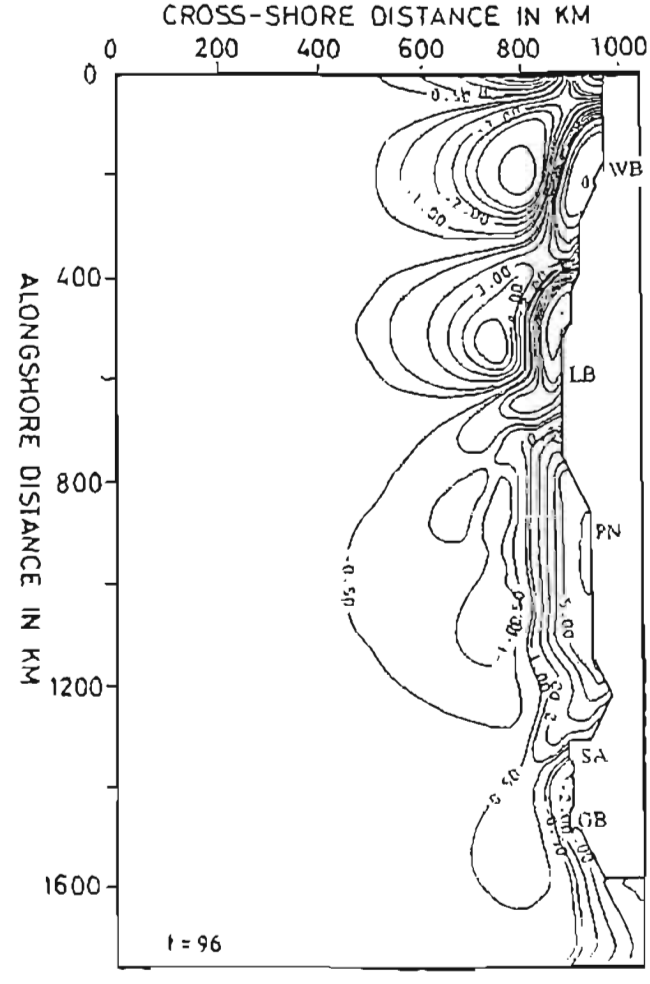

Fig. 7.6g Snapshot of the sea level at time, t = 96 hours. [numerical experiment 3]

The relative contribution of the slope response (B) to the total energy (A) in the cross-shore transect at $j = 60$ (Fig. 7.6h) is much greater here than in numerical experiment 1 (Fig. 7.4d, p146). The alongshore variations in the bottom topography result in the energy being not so strongly trapped over the shelf and a significant response is observed at the shelf edge. Topographic scattering of the free CTW input results in of higher mode and higher wavenumber motions which have significantly larger amplitudes over the shelf slope than the lower mode and wavenumber motions, thus the increase in energy over the shelf slope.

The total energy reaching the transect at j = 60 is greatly reduced due to this topographic scattering of the input wave (Fig. 7.6h).

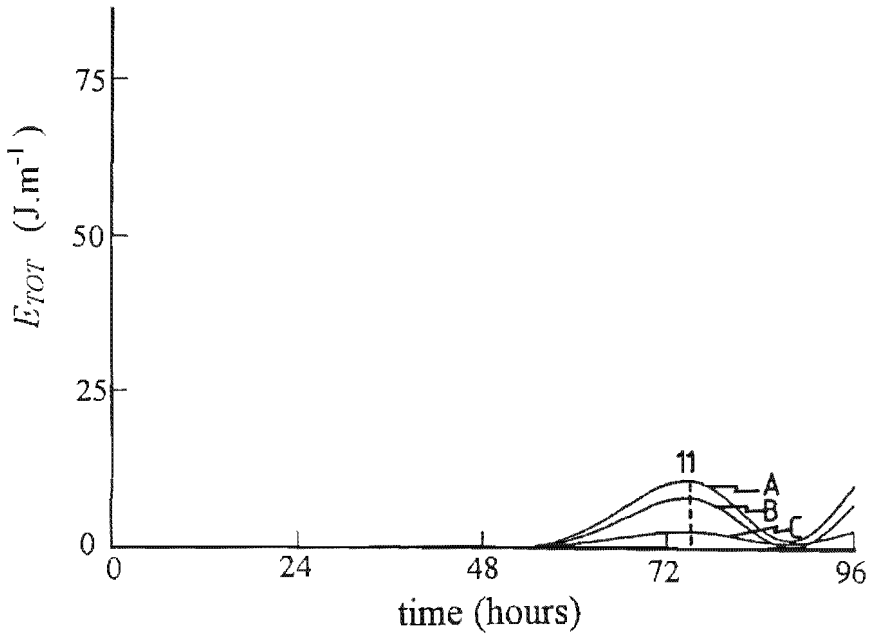

Fig. 7.6h Plot of the total energy at a transect at j = 60 versus time (E_{TOT} vs t). The labels refer to the total cross-shore integrated CTW energy (denoted A), the cross-shore integrated CTW energy in only the shallow shelf waters (denoted B), and the cross-shore integrated CTW energy both over the shelf break and in deeper waters (denoted C). [numerical experiment 3]

Numerical experiment 4 (realistic shelf topography with bottom friction)

This numerical experiment is identical to numerical experiment 3 except that here bottom friction effects are included ($r = 2.5 \times 10^{-4}$ m.s^{-1}). The only significant difference between the results of this experiment is those of numerical experiment 3 is that the amplitude of the input free CTW (I) is further reduced due to bottom friction (compare Fig. 7.7a with Fig. 7.6f). This is also reflected in the total energy in a cross-shore transect measured at $j = 60$ (Fig. 7.7b).

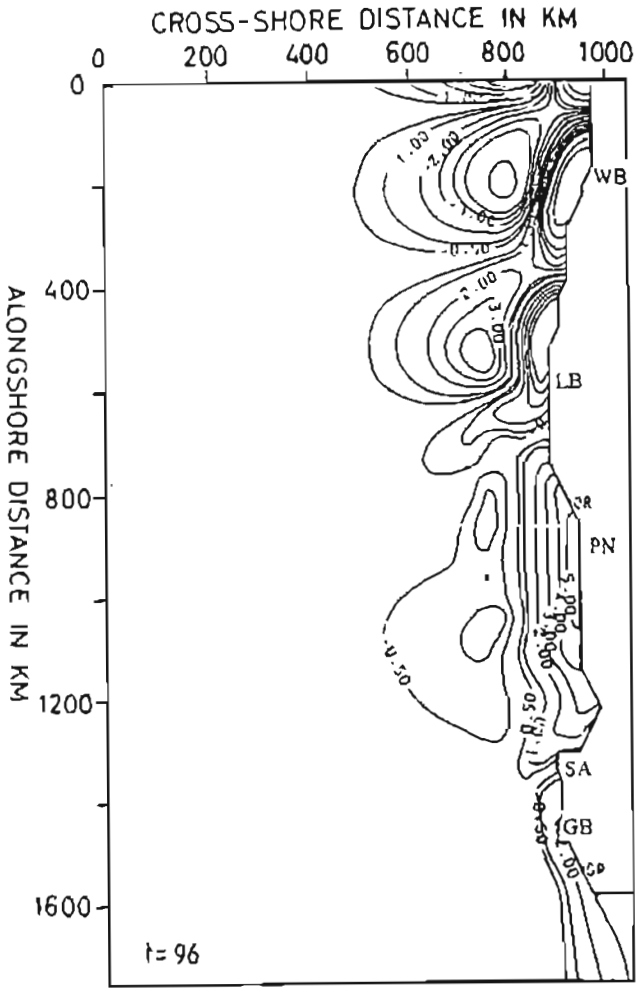

Fig 7.7a Sea level contours for time t = 96 hours. [numerical experiment 4]

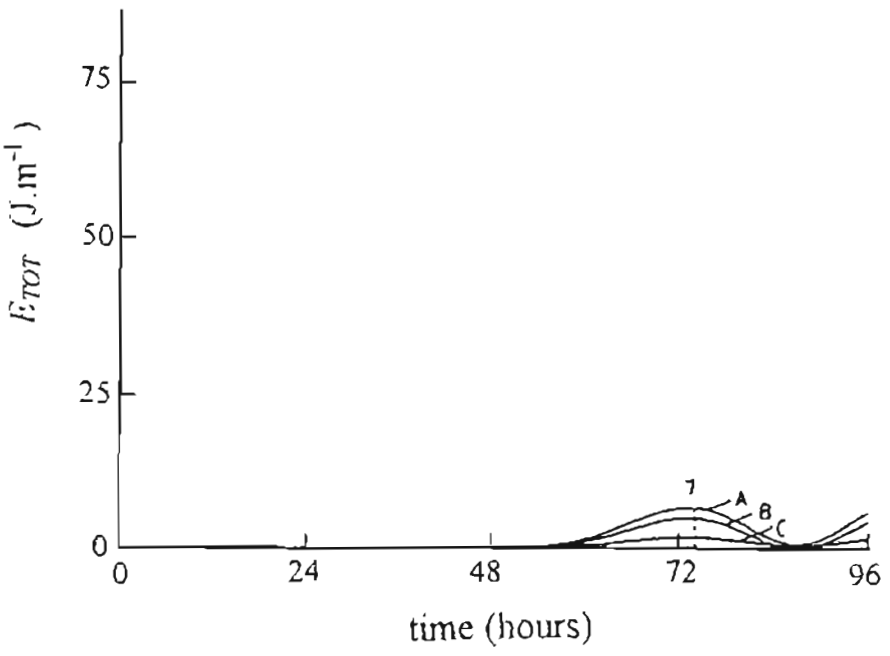

Fig 7.7b Plot of the total energy at a transect at j = 60 versus time (E_{TOT} vs t). The labels refer to the total cross-shore integrated CTW energy (denoted A), the cross-shore integrated CTW energy in only the shallow shelf waters (denoted B), and the cross-shore integrated CTW energy both over the shelf break and in deeper waters (denoted C). [numerical experiment 4]

Experiments 1 to 4 may be summarised as follows. The energy reaching the cross-shore transect to the south is greatly reduced due to the dispersive nature of the free CTW input (I), strong topographic scattering and frictional dissipation of the free CTW as it propagates along the shelf. Strong quasi-steady cross-shore velocities are observed to develop in the vicinity of large longshore changes in the shelf topography due to topographic scattering.

In numerical experiments 5 and 6 which follow, the less dispersive free wave input (II) is used to determine if above results hold for less dispersive free CTW inputs.

Numerical experiment 5 (idealised shelf topography and bottom friction)

This numerical experiment is identical to numerical experiment 4 (that is, an idealised shelf topography is used and bottom friction effects are included) except that here the less dispersive free wave input (II) is used

The total energy in the cross-shelf transects at j = 5 (input energy of free wave), j = 42 and j = 60, is calculated (see Fig 7.9a for the location of these transects). The quantity of free wave energy reaching the southern regions is once again reduced due both to the frictional dissipation and dispersive nature of the wave. Only 23 % of the first energy peak in the input wave reaches the transect at j = 42 while only 13 % reaches the transect at j = 60 (Fig. 7.8).

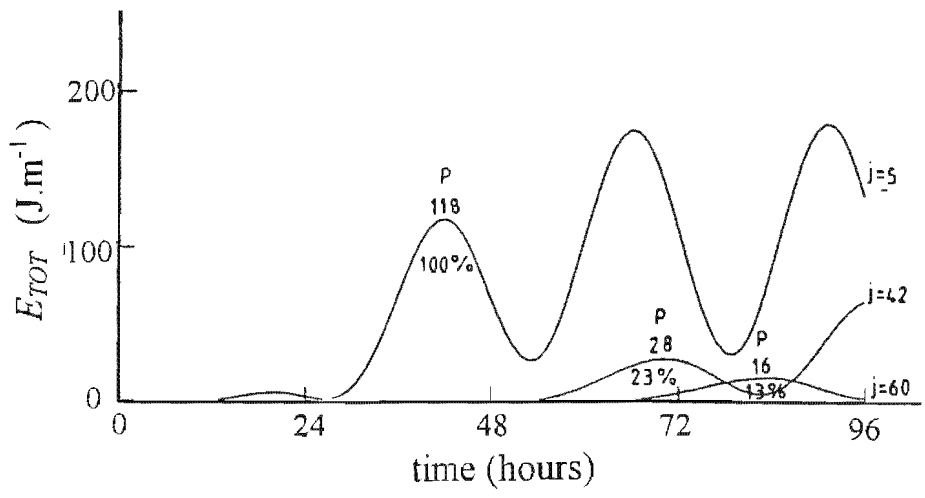

Fig. 7.8 Plot of the total energy in cross-shelf transects at j=5 (input energy), j=42 and j=60 as a function of time (E_{TOT} vs t). [numerical experiment 5]

Numerical experiment 6 (realistic shelf topography and bottom friction)

This numerical experiment is identical to numerical experiment 5, except here the real shelf topography is used. As in the previous numerical experiments using the real shelf topography, quasi-steady flow also starts to develop south of Lüderitz Bay and in the vicinity of Hondeklip Bay (Fig. 7.9a). However, these cross-shore flows are weaker than those developed in an in numerical experiments using the more dispersive wave input (I). Here only 10 % of the first energy peak in the input wave reaches the transect at j = 42 while only 6 % reaches the transect at j = 60 (Fig. 7.9b).

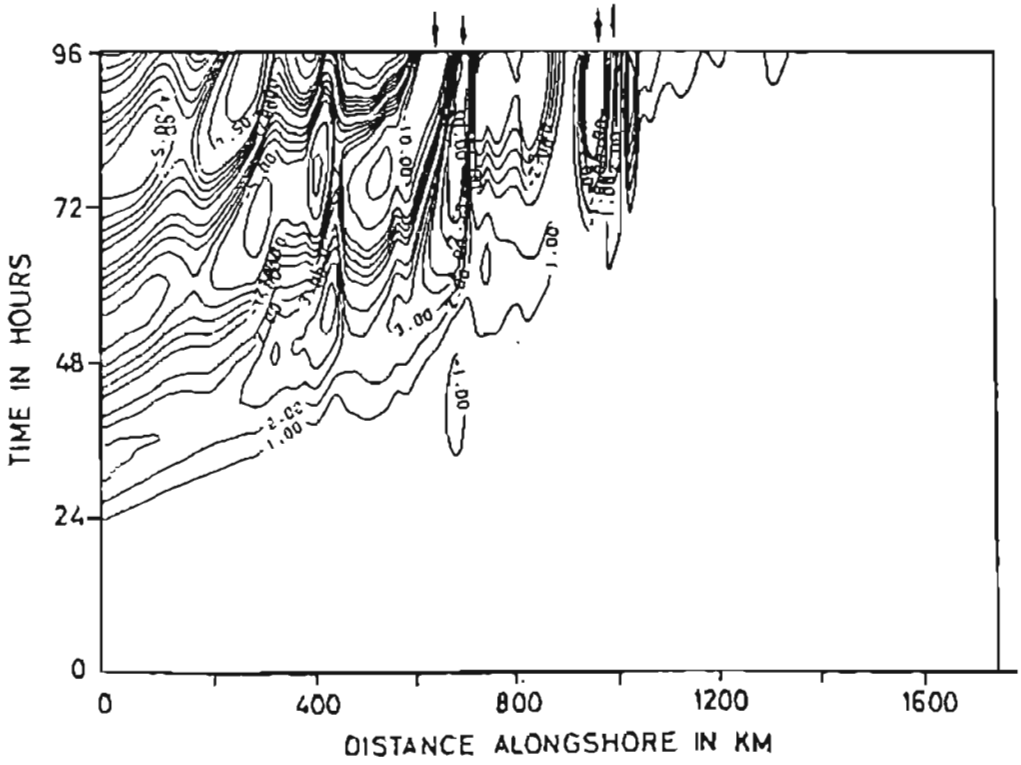

Fig. 7.9a Longshore "space-time plots of the cross-shore velocities at the shelf edge. [numerical experiment 6]

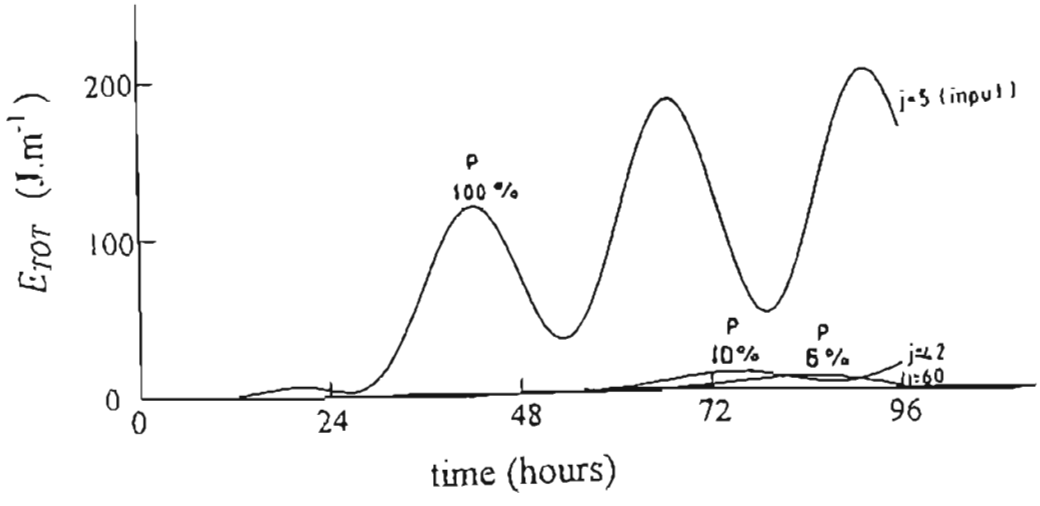

Fig. 7.9b Plot of the total energy in cross-shelf transects at j=5 (input energy), j=42 and j=60 as a function of time (E_{TOT} vs t). [numerical experiment 6]

In experiments 1 through to 6 the nature of the free CTW propagation along both an idealised and real shelf topography has been demonstrated. In experiments 1 through to 4, where the highly dispersive wave input (I) is used, the amplitude of the free CTW decreases rapidly downstream and very little energy is transmitted along the shelf due to the fact that the group velocity of the input free CTW is approximately zero. For the less dispersive wave input (II), used in experiments 5 and 6, more energy is transmitted along the shelf since $C_g \sim 0$ (C_{ph}). Further experiments (not reported here) with long, non-dispersive free wave inputs show that, if $C_g \approx C_{ph}$, the energy transmitted along the shelf is much greater.

The dispersive nature of the free wave is not the only reason for the energy transmission along the shelf being less for the more dispersive waves. Wang (1980) shows that the more dispersive waves are also more strongly scattered by the topography, further reducing the energy propagating along the shelf. This topographic scattering of the free wave into higher wavenumber and higher frequency motions (where C_g is generally very small) result in energy being trapped in the vicinity of large longshore changes in the shelf topography. Consequently, the quasi-steady flows reported in experiment 3 occur for all the free wave inputs. However, since the topographic scattering of almost non-dispersive waves is greatly reduced, the cross-shore flows developing at these sites are weaker and not so strongly trapped. Lastly, the results indicate that energy loss due to topographical scattering of the free CTW as it propagates along the shelf, is much greater than that due to bottom friction

One may thus conclude that the topographic scattering and frictional dissipation of the free wave as it travels along the shelf is large, especially for the shorter wavelength and shorter period motions. It would seem that these more dispersive, shorter wavelength CTW's are not able to propagate along the shelf for any appreciable distance without an energy input by wind. However, this is not the case for longer wavelength (> 2 000 km), longer period (> 10 days) free CTW's which are less strongly scattered by the topography. The above conclusions are strongly supported by the observation of low frequency, long wavelength, remotely forced CTW's which propagate for appreciable distances along the southern African shelf (see section 5.4.3)

7.3 The Forced Response over an Idealised Shelf Topography

In numerical experiments 7 to 11, the forcing comprises of a band of longshore wind stress (having a "$\sin^2 y$" longshore dependence) which propagates from north to south along the continental shelf at various phase speeds. The cross-shore amplitude of the wind stress field is constant over the shelf and rapidly decays offshore from the shelf slope to the open ocean boundary, where it is zero (This form of wind stress field is adequate as the wind-forcing is relatively ineffective in deep water due to the h^{-1} dependence of the wind stress term in the shallow water equations). In all the experiments the wind-forcing is impulsively applied at $t = 0$ and the alongshore wind stress is specified using

$$\tau^{y}_{w}(x,y,t) = \begin{cases} 0 & y < \psi_0 \text{ or } y > \psi_0 + W \\ \pm\left|\tau^{y}_{w}\right|_{max} \Pi(x)\,\Pi(y) & \psi_0 < y < \psi_0 + W \end{cases} \quad \text{for}$$

where

$\Pi(x)$ defines the offshore ($\sin^2 x$) decay of the wind stress field

$\Pi(y) = \sin^2[\pi(y - \psi_0)/W]$ defines the alongshore form of the wind stress field

$\psi_0 = y_0 + C_f t$ where $y_0 = 0$ in the numerical model

W is the longshore extent of the wind stress field (in this case 500 km)

and C_f is the phase speed of propagation of the wind stress field along the shelf.

The maximum amplitude of the wind stress field (τ^{y}_{w}) is 0.12 N.m^{-2} which roughly corresponds to a NNW wind of 8 m.s^{-1}. Since the model is linear and only a small bottom friction parameter is used ($r = 2.5\times10^{-4}$ m.s^{-1}), the magnitude/sign of the maximum wind stress amplitude is not important. A change in magnitude/sign of the wind stress maximum only changes the magnitude/sign of the response. However, if non-linear effects are included (Brink, 1987), an asymmetry develops (even in an inviscid fluid) which theoretically results in a net southward flow along the West Coast and a net eastward flow along the South Coast.

Before reporting the results of the numerical experiments 7 to 11, a description is given of the nature of the expected CTW response and the nomenclature used in reporting the results The wind-forcing is expected to generate a response comprising an infinite number of discrete modes (σ_n, ℓ), each mode consisting of both a free and a

forced wave (see Chapter 4). The amplitude of each mode in the response is proportional to $(C_f - C_n)^{-1} \tau^y_w$, where $C_f = \sigma_f/\ell$ is the propagation velocity of the wind stress field along the shelf and C_n is the free wave phase speed for each mode, n, as determined from the dispersion curve characteristic of the underlying shelf topography. Theoretically, a significant response occurs only when $C_n \approx C_f$, that is, the response to the forcing function has frequency-wavenumber properties such that $\sigma_n/\ell \approx C_f$. This implies that the frequency-wavenumber (σ_n/ℓ) characteristics of the response are primarily those given by the intersection of the dispersion curves (for each mode n) with the straight line $C_f = \sigma_f/\ell$ denoting the phase speed of the forcing function. For example, if $C_f = 6$ m.s^{-1} then the appropriate values of (σ_n/ℓ) are those at the intersection denoted (F) in Fig. 7.2 (p143).

As noted above, the total response observed at any particular location is due to the combination of a number of modes, each having their own frequency-wavenumber characteristics depending on the forcing at some "upstream" location as well as local forcing. Usually only a few modes dominate the low frequency response. In reality a significant part of the observed motion may be due to some remotely forced signal generated far "upstream" that travels along the shelf into the region of interest (see section 5.4.4 in chapter 5). Any such remotely forced CTW's generated outside the numerical domain are ignored and will not appear in the modelling results. In all numerical experiments we assume a "cold start" of the numerical model (that is, the shelf waters are assumed to be at rest at $t = 0$)

The numerical results which follow all indicate that the propagating wind stress field generates a response in the numerical domain that consists of both forced and free CTW's. The CTW signal which propagates along the shelf under the band of wind stress is closely associated with the forcing function and is referred to as the "forced wave" in the numerical results. (It will, however, contain free wave contributions). The periodic motions which precede or follow the wind-forcing are divorced from immediate effects of wind-forcing. These motions which no longer directly receive energy from the forcing function are referred to as "free wave" motions in the

numerical results. The above nomenclature, although not strictly accurate, is used in describing the results of all the numerical experiments which follow.

In experiments 7 to 10, the longshore extent of the wind stress field remains a constant of W = 500 km, while the phase speed of the forcing function is varied from 1 $m.s^{-1}$ to 10 $m.s^{-1}$. In experiment 11, the phase speed of the forcing is held constant at C_f = 5 $m.s^{-1}$, while the longshore extent of the wind stress field is increased to 800 km.

Numerical experiment 7 (C_f=5 $m.s^{-1}$, idealised topography, bottom friction)

In this numerical experiment bottom friction is included, an idealised shelf topography is used and the wind stress field propagates southwards with a phase velocity of 5 $m.s^{-1}$. The response (Figs. 7.10a, b and c) consists of a forced CTW (FOR) and a train of trailing free CTW's (FREE). The forced wave moves along the shelf in sympathy with the band of wind stress while the trailing free wave response has

a frequency, $\sigma = 4.48 \times 10^{-5}$ s^{-1} (period T = 38.8 hours),
a wavenumber, $\ell = 8.85 \times 10^{-6}$ m^{-1} (wavelength λ_ℓ = 716 km)
and a phase velocity, C_{ph} = 5.06 ms^{-1}.

The (σ,ℓ) eigenvalue pair typical of the free CTW is given by the point (A5) lying very close to the intersection of the first mode dispersion curve and the line representing a constant phase velocity of 5 $m.s^{-1}$ and, as expected, the (σ,ℓ) characteristics of the forced response lie in a small band either side of the line representing a constant phase velocity of 5 $m.s^{-1}$ (see Fig. 7.10d).

The group velocity of the free CTW is estimated from Fig. 7.10d to be C_g = 1.65 $m.s^{-1}$. The CTW energy thus propagates along the shelf more slowly than the directly forced response, resulting in a train of free waves following the forced CTW. This phenomenon is clearly seen in the sea level field (Fig. 7.10b and c) and the longshore "space-time" contours of the nearshore sea level response (Figure 7.10a)

A plot of the total energy in a cross-shore transect at j = 60 indicates energy maxima associated with the free (FREE) and forced (FOR) CTW responses. As noted above the energy in the free wave response is relatively large (see Fig. 7.10e) due to the small group velocities associated with the CTW response.

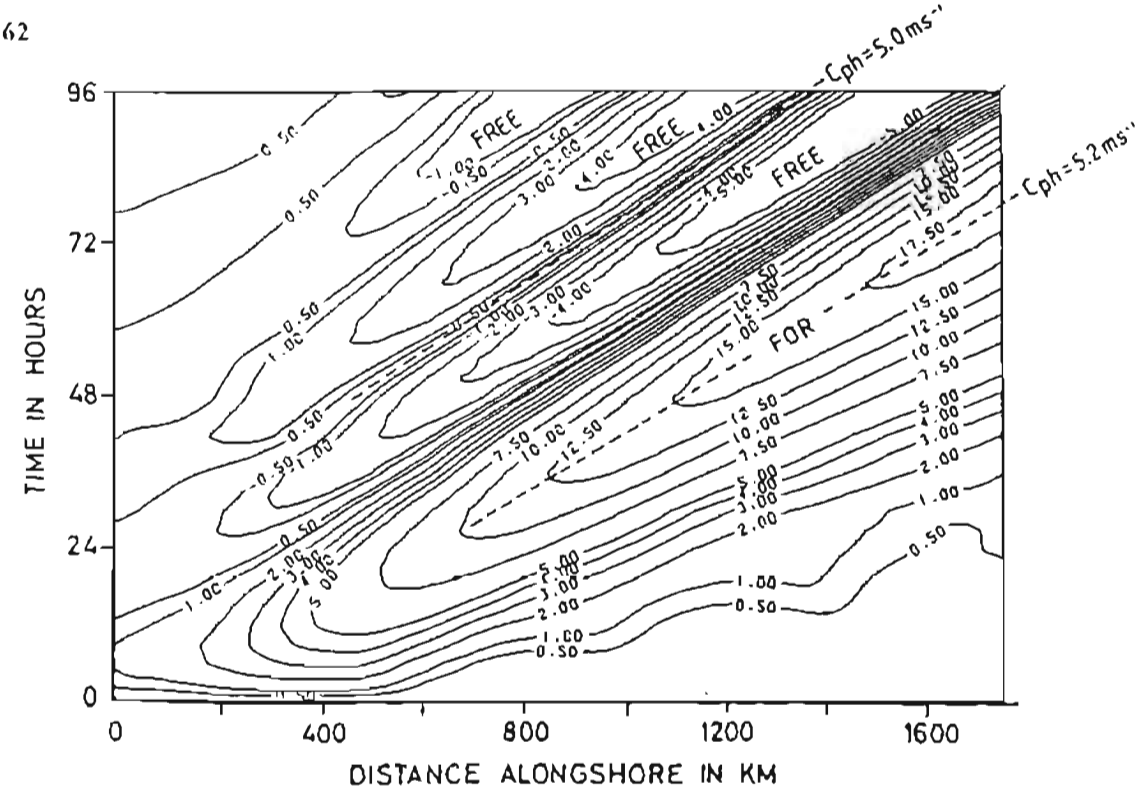

Fig. 7.10a Longshore "space-time" contours of the nearshore sea level response where the forced "FOR" and free "FREE" wave response are labelled. The dashed lines denote the phase speeds of the two waves. [numerical experiment 7]

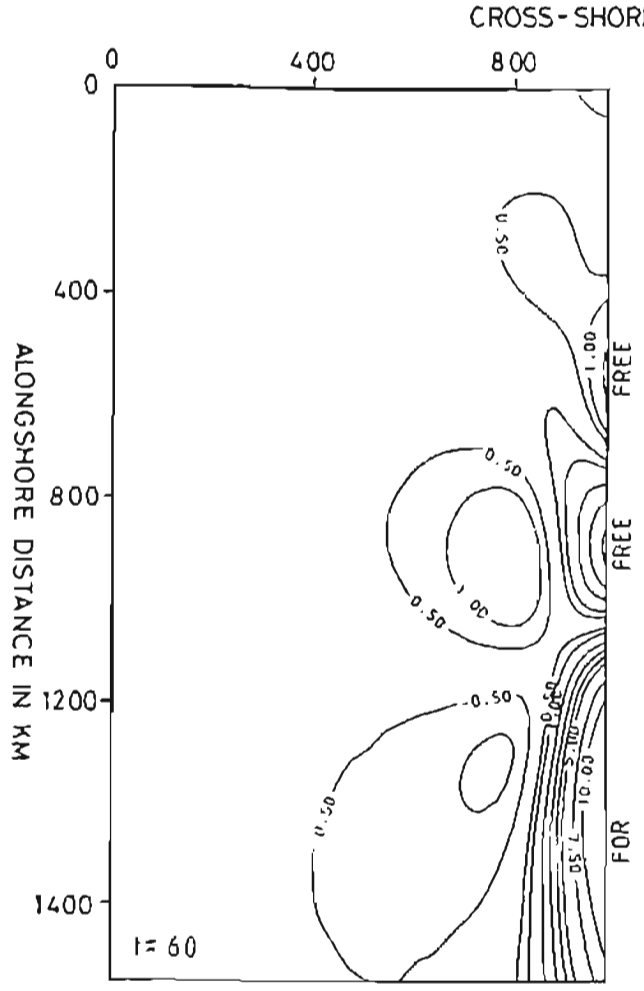

Fig. 7.10b Contours of the sea level response at time, t = 60 hours. [numerical experiment 7]

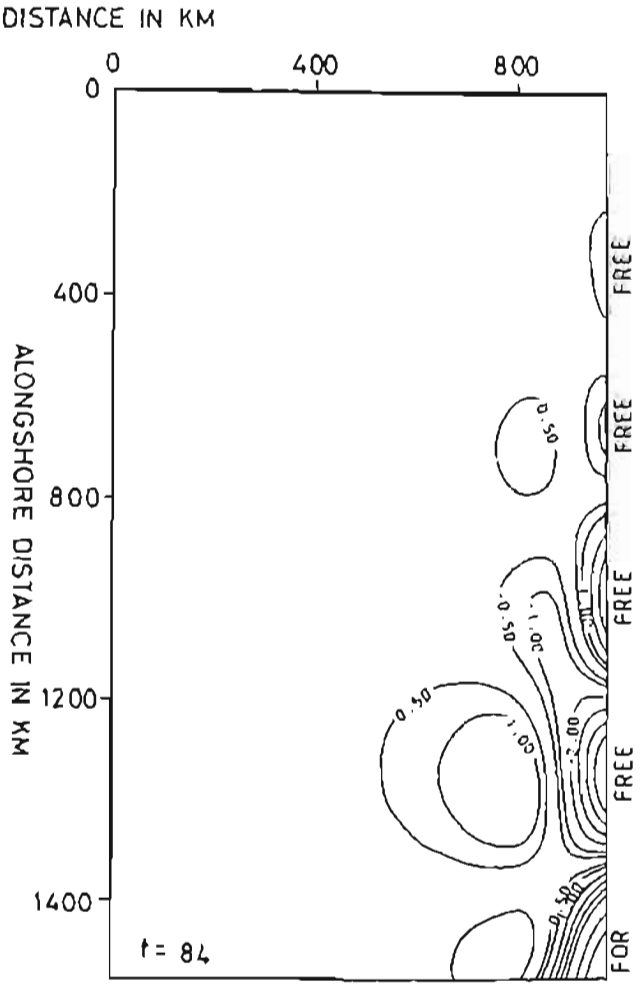

Fig. 7.10c Contours of the sea level response at time, t = 84 hours. [numerical experiment 7]

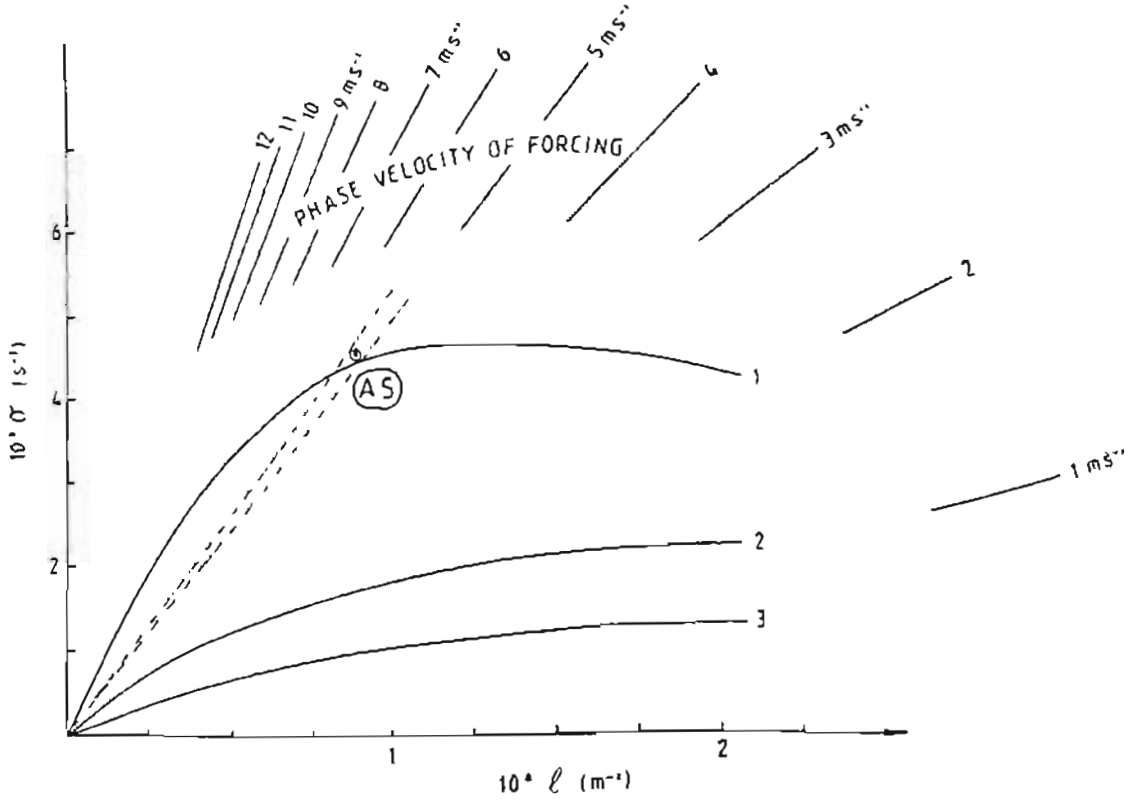

Fig. 7.10d Dispersion curve typical of the "idealised" shelf topography, showing the (σ, ℓ) characteristics (AS) of the response to a wind stress field propagating southwards at 5 m.s-1. [numerical experiment 7]

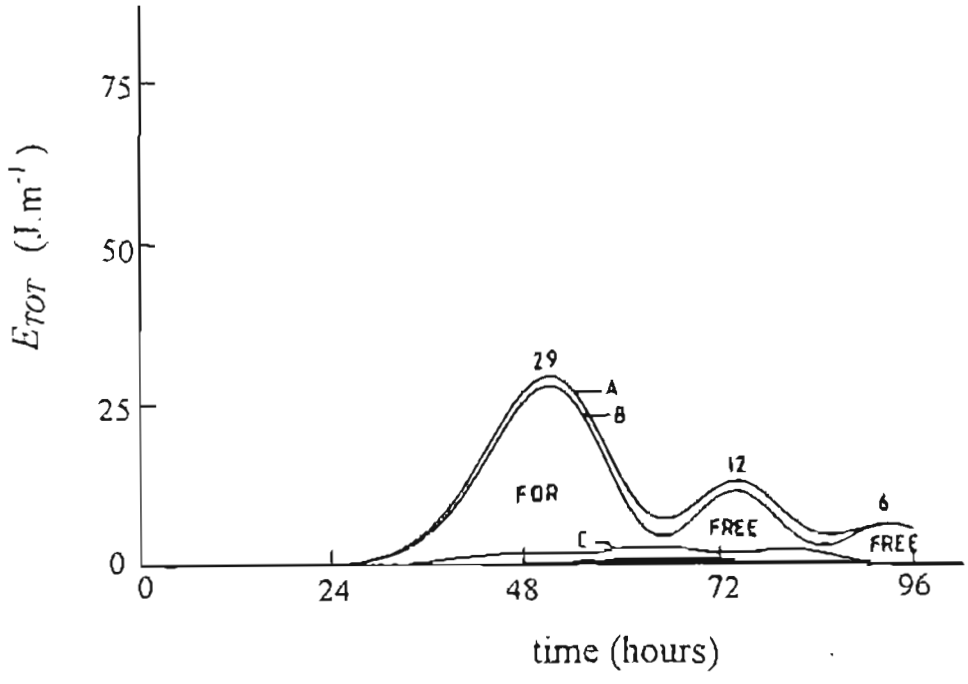

Fig. 7.10e Plot of the total energy at a transect at j = 60 versus time (E_{TOT} vs t). The labels refer to the total cross-shore integrated CTW energy (denoted A), the cross-shore integrated CTW energy in only the shallow shelf waters (denoted B), and the cross-shore integrated CTW energy both over the shelf break and in deeper waters (denoted C). [numerical experiment 7]

Fig 7.10f gives the growth of the forced sea level amplitude with time The growth is initially linear as predicted by Gill and Schumann (1974), but slows down as bottom friction effects become significant.

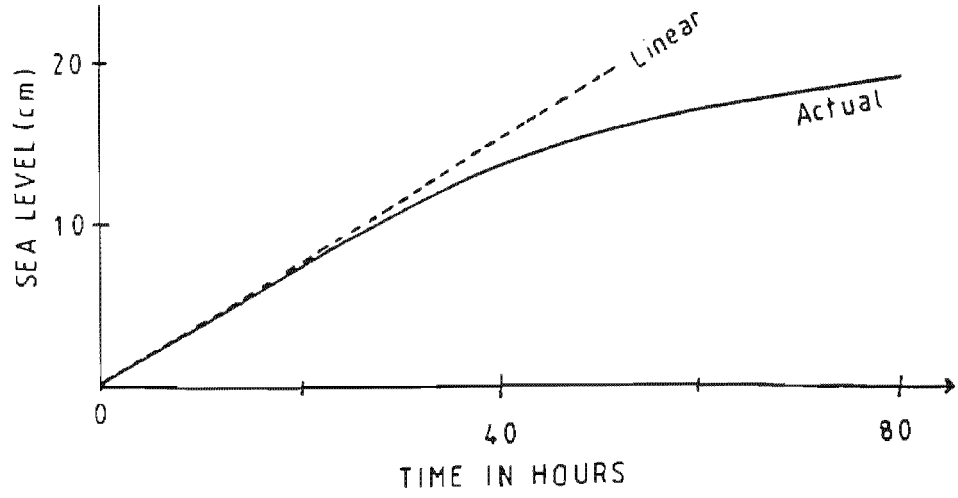

Fig 7.10f Growth of the amplitude of the sea level response with elapsed time. The actual growth observed is contrasted with the linear growth rate of the sea level response anticipated in the absence of bottom friction. [numerical experiment 7]

Numerical experiment 8 (C_f=7 m.s^{-1}, idealised topography, bottom friction)

In this numerical experiment (8), the phase velocity of the forcing function is increased to 7 m.s^{-1}.

The forced CTW is observed to move downstream with the phase velocity of the forcing function, namely 7 m.s^{-1} and a trailing free wave response is generated having

a frequency $\sigma = 4.11 \times 10^{-5}$ s-1 (period T = 42.4 hours),

a wavenumber $\ell = 6.28 \times 10^{-6}$ m^{-1} (wavelength λ_ℓ = 1 000 km),

and a phase velocity C_{ph} = 6.0 to 6.5 m.s^{-1}.

The eigenvalue pair (σ,ℓ) characteristic of the free CTW response are denoted (A7) in Fig. 7.11a, that is, the (σ,ℓ) characteristics of the response lie in a narrow band about the 7 m.s^{-1} line of constant phase velocity of the forcing function. The estimated group velocity of the free wave response is estimated from the dispersion curve in Fig. 7.11a to be $C_g \approx 3.2$ m.s^{-1} which results in more rapid propagation of free wave energy along the shelf. Consequently, the amplitude of the trailing free wave response is significantly reduced (Fig. 7.11b). In general, the energy is the CTW response is less than that in numerical experiment 7 (Fig 7.11c).

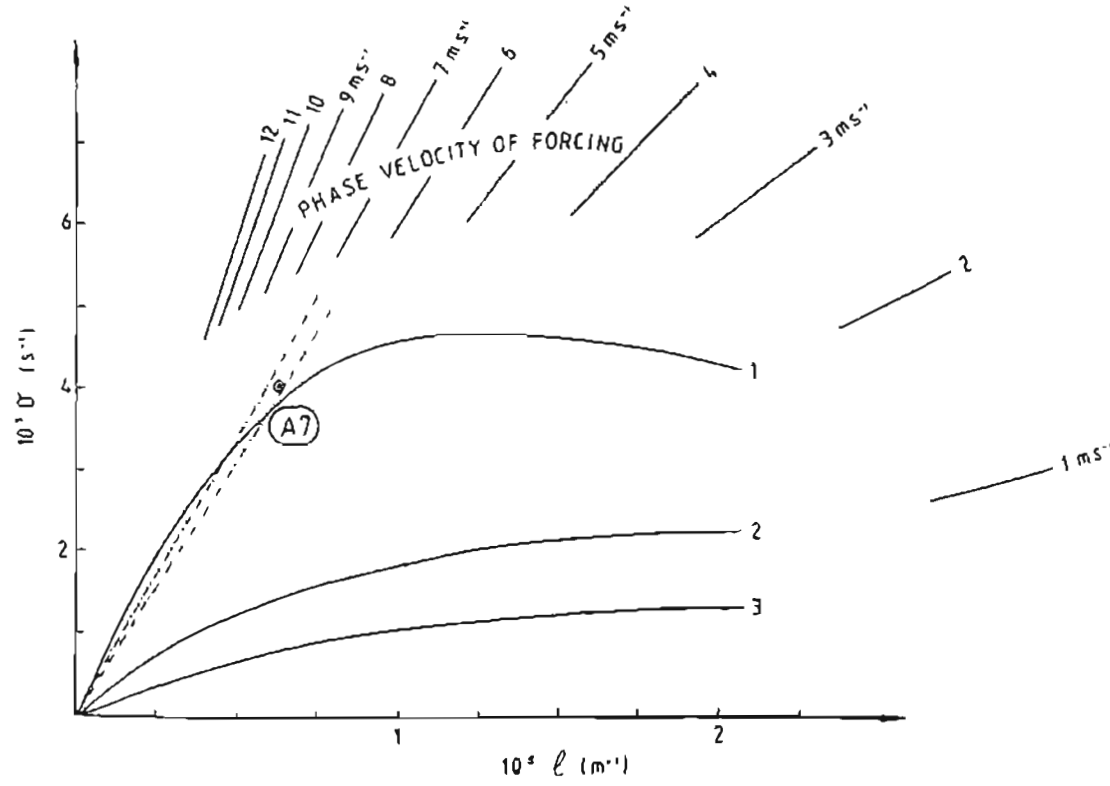

Fig 7.11a Dispersion curve typical of the "idealised" shelf topography, showing the (σ, ℓ) characteristics (A7) of the response to a wind stress field propagating southwards at 7 m.s-1. [numerical experiment 8]

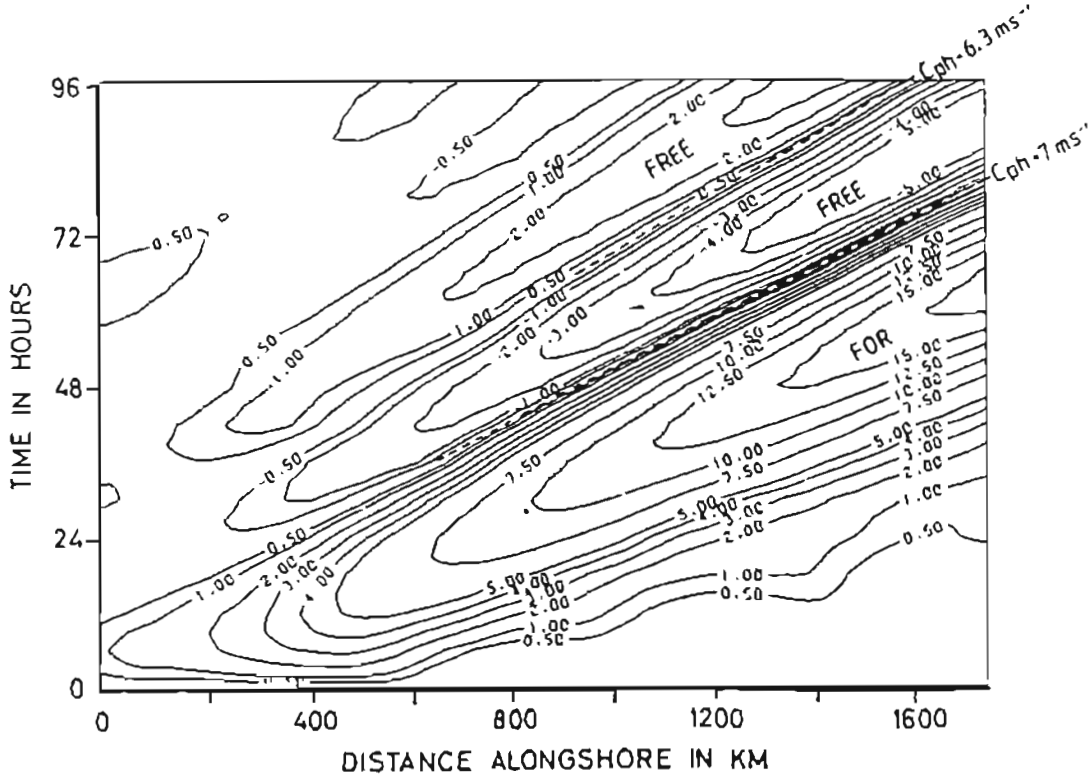

Fig 7.11b Longshore "space-time" plot of the nearshore sea level response [numerical experiment 8]

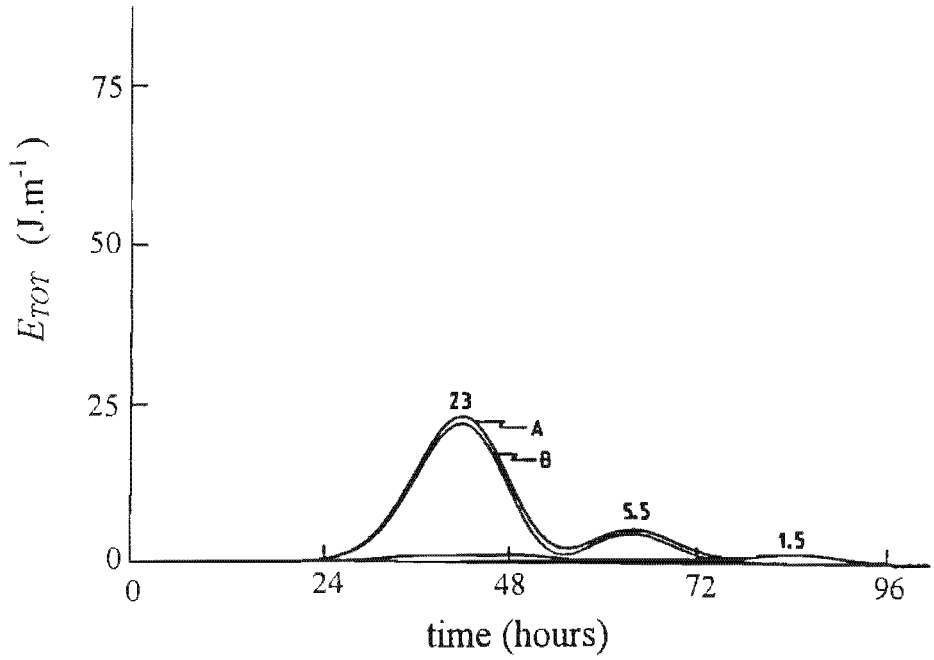

Fig. 7.11c Plot of the total energy at a transect at j = 60 versus time (E_{TOT} vs t). The labels refer to the total cross-shore integrated CTW energy (denoted A), the cross-shore integrated CTW energy in only the shallow shelf waters (denoted B), and the cross-shore integrated CTW energy both over the shelf break and in deeper waters (denoted C). [numerical experiment 8]

Numerical Experiment. 9 (C_f=10 m.s^{-1}, idealised topography, bottom friction)

In numerical experiment 9, all model parameters are kept the same, except for the propagation velocity of the wind stress field which is increased to 10 m.s^{-1}.

The 10 m.s^{-1} line of constant phase speed of the forcing function in Fig. 7.12a does not intersect the dispersion curve of the first mode free CTW because the phase velocity of the forcing is greater than any natural response of the shelf waters. This does not imply that there is no forced motion. On the contrary, both a forced and a very weak free CTW response are discernable in Fig. 7.12b. The forced CTW response is observed not to propagate at the phase velocity of the forcing function, rather the forced CTW propagates at the theoretical maximum phase velocity of free CTW's indicated by the dispersion relation, namely that of the 8 to 9 m.s^{-1} non-dispersive long wave. The free wave response has

a frequency $\sigma = 3.52 \times 10^{-5}$ s^{-1}

a wavenumber $\ell = 5.24 \times 10^{-6}$ m^{-1} (wavelength λ_ℓ = 1 200 km),

and a phase velocity $C_{ph} \approx 7$ m.s^{-1}.

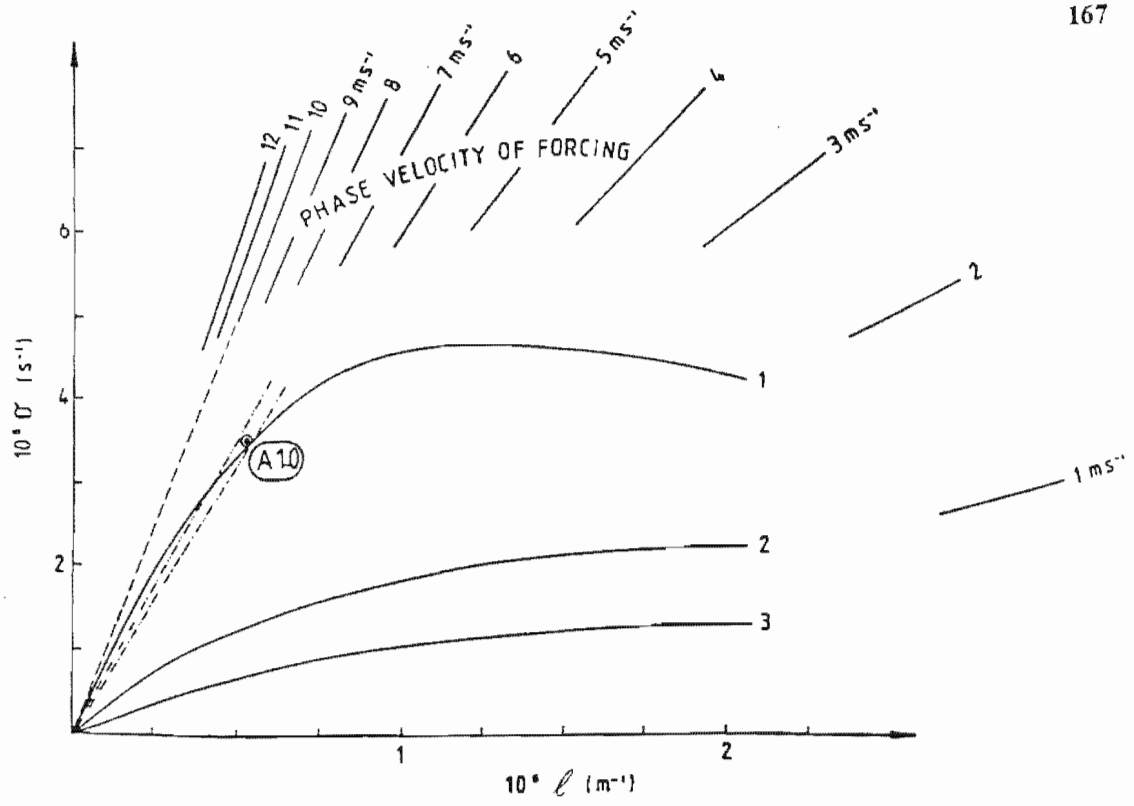

Fig 7.12a Dispersion curve typical of the "idealised" shelf topography, showing the (σ, ℓ) characteristics (A10) of the response to a wind stress field propagating southwards at 10 m.s-1. [numerical experiment 9]

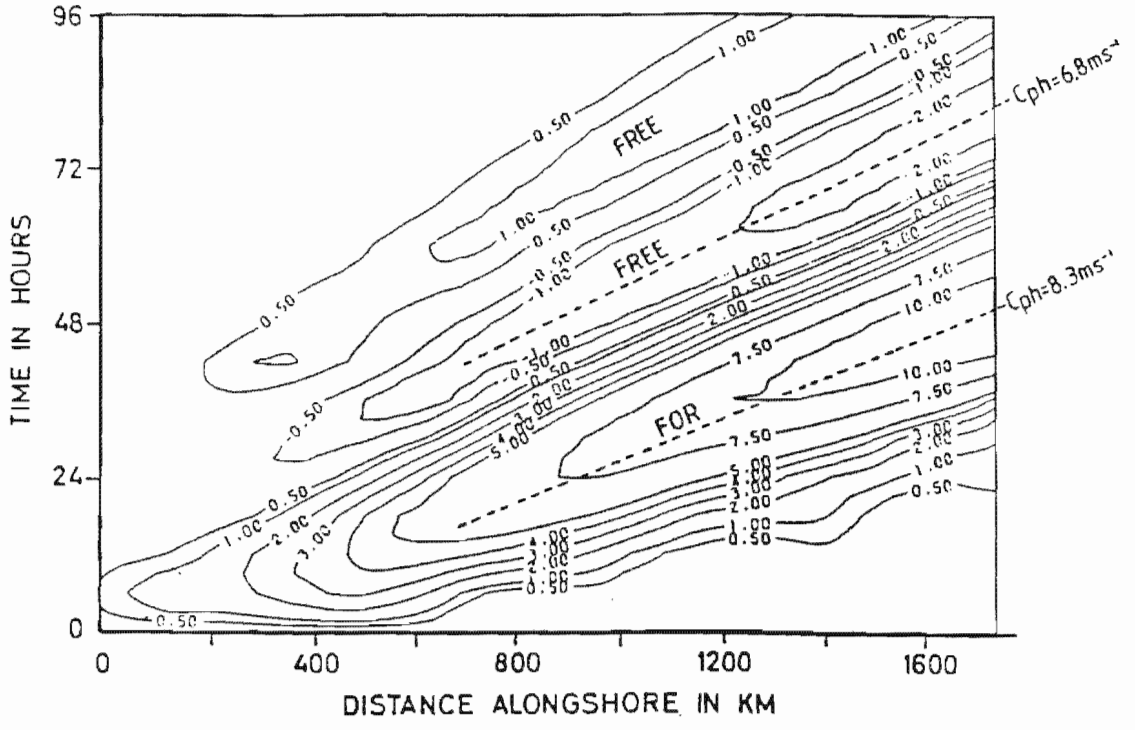

Fig. 7.12b Longshore "space-time" contours of the nearshore sea level response. Note the relatively weak forced and free wave response. [numerical experiment 9]

The estimated group velocity of the free wave is $C_g \approx 4.3$ m.s^{-1}, however the energy in this free wave response is negligible (Fig. 7.12c).

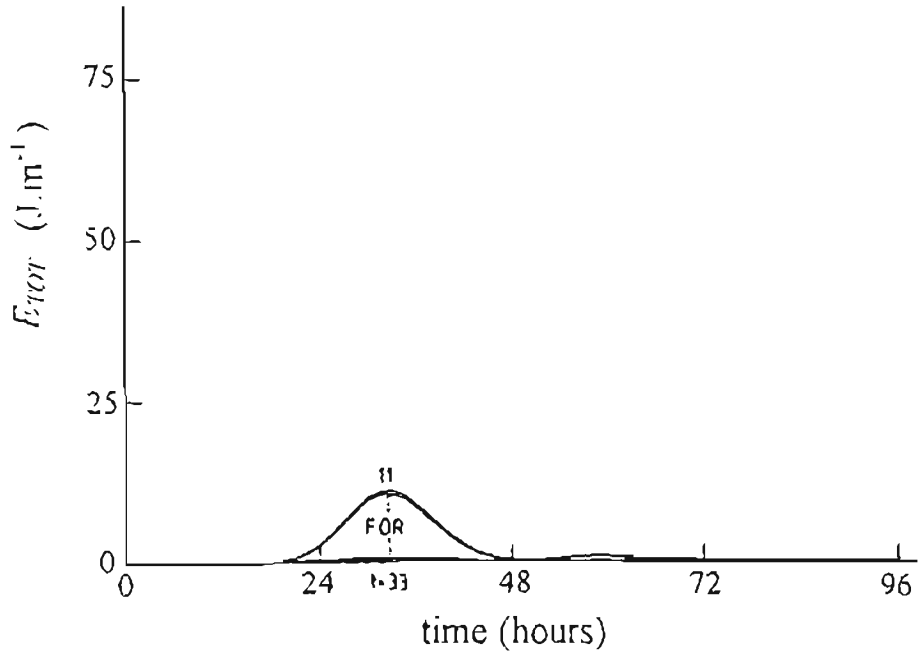

Fig. 7.12c Plot of the total energy at a transect at j = 60 versus time (E_{TOT} vs t). The labels refer to the total cross-shore integrated CTW energy (denoted A), the cross-shore integrated CTW energy in only the shallow shelf waters (denoted B), and the cross-shore integrated CTW energy both over the shelf break and in deeper waters (denoted C) [numerical experiment 9]

The rapidly propagating (10 m.s^{-1}) forcing function is only able to generate a small amplitude response on the essentially non-dispersive region of the dispersion curves (Fig. 7.12a). Since the group velocity is approximately equal to the phase velocity in these non-dispersive CTW's, the free CTW energy propagates at approximately the phase velocity of the forced response. Consequently, the amplitude of the trailing free CTW's is small. The plot of total cross-shelf energy in a transect at j = 60 indicates that the energy in the forced response is very small and that the energy in the trailing free wave response is all but non-existent (see Fig. 7.12c).

Numerical experiment 10 (C_f=1 m.s^{-1}, idealised topography, bottom friction)

In this numerical experiment the phase velocity of the forcing function is reduced to 1 m.s^{-1}. Such a slowly propagating forcing field is able to generate not only first mode shelf waves, but also higher mode waves (see Fig. 7.13a). In a situation such as this the first mode free wave (and often higher mode free waves) propagates more rapidly along the shelf than the forcing function, enabling the free wave response to propagate ahead of the wind stress field (Fig. 7.13b).

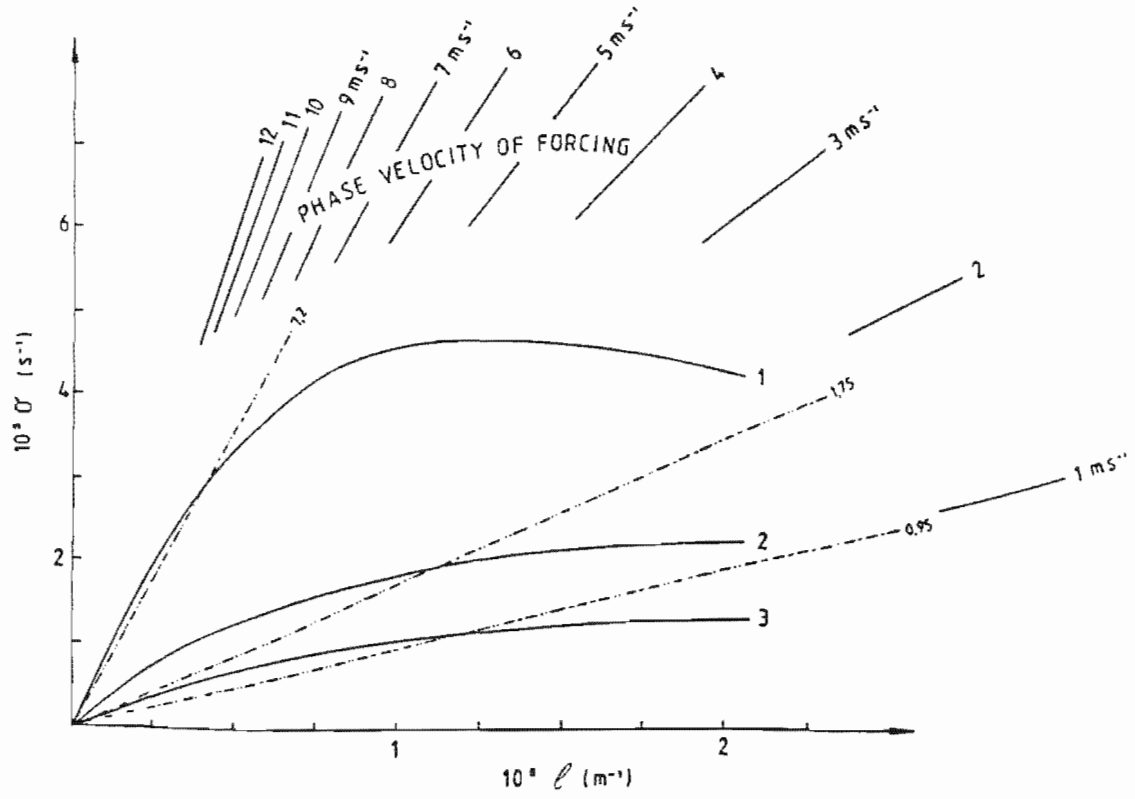

Fig. 7.13a Disperstion curve typical of the idealised shelf topography, where the dotted lines indicate the phase speeds of the different wave motions identified in numerical experiment 10.

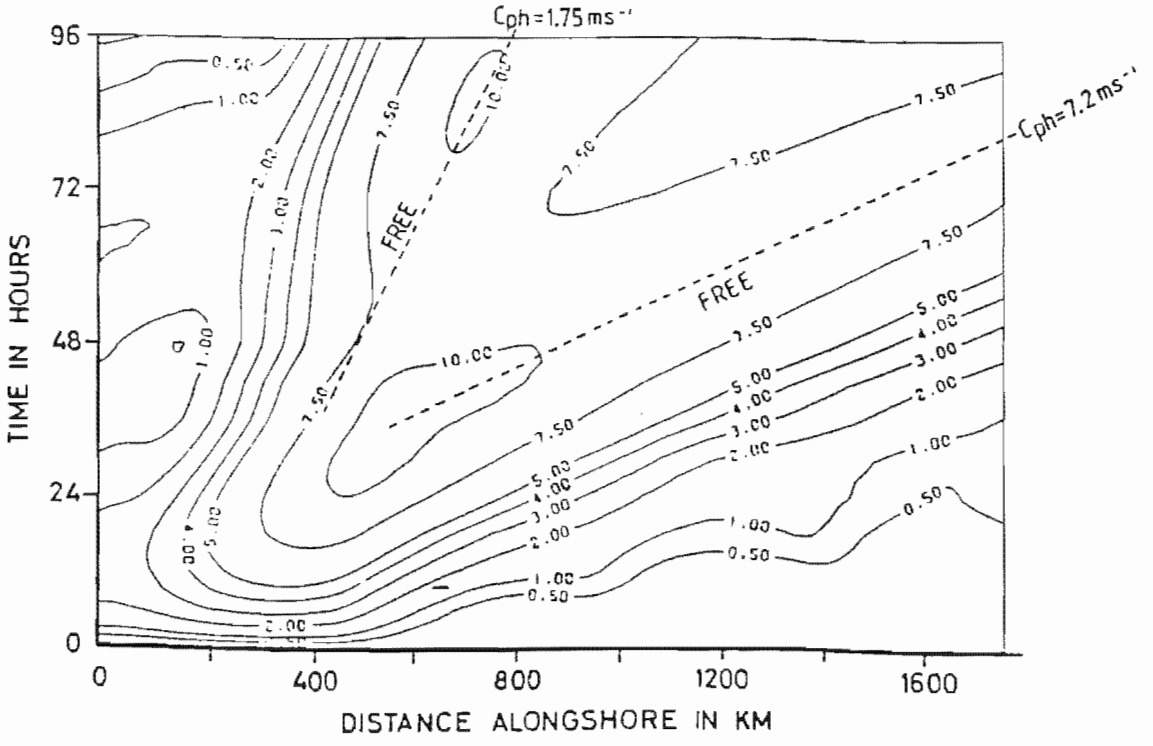

Fig 7.13b Longshore "space-time" contours of nearshore sea level response [numerical experiment 10]

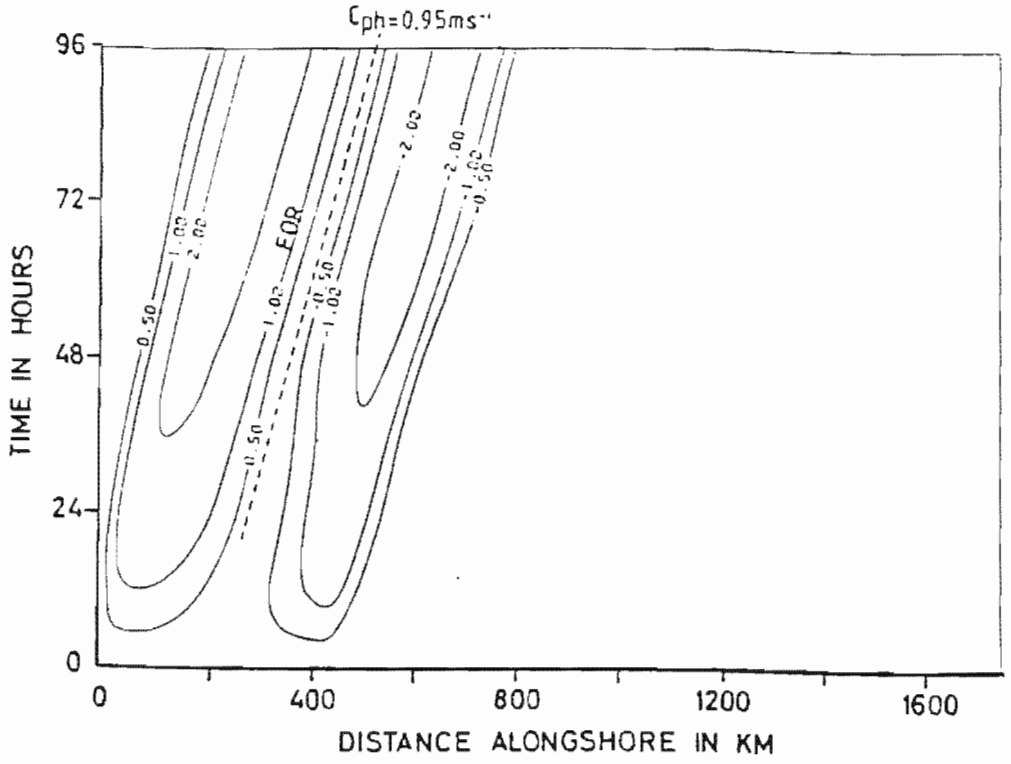

Fig 7.13c Longshore "space-time" contours of the cross-shore velocity response at the shelf edge [numerical experiment 10]

The phase velocities of the motions identified in Fig. 7.13b and Fig. 7.13c are:

i) a phase velocity C_{ph} (n=1) = 7,2 m.s^{-1} which is the non-dispersive first mode (n=1) wave which propagates along the shelf ahead of the forcing.

ii) a phase velocity C_{ph} (n=2) = 1,75 m.s^{-1} which are higher mode (n=2) wave motions which are generated by the slowly propagating wind stress field.

iii) a phase velocity C_{ph} (n=3) ≈ 0,95 m.s^{-1} which is the forced wave (Fig. 7.13c).

Note that the free wave motions in (ii) and (iii) above have an alongshore scale comparable to that of the wind stress field (Fig. 7.13a) and, as expected for higher mode observations, are clearly observable at the shelf-edge.

A plot of the energy in a cross-shelf transect at j = 60 (not shown) indicates that the total energy in the free CTW preceding the forcing is equal in magnitude to the total energy in the directly forced CTW response.

Numerical experiment 11 (C_f=5 m.s^{-1}, W=800km, idealised topography, bottom friction)

The forcing function in numerical experiment 11 is a wind stress field of increased longshore extent (W = 800 km) which propagates southwards along the shelf at a phase velocity of 5 m.s^{-1}.

Since greater energy is available in the more extensive wind field, the energy in the forced wave motion is larger than in numerical experiment 7. A free wave response is present (Figure 7.14a) having

a frequency $\sigma = 4.45 \times 10^{-5}$ s^{-1},

a wavenumber $\ell = 8.85 \times 10^{-6}$ m^{-1}, ($\lambda_\ell \approx 710$ km) and

a phase velocity C_{ph} = 5.0 m.s^{-1}.

Although the free wave has almost the same frequency-wavenumber characteristic as in numerical experiment 7, the energy in the trailing free waves is greatly reduced (Fig. 7.14b).

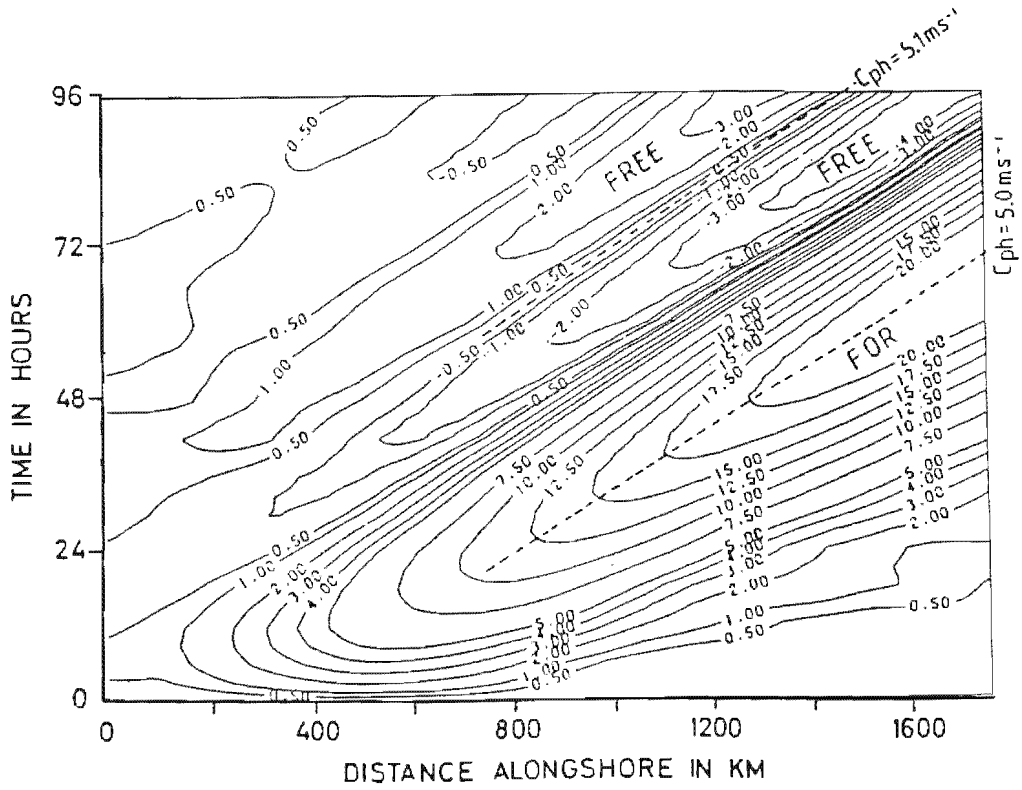

Fig 7.14a Longshore "space-time" contours of the nearshore sea level response in experiment 11.

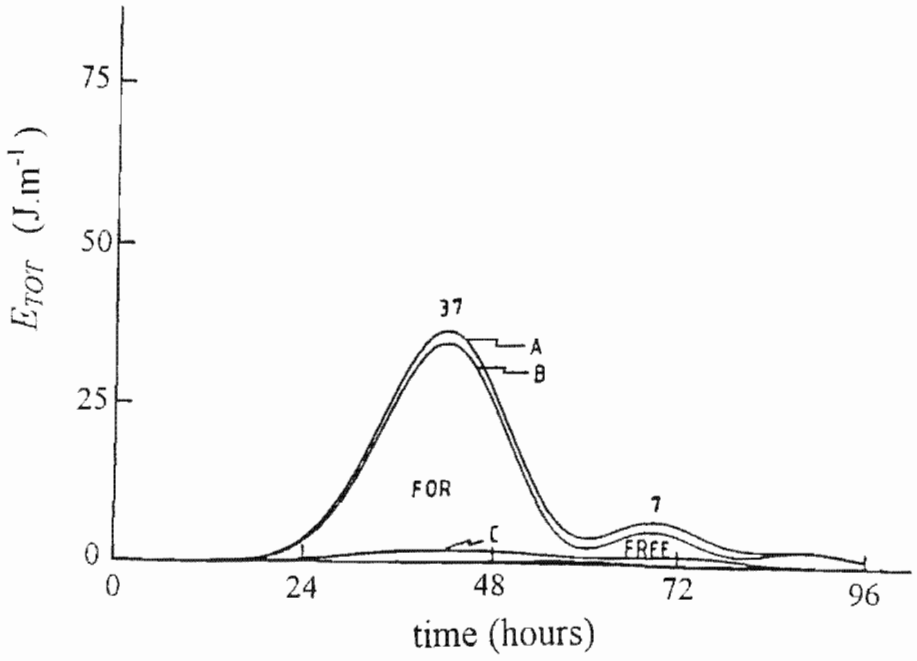

Fig 7.14b Plot of the total energy at a transect at j = 60 versus time (E_{TOT} vs t). The labels refer to the total cross-shore integrated CTW energy (denoted A), the cross-shore integrated CTW energy in only the shallow shelf waters (denoted B), and the cross-shore integrated CTW energy both over the shelf break and in deeper waters (denoted C). [numerical experiment 9]

The results of experiments 7 to 11 may be summarised as follows:

i) Provided the phase speed of the forcing field is equal to or less than that of the first mode, non-dispersive free CTW characteristic of the particular shelf profile under consideration, then both forced and free waves are clearly distinguishable. The forced wave develops (σ,ℓ) characteristics typical of the forcing field, while the trailing free waves develop (σ,ℓ) characteristics given by the approximate intersection of the dispersion curves with a line specifying the phase velocity of the forcing function.

If the response generated lies on the non-dispersive region of the dispersion curve then the group velocity of the response is approximately equal to the phase velocity of the response and the energy then propagates along the shelf at the phase speed of both the free and forced CTW as well as that of the forcing function. Consequently, very little energy is present in the trailing free wave response (numerical experiment 8 and 9). Since the response is essentially non-dispersive, it is seen as a single "event". This is typically the situation along most of the southern African continental shelf.

Conversely, if the response generated lies on the highly dispersive region of the curve then the group velocity is much smaller than the phase velocity of the free CTW motions. This results in a significant train of free CTW's trailing the forced CTW (numerical experiment 7).

ii) If the phase speed of the forcing function is greater than that of the first mode, non-dispersive free CTW characteristic of the particular shelf profile under consideration, a weaker non-dispersive CTW response is generated (where the group velocity is equal to the phase velocity). Since the response is non-dispersive, there is little evidence of the trailing free CTW's. The forced and free CTW response are indistinguishable since $C_g \approx C_{ph}$.

In general, the amplitude of the response is inversely proportional to the difference in phase speed of the forcing function and the non-dispersive first mode free CTW, that is, the greater the mismatch in these phase speeds the smaller is the amplitude of the response. Where the forcing function propagates along the shelf at velocities exceeding the maximum, non-dispersive free CTW phase velocitiy characteristic of the shelf topography under consideration, the amplitude of the CTW response drops off very rapidly with increasing propagation velocitiy of the forcing. This is most probably due to the fact that the forcing moves through the system (model domain) so rapidly that the response does not have time to develop its full amplitude.

iii) If the phase speed of the forcing function is sufficiently small, higher mode CTW's may be generated. These higher mode CTW which have small group and phase velocities are particularly susceptible to topographic scattering. The first mode free CTW generated by such a slowly propagating wind stress field has a phase velocity that exceeds that of the wind stress field and is observed to propagate (southwards) ahead of the wind stress field. Under these circumstances, the free CTW response is observed to arrive at a particular site before the wind stress field responsible for generating these CTW motions.

iv) If the longshore extent of the wind stress field is increased, the amplitude of the directly forced response increases while the amplitude of the trailing free wave response is reduced.

One may conclude that the greater the longshore extent of the wind stress field and the greater the phase speed of the forcing, the smaller is the amplitude of the trailing free wave motions. This implies that the response to the relatively rapid propagating wind stress fields on the West Coast and South Coast (as indicated in chapter 5) may be considered to be a single "event" resonant with the wind-forcing. No periodic (free CTW) motion associated with the forcing is likely to be observed. This does not preclude the observation of remotely forced periodic motions at sites along the West Coast On the contrary, such remotely forced CTW's, originating north of the study area (that is, north of Walvis Bay), are documented in chapter 5.

7.4 The Forced Response over the West Coast Shelf Topography

The forcing in numerical experiments 12 is the same as that used in numerical experiment 11 (C_f = 5 m.s^{-1}, W = 800 km), however here the longshore band of wind stress propagates over a realistic parameterisation of west coast continental shelf topography. In numerical experiment 13, the phase speed of propagation of the wind stress field is increased to 7 m.s^{-1}

Numerical experiment 12 (C_f=5 m.s^{-1}, W=800km, realistic topography, bottom friction)

Here the forcing comprises a wind stress field having a longshore extent of 800 km which propagates along the shelf at 5 m.s^{-1}. As before, the maximum amplitude of the wind stress field is 0.12 N.m^{-2} (which roughly corresponds to a NNW wind of 8 m.s^{-1}).

The coastal sea level (Fig. 7.15a) and longshore velocity response (Fig. 7.15b) are less coherent than in numerical experiments 7 to 11. The coastal sea level response reaches a maximum amplitude of 10 cm, while the longshore velocity response is typically 20 cm.s^{-1}. Acceleration of the longshore velocity occurs in the vicinity of prominent capes and where the shelf narrows due to a steeper slope in the offshore topography. The amplitude of the response grows rapidly over the Orange River cone and the regions just to the south of the Orange River cone.

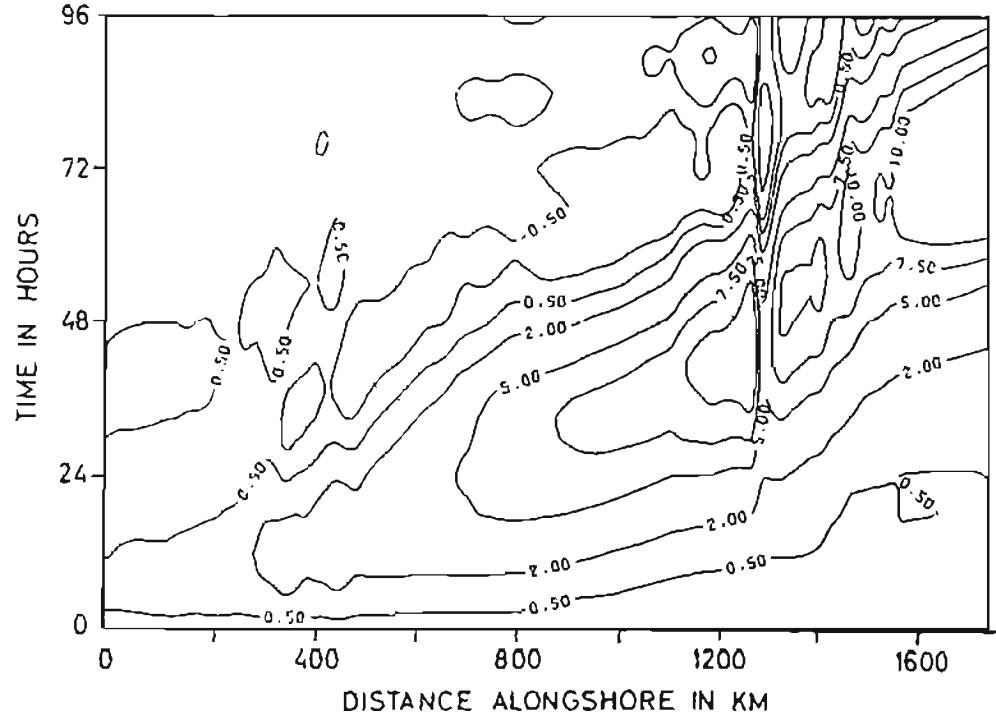

Fig. 7.15a Longshore "space-time" contours of the coastal sea level response [numerical experiment 12]

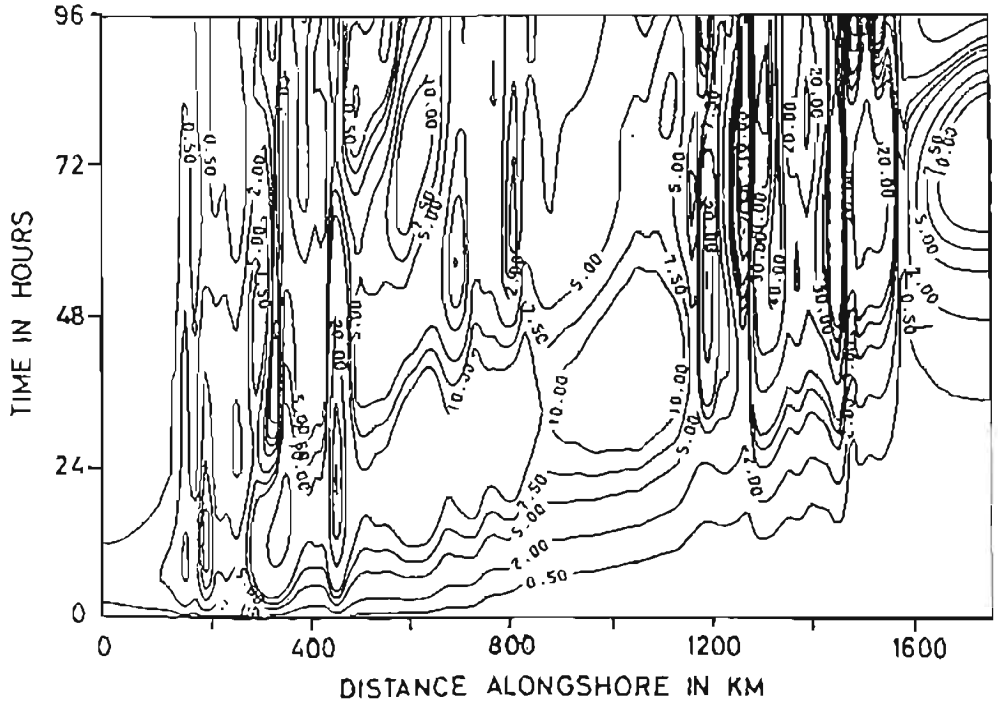

Fig 7.15b Longshore "space-time" contours of the longshore velocity response at the coast [numerical experiment 12]

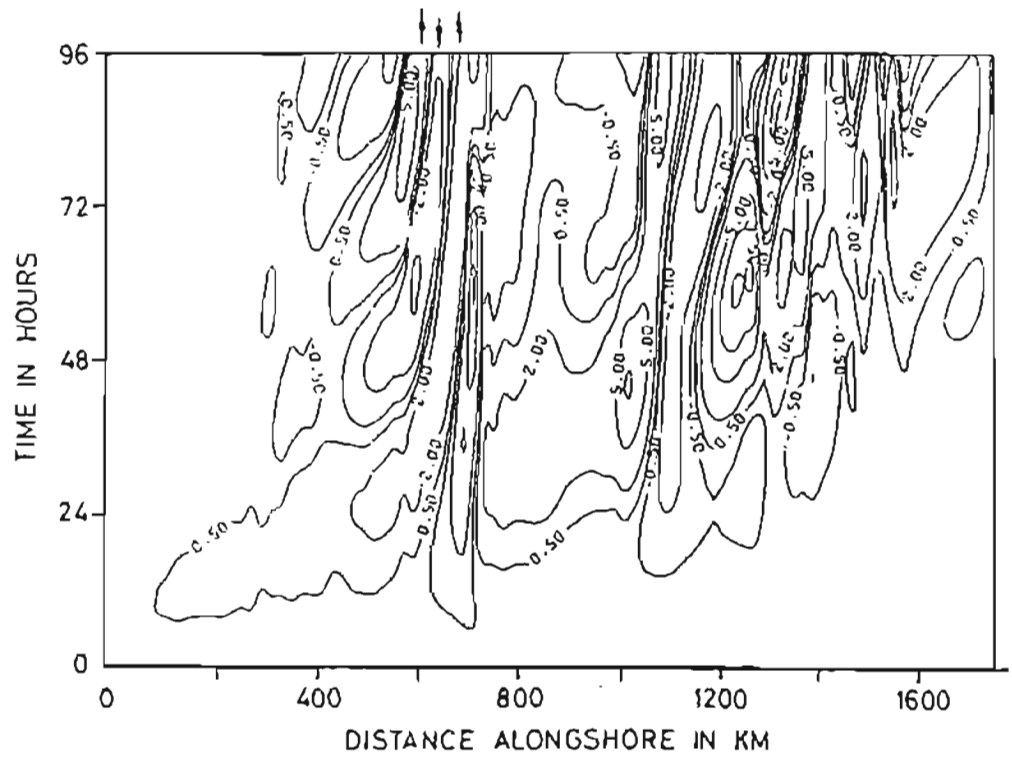

Fig. 7.15c Longshore "space-time" contours of the cross-shore velocity response in the nearshore transect. The arrows indicate the direction of the strong cross-shore flows that develop [numerical experiment 12]

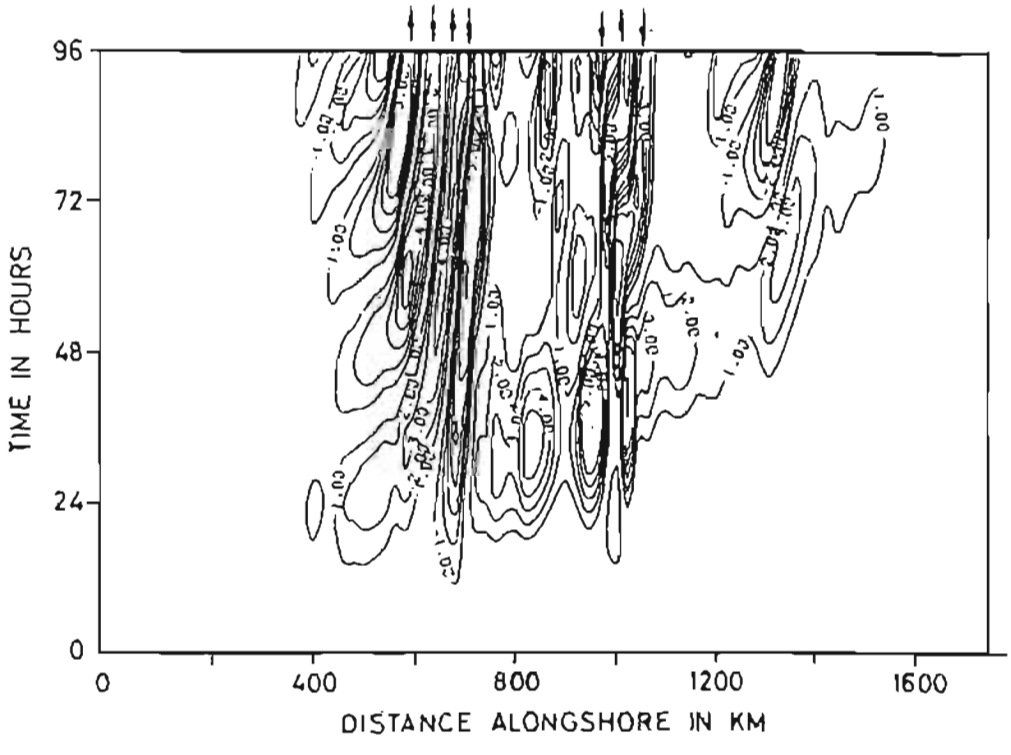

Fig. 7.15d Longshore "space-time" contours of the cross-shore velocity response at the shelf edge. The arrows indicate the direction of the strong cross-shore flows that develop [numerical experiment 12]

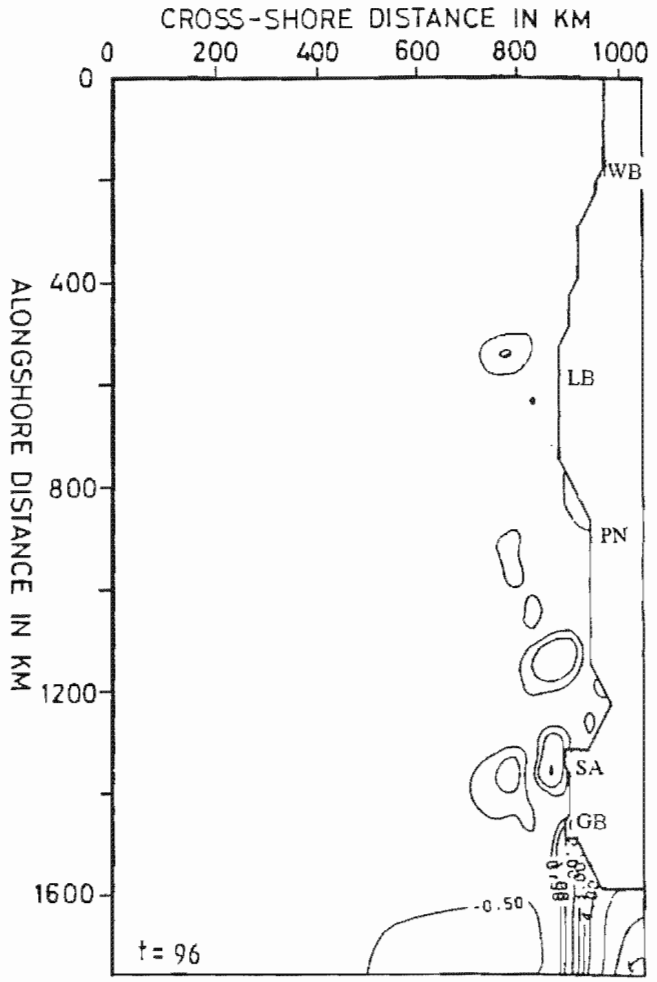

Fig. 7.15e Contours of the sea level response (at time t = 96 hours) when the wind-forcing has propagated out of the numerical domain through the southern boundary. Note the sea level anomalies which remain trapped in the vicinity of large changes in the shelf topography. [numerical experiment 12]

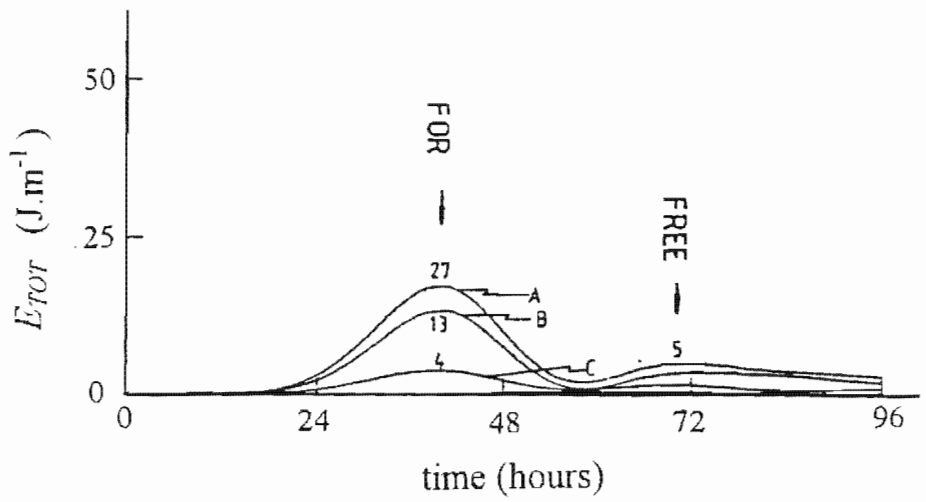

Fig. 7.15f Plot of the total energy at a transect at j = 60 versus time (E_{TOT} vs t). The labels refer to the total cross-shore integrated CTW energy (denoted A), the cross-shore integrated CTW energy in only the shallow shelf waters (denoted B), and the cross-shore integrated CTW energy both over the shelf break and in deeper waters (denoted C). [numerical experiment 12]

The development of strong, quasi-steady onshore/offshore flows just south of Lüderitz and in the vicinity of Hondeklip Bay is observed in the coastal (Fig. 7.15c) and shelf-edge (Fig. 7.15d) cross-shore velocity response. These strong onshore/offshore flows are associated with backscattered CTW motions which propagate slowly northwards (see Fig. 7.15d). These cross-shelf motions and their associated sea level anomalies (Fig. 7.15e) decay relatively slowly. Weaker cross-shelf motions, associated with large changes in the coastline orientation, occur just north of Cape Columbine. The shorter scales of motion that develop in the region south of Cape Columbine are associated both with the topographic scattering of the forced and free wave response as well as the narrowing shelf in these southern regions.

A significantly larger proportion of the total cross-shelf energy in a transect at j = 60 lies over the shelf slope (compare curve C in Fig. 7.15f with that in Fig 7.14b). This is indicative of topographic scattering of the forced response into higher mode and higher wavenumber motions. The energy in the trailing free wave response is seen in Fig. 7.15f to be very small.

Numerical experiment 13 (C_f=7 m.s^{-1}, W=800km, realistic topography, bottom friction)

In this numerical experiment the phase velocity of the wind stress field is increased to 7 m.s^{-1}. The direction of the wind stress is reversed (the maximum amplitude of the wind stress is changed to -0,12 N.m^{-2} representing a SSE wind). For the small bottom friction parameters used, the 180° change in direction of the wind results in a 180° change in the direction of the response, but does not qualitatively modify the results.

As expected from previous results (Section 7.3), the amplitude of the response (Fig. 7.16a) decreases with an increase in the phase velocity of the moving wind stress field and the energy in the free wave response is negligible (Fig. 7.16b).

Significant cross-shelf motions develop at the same locations as in numerical experiment 12 (Figs 7.16c and d) but are not as steady or as intense as the motions in numerical experiment 12. Once again these cross-shore flows are seen to persist in the vicinity of these locations long after the forcing field has passed (Figure 7.16e). In fact, the energy in the backscattered wave motions comprising these cross-shelf flows,

are observed to travel slowly northwards away from the regions of strong topographic change (Fig. 7.16d) This observation is consistent with the theory of topographic scattering reviewed in chapter 4. The apparent incoherence of the velocity vectors over the shelf south of Cape Columbine (see Fig. 7 16e) is indicative of the shorter scales of motion developed in these southern regions of the West Coast.

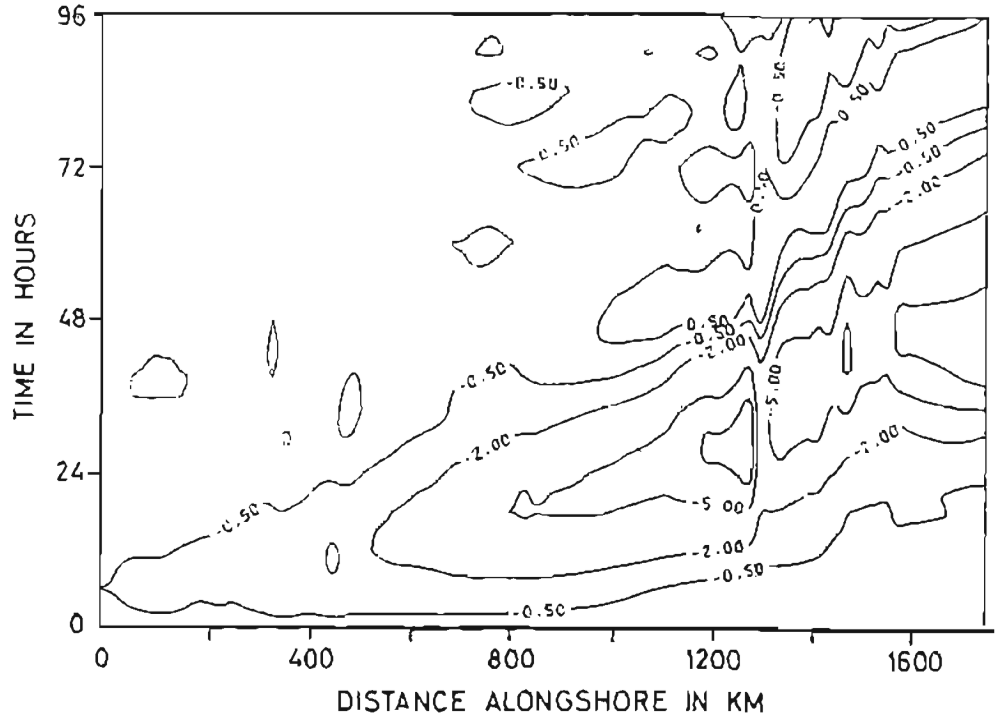

Fig 7.16a Longshore "space-time" plot of coastal sea level response, showing a decreased response to the faster propagating wind stress field in numerical experiment 13.

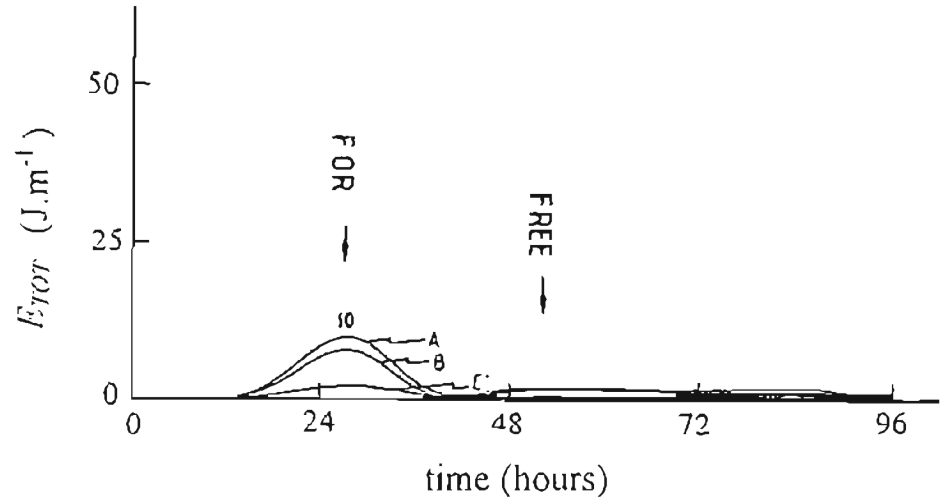

Fig. 7.16b Plot of the total energy at a transect at j = 60 versus time (E_{TOT} vs t). The labels refer to the total cross-shore integrated CTW energy (denoted A), the cross-shore integrated CTW energy in only the shallow shelf waters (denoted B), and the cross-shore integrated CTW energy both over the shelf reak and in deeper waters (denoted C). [numerical experiment 13]

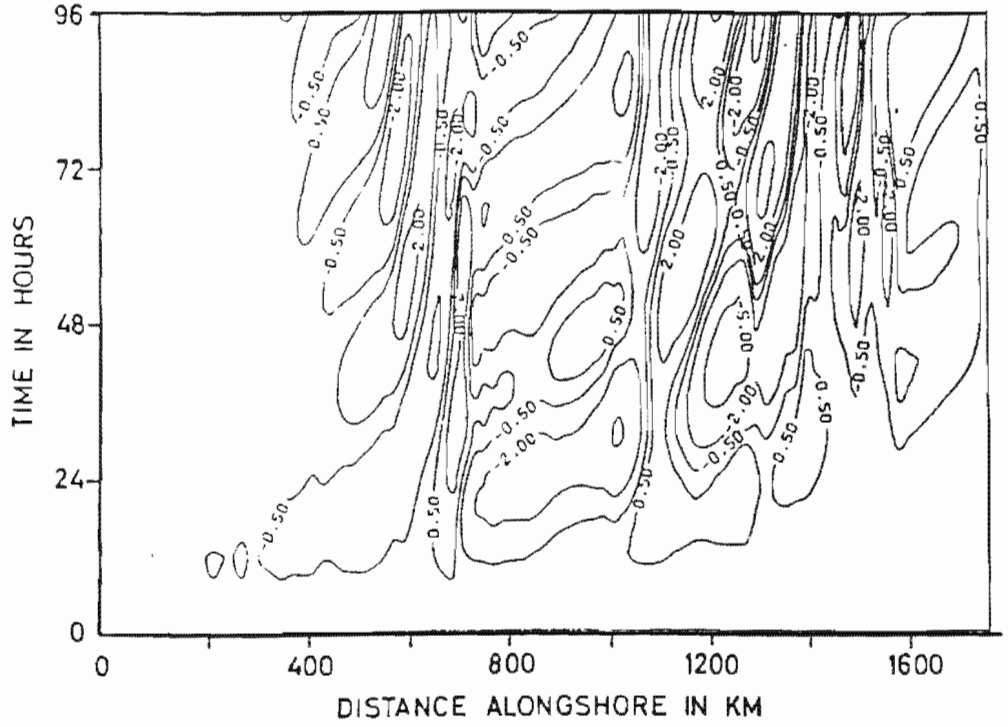

Fig 7.16c Longshore "space-time" plot of cross-shore velocities in a nearshore transect [numerical experiment 13].

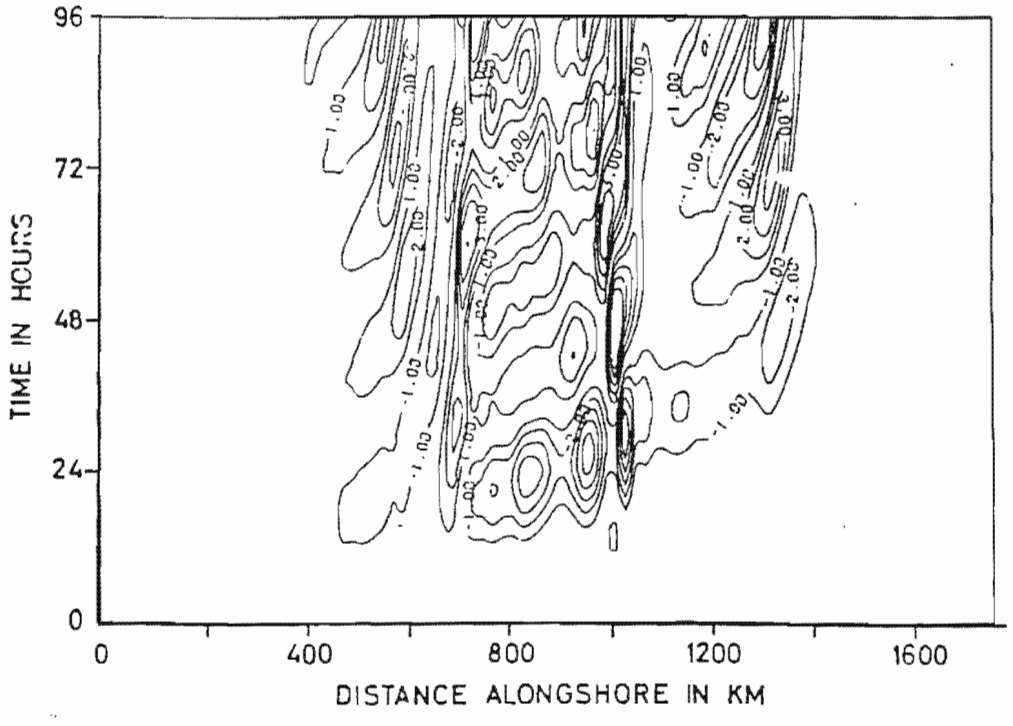

Fig 7.16d Longshore "space-time" plot of cross-shore velocities at the shelf edge [numerical experiment 13].

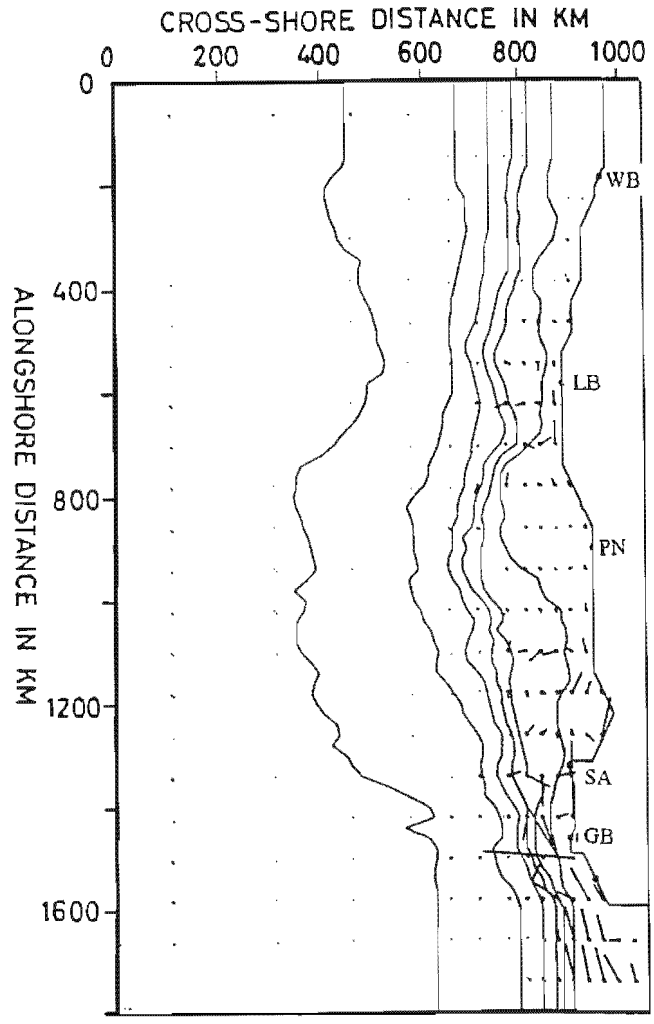

Fig. 7.16e Velocity field (at time t = 96 hours) after the wind-forcing has propagated southwards of the numerical domain through the southern boundary. [numerical experiment 13]

Comparison of numerical experiments 12 and 13 show that the stronger and more coherent cross-shore flows develop where the forcing propagates southwards at lower phase speeds. This is because the wave motions generated in experiment 12 have frequency and wavenumber properties such that their group velocity is close to zero. Not only are these waves more easily scattered by variations in the topography (Brink, 1980), but also the resultant scattered waves have a group velocity very close to zero. This implies that the energy in the backscattered motions is stationary, resulting in quasi-steady, cross-shore flows over the large changes in topography observed in numerical experiment 12. (These flows are considered quasi-steady in that they remain oscillatory, but are trapped over the large changes in bottom topography and consequently do not move much along the shelf.) There is reduced topographic scattering of the less dispersive wave motions generated in experiment 13. The backscattered wave motions also have a small negative group velocity, resulting in a

slow northward propagation of energy away from the large charges in bottom topography. Consequently, the cross-shore flows developed are less intense and less steady.

The backscattered motions typically have wavelengths of greater than 120 km and are thus adequately resolved in the numerical model (see Appendix D). Consequently these trapped or almost steady motions are real physical results of the model rather than artefacts of the numerical model resulting from numerical dispersion.

7.5 The Forced Response due to Realistic Wind-forcing over the West Coast Shelf Topography

In experiments 14 and 15, a more realistic wind stress profile is used. A SSE wind, with a maximum amplitude at Lüderitz, is assumed to be present over the whole model domain. An offshore decaying band of NNW wind stress travels southwards at 5 ms^{-1} through the SSE wind stress field. Although the propagation velocity of wind stress fields along the West Coast is generally greater than 5 $m.s^{-1}$, the results of the numerical experiments which follow are nevertheless representative of CTW generation by more rapidly propagating wind stress fields.

Numerical experiment 14 (realistic wind-forcing, idealised topography, bottom friction)

In this numerical experiment the response to realistic wind forcing over an idealised shelf topography is investigated. Fig. 7.17a indicates that there is a general drop in the nearshore sea level due to the SSE wind. A positive sea level anomaly travels along the shelf in sympathy with the moving NNW wind stress field. There is slight evidence of a free wave response but these motions have a very small amplitude.

Fig. 7.17b indicates how the coastal sea level at a particular longshore site develops with time. The energy diagnostic normally used is not useful here as the energy diagnostic is dominated by a strong almost steady longshore velocity driven by the SSE wind stress field.

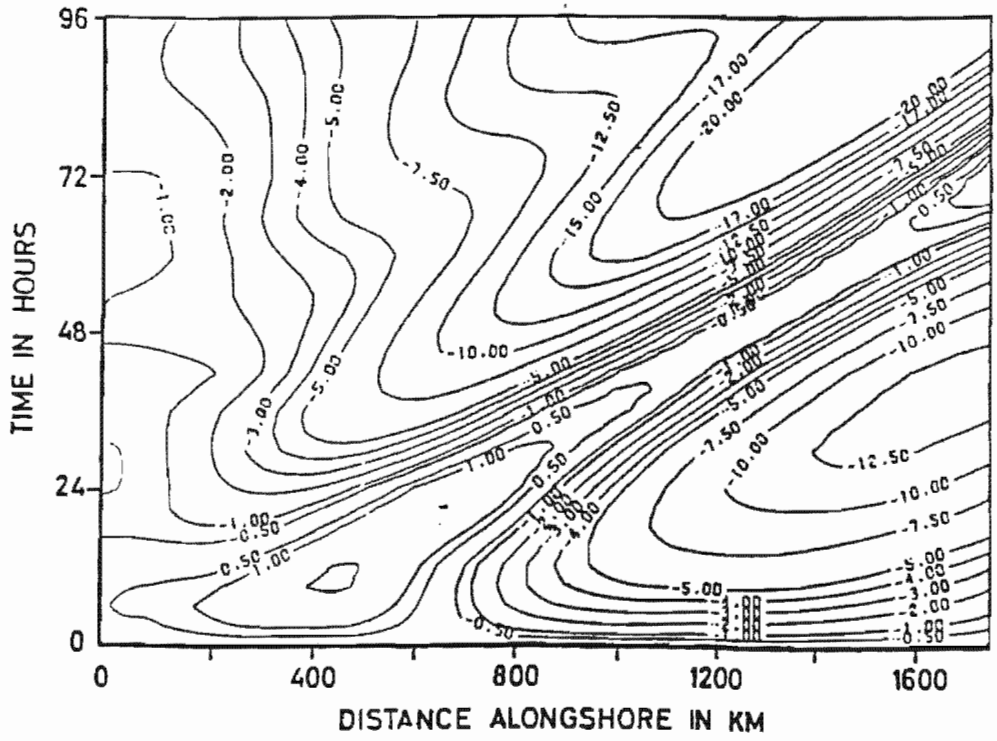

Fig 7.17a Longshore "space-time" contours of the nearshore sea level response. [numerical experiment 14]

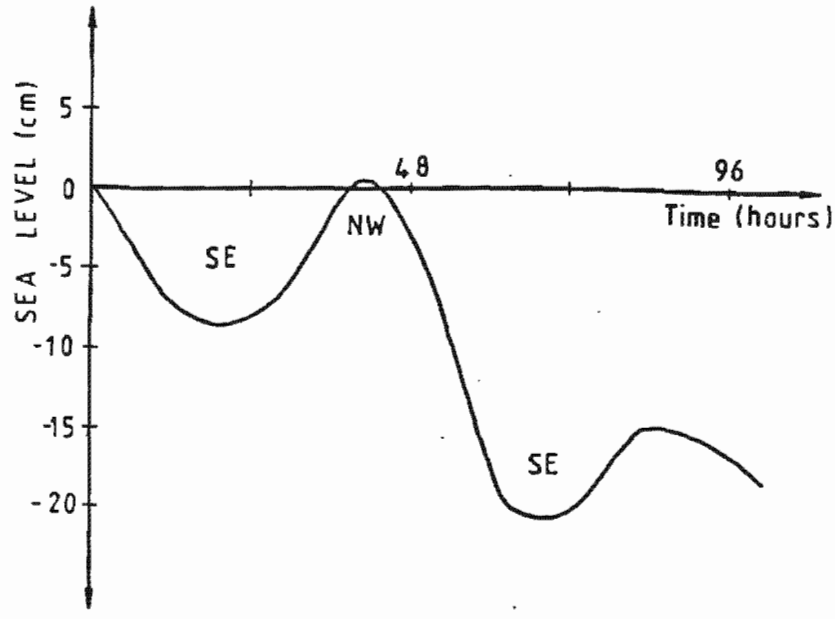

Fig 7.17b Plot of the evolution of sea level with time at a particular site along the shelf. [numerical experiment 14]

Numerical experiment 15 (realistic wind-forcing, realistic topography, bottom friction)

In this numerical experiment the response to realistic wind-forcing over the West Coast shelf topography is investigated. There is a general decrease in coastal sea level in response to the SSE winds with the largest negative anomalies in the sea level occurring just south of Lüderitz and between Cape Columbine and Cape Point (Fig. 7.18a).

Figs. 7.18b and 7.18c indicate the development of strong cross-shelf motions just south of Lüderitz and in the vicinity of Hondeklip Bay, however the flow off Hondeklip Bay is less steady and shows evidence of northward propagation of short wavelength CTW's.

Experiments 14 and 15 indicate a response in which the forced wave dominates. There is little or no evidence of the trailing free wave response. The only significant motions besides the strong longshore velocity response driven by the SSE wind, are the amplitude cross-shore flows which develop in the vicinity of large alongshore variations in the bottom topography.

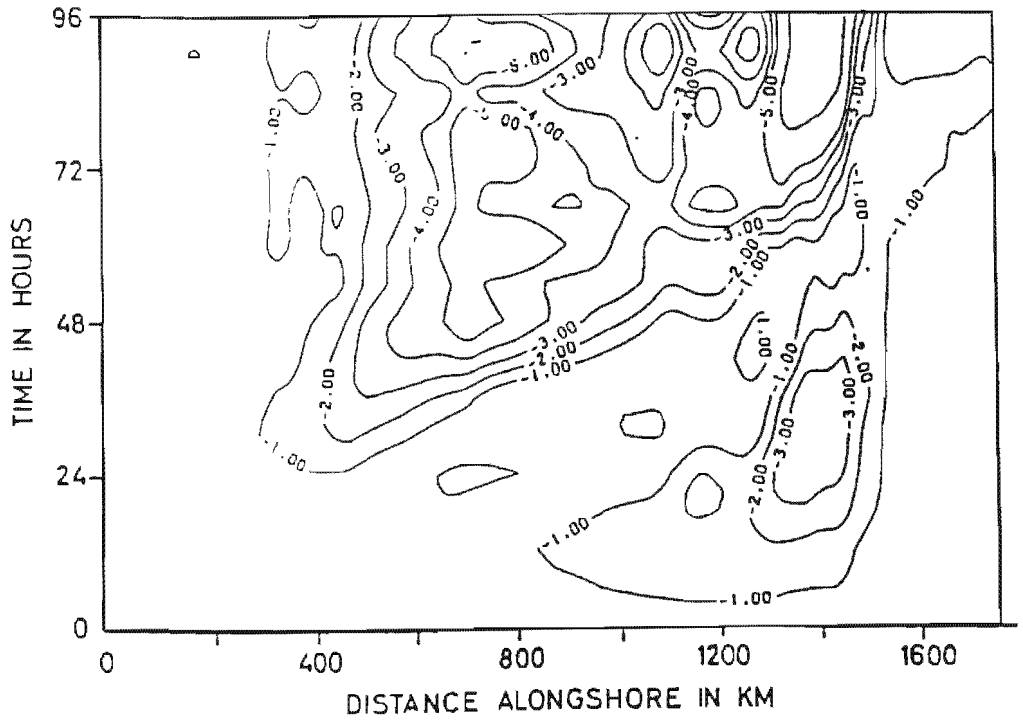

Fig. 7.18a Longshore "space-time" contours of the coastal sea level response [numerical experiment 15]

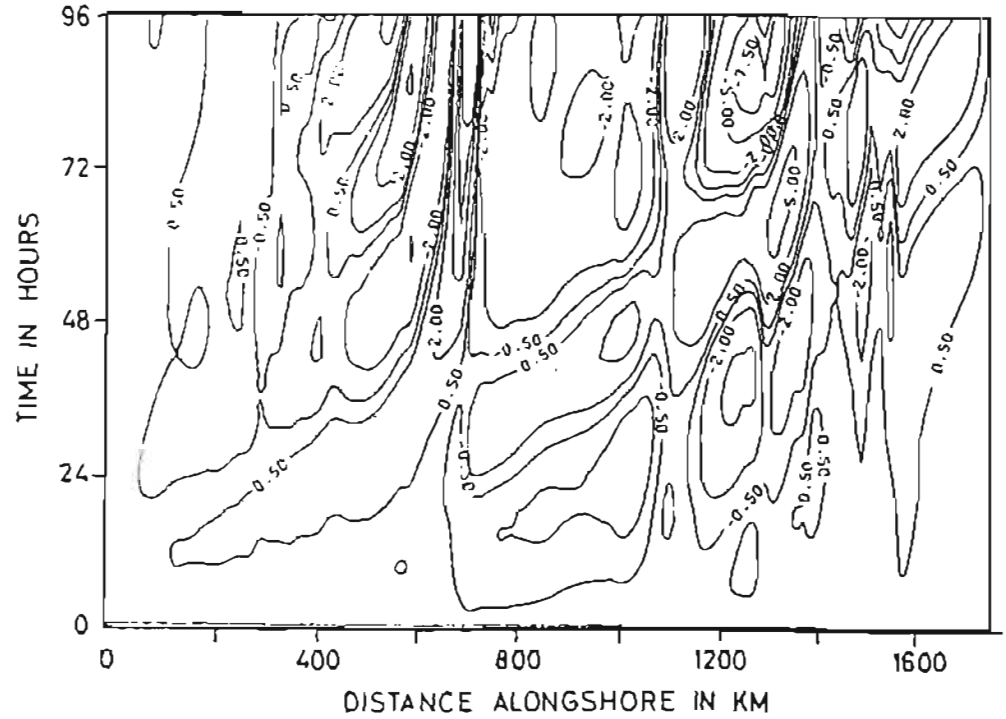

Fig. 7.18b Longshore "space-time" contours of cross-shore velocities in the nearshore transect.

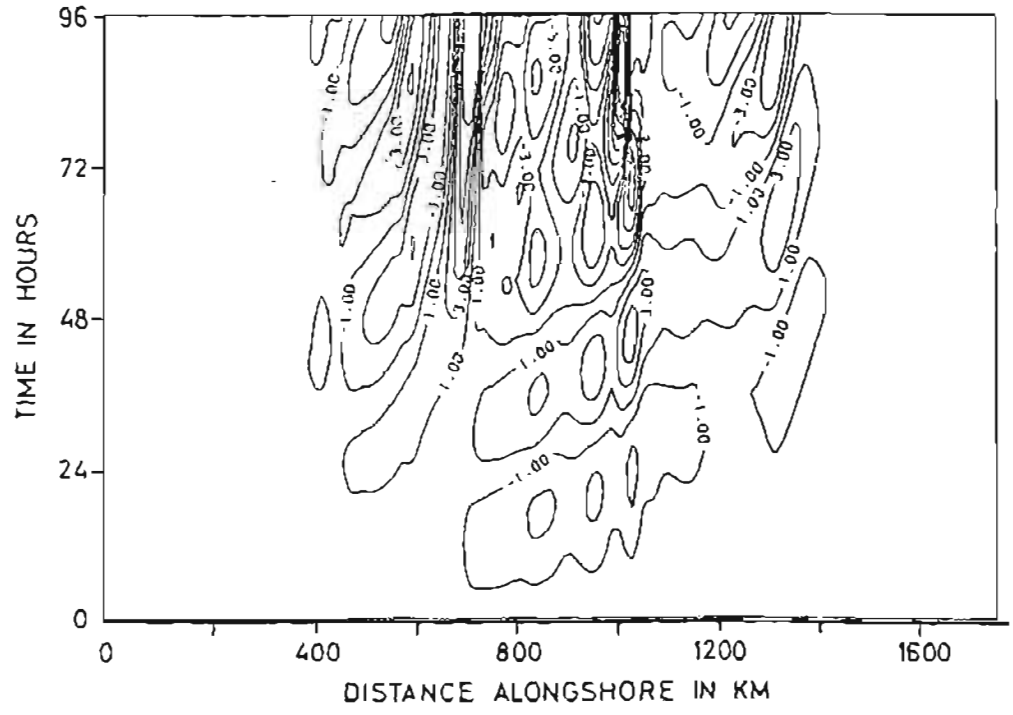

Fig. 7.18c Longshore "space-time" contours of cross-shore velocity at the shelf edge. [numerical experiment 15]

The most important result of all of the above numerical experiments is that strong, almost steady cross-shore flows develop in the vicinity of large alongshore changes in the shelf topography. In reality, the rapidly propagating wind stress fields along the West Coast and the water column stratification both tend to reduce the amplitude of these cross-shore flows, however observations tend to support these numerical model results.

8. DISCUSSION

In the introduction, reference was made to the presently limited data set available for investigating CTW motions along the southern African coastline, thus identifying the need for a more theoretical investigation of the generation, propagation and dissipation of CTW motions in southern African shelf waters. Particular aspects of the CTW response along the southern African coastline have been identified as being important and their proposed investigation constitutes the research objectives of this dissertation. The results of this investigation are summarised below, followed by an assessment of the extent to which the research objectives have been fulfilled and suggestions for further research.

First, the dynamics governing CTW activity on the southern African shelf are discussed. The shelf water response is largely determined by the "resonance" between the free CTW phase velocities and the propagation velocities of atmospheric weather systems. The exact nature of this response is further determined by the water column stratification and alongshore variations in topography, both factors which have been investigated in this dissertation. The dominant spatial and temporal scales of CTW activity and the propagation velocities associated with CTW's have been obtained from the analysis of pressure-adjusted sea level data and this information is discussed within a framework provided by both theoretical considerations and the research results of others. Lastly, seasonal differences in the CTW response and both remotely forced CTW and open-ocean forcing of shelf waters are discussed.

8.1 The Dynamics Governing the CTW Response of Southern African Shelf Waters

The scales associated with CTW's are such that the "long wave" approximation can generally be made whereby the cross-shore length scales of the response are assumed to be much smaller than the longshore scales and the frequency of the CTW's are assumed to be less than the inertial frequency. Where such a "long wave" scaling is appropriate, the importance of stratification in the CTW response may be determined using the non-dimensional stratification parameter (S). The magnitude of this parameter is determined by the average shelf slope, the mean shelf stratification and the

magnitude of the Coriolis parameter. Where $S^2 \ll 1$, the effects of stratification are negligible and may be ignored. Stated more precisely, if $S^2 < 0.04$ ($S < 0.2$), the CTW response may be considered to be governed by the linearised, barotropic shallow water wave equations (Chapman and Henderschott, 1982). For the water column stratification typically observed over the southern African shelf, scaling analyses indicate that the CTW response of shelf waters on the West and South Coasts are governed by the barotropic, linearised shallow water wave equations while the CTW response on East Coast is significantly baroclinic. Further, if $S \ll 1$, the wind-forced CTW response is not only barotropic but also is restricted to the shelf with no significant CTW activity over the shelf slope. This is typically the situation over the wide, gently-sloping shelf regions such as the Orange River cone and the Agulhas bank (see Table 1).

Scale analyses of the appropriate barotropic equations of motion indicate that subinertial CTW's are essentially non-divergent motions where the "rigid lid" assumption may be made. Further, the scales of motion are such that non-linear and β-effects are negligible. The analyses also indicate that the longshore velocities are in geostrophic balance with the offshore gradient in pressure-adjusted sea level. This has been confirmed for the shelf response off East London (Schumann and Brink, 1990) and is probably true for most West and South Coast sites. This observation is important as it provides justification for the use of pressure-adjusted sea levels in analysing CTW response along the southern African coastline.

If the "long wave" approximation holds, the forcing of CTW's is primarily due to longshore wind stress and forcing by cross-shore wind stresses is negligible except in the vicinity of large alongshore variations in bottom topography where strong cross-shore flows develop resulting in cross-shore and longshore scales of similar magnitude. Under these conditions the "long wave" approximation breaks down and the effects of stratification may be important despite the fact that $S^2 \ll 1$ in these regions. Scale analyses also show the wind stress curl forcing of CTW motions to be negligible provided that the offshore scale of variations in the longshore wind stress fields and the longshore scale of variations in the cross-shore wind stress fields greatly exceed the spatial scales of the response (typically given by the shelf width). Near headlands and

prominent capes this is rarely true and wind stress curl forcing and Ekman dynamics predominate resulting in localised upwelling. Similarly, wind stress curl forcing may be significant over wide, gently-sloping, shallow shelf regions such as the Orange River cone and the Agulhas Bank. López-Mariscal and Clarke (1993) have found that the wind stress curl is important in determining the low frequency response over the Californian shelf and state that it is not possible understand the low frequency shelf dynamics in this region without carefully measuring the cross-shore variations in the wind stress field. This is most probably also true for the shelf surrounding southern Africa and thus the importance of determining the spatial scales and variability of the offshore wind field along our coastline.

Atmospheric pressure forcing by atmospheric pressure systems propagating along the coastline is shown in chapter 4 to be generally small in comparison to forcing by longshore wind stress, however such forcing is more effective over wide, shallow shelf regions. Tidal forcing of CTW motions may be assumed to be limited along the southern African coastline. Finally, the analysis of pressure-adjusted sea level data in chapter 5 indicate that remotely forced CTW's and open-ocean forcing are significant along most of the southern African coastline and cannot be ignored.

Where there are substantial longshore variations in shelf topography the scale analyses indicate two significant responses of shelf waters to synoptic-scale wind-forcing, namely a strong response to strong alongshore topographic control and a strong response to weak alongshore topographic control. As noted above, the CTW response develops cross-shelf and longshore scales of similar magnitude in the vicinity of these large alongshore changes in shelf topography, leading to the break down of the "long wave" assumptions. Further, the scale analyses indicate that the subinertial CTW response is such that motions developing in these regions are largely slowly-varying or quasi-steady. The scale analyses also indicate that the very low frequency response in these regions comprises an essentially steady-state flow that follows the bottom topography.

8.2 The Generation of CTW's by Propagating Wind Stress Fields

The response of shelf waters to wind-forcing is determined primarily by the nature of the forcing and the structure of the free CTW dispersion curves characteristic of the particular shelf region. The maximum possible phase speed of low wavenumber free CTW's largely determine the nature and amplitude of the shelf response along the coastline of southern Africa, while the high wavenumber structure of the dispersion curves give an indication of the extent of the expected topographic scattering of CTW's by alongshore variations in the shelf topography. Both theory and the numerical results in chapter 7 show that the magnitude of the CTW response is directly proportional to the magnitude of the longshore wind stress and inversely proportional to the difference between the phase velocity of the propagating wind stress field and the free CTW phase speed characteristic of the underlying topography. Similarly the numerical results indicate that the forced response generally assumes the spatial and temporal scales of the propagating wind stress fields with a more extensive wind stress field generating a more energetic CTW response. The CTW motions generated by moving wind stress fields therefore develop longshore scales concomitant with those of the longshore extent of the wind field, thus the large longshore coherence in pressure-adjusted sea levels and in the shelf currents observed by Nelson (1987).

In the absence of appropriate wind data, the CTW response on the West Coast has been investigated numerically. In chapter 7, the numerical results indicate that wind stress fields propagating along the shelf more rapidly that the maximum free CTW phase velocities characteristic of the particular shelf topography, result in a greatly reduced CTW response over the spatial scales used in the modelling study. For very high phase speeds of propagation of the wind stress fields, the modelling results indicate that the response does not travel at the phase speed of the wind stress field, but rather at the phase speed of the fastest non-dispersive free wave typical of the local shelf topography. Further, very slowly propagating wind stress fields generate smaller amplitude first mode CTW's which may propagate along the coastline ahead of the moving wind stress field and also generate higher mode CTW's if the propagation velocity of the wind stress field is less than or equal to free CTW phase speeds of these higher free CTW modes.

Observations of higher mode CTW's are most likely over the wider shelf regions where second mode free CTW phase velocities are the largest, in the southern Benguela region where the first and second mode free CTW phase velocities are of a similar magnitude and in regions where there is substantial topographic scattering of CTW's. The significant presence of higher mode CTW's in the shelf response will lead to reduced estimates of the phase velocity of sea level events propagating along the southern African coastline. The pressure-adjusted sea level analyses of Schumann and Brink (1990) and those in chapter 5 suggest that higher mode CTW motions are not significant along the southern African coastline. Schumann and Brink (1990) do however caution that higher mode CTW's are unlikely to be detected in analyses of coastal sea levels. In particular, topographic scattering of CTW's could lead to significant higher mode CTW activity which would typically not be reflected in coastal sea level data and consequently not detected in the sea level analysis.

At downstream sites along the shelf, the free waves generated by slowly propagating wind stress fields may be perceived to be "remotely forced" as changes in sea levels and shelf currents lead the changes in the wind stress fields responsible for their generation Such a mechanism could explain the observation of apparently "remotely forced" CTW's in the southern Benguela region. In the southern regions of the West Coast there is evidence of the response leading the changes in the wind. Bang (1973) observed the intensification of the upwelling front to occur before the onset of southeasterly winds off the Cape Peninsula, while the atmospheric pressure and sea level composites of Jury *et al*, (1990a) indicate that the CTW response coincided or even preceded the atmospheric forcing in the southern Benguela. Similarly, de Cuevas (1985) found the sea level response to precede changes in the local wind field at Gansbaai. The sea level as Gansbaai also showed very little response to the local winds, but correlated very well with the "upstream" winds at Lambert's Bay. The above observations could be indicative of a free wave response preceding the changes in the wind stress field which on occasion may propagate more slowly towards these southern regions, or the observations could be due to the lack of effective large-scale forcing by local winds in these southern regions.

The free CTW dispersion curves for narrow, steeply-sloping shelves are characterised by low phase velocities, implying that these narrow shelf region will not respond as readily to rapidly propagating wind stress fields. The low free CTW phase speeds (≈ 6 m.s^{-1}) associated with the narrow shelf regions of the southern Benguela suggest a greatly reduced response to local winds for wind stress fields with propagation velocities exceeding approximately 6 m.s^{-1}. The poor response of the sea level at Gansbaai to the relatively strong local winds therefore is not unexpected.

Conversely, the free CTW dispersion curves for wide, gently-sloping shelf regions are characterised by large phase velocities at low wavenumbers which suggest that the shelf waters in these region respond more readily to more rapidly propagating wind stress fields. The shallow waters of these wide shelf regions also respond very rapidly and energetically to wind-forcing (due to the high free CTW phase speeds characteristics typical of these shelf regions and the inverse water depth relationship that exists in the wind-forcing terms of the equations of motion, respectively). The above factors lead to a larger amplitude CTW response to local forcing in these regions. Further, the scale analyses (Appendix A) suggest that the response of shelf waters to atmospheric pressure fluctuations may also become appreciable over wide, gently-sloping shelves.

These results suggest that propagating wind stress fields having a wide range of propagation velocities will be effective in generating locally forced CTW motions the wider, shallow shelf regions such as the Orange River cone (profile 3) and the wide Agulhas Bank (profile 8). This could explain the relative independence of the sea level signals observed at the sites on these wider shelf regions. Wind stress fields with propagation velocities as high as 12 to 13 m.s^{-1} will elicit a large amplitude, locally-forced response on the Orange River cone. Similarly, fast moving wind stress fields propagating at velocities exceeding 15 m.s^{-1} will still be effective in generating a large amplitude locally-forced response on the Agulhas Bank. Since wind-forcing on these wide, shallow shelf regions is particularly effective, they may be considered to be geographical origins for CTW motions (for example, Middleton and Cunningham, 1984). In particular, the Orange River cone may be a source region for "event scale" CTW wave motions in the southern Benguela regions. The data analyses of de Cuevas

(1985), Schumann and Brink (1990) and those in chapter 5 show that the sea level anomalies which propagate southwards along the West Coast are often only apparent from Port Nolloth southwards. This may reflect the nature of the development of the synoptic wind field (coastal low) rather than the wider shelf acting as a geographical origin for CTW motions, however the pressure-adjusted sea level contours and power spectra suggest otherwise. A similar maximum in the amplitude of the CTW response is observed on the South Coast between Mossel Bay and Port Elizabeth which suggests that the wide Agulhas Bank also serves as a geographical origin for CTW's. These two energy maxima are reflected in the power spectra of pressure-adjusted sea levels along the southern African coastline.

In general, the propagation velocities of the wind stress fields seem to match the theoretical free wave CTW phase speeds along most of the southern African shelf resulting in a strong CTW response (Schumann and Brink, 1990), however along the East Coast the propagating wind stress fields seem to "outrun" the CTW response of the shelf waters in the vicinity of East London. This lack of resonance between the wind-forcing and shelf waters along the East Coast results in a reduced amplitude, free CTW which propagates slowly along the shelf towards Durban.

The quantity of CTW energy that propagates along the shelf is determined by the frequency-wavenumber properties of the CTW (i.e. the dispersion properties of the CTW), the extent of bottom friction and the extent of topographic scattering of the CTW. The numerical results indicate that the higher frequency, shorter wavelength motions are most dispersive and consequently have the lowest group velocities. Further these higher frequency, shorter wavelength motions are more susceptible to topographic scattering. Both theoretical studies (Webster, 1987; Middleton and Wright, 1988) and the modelling results in chapter 7 indicate how longshore variations in the topography, in scattering incident CTW's, tend to act as a low pass filter for forward scattered CTW's in both the frequency and wavenumber domain. The reduced high frequency variability observed at the southern Benguela sites (Saldahna Bay and Granger Bay) is consistent with both topographic scattering of CTW's along the West Coast and limited forcing by local winds in the southern Benguela. Since extensive topographic scattering reduces the propagation of high frequency CTW's

along the shelf, it can be assumed that the higher frequency components of the shelf response are largely locally forced. The absence of these higher frequency components at these southern sites may be interpreted as being indicative of both a high degree of topographic scattering and a lack of local forcing. The higher propagation velocities observed in this region are also consistent with the hypothesis that only the higher velocity, lower frequency components of the CTW response propagate between Port Nolloth and these southern sites.

8.3 Topographic Control of the Wind-forced CTW Response

The topographic control of the CTW response occurs both through the determination of the free CTW dispersion properties by the underlying topography and by alongshore changes in the topography which result in topographic scattering of CTW's propagating along the shelf. The topographic scattering of CTW motions has been comprehensively reviewed in chapter 4 and is essentially a process whereby incident CTW modes are forward- and backscattered into propagating and evanescent CTW modes by large alongshore changes in bottom topography.

The variations in the bottom topography have a strong dissipative effect on the CTW's propagating along the shelf. Small random changes in the bottom topography have the same dissipative effect as bottom friction (Brink, 1980), while large longshore variations in the bottom topography result in strong topographic scattering of the free wave as it propagates along the shelf. This scattering of the incident CTW, generally into higher wavenumber and higher mode wave motions, results in a cascade of energy to shorter scale motions (Chao *et al.*, 1979) which are very efficiently damped by the effects of bottom friction. Thus longshore changes in the bottom topography inhibit the propagation of CTW energy along the shelf and also acting as a low pass filter in both the frequency and wavenumber domain for CTW's propagating along the shelf.

The amount of CTW energy transmitted along the shelf is highly dependent on the dispersion characteristics of the CTW's. Both theory and the numerical results indicate that the higher wavenumber CTW's are highly dispersive (i.e. have $C_g \ll C_{ph}$), resulting in very little propagation of free wave energy along the shelf. The results of the numerical experiments also indicate that the shorter wavelength CTW's are more

strongly dissipated on propagating over the longshore changes in the bottom topography. Conversely, low wavenumber CTW's are less dispersive, resulting in greater energy propagation along the shelf and both theory and the numerical results indicate that low wavenumber CTW's are less susceptible to topographic scattering.

Although bottom friction also results in the alongshore decay of CTW's, the model results indicate that (for the specific bottom friction parameters chosen) the dissipative effect of topographic scattering on CTW amplitudes exceeds that of bottom friction. This is true for both the highly dispersive ($C_g \ll C_{ph}$) and the less dispersive free wave motions ($C_g \approx C_{ph}$). The extent of CTW propagation along the shelf in regions where there is substantial alongshore variations in topography is therefore determined by the extent of topographic scattering rather than dissipation due to bottom friction. This implies that only the lower frequency and longest wavelength CTW's are able to propagate for appreciable distances along the shelf as free CTW's and that shorter wavelength motions generated by "upstream" winds are not able to propagate for appreciable distances along the shelf without energy input by local wind-forcing. The extensive propagation of the remotely-forced low frequency CTW's along the shelf in Autumn 1985 are an indication of the limited topographic scattering and dissipation characteristic of low frequency, low wavenumber free CTW's.

It should be noted that the effective shelf width (chapter 3) determines the high wavenumber structure of the dispersion curves which in turn determine the extent of topographic scattering. The rapid decrease in frequency with increasing wavenumber in the dispersion curves of wide, gently-sloping shelf regions suggests that topographic backscattering in such a region may be particularly severe. This suggests that the ridge extending across the Agulhas Bank in a southwesterly direction from Mossel Bay strongly modifies the low frequency response in this region. In narrow shelf regions where the frequency in the dispersion curves continues to increase with increasing wavenumber, topographic backscattering is limited.

The numerical modelling results indicate that the effect of longshore variations in the bottom topography on the wind-forced response, is quite dramatic. In all the numerical experiments, strong almost steady-state cross-shore flows developed in the

region south of Lüderitz and in the vicinity of Hondeklip Bay. In these regions of large longshore variability in shelf topography the large-scale CTW motions are scattered into higher wavenumber and higher mode number CTW motions. These shorter scale motions have greatly reduced or small negative group velocities resulting in the trapping of energy over the large changes in bottom topography. These trapped, higher mode CTW motions also have larger amplitudes at the shelf edge, thus explaining the strong cross-shelf flows at the shelf edge. The topographic scattering is particularly strong for the shorter period and wavelength motions which are highly dispersive. This implies that a slowly changing or slowly propagating wind stress field (which is expected to generate higher modes) may result in significant cross-shore velocities at the shelf-edge.

Copenhagen (1953) and Shannon (1985) identified a number of upwelling centres along the west coast where enhanced upwelling occurs. The above results suggest that the enhanced upwelling and large offshore filaments which develop off Lüderitz and Hondeklip Bay (Lutjeharms and Stockton, 1987) have their origin in the interaction of the large-scale, wind-forced shelf motions with the strong longshore changes in the bottom topography at these sites. The preferential location of these strong cross-shore flows could explain the fact that large filaments in eastern boundary shelf regions are often topographically anchored. The further upwelling centres typically identified near Cape Columbine and Cape Point are due to the enhanced upwelling typical of capes (Nelson and Hutchings, 1983; Nelson, 1981) rather than the mechanism postulated above.

The above observations off strong offshore/onshore flows are also consistent with those of Nelson (1994) and Monteiro (pers. comm.) that suggest the presence of cross-shelf flows in the vicinity of one or more of the above locations. In particular, Nelson (1994) provides strong evidence of a divergence of surface waters at the shelf edge between 27°S and 28°S. These potential cross-shore flows at the shelf edge are important as they lead to the loss of biota from the shelf waters.

The numerical results also indicate the development of shorter scale cross-shelf motions south of Cape Columbine which result in a cross-shore velocity response

which is not well correlated with the longshore velocity response. This could explain the different time scales of the cross-shore and longshore velocity responses in the current meter data of Nelson (1987), however these observations may simply be a reflection of the different dynamics and the inherent disparity in the cross-shore and longshore scales of the CTW response.

Changes in the CTW energy density over the shelf occur when the shelf width changes. Where the shelf narrows the group velocity of the free CTW response decreases, resulting in an increase in the energy density. The energy in the free wave is thus concentrated over a more narrow shelf, leading to locally enhanced CTW amplitudes due to the increased energy density (Wang, 1980). There is evidence of this effect in the current meter data of Nelson and Polito (1987) and Nelson (1989) where the shelf currents observed at a number of longshore current meter sites intensify as the shelf narrows in the southern Benguela regions.

Extreme care should be taken when extrapolating the results from current meter observations obtained over a complex bottom topography as the observations may be highly site specific.

8.4 The Effect of Stratification on CTW Generation and Propagation

Theoretical considerations lead to the conclusion that the low frequency response over most of the southern African continental shelf is essentially barotropic. The kinetic to potential energy ratio (R_{kp}), as determined by the Brink and Chapman (1987) software, indicates the baroclinicity of the CTW response. Values of R_{kp} listed in Table 2 indicate that, for water column stratification typical of the southern African shelf, the CTW response over the West and South Coasts is essentially barotropic, while the CTW response along the East Coast is highly baroclinic. In the southern Benguela, the more steeply sloping shelf and generally higher water column stratification leads to higher values of R_{kp}, suggesting a not so highly barotropic response. The current meter data of Nelson and Polito (1987) show evidence of bottom-trapping in the Cape Peninsula area, however both the current meter data of Holden (1987) and Nelson (1985) and the theoretical longshore response calculated using the programs of Brink

and Chapman (1987), indicate a strongly barotropic response in alongshore velocities in this region.

While the direct effect of stratification on the response may be limited, changes in water column stratification are expected to impact on topographic scattering. Increasing stratification modifies the free CTW dispersion properties by increasing the frequency of the free CTW's (and consequently both the phase and group velocity) at all wavenumbers. The effect, however, is greatest for the higher wavenumber and higher mode CTW's. The increase in free CTW phase velocities imply that the shelf waters will respond more readily to rapidly propagating wind stress fields, however more important is the change in group velocity of the free CTW's. Should the stratification increase sufficiently, the high-frequency cut-off in the dispersion curves may no longer exist and theoretically no topographic backscattering of incident CTW's is possible. While this may be true for the narrow shelf regions, the dispersion curves in Appendix B indicate that over wide, gently-sloping shelf regions even the strongest water column stratification does not lead to the loss of this high frequency cut-off and topographic backscattering remains a possibility

Unfortunately the stratification parameter (S) assumes its largest values in the regions of greatest interest, namely the narrow shelf regions off Lüderitz (where the barotropic model results indicate the development of strong cross-shore flows) and the region south of Cape Columbine. Topographic scattering results in smaller scale motions which are more strongly modified by the inclusion of stratification effects. Thus in these regions where strong scattering of CTW motions occurs, the effects of stratification are more important and significant baroclinic motions may result.

In general, the inclusion of stratification is expected to limit the extent of backscattering and increase the forward scattering away from the large changes in topography. This results in reduced trapping of energy over these large changes in topography which limits the development of strong, almost steady-state, cross-shore velocities at the shelf edge. In very strongly stratified waters, the CTW's may be able to propagate over large changes in the bottom topography by changing their nature from that of a barotropic CTW (more typical of the wide, shallow shelf regions) to the

more baroclinic nature of internal Kelvin waves (more typical of the narrow shelf regions) and in so doing accommodate changes in the bottom topography by adjustment of their internal density fields without significant topographic scattering of the CTW signal.

The modification of the dispersion curves seems sufficiently small to conclude that the barotropic model results will not change qualitatively when stratification is explicitly considered.

8.5 Dominant Temporal and Spatial Scales of CTW's along the Southern African Coastline

The data analyses in chapter 5 clearly indicate the quasi-periodic nature of the atmospheric forcing and CTW response. It is difficult to identify dominant temporal and spatial scales in CTW activity when the dominant scales of the atmospheric forcing change in such an irregular manner (Jury and Brundrit, 1992 and Nelson, 1992a,b). In chapter 5 a number of dominant frequencies are identified in the atmospheric pressure and pressure-adjusted sea level data. There is an ubiquitous 22 to 25 day signal in both the atmospheric pressure and pressure-adjusted sea level data that is not resolved by the spectral analysis techniques used. This signal is particularly strong at the South Coast sites in winter and weakest at the northern West Coast sites in summer. Energy peaks in the atmospheric spectra are observed at periods of approximately 50 days, 13 to 15 days, 10 days, 6 to 7 days, 5 days, 3 days and 2,7 days. The energy peaks are not consistent throughout the year and a time-lagged spectral analysis indicates that the energy at a specific frequency typically persists for 25 to 50 days, with the energy at lower frequencies (< 0,1 cpd) having a greater persistence.

Similarly energy peaks in the pressure-adjusted sea level spectra are observed at 25 to 30 days, 14 days. 10 days, 7 to 8 days, 4,5 days 3 days and 2,3 days. As with atmospheric pressure, the energy peaks in the pressure-adjusted sea level data only persist for periods of approximately one to two months. To investigate common CTW dynamics, the coherence was determined between the various sites along the coast. These results indicate a strong coherence in sea level along the southern African coastline at periodicities of 22 to 25 days (all year round), 18 to 22 days (summer),

approximately 10 days (winter), approximately 4 to 5 days and at higher frequencies of approximately 2 to 3 days.

Modelling studies (Johnson, 1982) indicate that longshore currents react quite quickly to changes in wind stress, however significant changes in environmental variables such as temperature and nutrients require longer periods of wind-forcing. This observation is supported by Jury and Brundrit (1992) who show that the environmental variables on the West Coast only show an appreciable response to longer period wind-forcing. Thus higher frequency CTW motions may well result in strong current fluctuations over the shelf, however the impact on environmental variables may be negligible. Consequently the impact of higher frequency variability on environmental parameters such as nutrients and temperature may be limited.

General CTW activity extends from north of Walvis Bay to Durban and beyond, however CTW activity in the "weather band" is only significant between Port Nolloth and East London, with small amplitude free CTW activity extending as far as Durban. The wide shelf region off the Orange River (Port Nolloth) and the wide Agulhas Bank act as geographic origins for CTW's while the narrow East Coast shelf region acts as a sink for synoptic-scale CTW motions. Not only are the CTW's strongly damped in the Agulhas Current north of East London, but the resonance between the shelf waters and the propagating atmospheric weather systems ceases to exists as the atmospheric pressure systems accelerate and the free CTW phase velocities decrease dramatically over the narrow East Coast shelf. Fig 15.15a (p119) indicates that the propagation velocities of CTW's along the southern African coastline are quite variable and typically range between 7 $m.s^{-1}$ and 14 $m.s^{-1}$ on both the West and South Coasts, between 5 and 10 $m.s^{-1}$ in the vicinity of Cape Town and rapidly decreases from approximately 7 $m.s^{-1}$ in the vicinity of Port Elizabeth to approximately 2 $m.s^{-1}$ along the East Coast. The lack of variability in the estimates of phase velocities of CTW's along the East Coast suggest that these are free rather than forced CTW motions. The above phase velocity estimates are of a similar magnitude to those obtained from the sea level composites of Jury *et al.* (1990a), but are generally larger than those estimated by Schumann and Brink (1990) from the coherency and phase spectra of pressure adjusted sea levels.

The numerical modelling results suggest that, for rapidly propagating wind stress fields, the velocity of any significant CTW response does not exceed the "long wave" free CTW phase velocity. Within observational error, the estimated phase velocities of the forced CTW's in chapter 5 support the above conclusion. (An exception is the high CTW phase velocities observed between Port Nolloth and Saldahna, however local bay dynamics may account for these seemingly anomalous observations.)

8.6 Seasonal and Interannual Variability in the CTW Response

The two factors that change seasonally are the stratification of the water column and the nature of the atmospheric forcing. The direct impact of changing water column stratification is negligible, nevertheless these changes in water column stratification (through their impact on topographic scattering of CTW's) may be indirectly important in determining the subinertial response of shelf waters. The seasonal changes in wind-forcing, however, are much more significant than those due to changes in stratification.

The data analyses in chapter 5 indicate that the forcing over the southern African shelf is much more energetic in the winter/spring period and consists of a higher frequency of events. In general there is a higher frequency of events on the South Coast than on the West Coast, especially in summer. These higher frequency, larger amplitude events do not necessarily imply greater variability in environmental parameters over the shelf. On the contrary, the lower frequency forcing and more persistent winds on the West Coast in summer may lead to larger variability (Johnson, 1982) in the environmental parameters affecting biological production.

The data analyses in chapter 5 indicate a strong interannual variability in the frequency characteristics of the shelf water response. One example is the lower frequency variability observed during spring 1984 compared to that of spring 1985 and spring 1986. The postulation of an optimum environmental window for biological productivity in such a shelf region is common. The existence of an optimum environmental window suggests that large changes in the frequency characteristics of shelf variability may impact strongly on biological productivity over the shelf.

Other well-documented large scale perturbations of the shelf environment during the 1980's include the 1982 short-lived warm event that occurred in the southern Benguela due to the failure of local winds (Brundrit *et al.*, 1987) and the 1984 Benguela Niño type event which seemed to have its origin in the equatorial Atlantic Ocean (Shannon *et al.* 1986).

8.7 Remote and Open Ocean Forcing of Shelf Circulation

In shelf regions where the wind systems propagate in the opposite direction to the free CTW motions, the forced and free CTW responses are clearly distinguishable (Mooers and Smith, 1968), however along the southern African coastline the wind stress field propagates in the same direction as the free wave response and such a distinction is not as simple. The sea level data and modelling results suggest that it is more appropriate to treat the CTW response along the southern African coastline as an "event" comprising both forced and free waves, however along the East Coast the forcing outruns the CTW response and the sea level events propagating between East London and Durban may be considered to be freely propagating CTW's.

Pressure-adjusted sea level data from 1985 provide evidence of remotely forced CTW's originating north of Walvis Bay and propagating along the shelf in an anticlockwise direction from Walvis Bay to the East Coast sites at velocities of approximately 2 $m.s^{-1}$. These low frequency waves have a periodicity of approximately 40 days and are observed in March, April and May, a period of the year when there is often substantial movement of the Angola Front and salinity intrusions into the northern Benguela region (Boyd, 1987). The source of these low frequency CTW motions is uncertain, however it is possible that they are of equatorial origin. It is not clear from the limited data from other years whether this is a common occurrence along the coastline of southern Africa. These remotely forced CTW's are important in that they are able to modulate the synoptic-scale perturbations of all of the shelf environment of southern Africa. This could lead to observations of an atypical response of shelf waters to local wind-forcing (for example, Nelson, 1992a).

The low frequency variability observed along the East Coast is related to open-ocean forcing rather than remotely forced CTW's travelling along the southern African

coastline. These large sea level perturbations are associated with large perturbations in the Agulhas Current called Natal Pulses. In general, these Natal Pulses causes strong reversals of the shelf circulation along the East Coast. The severity of these episodic perturbations of the shelf circulation varies with the size of each Natal Pulse. Preliminary indications are that there are about two large perturbations and a further number of smaller such perturbations each year.

8.8 Fulfilment of Research Objectives

The aim of this dissertation is to provide a basic characterisation of the subinertial circulation over the continental shelf surrounding southern Africa in terms of CTW theory. Specifically, the research objectives are

a) to describe the dynamics governing the CTW response along the coastline of southern Africa,
b) investigate the role of topographic scattering and stratification in the generation and propagation of CTW waves along the southern African coastline,
c) determine the dominant temporal and spatial scales and phase speeds associated with these CTW's,
d) document the seasonal differences (if any) in forcing and propagation of the CTW's, and
e) investigate to what extent the low frequency response on the shelf surrounding southern Africa is attributable to remotely forced CTW motions or open-ocean forcing.

The main results of the research (summarised below) indicate that the research objectives set out in chapter 1 mostly have been fulfilled.

Theory and scale analyses provide a clear indication of the dynamics of CTW activity along the southern African shelf. The CTW motions and subinertial currents over the shelf are predominantly forced by longshore winds with atmospheric pressure forcing only being of some significance at higher frequencies on wide, gently-sloping shelf regions. In the vicinity of regions such as headlands where there are large spatial changes in wind stress, wind stress curl is a significant and strong localised upwelling occurs. Further, cross-shore wind stresses are important in the vicinity of large

alongshore variations in shelf topography where significant cross-shore flows (having cross-shore and longshore response scales of a similar magnitude) are expected to develop

Alongshore changes in shelf topography impact significantly on CTW's and the low frequency circulation on the West Coast. In the vicinity of large alongshore changes in the shelf topography, strong topographic scattering leads to almost steady-state, cross-shelf flows near the shelf edge. This could partially explain why large offshore filaments observed in eastern boundary shelf regimes are often topographically or geographically anchored. There is some agreement between observations (Lutjeharms and Stockton, 1987; Lutjeharms *et al.*, 1991; Nelson, 1994) and the numerical model results. Further, topographic scattering of CTW's significantly decreases the energy propagating along the shelf and thus impacts on the extent of "upstream" (remote) forcing experienced at particular sites along the coast.

The scale analyses, numerical results and numerous current meter observations indicate that the "weather band" response of the shelf waters on the West and South Coasts is predominantly barotropic, however on the narrow East Coast shelf regions the response is significantly baroclinic. The impact of strong stratification on the free CTW phase velocities is small and consequently their is very little effect on the forcing of low wavenumber CTW's. However, the impact of strong stratification on CTW group velocities at higher wavenumbers is significant thus stratification is expected to modify the extent of topographic scattering of CTW's and consequently the energy propagation along the shelf and the development of cross-shore flows at the shelf edge.

It is difficult to identify dominant temporal and spatial scales in CTW activity as the dominant scales of the atmospheric forcing changes in a somewhat irregular manner (Jury and Brundrit, 1992 and Nelson, 1992a,b). The results in this dissertation do however indicate a strong coherence in sea level along the southern African coastline at periodicities of 22 to 25 days (all year round), 18 to 22 days (summer), approximately 10 days (winter), approximately 4 to 5 days and at higher frequencies of approximately 2 to 3 days. Theoretical considerations (Johnson, 1982) and data (Jury and Brundrit, 1992) indicate that the impact of the higher frequency fluctuations on

environmental variability is limited. General CTW activity extends from north of Walvis Bay to Durban and beyond, however CTW activity in the "weather band" is only significant between Port Nolloth and East London. The wide shelf region off the Orange River (Port Nolloth) and the wide Agulhas Bank act as geographic origins for CTW's while the narrow East Coast shelf region acts as a sink for synoptic-scale CTW motions. Not only are the CTW's strongly damped by the Agulhas Current north of East London, but the resonance between the shelf waters and the propagating atmospheric weather systems ceases to exists as the atmospheric pressure systems accelerate and the free CTW phase velocities decrease dramatically over the narrow East Coast shelf. Fig 15.15a (p119) indicates that the propagation velocities of CTW's along the southern African coastline are quite variable, however they typically reflect the free CTW phase velocities of the local shelf topographies. These phase velocities typically range between 7 $m.s^{-1}$ and 14 $m.s^{-1}$ on both the West and South Coasts, between 5 and 10 $m.s^{-1}$ in the vicinity of Cape Town and rapidly decreases from approximately 7 $m.s^{-1}$ in the vicinity of Port Elizabeth to approximately 2 $m.s^{-1}$ along the East Coast.

Although the water column stratification over the shelf may vary quite substantially during the year (especially along the South Coast), the direct impact on CTW activity is expected to be minimal. Changes in stratification do affect the topographic scattering of CTW motions, but the impact of changes in the wind-forcing far exceed those due to changes in the stratification of shelf waters. The wind-forcing is more energetic in winter/spring rather than in summer/autumn, however the lower frequency forcing observed on the West Coast during summer may result in greater variability in environmental parameters than the higher frequency variability of winter. The interannual variability in the spectral characteristics of CTW activity over the shelf is substantial. Given the different environmental response at different frequencies, the impact of these interannual changes in the spectral characteristics of the shelf water response on biological productivity may be significant.

There is evidence of remotely forced low frequency CTW motions originating north of Walvis Bay. These low frequency CTW motions have a periodicity of approximately 40 days and propagate along the shelf from Walvis to the East Coast at velocities of

approximately 2 $m.s^{-1}$. The source of these low frequency CTW motions is uncertain, however it is possible that they are of equatorial origin. The data coverage for years other than 1985 is inadequate to determine if these events are a common occurrence. Further low frequency variability is observed on the East Coast, however this is related to open-ocean forcing of the shelf circulations. These large sea level perturbations which travel from north to south along the East Coast are associated with large perturbations in the Agulhas Current called Natal Pulses. These Natal pulses causes strong reversals of the shelf circulation, however their direct influence the shelf circulation is limited to the East Coast.

8.9 Future Research

Ideally one would like to accurately model or predict the currents, sea levels and environmental variability associated with CTW activity over the shelf as this would

a) assist in predicting extreme sea levels at the coast,
b) provide the necessary inputs into studies of the circulation in coastal embayments,
c) provide a characterisation of Lagrangian flows over the shelf that impact on human activities such as mining and oil and gas exploration/production, and
d) provide the necessary environmental information required to investigate how variability in the shelf environment affects the biological productivity and ultimately the various regional fisheries of southern Africa.

The usual methods of analysis (spectral analysis techniques) which attempt to identify the "statistical mean" temporal and spatial scales of the dominant response are not particularly effective as the processes being investigated are at best quasi-periodic. Cross-correlation techniques are useful in this regard, however a more successful approach is to use models to predict the shelf response both as time series of the sea level and currents and in terms of the statistical properties of these fields. The implementation of wave-based CTW wave models on other shelf regions (for example Clarke and Van Gorder, 1986; Chapman, 1987, Zamuido and López, 1994) have been reasonably successful in hindcasting the low frequency shelf currents using a relatively well-documented wind stress field. Similarly, more general models have been used to

describe the statistical properties of shelf variability (for example Brink *et al.*, 1987). Unfortunately this is not possible along the southern African coastline as the marine wind field data are too limited. Hunter (1987) and Schumann (1989) have provided a rudimentary characterisation of the marine meteorology of the coastal regions of Southern Africa, however these data are too limited to provide the detailed characterisation of marine winds that is required to model the CTW response on the southern African continental shelf. Further, there is strong evidence of remotely forced CTW's and open-ocean forcing which further limit our ability to operationally predict the currents and sea level variability over the shelf.

Thus, although the limited availability of more extensive current meter data over the shelf is also problematic, the lack of adequate information on the marine wind field is *the* limiting factor in investigating CTW activity along the coastline of southern Africa. It is difficult to characterise the response of shelf waters to a relatively unknown forcing function and this inadequacy needs to be addressed before substantial progress can be made in investigating the subinertial response of the shelf waters surrounding southern Africa.

9. REFERENCES

ADAMS, J.K. AND BUCHWALD, V.T. (1969) The generation of continental shelf waves. *J. Fluid Mech.*, **35**, 815-826.

AHN, N.N. AND GILL, A.E. (1981) Generation of coastal lows by synoptic scale waves. *Quart. J. R. Met. Soc.*, **107**, 521-530.

ALLEN, J.S. (1975) Coastal trapped waves in a stratified ocean. *J. Phys. Oceanogr.*, **5**, 300-325.

ALLEN, J.S. (1976) Continental shelf waves and alongshore variations in bottom topography and coastlines. *J. Phys. Oceanogr.*, **6**, 564-578.

ALLEN, J.S. (1980) Models of wind-driven currents on the continental shelf. *Ann. Rev. Fluid Mech.*, **12**, 389-433.

ALLEN, J.S. AND D.W. DENBO (1984) Statistical characteristics of the large-scale response of coastal sea level to atmospheric forcing. *J. Phys. Oceanogr.*, **14**, 1079-1094.

BAKUN, A. AND G.S. NELSON (1991) The seasonal cycle of wind-stress curl in Subtropical eastern boundary regions. *J. Phys. Oceanogr.*, **21**, 1815-1834.

BANE, J.M. AND HSUEH, Y. (1980) On the theory of coastal trapped waves in an upwelling frontal zone. *J. Phys. Oceanogr.*, **10**, 270-285.

BANG, N.D. (1973) Characteristics of an intense ocean frontal system in the upwell regime west of Cape Town. *Tellus*, **25**, 256-265.

BANG, N.D. AND W.R.H. ANDREWS (1974) Direct current measurements of a shelf-edge frontal jet in the southern Benguela system. *J. Mar Res.*, **32(3)**, 405-417.

BATTEEN, M.L. AND HAN, Y.-J. (1981) On the computational noise of finite-difference schemes used in ocean models. *Tellus*, **33**, 287-396.

BATTISTI, D.S. AND B.M. HICKEY (1984) Application of remote wind-forced coastal trapped wave theory to the Oregon and Washington coasts. *J. Phys. Oceanogr.*, **14**, 887-903.

BEARDSLEY, R.C. AND HAIDVOGEL, D.B. (1981) Model studies of the wind-driven transient circulation in the Middle Atlantic Bight. Part I: Adiabatic boundary conditions. *J. Phys. Oceanogr.*, **11**, 355-375.

BENDAT, J.S. AND A.G. PIERSOL (1971) Random data: Analysis and measurement procedures. *Wiley-Interscience, New York*, 407pp.

BENIGNUS,V.A. (1969) Estimation of the coherence spectrum and its confidence interval using the Fast Fourier transform. *IEEE Transactions on Audio and Electroacoustics, Vol. AU-17, No. 2.*

BLUMBERG, A.F. AND KANTHA, L.H. (1985) Open boundary conditions for circulation models. *ASCE J. Hydraulic Eng.*, **111**, 237-255.

BOYD, A.J. (1987) The oceanography of the Namibian shelf. *PhD Thesis*, University of Cape Town, 188pp.

BOYD, A.J., J. SALAT AND M. MASO (1987) The seasonal intrusion of relatively saline water on the shelf of northern and central Namibia. *S. Afr. J. mar. Sci.*, **5**, 107-120.

BOYD, A.J., J. TAUNTON-CLARK AND G.P.J. OBERHOLSTER (1992) Spatial features of the near-surface and midwater circulation patterns off western and southern South Africa and their role in the life histories of various commercially fished species. *S. Afr. J. mar. Sci.*, **12**, 189-206.

BRINK, K.H. (1980) Propagation of barotropic continental shelf waves over irregular bottom topography. *J. Phys. Oceanogr.*, **10**, 765-778.

BRINK, K.H. (1982a) On the effect of bottom friction on low-frequency coastal trapped waves. *J. Phys. Oceanogr* , **12**,127-133.

BRINK, K.H. (1982b) A comparison of long coastal-trapped wave theory with observations off Peru. *J. Phys. Oceanogr.*, **12**, 897-913.

BRINK, K.H. (1986) Scattering of long coastal-trapped waves due to bottom irregularities. *Dyn. Atmos. Oceans*, **10**, 149-164.

BRINK, K.H. (1987) Coastal ocean physical processes. *Rev. Geophys.*, **25(2)**, 204-216.

BRINK, K.H. (1989) Energy conservation in coastal-trapped wave calculations. *J. Phys. Oceanogr.*, **19**, 1011-1016

BRINK, K.H. (1990) On the damping of free coastal-trapped waves *J. Phys. Oceanogr.*, **20**, 1219-1225.

BRINK, K.H. (1991) Coast-trapped waves and wind-driven currents over the continental shelf. *Rev. Geophys.*, **25(2)**, 204-216.

BRINK, K.H. AND ALLEN, J.S. (1978) On the effect of bottom friction on barotropic motion over the continental shelf. *J. Phys. Oceanogr.*, **8**, 919-922.

BRINK, K.H. AND ALLEN, J.S. (1983). Reply to "Comments on the effects of bottom friction on continental shelf waves" *J. Phys. Oceanogr.*, **13**, 149-150

BRINK, K.H. AND CHAPMAN, D.C (1987) Programs for computing properties of coastal-trapped waves and wind-driven motions over the continental shelf and slope.). *Woods Hole Oceanog. Inst. Tech. Rep (2nd Edition)*, WHOI-87-24, 119pp.

BRINK, K.H., CHAPMAN, D.C. AND HALLIWELL, G.R. (Jr) (1987) A stochastic model for wind-driven currents over the continental shelf. *J. Geophys. Res.*, **92**, 1783-1797.

BRUNDRIT, G.B. (1984). Monthly mean sea level variability along the west coast of Southern Africa. *S. Afr. J. mar. Sci.*, **2**, 195-203.

BRUNDRIT, G.B., DE CUEVAS, B. AND SHIPLEY, A.M. (1984) Significant sea level variations along the west coast of Southern Africa 1979-1983. *S. Afr. J. Sci.*, **80**, 80-82.

BRUNDRIT, G.B., DE CUEVAS, B. AND SHIPLEY, A.M. (1987) Long-term sea-level variability in the eastern South Atlantic and a comparison with that in the eastern Pacific. *S. Afr. J. mar. Sci.*, **5**, 73-78.

BUCHWALD, V.T. AND ADAMS, J.K. (1968) The propagation of continental shelf waves. *Proc. Roy. Soc. London*, Ser., **A305**, 235-250

CALDWELL, D.R., CUTCHIN, D.L. AND LONGUET-HIGGINS, M.S (1972) Some model experiments on continental shelf waves. *J. Mar. Res.*, **30**, 39-53.

CAMERLENGO, A.L. AND O' BRIEN, J.J. (1980) Open boundary conditions in rotating fluids. *J. Comput. Physics*, **35**, 12-35.

CARTWRIGHT, D (1969) Extraordinary tidal currents near St. Kilda. *Nature*, **223**, 928-932.

CHAO, S.-Y, PIETRAFESA, L.J. AND JANOWITZ, G.S. (1979) The scattering of continental shelf waves by an isolated topographic irregularity. *J. Phys. Oceanogr.*, **9**, 687-695.

CHAPMAN, D.C. (1985) Numerical treatment of cross-shelf open boundaries in a barotropic coastal model. *J. Phys. Oceanogr.*, **15**, 1060-1075

CHAPMAN, D C (1987) Application of wind-forced, long coastal-trapped wave theory along the California coast. *J. Geophys Res.*, **92**, 1798-1816.

CHAPMAN, D.C. AND K H. BRINK (1987) Shelf and slope circulation induced by fluctuating offshore forcing. *J. Geophys. Res.*, **92**, 11741-11759.

CHAPMAN, D.C. AND HENDERSCHOTT, M.R. (1982) Shelf wave dispersion in a geophysical ocean. *Dyn. Atmos. and Oceans*, **7**, 17-31.

CHAPMAN, D.C., S.J. LENTZ AND K.H. BRINK (1988) A comparison of empirical and dynamic hindcasts of low frequency wind-driven motions over a continental shelf. *J. Geophys. Res.*, **93**, 12409-12422

CHURCH, J.A., N.J WHITE A.J. CLARKE, H.J. FREELAND AND R.L. SMITH (1986) Coastal-trapped waves on the east Australian continental shelf. Part II: Model verification. *J. Phys. Oceanogr.*, **16**, 1945-1957.

CLARKE, A.J. (1977a) Observations and numerical evidence for wind-forced coastal trapped waves. *J. Phys. Oceanogr.*, 7, 231-247

CLARKE, A.J. (1977b) Wind-forced linear and non-linear Kelvin waves along an irregular coastline. *J. Fluid Mech.*, **83**, 337-348

CLARKE, A.J. AND BRINK, K.H. (1985) The response of stratified frictional flow of shelf and slope waters to fluctuating, large-scale low-frequency wind forcing. *J. Phys. Oceanogr.*, 15, 439-453

CLARKE, A.J. AND VAN GORDER, S. (1986) A method for estimating wind-driven frictional, time-dependent, stratified shelf and slope water flow. *J. Phys. Oceanogr.*, **16**, 1013-1028.

COASTAL LOW WORKSHOP (1984) Abstracts and summary, G.B. Brundrit, R.P. Dias and M.R. Jury (eds), IMT, 15-16 March 1984, Simonstown, 67 pp.

CODE (1983) CODE-1: Moored array and large-scale data report. Woods Hole Oceanog. Inst. Tech Rept., WHOI, **83-23**, 186pp.

CODE (1985) CODE-2: Moored array and large-scale data report. Woods Hole Oceanog. Inst Tech Rept., WHOI, **85-35**, 234pp.

COPENHAGEN, W.J. (1953) The periodic mortality of fish in the Walvis region: a phenomenon within the Benguela Current. *Investl. Rep. Div. Fish. S. Afr.*, **14**, 35 pp.

CRAIG, P D. (1988) Space and time scales in shelf circulation modelling. *Cont. Shelf. Res.*, **8(11)**, 1221-1246.

CRAIG, P.D. AND P.E. HOLLOWAY (1991) The influence of coastally trapped waves on the circulation in Jervis Bay, New South Wales, In: *Dynamics and exchanges in Estuaries and the Coastal Zone*, (ed D.Prandle), pp9-33, Springer-Verlag, New York, 747pp.

CRAWFORD, W.R. AND R.E. THOMSON (1984) Diurnal period continental shelf waves along Vancouver Island: a comparison of observations with theoretical models. *J. Phys. Oceanogr.*, **14**, 1629-1646.

CSANADY, G.T. (1976) Mean circulation in shallow seas. *J. Geophys. Res.*, **81**, 5389-5399.

CUTCHIN, D.L. AND SMITH, R.L. (1973) Continental shelf waves: low-frequency variations in sea level and currents over the Oregon continental shelf. *J. Phys. Oceanogr.*, **3**, 73-82.

DAIFUKU, P.R AND R.C BEARDSLEY (1983) The K1 tide on the continental shelf from Nova Scotia to Cape Hatteras. *J. Phys. Oceanogr* , **13**, 3-17.

DAVIS, R.E. (1976) Predictability of sea surface temperature and sea level anomalies of the North Pacific. *J. Phys. Oceanogr.*, **6**, 249-266.

DAVIS, A.M.J. (1981) The scattering by a peninsula of the dominant continental shelf wave. *Phil. Trans. R. Soc. London, Ser. A*, **303**, 383-431.

DAVIS, A.M.J. (1983) Shelf similar topographies for free continental shelf waves. *Geophys. Astrophys. Fluid Dyn.*, **23**, 321-331.

DE CUEVAS, B (1985) Characteristics of sub-tidal coastal trapped disturbances in sea level along the coasts of Namibia and South Africa. *MSc Thesis*, Oceanogr. Dept., Univ. of Cape Town, 118 pp.

DE CUEVAS, B.A., BRUNDRIT, G.B. AND SHIPLEY, A.M (1986) Low-frequency sea-level fluctuations along the coasts of Namibia and South Africa. *Geophys. J. R. astr. Soc.*, **87**, 33-42.

DINGLE, R.V., MOIR, S.J. AND BREMNER, J.M. (1977) Bathymetry of the continental shelf off South Africa and South West Africa. *Geol. Surv. S. Afr., Pretoria, Map and Text.*

DORR, A.R. AND GRIMSHAW, R. (1986) Barotropic continental shelf waves on a β-plane. *J. Phys. Oceanogr.*, **16**, 1345-1358.

DUNCOMBE RAE, C.M., F.A. SHILLINGTON, J.J. AGENBAG, J. TAUNTON-CLARKE AND M.L. GRÜNDLINGH (1992) An Agulhas ring in the South Atlantic Ocean and its interaction with the Benguela upwelling frontal system.. *Deep-Sea Res.*, **39(11/12)**, 2009-2027.

EAGLE, G.A. AND M.J. ORREN (1985) A seasonal investigation of the nutrients and dissolved oxygen in the water column along two lines of stations south and west of south Africa. *National Research Institute for Oceanology, CSIR Research Report 567*, 52pp + 119 figures.

ENGEDAHL, H. (1992) Some experiments with explicit finite-difference schemes in a linear barotropic ocean model. *Cont. Shelf Res.*, **12(9)**, 1059-1073.

ESTIE, K.E. (1984) Forecasting the formation and movement of the coastal low. In: *Coastal Low Workshop. Abstracts and Summary.* G.B. Brundrit, Dias, R.D. and M.R. Jury (eds), IMT, 15-16 March 1984, Simonstown, 67 pp.

FOREMAN, M.G.G. (1987) An accuracy analysis of selected finite difference methods for shelf waves. *Cont. Shelf Res.*, **7(7)**, 773-803.

FLATHER, R.A. (1988) A numerical model investigation of tides and diurnal period continental shelf waves along Vancouver Island. *J. Phys. Oceanogr.*, **18**, 115-139.

GILL, A.E. (1977) Coastally trapped waves in the atmosphere. *Quart. J. R. Met. Soc.*, **103**, 431-440.

GILL, A.E. (1982) Atmosphere-ocean dynamics. Academic Press, New York, 662pp.

GILL, A.E. AND P.P. NIILER (1973) The theory of seasonal variability in the ocean. *Deep-Sea Res.*, **20**, 141-177.

GILL, A.E. AND CLARKE, A.J. (1974) Wind-induced upwelling, coastal currents and sea level changes. *Deep-Sea Res.*, **21**, 325-345.

GILL, A.E. AND SCHUMANN, E.H. (1974) The generation of long-shelf waves by the wind. *J. Phys. Oceanogr.*, **4**, 83-90.

GRANT, N.D. AND MADSEN, O.S. (1979) Combined wave and current interaction with a rough bottom. *J. Geophys. Res.*, **84**, 1797-1808.

GRANT, N.D. AND MADSEN, O.S. (1986) The continental shelf boundary layer. *Ann. Rev. Fluid Mech.*, **18**, 265-305.

GRIFFIN, D.A. AND J.H. MIDDLETON (1991) Local and remote forcing of New South Wales inner shelf currents and sea level. *J. Phys. Oceanogr.*, **21**, 304-322.

GRIMSHAW, R. (1977) The effects of a variable Coriolis parameter, coastline curvature and variable bottom topography on continental shelf waves. *J. Phys. Oceanogr.*, **7**, 547-554.

HAGEN, E. (1985) Meso-scale upwellings off Namibian coast. *Int. Symp. Upw. W Afr., Inst. Inv. Perq.*, Barcelona, Vol. **1**, 161-179.

HALTINER, G.J. AND WILLIAMS, R.T. (1980) Numerical prediction and dynamic meteorology, *John Wiley and Sons, New York*, 250pp.

HAMON, B.V. (1962) The spectrums of mean sea level at Sydney, Coffs Harbour and Lord Howe Island. *J. Geophys. Res.*, **67**, 5147-5155. (Correction : *J. Geophys. Res.*, **68**, 4635, 1963).

HAMON, B.V. (1966) Continental shelf waves and the effect of atmospheric pressure and wind stress on sea level. *J. Geophys. Res.*, **71**, 2883-2893.

HAMON, B.V. AND HANNAN, E.J. (1962) Estimating relations between time series. *J. Geophys. Res.*, **68**, 6033-6041.

HAYASHI, T., D.A. GREENBERG AND C.J.R. GARRETT (1986) Open ocean boundary conditions for numerical models of shelf sea circulation. *Cont. Shelf Res.*, **5**, 487-497.

HEAPS, N.S. (1978) Linearized vertically-integrated equations for residual circulation in coastal seas. *Deuts. Hydrog. Zeit.*, **31**, 147-169.

HOLDEN, C. (1986) Spatial and temporal scales of coastal currents in the St. Helena Bay - Cape Columbine region. *MSc Thesis*, Oceanogr. Dept., Univ. of Cape Town, 103 + A pp.

HOLDEN, C. (1987) Observations of low-frequency currents and continental shelf waves along the west coast of South Africa. *S. Afr. J. mar. Sci.*, **5**, 197-208.

HOLLOWAY, P.E., G. SYMONDS AND R. NUNES VAZ (1992) Observations of circulation and exchange processes in Jervis Bay, New South Wales. *Aust. J. Mar. Freshwater Res.*, **43**, 1487-1515.

HSUEH, Y. (1980) Scattering of continental shelf waves by longshore variations in bottom topography. *J. Geophys. Res.*, **85**, 1147-1150.

HUNTER, I.T. (1987) Weather of the Agulhas Bank and the Cape South Coast. *MSc Thesis*, Oceanogr. Dept., Univ. of Cape Town, 164 pp.

HUTHNANCE, J.M. (1975) On trapped waves over a continental shelf. *J. Fluid Mech.*, **69**, 689-704.

HUTHNANCE, J.M. (1978) On coastal trapped waves: Analysis and numerical calculation by inverse iteration. *J. Phys. Oceanogr.*, **8**, 74-92.

HUTHNANCE, J.M. (1981) Waves and currents near the continental shelf edge. *Prog. Oceanog.*, **10**, 193-226.

HUTHNANCE, J.M. (1987) Effects of longshore shelf variations on barotropic continental shelf waves, slope currents and ocean modes. *Prog. Oceanog.*, **19**, 177-220.

JACKSON, S.P. (1947) Air masses and the circulation over the plateau and coast of South Africa. *S. Afr. Geogr. J.*, **29**, 15pp.

JENKINS, G.M. AND D.J. WATTS (1968) Spectral Analysis and its applications *Holden-Day, San Francisco*, 525pp.

JOHNSON, A. (1982) A two time-scale model of stratified shelf currents *Cont. Shelf Res.*, **2**, 143-157.

JOHNSON, E.R (1991) The scattering at low frequencies of coastally trapped waves. *J. Phys. Oceanogr.*, **21**, 913-932.

JURY, M.R. C.I. MACARTHUR AND G.B. BRUNDRIT (1990a) Pulsing of the Benguela upwelling region: large-scale atmospheric controls *S. Afr. J. mar. Sci.*, **9**, 27-41

JURY, M.R. C.I. MACARTHUR AND C. REASON (1990b) Observations of trapped waves in the atmosphere and the ocean along the coast of southern Africa. *S. Afr. geogr. J.*, **72**, 33-46.

JURY, M.R. AND G.B. BRUNDRIT (1992) Temporal organisation of upwelling in the southern Benguela ecosystem by resonant coastal trapped waves in the ocean and atmosphere *S. Afr. J. mar. Sci.*, **12**, 219-224

KAMSTRA, F (1987) Interannual variability in the spectra of daily surface pressure at four stations in the southern hemisphere *Tellus*, **39A**, 509-514

KELLY, K.A. AND D.C. CHAPMAN. (1988) The response of stratified shelf and slope waters to steady offshore forcing. *J. Phys. Oceanogr.*, **18**, 906-925.

KILLWORTH, P.D. (1978). Coastal upwelling and Kelvin waves with small longshore topography. *J. Phys. Oceanogr.*, **8**, 188-205.

KRAUSS, T P, L. SHIYRE, J.N LITTLE (1995) Signal processing toolbox for use with MATLAB. The Mathsworks Inc., Massachusetts, U.S.A , 347 pp.

KRAUSE, G. AND R. RADOK (1976) Long waves on the Southern Ocean. In: *Waves in water of variable depth*, D.G. Provis, R. Radok, eds., Springer-Verlag, 221-231

KUBOTA, M. (1982) Continental shelf waves off the Fukushima coast. Part II: Theory of generation. *J. Oceanog. Soc. Jap.*, **38**, 323-329.

LE BLOND, P.H. AND MYSAK, L.A. (1977) Trapped coastal waves and their role in shelf dynamics. In: *"The Sea"* (E.D. Goldberg et al., eds.), Vol. 6, p459-495, Wiley (Interscience), New York.

LOUIS, J.P (1989) Current-shelf interactions during the Australian Coastal Experiment *Aust. J. Mar. Freshwater Res.*, **40**, 571-585.

LOPEZ, M AND A J. CLARKE (1989) The wind-driven shelf and slope water flow in terms of a local and a remote response. *Aust. J. Mar. Freshwater Res.*, **40**, 571-585

LÓPEZ-MARISCAL, M. AND A.J. CLARKE (1993) On the influence of wind stress curl on low frequency shelf water flow *J. Phys. Oceanogr.*, **23**, 2717-2727.

LUTJEHARMS, J.R.E. AND H.R. ROBERTS (1988) The Natal Pulse: an extreme transient on the Agulhas Current. *J. Geophys. Res.*, **93**, 631-645.

LUTJEHARMS, J.R.E. AND STOCKTON, P.L. (1987) Kinematics of the upwelling front off Southern Africa. In: The Benguela and comparable ecosystems, Payne, A.I.L., J.A. Gulland and K.H. Brink (Eds). *S. Afr. J. mar. Sci.*, **5**, 35-50.

LUTJEHARMS, J.R.E. AND A.D. CONNEL (1989) The Natal Pulse and inshore counter currents of the South African east coast. *S. Afr. J. Sci.*, **85**, 533-534.

LUTJEHARMS, J.R.E., F.A. SHILLINGTON AND C.M. DUNCOMBE RAE (1991) Observations of extreme upwelling filaments in the Southeast Atlantic Ocean. *Science*, **253**, 774-776.

MARTINSSEN, E.A., GJEVIK, B. AND RØED, L.P. (1979) A numerical model for long barotropic waves and storm surges along the western coast of Norway. *J. Phys. Oceanogr.*, **9**, 1126-1138.

MESINGER, F. AND ARAKAWA, A. (1976) Numerical methods used in atmospheric models. *GARP Publication series*, Vol. **17**, 66 pp.

MIDDLETON, J.F. (1988) Long shelf waves generated by a coastal flux. *J. Geophys. Res.*, **93**, 10724-10730.

MIDDLETON, J.H. AND CUNNINGHAM, M, A. (1984) Wind-forced continental shelf waves from a geographical origin. *Cont. Shelf Res.*, **3**, 215-232.

MIDDLETON, J.F. AND D G. WRIGHT (1988) Shelf wave scattering due to a longshore jump in the topography. *J. Phys. Oceanogr.*, **18**, 230-242.

MILLER, M J. AND THORPE, A.J. (1981) Radiation conditions for the lateral boundaries of limited area numerical models. *Quart. J. R. Met. Soc.*, **107**, 615-628.

MITCHUM, G.T. AND A. J. CLARKE (1986a) The frictional nearshore response to forcing by synoptic scale winds. *J. Phys. Oceanogr.*, , **16**, 934-946.

MITCHUM, G.T AND A. J. CLARKE (1986b) Evaluation of frictional wind-forced long-wave theory on the west Florida shelf.. *J. Phys. Oceanogr.*, , **16**, 1029-1037.

MONTIERO, P.M.S. AND G.B. BRUNDRIT (1995) Shelf-bay interactions in the southern Benguela upwelling system: Implications for eutrophication. *Coast. Est. Shelf Res.*, (submitted).

MOOERS, C.N.K. AND SMITH, R.L. (1968) Continental shelf waves off Oregon. *J. Geophys. Res.*, **73**, 549-557.

MYSAK, L.A. (1967) On the very low frequency spectrum of the sea level on a continental shelf. *J. Geophys. Res.*, **72**, 3043-3047.

MYSAK, L.A. (1968a) Edge-waves on a gently sloping continental shelf of finite width. *J. Mar. Res.*, **26**, 24-33.

MYSAK, L.A. (1968b) Effects of deep-sea stratification and current on edge-waves. *J. Mar. Res.*, **26**, 34-42.

MYSAK, L.A. (1980a) Recent advances in shelf wave dynamics. *Rev. Geophys. Space Phys.*, **18**, 211-241.

MYSAK, L.A. (1980b) Topographically trapped waves. *Ann. Rev. Fluid Mech.*, **12**, 45-76.

NELSON, G. (1981) Upwelling plumes. *Trans. Roy. Soc. S. Afr.*, **44**, 303-308.

NELSON, G. (1985) Notes on the physical oceanography of the Cape Peninsula upwelling system. In: *South African Ocean Colour and Upwelling Experiment*, edited L.V. Shannon, Sea Fisheries Research Institute, Cape Town, pp 63-95.

NELSON, G. (1987) Low frequency currents along the west coast of South Africa. Sixth National Oceanographic Symposium, Stellenbosch, 6-10 July 1987, Abstracts of papers and posters, p C-19.

NELSON, G. (1989) Poleward motion in the Benguela area. In: *Polewards Flows along Eastern Ocean Boundaries, Coastal and Estuarine Studies 34*, eds. S.J Neshyba, C.N.K. Mooers, R.L. Smith and R.T. Barber, , Springer-Verlag, Berlin, p110-130.

NELSON, G (1992a) Equatorward wind and atmospheric pressure spectra as metrics for primary productivity in the Benguela System. *S. Afr. J. mar. Sci.*, **12**, 19-28.

NELSON, G. (1992b) Longshore wind variation on the west coast of southern Africa and its influence on the shelf sea. *S. Afr. J. Sci.*, **88**, 418-423.

NELSON, G. (1994) Deep currents along the eastern boundary of the Cape Basin. Symposium Abstracts, *The South Atlantic: Present and Past Circulation*, 15-19 August, Bremen, Germany, pp 102.

NELSON, G. AND HUTCHINGS, L. (1983) The Benguela upwelling area. *Prog. Oceanogr.*, **12**, 333-356.

NELSON, G. AND A. POLITO (1987). Information on currents in the Cape Peninsula area, South Africa. *S. Afr. J. mar. Sci.*, **5**, 287-304.

NELSON, G., R.M. COOPER AND S. CRUICKSHANK (1987). Time-series from a current-meter array near Cape Point. *Trans. Roy. Soc. S. Afr.*, **47(4&5)**, 471-482.

ORLANSKI, I (1976) A simple boundary condition for unbounded hyperbolic flows. *J. Comp. Physics.*, **21**, 251-269.

OTNES, R.K. AND L. ENOCHSON (1978) Applied time series analysis. *John Wiley and Sons, New York*, 450pp.

PEDERSON, G. (1986). On the effects of irregular boundaries in finite difference models. *Int. J. Num. Meth. in Fluids*, **6**, 497-505.

PHILANDER, S.G.H. (1978) Forced oceanic waves. *Rev. Geophys. Space Phys.*, **16**, 15-46.

PONTE, R.M. (1992) The sea level response of a stratified ocean to barometric pressure forcing. *J. Phys. Oceanogr.*, **22**, 109-113.

PONTE, R.M. (1993) Understanding the relation between wind- and pressure-driven sea level variability. *J. Geophys. Res.*, **99(C4)**, 8033-8039.

PONTE, R.M., D.A. SALSTEIN AND R.D. ROSEN (1991) Sea level response to pressure forcing in a barotropic numerical model. *J. Phys. Oceanogr.*, **21**, 1043-1057.

POTGIETER, E., I.T. HUNTER AND M.L. GRÜNDLINGH (1987). Wind and bottom flow at the entrance to False Bay. Sixth National Oceanographic Symposium, Stellenbosch, 6-10 July 1987, Abstracts of papers and posters, pC-11.

PRESTON-WHYTE, R.D. AND P.D. TYSON (1973) Note on pressure oscillations over South Africa. *Mon. Weath. Rev.*, **101**, 650-659.

PRESS, W.H., B.P FLANNERY, S.A. TEUKOLSKY AND W.T. VETTERLING (1989) Numerical recipes in C: The art of scientific computing. *Cambridge University Press, Cambridge*, 735pp.

PUGH, D.T. (1987) Tides, surges and mean sea level. *John Wiley and sons, New York.*

REASON, C.J.C AND M.R. JURY (1993) On the generation and propagation of the southern African coastal low. *Quart. J. R. Met. Soc.*, **116**, 1133-1151.

RHINES, P.B. (1970) Edge, bottom and Rossby waves in a rotating stratified fluid. *Geophys. Fluid Dyn.*, 1, 273-302.

ROBINSON, A.R. (1964) Continental shelf waves and the response of sea level to weather systems. *J. Geophys. Res.*, **69**, 367-368.

ROED, L.P. AND COOPER, C.K. (1986) Open boundary conditions in numerical models. In: *Advanced physical oceanographic numerical modelling*, J.J. O'Brien (Ed), NATO ASI Series C, Vol. 186, Reidel Publ. Co., p411-436.

ROED, L.P. AND COOPER, C.K. (1987) A study of various open boundary conditions for wind-forced barotropic numerical ocean models. In: *Three-dimensional models of marine and estuarine dynamics*. Eds. Nihoul, J.C.J. and B.M. Jamart, Elsevier, Amsterdam, 629 pp.

ROED, L.P. AND O.M. SMEDSTAD (1984) Open boundary conditions for forced waves in a rotating fluid. *SIAM J. Sci. Stat. Comput.*, **5**, 414-426.

ROOTH, C. (1972) A linearized bottom friction law for large-scale oceanic motions. *J. Phys. Oceanogr.*, **4**, 509-510.

SCHUMANN, E.H. (1973) Trapped low frequency waves in a homogeneous ocean. *MSc Thesis*, Univ. of Cambridge, 67 pp.

SCHUMANN, E.H. (1983) Long-period coastal trapped waves off the south-east coast of Southern Africa. *Cont. Shelf Res.*, **2**, 97-107

SCHUMANN, E.H. (1987) The coastal ocean off the east coast of South Africa. *Trans. Roy. Soc. S. Afr.*, **46**, 215-229.

SCHUMANN, E.H. (1989). The propagation of air pressure and wind systems along the South African coast. *S. Afr. J. Sci.*, **85**, 382-385.

SCHUMANN, E.H. AND L.J. BEEKMAN (1984) Ocean temperature structures on the Agulhas Bank. *Trans. Roy. Soc. S. Afr.*, **45 (2)**. 191-203.

SCHUMANN, E.H AND K.H. BRINK (1990) Coastal-trapped waves off the coast of South Africa: generation, propagation and current structures. *J. Phys. Oceanogr.*, **20**, 1206-1218.

SCIREMAMMANO JR., F. (1979) A suggestion for the presentation of correlations and their significance levels. *J. Phys. Oceanogr.*, **9**, 1273-1276.

SEARSON, S. (1994) Extreme sea levels around the coast of southern Africa. *MSc thesis*, Science Faculty, University of Cape Town, 101pp.

SEARSON, S. AND G.B. BRUNDRIT (1995) Extreme high sea levels around the coast of southern Africa. *S. Afr. J. Sci.*, (submitted)

SHANNON, L.V. (1985). The Benguela ecosystem. Part I: Evolution of the Benguela, physical features and processes. In: *Oceanography and Marine Biology. An Annual Review*, **23**, Bannes, M. (ed). Aberdeen, University Press, 105-182.

SHANNON, L.V , A.J. BOYD, G.B. BRUNDRIT AND J TAUNTON-CLARK (1987) On the existence of an El niño type phenomenon in the Benguela system. *J. Mar. Res.*, **44**, 495-520.

SHANNON, L.V , R.J.M CRAWFORD, D.E. POLLOCK, L. HUTCHINGS, A J. BOYD, J. TAUNTON-CLARK, A. BADENHORST, R. MELVILLE-SMITH, C.J. AUGUSTYN, K L COCHRANE, I. HAMPTON, G. NELSON, D.W JAPP AND R.J.Q. TARR. (1992) The 1980s - a decade of change in the Benguela ecosystem. *S. Afr. J. mar. Sci.*, **12**, 271-296.

SHILLINGTON, F.A (1985). Long period edge waves off Southern Africa *PhD Thesis*, Univ. of Cape Town, South Africa, 171 pp.

SHILLINGTON, F.A AND D. VAN FOREEST (1986). Numerical model studies of long-period edge waves. *J. Phys. Oceanogr.*, **16**, 1487-1492.

SHILLINGTON, F A. AND BRUNDRIT, G.B. (1986). Energy flux of continental shelf waves. In: *Proceedings of 9th Australian Fluid Mechanics Conference*, Auckland, 8-16 December 1986, pp. 284-287

SHOJI, P. (1955). On the variations of the daily mean sea levels along the Japanese Islands. *J. Oceanogr. Soc. Jap.*, **17**, 21-32.

SHUMWAY, R.H. (1988) Applied statistical time series analysis. *Prentice Hall, New Jersey*, 379pp.

SIMONS, T.J. (1983). Comments "On the effects of bottom friction on continental shelf waves". *J. Phys. Oceanogr* , **13**,147-148

SMITH, R. (1972). Non-linear Kelvin and continental shelf waves. *J. Fluid Mech.*, **52**, 379-391.

SWART, V (1987) Agulhas Current - shelf interaction on the Agulhas Bank. Paper OPS7-P8, Abstracts, IUGG 19th Gen. Assembly, Vancouver, 9-22 August 1987

TAUNTON-CLARK, J., AND L.V. SHANNON (1988) Annual and interannual variability in the southeast Atlantic during the 20th century. *S. Afr. J. mar. Sci.*, **6**, 97-106.

THOMSON, R.E. AND J.H. MIDDLETON (1985) On wavenumber estimates for forced continental shelf waves. *J. Phys. Oceanogr.*, **15**, 33-45.

VAN BALLEGOOYEN, R.C (1991) The dynamics relevant to modelling of synoptic scale circulations within False Bay. *Trans. Roy. Soc. S. Afr.*, **45 (4/5)**, 419-431.

VAN FOREEST, D. AND BRUNDRIT, G. (1985). Numerical modelling of the Southern Benguela system. In: *South African Ocean Colour and Upwelling Experiment, Shannon, L.V. (ed)*, Sea Fisheries Research Institute, Cape Town, p111-123.

WAINMAN, C.K., A POLITO AND G. NELSON (1987) Winds and subsurface currents in the False Bay region, South Africa. *S. Afr. J. mar. Sci.*, **5**, 337-346.

WALKER, N.D (1984). Passage of coastal lows on the west coast as shown in coastal weather station data. In: *Coastal Low Workshop. Abstracts and Summary.* G.B. Brundrit, Dias, R.D. and M.R. Jury (eds), IMT, 15-16 March 1984, Simonstown, 67 pp.

WANG, D -P. (1975). Coastal trapped waves in a baroclinic ocean. *J. Phys. Oceanogr* , **5**, 326-333.

WANG, D.-P. (1980). Diffraction of continental shelf waves by irregular alongshore geometry. *J. Phys. Oceanogr.*, **10**, 1187-1199

WANG, D.-P (1982). Effects of continental slope on the mean shelf circulation. *J. Phys. Oceanogr.*, **12**, 1524-1526.

WANG, D.-P. AND MOOERS, C.N.K. (1976) Coastal trapped waves in a continuously stratified ocean. *J. Phys. Oceanogr.*, **6**, 853-863.

WEAVER, A.J. (1987) Bass strait as a reverse estuary source for coastally trapped waves. *Aust. J. Mar. Freshwater res.*, **38**, 685-699.

WEBSTER, I. (1985). Frictional continental shelf waves and the circulation response of a continental shelf to wind forcing. *J. Phys. Oceanogr.*, **15**, 855-864.

WEBSTER, I. (1987). Scattering of coastally trapped waves by changes in continental shelf width. *J. Phys. Oceanogr.*, **17**, 928-937.

WELCH, P D (1967). The use of Fast Fourier Transform for the estimation of Power Spectra: A method based on time averaging over short, modified periodograms. *IEEE Trans. Audio Electracoust.*, AU-15 (June 1967), 70-73.

WILKIN, J.L (1988) Scattering of coastal-trapped waves by irregularities in coastline and topography. *PhD thesis*, Mass. Inst. Technol./Woods Hole Oceanogr. Inst., Cambridge/Woods Hole, Mass (available as *Rep No. WHOI-88-47*, Woods Hole Oceanogr. Inst, Woods Hole, Mass.)

WILKIN, J.L. AND D.C. CHAPMAN (1990) Scattering of Coastal-Trapped Waves by Irregularities in Coastline and Topography. *J. Phys. Oceanogr.*, **20**, 396-421.

WRIGHT, D G (1986) On quasi-steady shelf circulation driven by along-shelf wind stress and open ocean pressure gradients *J. Phys. Oceanogr.*, **16**, 1712-1714.

WUNSCH, C. (1972) Bermuda sea level in relation to tides, weather and baroclinic fluctuations. *Rev. Geophys.*, **10**, 1-49.

YOSHIDA, K. (1960) The oceanic waves of days to months' periods. *Rec. Oceanogr. Works Jap.*, **5**, 11-24.

ZAMUDIO, M AND M. LÓPEZ (1994) On the effect of the alongshore pressure gradient on numerical simulations over the Northern California continental shelf. *J. Geophys. Res.*, **99(C8)**, 16117-16129

APPENDICES

APPENDIX A - Scaling of the homogenous, shallow water wave equations

The "long wave" CTW response has been shown to be predominantly barotropic in shelf regions where the Burger number is small (Clarke and Brink, 1985). Since the Burger number is generally small (i.e. S « 1) for the shelf waters surrounding southern Africa, it seems reasonable to use the homogenous shallow water wave equations to investigate the large-scale, low frequency response in these regions. The scale analysis which follows is used to analyse the efficacy of the different forcing mechanisms of barotropic CTW motions and their modification by longshore variations in the bottom topography of the shelf. Of particular importance is the situation where the "long wave" approximation is no longer valid as this results in the effects of stratification becoming important in the first order dynamics of CTW motions (Clarke and Brink, 1985).

The full homogenous shallow water equations governing the barotropic response of shelf waters to atmospheric pressure and wind forcing (p128, Le Blond and Mysak, 1978 and p337-338, Gill, 1982) are

$$\frac{\partial u}{\partial t}+u\frac{\partial u}{\partial x}+v\frac{\partial u}{\partial y}-fv=-g\frac{\partial}{\partial x}\left(\eta-\eta^{a}\right)+\frac{1}{\rho h}\left[\tau_{w}^{x}-\tau_{b}^{x}\right] \quad (A.1)$$

$$\frac{\partial v}{\partial t}+u\frac{\partial v}{\partial x}+v\frac{\partial v}{\partial y}+fu=-g\frac{\partial}{\partial y}\left(\eta-\eta^{a}\right)+\frac{1}{\rho h}\left[\tau_{w}^{y}-\tau_{b}^{y}\right] \quad (A2)$$

$$\left(\frac{\partial (hu)}{\partial x}+\frac{\partial (hv)}{\partial y}\right)+\frac{\partial \eta}{\partial t}=0 \quad (A.3)$$

A linearized boundary condition has been used for the pertubation pressure (p337, Gill, 1982), namely

$$p=p^{a}+\rho g\eta'$$

where $\eta' = \eta - \eta^{a}$, and η' is the atmospheric pressure-adjusted sea level, η is the observed sea level, η^{a} is given by the inverse barometer approximation $\eta^{a} = -p^{a}/\rho g$ and p^{a} is the atmospheric pressure. The above equations can be re-written such that the atmospheric pressure forcing only appears explicitly in the continuity equation

$$\frac{\partial u}{\partial t}+u\frac{\partial u}{\partial x}+v\frac{\partial u}{\partial y}-fv+g\frac{\partial \eta'}{\partial x}=\frac{1}{\rho h}\left[\tau_{w}^{x}-\tau_{b}^{x}\right] \quad (A.4)$$

$$\frac{\partial v}{\partial t} + u\frac{\partial v}{\partial x} + v\frac{\partial v}{\partial y} + f u + g\frac{\partial \eta'}{\partial y} = \frac{1}{\rho h}\left[\tau^{y}_{w} - \tau^{y}_{b}\right] \qquad (A.5)$$

$$\left(\frac{\partial (hu)}{\partial x} + \frac{\partial (hv)}{\partial y}\right) = -\frac{\partial \eta'}{\partial t} - \frac{\partial \eta^{a}}{\partial t} \qquad (A.6)$$

where it is assumed that $\left|\frac{\eta}{H}\right| \ll 1$ (H is a typical depth scale)

The following spatial and temporal scales are important in the scaling of the barotropic shallow water wave equations

a) Response scales

$T \approx \sigma^{-1}$	characteristic period of CTW motions
X	offshore spatial scale of CTW motions
Y	longshore spatial scale of CTW motions
η	characteristic magnitude of sea level pertubations
H	depth scale
U	cross-shore velocity scale
V	longshore velocity scale
f	characteristic magnitude of the Coriolis parameter, f, where $f = 2\Omega \sin\theta$ and θ is the latitude
R_0 $[=\sqrt{gH}/f]$	external Rossby radius
ε^2 $[= (X/R_0)^2]$	divergence parameter, i.e. $\varepsilon^2 = (f^2 X^2)/gH$
R $[= U/fX]$	Rossby number
Y_β $[\approx R_e \tan\theta]$	characteristic longshore scale for the variation of f
X_β $[\ll Y_\beta]$	characteristic cross-shore scale for the variation of f

b) Topographic scale

X_h	cross-shore topographic scale, typically interpreted as the width of the shelf.
Y_h	spatial scale of variations in longshore topography

c) Scales of forcing and bottom friction

S $[\approx \rho HfU]$	the characteristic magnitude of wind stresses

$B\ [\approx \rho HfU]$	the characteristic magnitude of bottom stresses
X_f	spatial scale of variations in cross-shore wind stress
Y_f	spatial scale of variations in longshore wind stress
X_B	spatial scale of variations in cross-shore bottom stress
Y_B	spatial scale of variations in longshore bottom stress

The characteristic scales for the wind stress and bottom stress have been defined by assuming the wind stress and bottom stress terms to be of the same order of magnitude as the Coriolis term in the alongshore momentum equation, however by making this assumption the importance of bottom stresses in CTW dynamics may be overestimated. Using the scales defined above and assuming the response over the shelf to be quasi-geostrophic, the equations A.4 to A.6 may be re-written in a non-dimensional form where x, y, h, u, v, η' and τ_w and τ_b now all represent non-dimensional variables

$$\left[\frac{U}{V}\right]\frac{\partial u}{\partial t} + \left[fT\frac{U}{V}\frac{U}{fX}\right]u\frac{\partial u}{\partial x} + \left[fT\frac{X}{Y}\frac{U}{fX}\right]v\frac{\partial u}{\partial y} - [fT]\,v + [fT]\frac{\partial \eta'}{\partial x} = \left[fT\frac{U}{V}\right]\left[\tau_w^x - \tau_b^x\right]$$

$$\frac{\partial v}{\partial t} + \left[fT\frac{U}{fX}\right]u\frac{\partial v}{\partial x} + \left[fT\frac{X}{Y}\frac{U}{V}\frac{U}{fX}\right]v\frac{\partial v}{\partial y} + \left[fT\frac{U}{V}\right]u + \left[fT\frac{X}{Y}\right]\frac{\partial \eta'}{\partial y} = \left[fT\frac{U}{V}\right]\left[\tau_w^y - \tau_b^y\right]$$

$$\left[\frac{U}{V}\right]h\frac{\partial u}{\partial x} + \left[\frac{U}{V}\frac{X}{X_h}\right]u\frac{\partial h}{\partial x} + \left[\frac{X}{Y}\right]h\frac{\partial v}{\partial y} + \left[\frac{X}{X_h}\frac{X_h}{Y_h}\right]v\frac{\partial h}{\partial y} = \left[\frac{\varepsilon^2}{fT}\right]\left(\frac{\partial \eta'}{\partial t} - \frac{\partial \eta^o}{\partial t}\right)$$

where $\varepsilon^2 = (X/R_0)^2 = \left(f^2X^2\right)/gH$ is the commonly defined "divergence" parameter.

The "long wave" approximation (Clarke and Brink, 1985) is made by assuming that

$fT \approx \delta^{-1}$ or $\sigma/f \approx \delta$ (temporal scales of 2 to 20 days, low frequency waves)

and $X/Y \approx U/V \approx \delta$ (longshore scales greatly exceed cross-shore scales)

where δ is a small parameter of magnitude $\delta \approx 10^{-1}$.

Typically $R = U/fX \approx \delta^2$, which allows the non-linear terms to be ignored in "long wave" CTW dynamics. Alternatively stated (Mysak, 1980a), the non-linear terms may be ignored if the magnitude of cross-shore and alongshore velocities are small in comparasion to the phase speeds typical of CTW motions (i.e $U \ll C_{ph}$ and $V \ll C_{ph}$). This is true for all scales of motion considered in this analysis.

For CTW motions the magnitude of the "divergence" parameter is typically $\varepsilon^2 \approx \delta$. Note that the atmospheric pressure forcing enters explicitly through the "divergence" term in the continuity equation and thus the extent of atmospheric pressure forcing depends on the magnitude of the non-dimensional ratio (ε^2 / fT). In the analysis which follows, the cross-shore spatial scale of the response is assumed to be of the same order of magnitude as the shelf width (i.e. $X \approx X_h$).

For "long wave" scaling ($fT \approx \delta^{-1}$ and $X/Y \approx U/V \approx \delta$), there are two possible responses of the shelf waters to synoptic scale forcing, namely

a) a strong response to strong alongshore topographic control where $X_h/Y_h \approx \delta$,

b) a strong response to weak alongshore topographic control where $X_h/Y_h \approx \delta^2$.

For "long wave" scales and $X_h/Y_h \approx \delta$, the first order response is governed by the following equations

$$-fv + g\frac{\partial \eta'}{\partial x} = 0$$

$$\frac{\partial v}{\partial t} + fu + g\frac{\partial \eta'}{\partial y} = \frac{1}{\rho h}\left[\tau^y_w - \tau^y_b\right]$$

$$h\frac{\partial u}{\partial x} + u\frac{\partial h}{\partial x} + h\frac{\partial v}{\partial y} + v\frac{\partial h}{\partial y} = 0$$

while for "long wave" scales and weak alongshore topographic control ($X_h/Y_h \approx \delta^2$), the term containing the longshore gradient in bottom topography may be ignored in the continuity equation. In summary, for the "long wave" approximation

a) the longshore velocities are in geostrophic balance with the cross-shore gradient in sea level,

b) both the cross-shelf wind stresses and the cross-shelf bottom stresses do not play a role in the first order CTW dynamics,

c) for small alongshore variations in bottom topography, the alongshore topographic gradients may be ignored, and

d) the response is non-divergent and a "rigid lid" boundary condition may be applied at the surface boundary. Since the atmospheric pressure forcing only appears explicitly in the "divergence term", atmospheric pressure forcing is not considered to be a first order effect.

For large alongshore variations in the bottom topography ($X_h / Y_h \approx 1$) and/or higher frequency motions ($fT \approx 1$), the cross-shore and alongshore spatial scales of the response are expected to be of the same order of magnitude ($X/Y \approx U/V \approx 1$) and thus boundary layer scaling ($X/Y \approx U/V \approx \delta$) is no longer valid. An analysis using $X_h / Y_h \approx 1$, $X/Y \approx U/V \approx 1$ and $fT \approx \delta^{-1}$, shows that where the response develops comparable cross-shore and long-shore scales due to strong alongshore variations in bottom topography,

a) the response remain non-divergent,

b) forcing by cross-shore wind stress becomes important (due to the fact that the response develops cross-shore and longshore scales of comparable magnitude, i.e. $X/Y \approx U/V \approx 1$), and

c) the time dependant terms in the equations are negligible and the response displays little temporal variability (i.e. the motions tend towards a quasi-steady state).

If one considers the same spatial scales ($X_h / Y_h \approx 1$, $X/Y \approx U/V \approx 1$) but allows for the higher frequency motions ($fT \approx 1$) that are expected in the presence of strong alongshore topographic variations (which scatter CTW motions into higher frequency and wavenumber motions), one finds that the response remains non-divergent, the cross-shelf (wind and bottom) stresses are a first order effect and time dependence once again becomes important.

Note that for $X/Y \approx U/V \approx 1$ (a consequence of the scaling $X_h / Y_h \approx 1$ and/or $fT \approx 1$), the scaling arguments of Clarke and Brink (1985) are no longer valid and the effects of stratification become important in CTW dynamics. The use of a barotropic model is thus not strictly justified in determining the subinertial CTW response of the shelf

waters surrounding southern Africa in the presence of large alongshore variations in the shelf topography

The dynamics of CTW are essentially those of the generation of vorticity over the sloping topography of a continental shelf and continuity at the coastal boundary (Gill and Schumann, 1974). An analysis of the vorticity equation is necessary to elucidate CTW dynamics and the relevant forcing mechanisms for CTW motions on the continental shelf surrounding southern Africa. The vorticity equation derived from the homogenous shallow water equations is

$$\frac{\partial}{\partial t}\left(\frac{\partial v}{\partial x}-\frac{\partial u}{\partial y}\right)-\frac{f}{h}\left(u\frac{\partial h}{\partial x}+v\frac{\partial h}{\partial y}+\frac{\partial \eta'}{\partial t}+\frac{\partial \eta^{a}}{\partial t}\right)+u\frac{\partial f}{\partial x}-v\frac{\partial f}{\partial y}$$
$$=\frac{1}{\rho h}\left(\frac{\partial \tau_w^y}{\partial x}-\frac{\partial \tau_w^x}{\partial y}\right)-\frac{1}{\rho h}\left(\frac{\partial h}{\partial x}\frac{\tau_w^y}{h}-\frac{\partial h}{\partial y}\frac{\tau_w^x}{h}\right)$$
$$-\frac{1}{\rho h}\left(\frac{\partial \tau_B^y}{\partial x}-\frac{\partial \tau_B^x}{\partial y}\right)+\frac{1}{\rho h}\left(\frac{\partial h}{\partial x}\frac{\tau_B^y}{h}-\frac{\partial h}{\partial y}\frac{\tau_B^x}{h}\right)$$

Using the scales as defined previously, the above equations may be written in a non-dimensional form

$$\frac{\partial}{\partial t}\left(\frac{\partial v}{\partial x}-\left[\frac{X}{Y}\frac{U}{V}\right]\frac{\partial u}{\partial y}\right)-\left[fT\frac{U}{V}\frac{X}{X_h}\right]\frac{f}{h}u\frac{\partial h}{\partial x}-\left[fT\frac{X}{X_h}\frac{X_h}{Y_h}\right]\frac{f}{h}v\frac{\partial h}{\partial y}$$
$$-\left[\varepsilon^{-1}\right]\left(\frac{\partial \eta'}{\partial t}+\frac{\partial \eta^{a}}{\partial t}\right)+\left[fT\frac{U}{V}\frac{X}{X_\beta}\right]u\frac{\partial f}{\partial x}-\left[fT\frac{X}{Y}\frac{Y}{Y_\beta}\right]v\frac{\partial f}{\partial y}$$
$$=\left[fT\frac{U}{V}\frac{X}{X_f}\right]\frac{1}{h}\frac{\partial \tau_w^y}{\partial x}-\left[fT\frac{U}{V}\frac{X}{Y}\frac{Y}{Y_f}\right]\frac{1}{h}\frac{\partial \tau_w^x}{\partial y}-\left[fT\frac{U}{V}\frac{X}{X_h}\right]\frac{\partial h}{\partial x}\frac{\tau_w^y}{h}+\left[fT\frac{U}{V}\frac{X}{Y}\frac{Y}{Y_h}\right]\frac{\partial h}{\partial y}\frac{\tau_w^x}{h}$$
$$-\left[fT\frac{U}{V}\frac{X}{X_B}\right]\frac{1}{h}\frac{\partial \tau_B^y}{\partial x}+\left[fT\frac{U}{V}\frac{X}{Y}\frac{Y}{Y_B}\right]\frac{1}{h}\frac{\partial \tau_B^x}{\partial y}+\left[fT\frac{U}{V}\frac{X}{X_h}\right]\frac{\partial h}{\partial x}\frac{\tau_B^y}{h}-\left[fT\frac{U}{V}\frac{X}{Y}\frac{Y}{Y_h}\right]\frac{\partial h}{\partial y}\frac{\tau_B^x}{h}$$

For "long wave" scaling ($X/Y \approx U/V \approx \delta$), atmospheric pressure forcing is negligible and the vorticity generated by the spatial gradients of the Coriolis parameter (beta effect) and cross-shore wind and bottom stresses are of secondary importance. The vorticity generated by wind stress curl and bottom stress curl and are also of secondary importance if a few additional scaling assumptions are made about their spatial scales

For the vorticity generated by the spatial gradients of the Coriolis parameter (beta effect) to be considered negligible, it is required that

$$\left| v\frac{\partial f}{\partial y} \right| \ll \left| \frac{f}{h} u \frac{\partial h}{\partial x} \right| \qquad or \qquad \left| v\frac{\partial f}{\partial y} \right| \ll \left| \frac{\partial}{\partial t}\left(\frac{\partial v}{\partial x}\right) \right|$$

Since $X \approx X_h$ and $Y_\beta = f / \beta \approx R_e / \cot\theta$ (where R_e = 6371 km is the radius of the earth and θ is the mean latitude of the region if interest), the above conditions reduce to

$$X_h \ll \frac{U}{V} R_e \tan\theta \qquad \text{or} \qquad X_h \ll \frac{1}{fT} R_e \tan\theta$$

Since $Y_\beta \ll X_\beta$, the above conditions are sufficient to ensure that the generation of vorticity by the β-effect is negligible. For the 'long wave' scaling, these conditions hold for all but very low frequency CTW motions where $(fT)^{-1} = \sigma / f \le \delta^2$

For the "long wave" scaling ($fT \approx \delta^{-1}$ and $X/Y \approx U/V \approx \delta$) subject to the above two conditions, the first order CTW dynamics are governed by the following (non-dimensional) vorticity equation

$$\frac{\partial}{\partial t}\left(\frac{\partial v}{\partial x}\right) - \frac{u}{h}\frac{\partial h}{\partial x} - \frac{v}{h}\frac{\partial h}{\partial y} = \left[\frac{X}{X_f}\right]\frac{1}{h}\frac{\partial \tau_w^y}{\partial x} - \frac{\partial h}{\partial x}\frac{\tau_w^y}{h^2} - \left[\frac{X}{X_B}\right]\frac{1}{h}\frac{\partial \tau_B^y}{\partial x} + \frac{\partial h}{\partial x}\frac{\tau_B^y}{h^2}$$

Note that the forcing of CTW's by the alongshore component of the wind stress curl may only be ignored if the cross-shore spatial scale associated with the alongshore wind stress is much greater than the cross-shore scale associated with the CTW response (given here by the shelf width), that is if $X \ll X_f$ or $X_h \ll X_f$. Likewise, the bottom stress curl term generally may be ignored if $X \ll X_B$ or $X_h \ll X_B$. Note, however, that wave conditions over the shelf may be such that these terms are significant. If the above restrictions on the spatial scales are valid, then the only effective forcing mechanism for shelf wave motions in the mid-latitudes is the alongshelf wind stress and the first order CTW dynamics are governed by the following (dimensional) vorticity equation

$$\frac{\partial}{\partial t}\left(\frac{\partial v}{\partial x}\right) - f\frac{u}{h}\frac{\partial h}{\partial x} - f\frac{v}{h}\frac{\partial h}{\partial y} = -\frac{\partial h}{\partial x}\frac{\tau_w^y}{\rho h^2} + \frac{\partial h}{\partial x}\frac{\tau_B^y}{\rho h^2}$$

In summary, for the 'long wave scaling with small alongshore variations in the bottom topography

a) the β-effect is negligible,

b) atmospheric pressure forcing is not a first order effect,

c) cross-shore wind and bottom stresses can be ignored,

d) if the spatial scale associated with the cross-shore variation in the longshore wind stress is much greater than the typical CTW response scale (here considered to be given by the shelf width), then wind stress curl is not an effective forcing mechanism and the only effective CTW forcing mechanism is the alongshore wind stress,

e) the alongshore component of the bottom stress curl would seem to be important as one would expect $X \approx X_B$, however in assuming that the bottom stresses are equal in magnitude to the wind stress at the surface the importance of frictional effects may be exaggerated Conversely, wave conditions over the shelf may be such that bottom stresses are sufficiently large for the bottom stress curl to play a significant role in the first order CTW dynamics.

If the response develops the comparable cross-shore and longshore scales (i.e. $X/Y \approx U/V \approx 1$), typically due to the presence of substantial alongshore variations in the bottom topography (i.e. $X_h / Y_h \approx 1$) and/or the presence of higher frequency motions ($fT \approx 1$), there are important changes in the first order vorticity dynamics of the CTW response.

a) For $X/Y \approx U/V \approx 1$ and $fT \approx \delta^{-1}$ (low frequency response), atmospheric pressure forcing remains negligible, however forcing by cross-shelf wind stress becomes important. Where the cross-shore scales of the alongshore wind stress and the longshore scales of the cross-shore wind stress are small in comparison to the typical CTW response scales (given here by the shelf width), forcing due to wind stress curl is significant and cannot be ignored. Further, the time dependence is removed from the first order equations and thus all motions are only slowly varying or quasi-steady

b) When $X/Y \approx U/V \approx 1$ and higher frequency motions are considered (i.e. $fT \approx 1$), the conclusions are the same as for $fT \approx \delta^{-1}$ except that the time-dependent terms are retained in the first order vorticity equation.

In summary, for "long wave" CTW dynamics, forcing by atmospheric pressure variations, wind stress curl and cross-shore wind stress are generally ineffective and the only forcing of consequence is that due to alongshore wind stress. Atmospheric pressure forcing is important if the CTW motions are divergent (which is only expected over very shallow, gently-sloping, extensive shelf regions or for motions having a frequency greatly exceeding the inertial frequency, that is, where $\varepsilon^2/fT \geq 1$). While cross-shelf wind stresses are generally ineffectual in forcing "long wave" CTW motions, wind stress curl forcing may become important where the atmospheric weather systems forcing CTW motions have an offshore scale comparable to or smaller than the cross-shore response scale of the CTW's which here is considered to be given by the shelf width (i.e. if $X \approx X_h \ll X_f$). In the vicinity of headlands and other regions where the spatial scales characteristic of wind stress fields are small (i.e $X_h \approx X_f$), forcing by wind stress curl becomes important and Ekman dynamics may predominate, resulting in upwelling.

Note that where the CTW response develops cross-shore and longshore scales of comparable magnitude (typically due to significant longshore variations in the bottom topography and/or the presence of higher frequency motions), forcing by cross-shelf wind stress is important. Further, where the development of similar cross-shore and longshore scales occurs solely due to to significant longshore variations in the bottom topography, the response is expected to display only a weak time dependence (i.e. quasi-steady flows are expected in regions where there are sharp alongshore changes in the bottom topography).

APPENDIX B - CTW Dispersion Curves for selected Shelf Topographies around Southern Africa

The CTW dispersion properties for selected offshore profiles of bottom topography (profiles 1 to 8 in Fig 3.1, p32) and three specification of the water column stratification (Fig 3.5, p41) are presented in Figures B1 to B8. At the top of each page is a plot of the dispersion properties (σ_n versus ℓ) of the first two CTW modes at each location. At the bottom of each page is a plot of the phase speeds of free CTW's as a function of wavenumber for the same shelf location. The above dispersion properties have been determined using local values of the Coriolis parameter at the different (see Table 1, p48). The labelling for the different modes and specifications of the water column stratification is as follows:

- b1 first barotropic mode
- b2 second barotropic mode
- w1 first mode for weak stratification
- w2 second mode for weak stratification
- m1 first mode for moderate stratification
- m2 second mode for moderate stratification
- s1 first mode for strong stratification
- s2 second mode for strong stratification

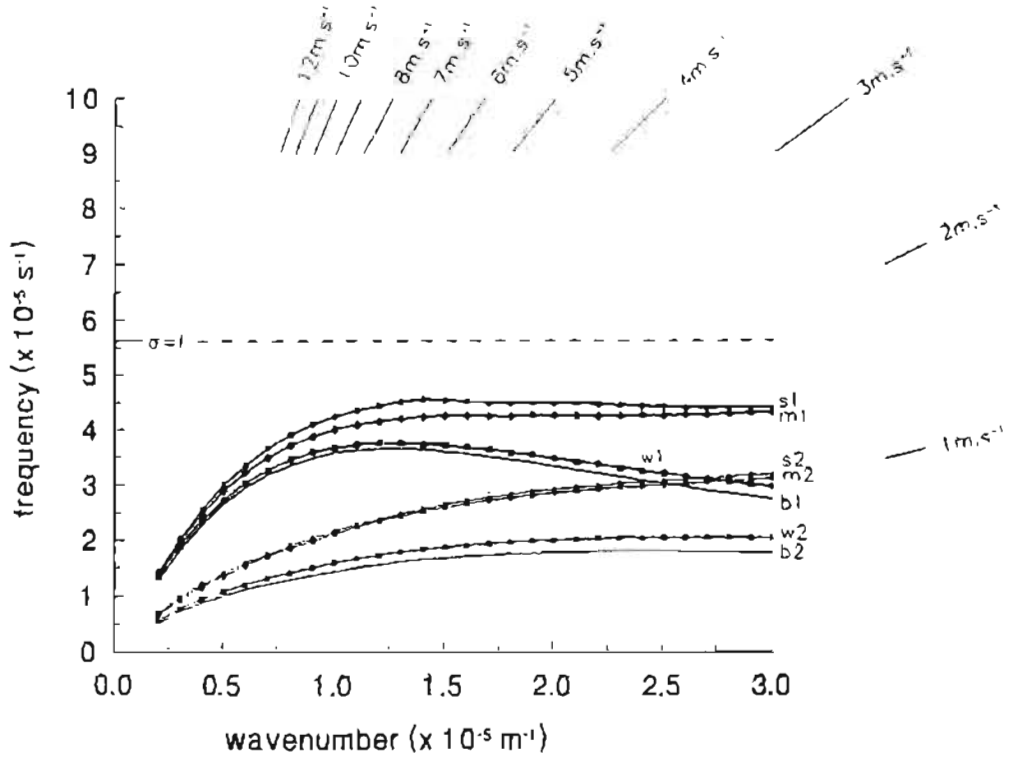

Fig B.1(a) The dispersion curves of free CTW motions characteristic of bottom topography profile 1.

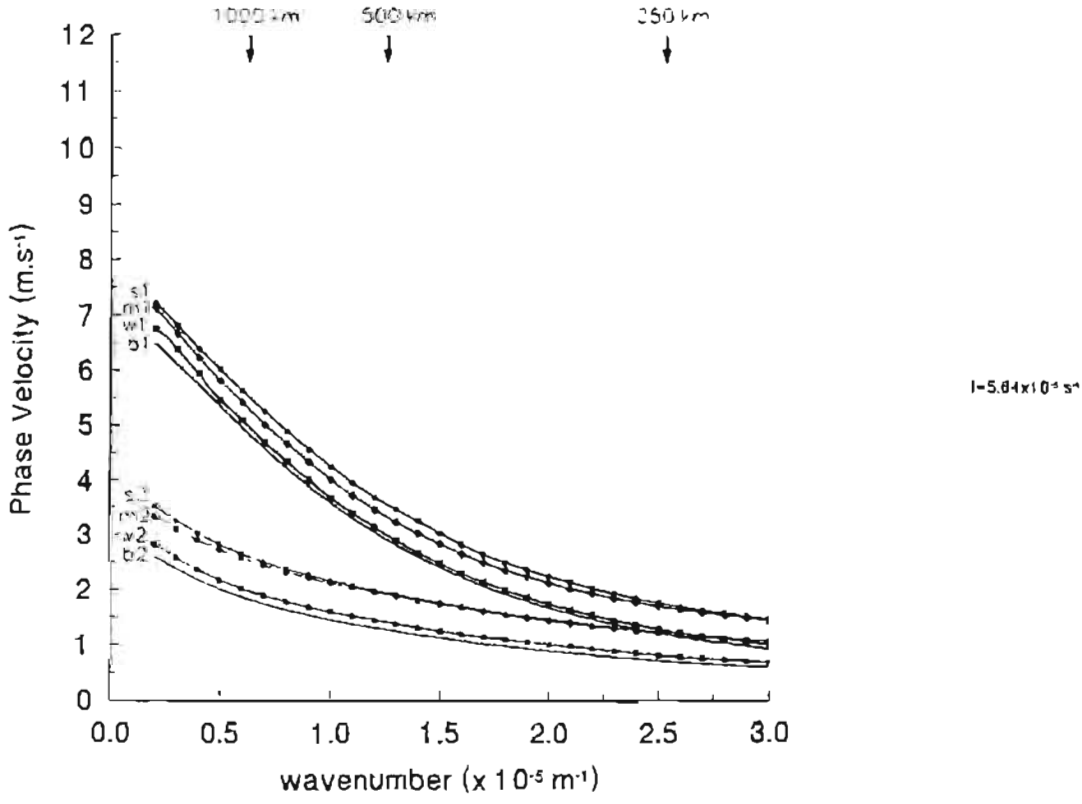

Fig B.1(b) The phase velocities of free CTW motions characteristic of bottom topography profile 1.

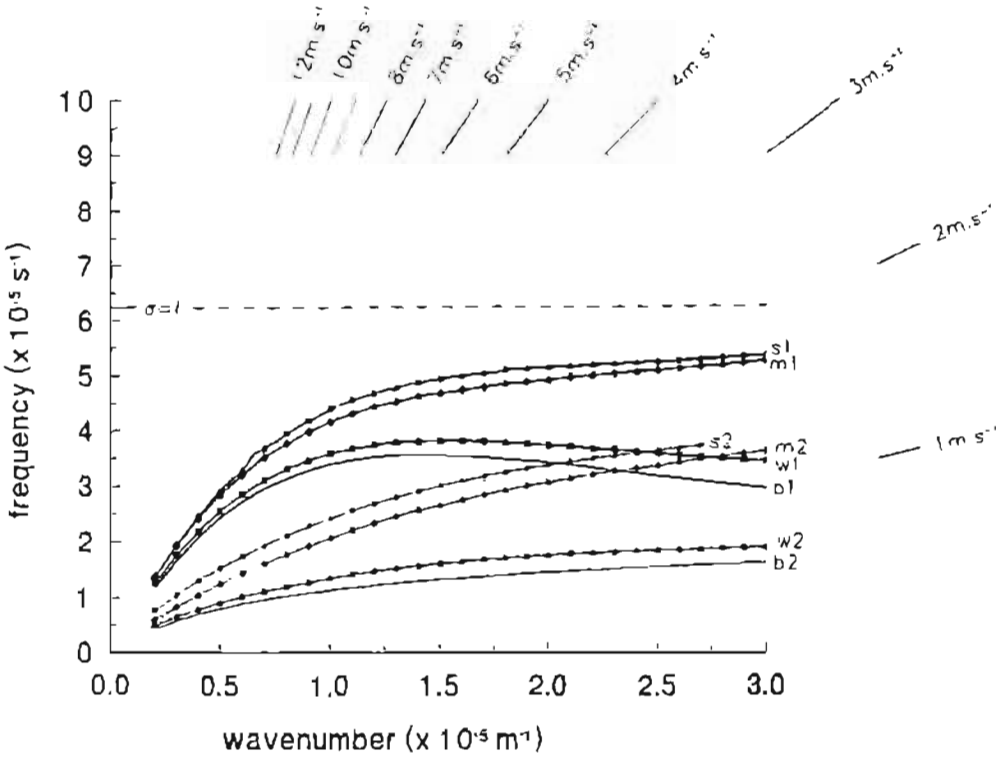

Fig B.2a) The dispersion curves of free CTW motions characteristic of bottom topography prolfile 2

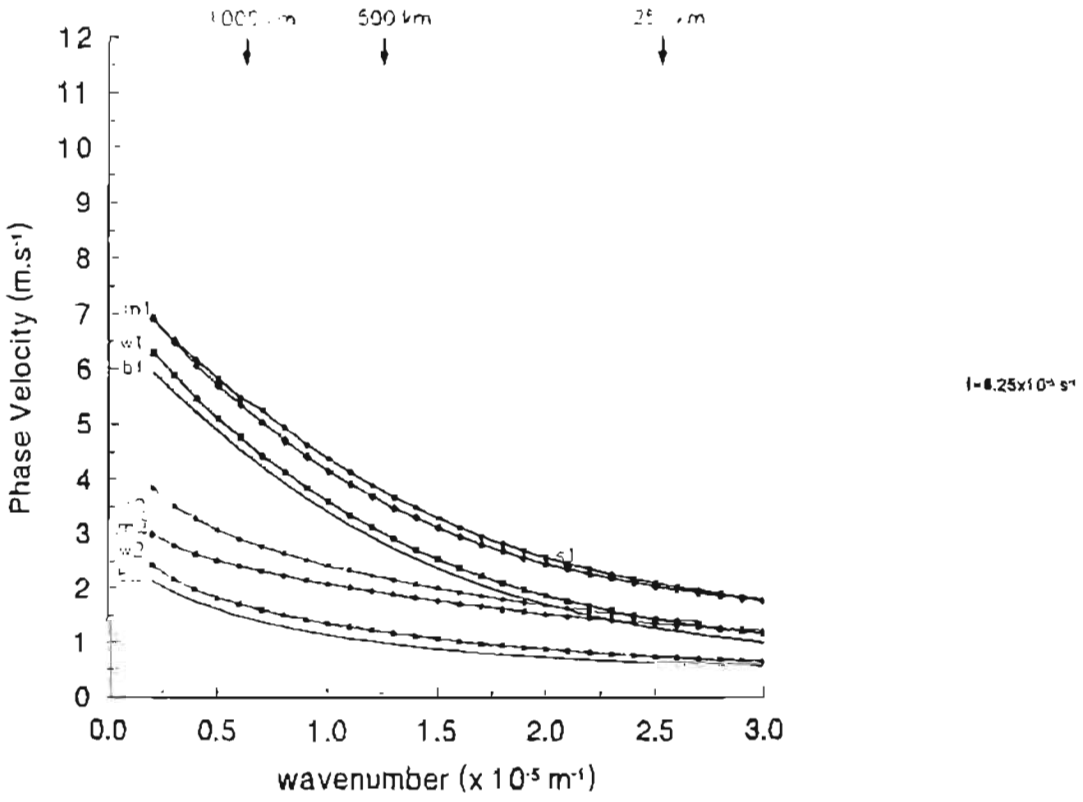

Fig B.2b) The phase velocities of free CTW motions characteristic of bottom topography prolfile 2

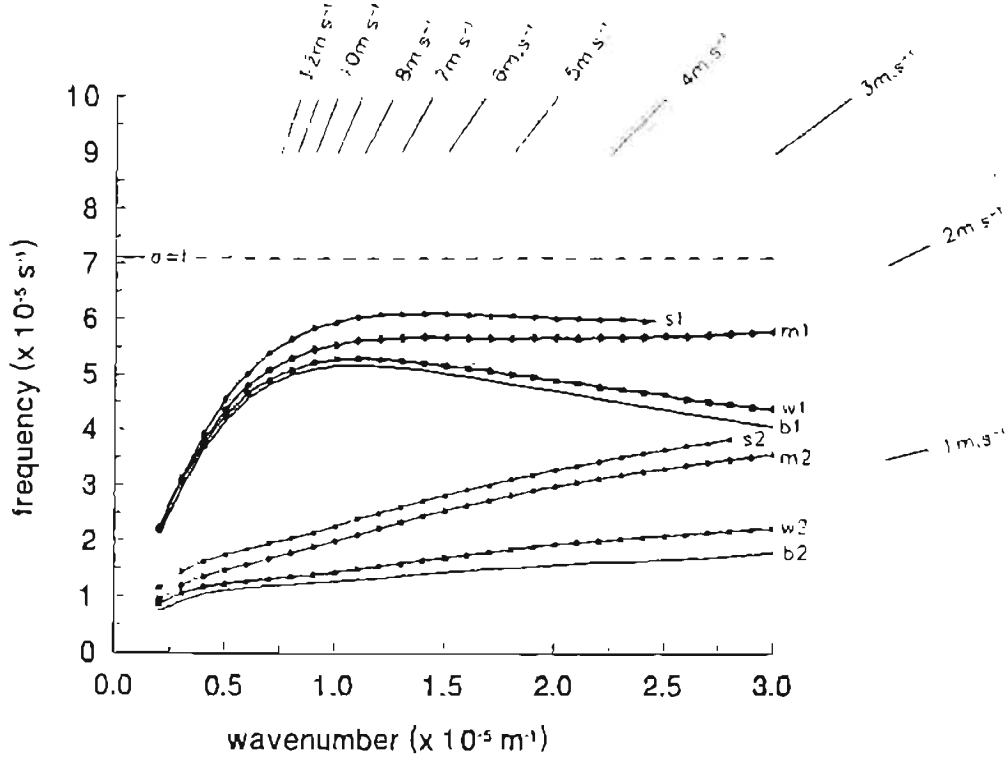

Fig B.3a) The dispersion curves of free CTW motions characteristic of bottom topography profile 3.

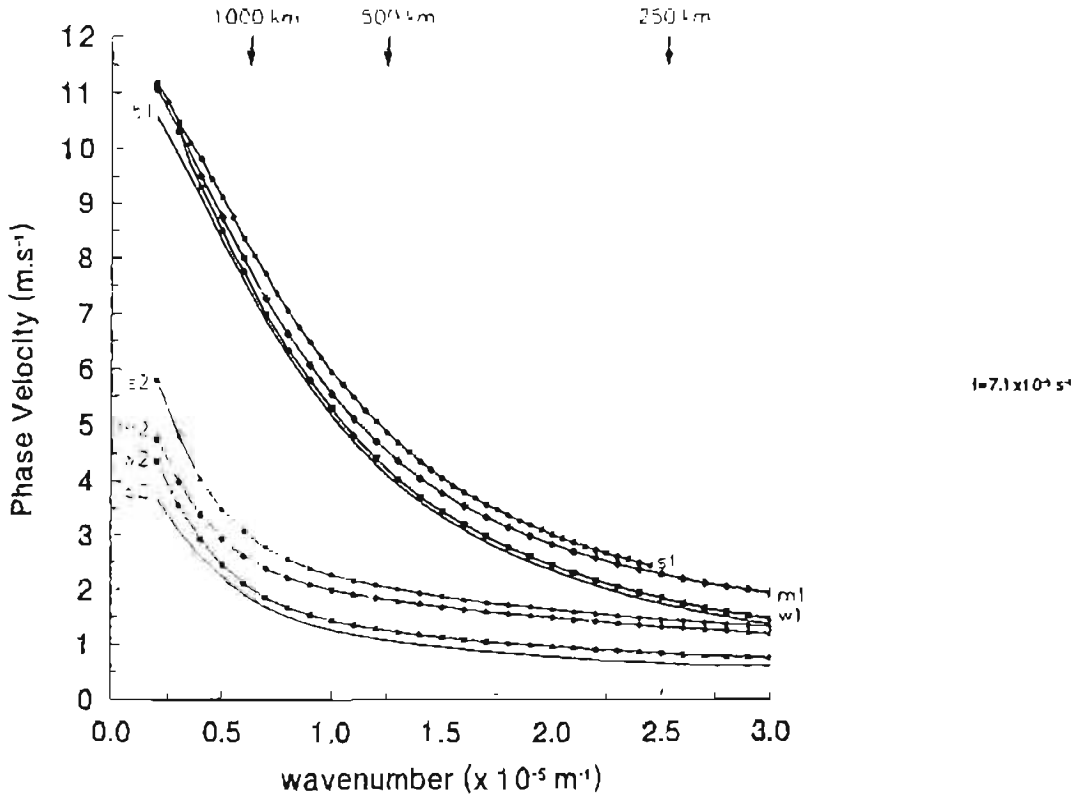

Fig B.3b) The phase velocities of free CTW motions characteristic of bottom topography profile 3.

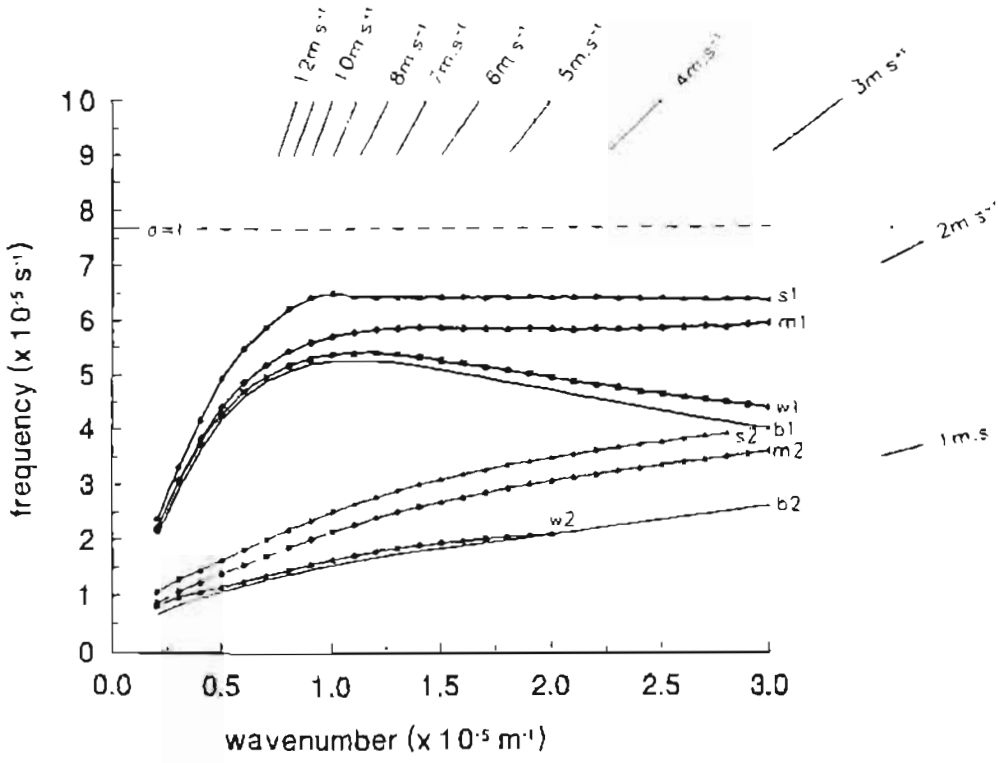

Fig B.4a) The dispersion curves of free CTW motions characteristic of bottom topography profile 4.

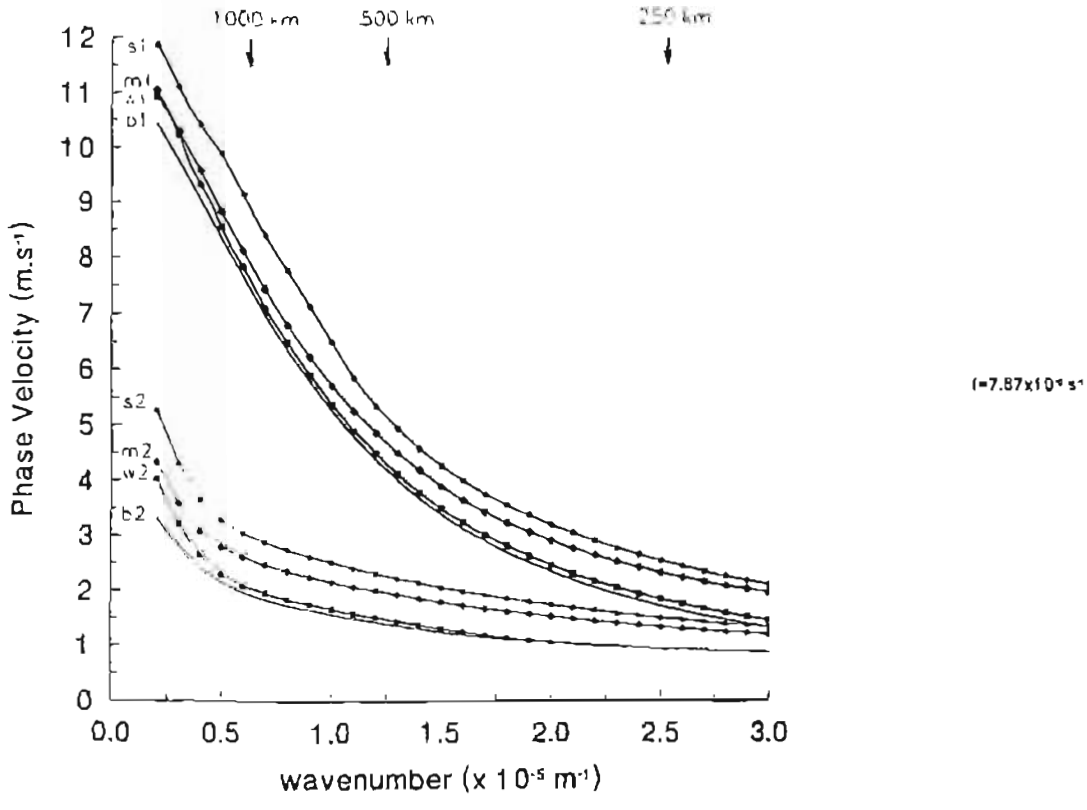

Fig B.4b) The phase velocities of free CTW motions characteristic of bottom topography profile 4.

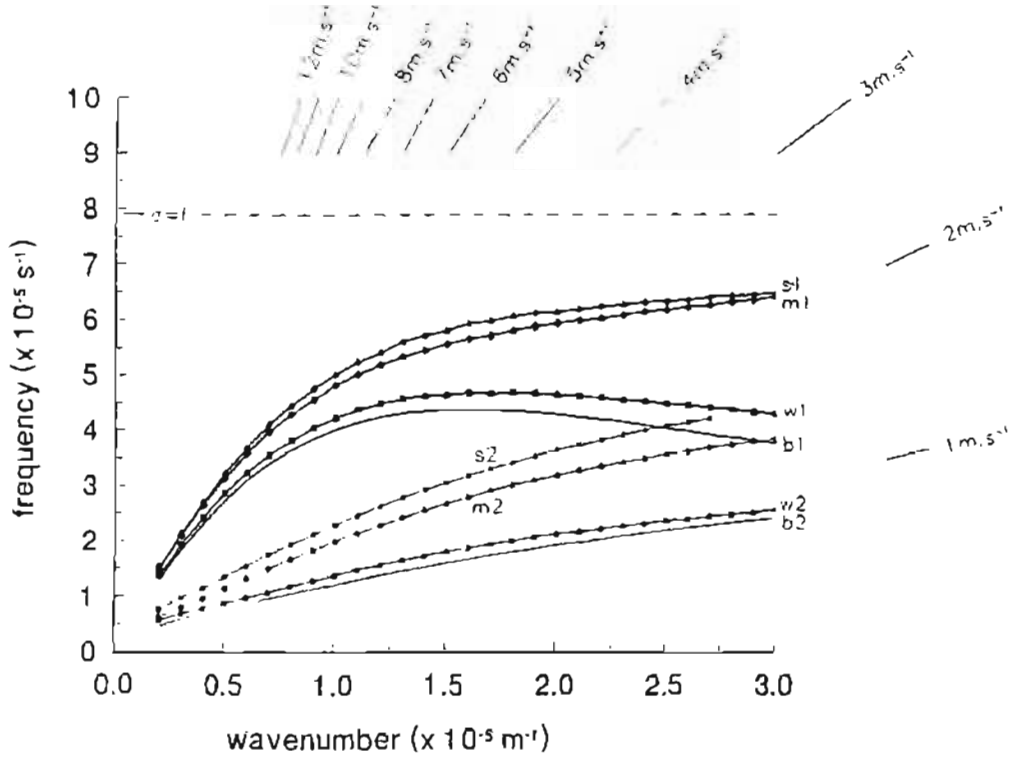

Fig B.5a) The dispersion curves of free CTW motions characteristic of bottom topography profile 5

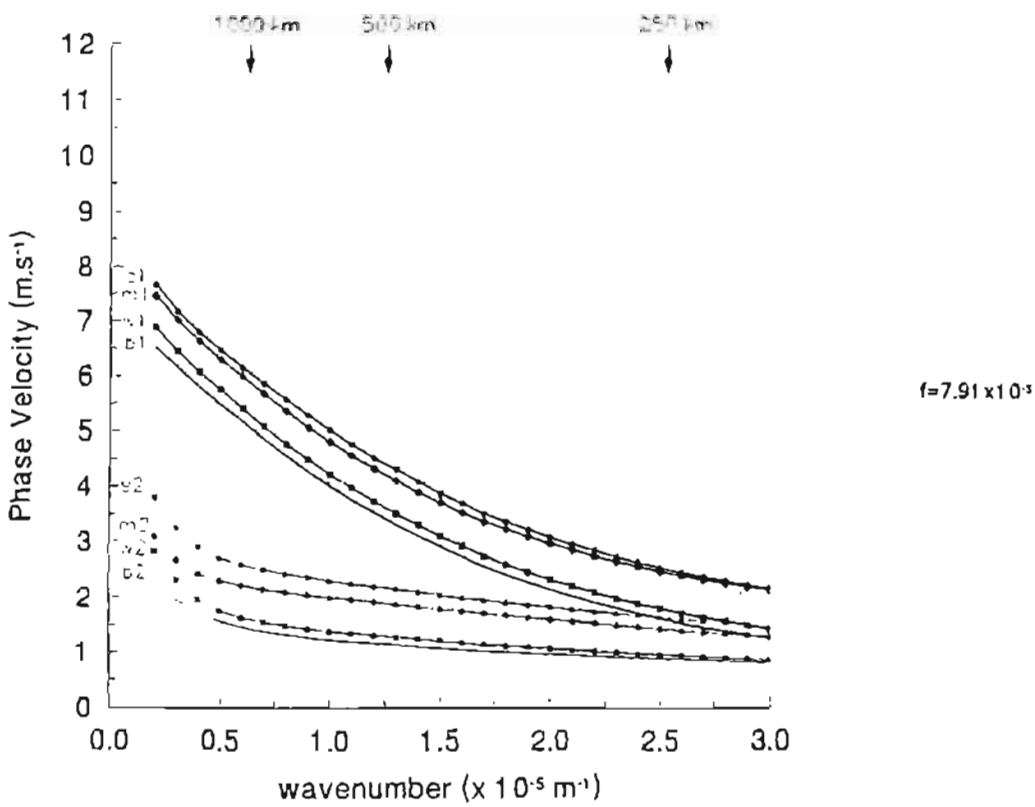

Fig B.5b) The phase velocities of free CTW motions characteristic of bottom topography profile 5

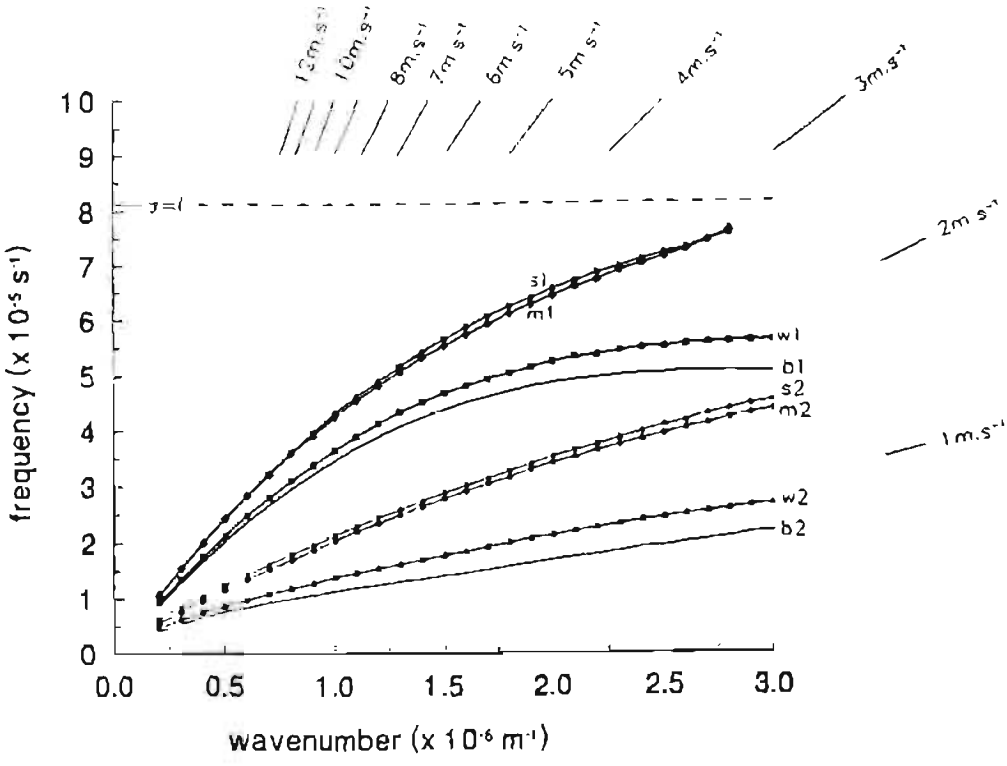

Fig B.6a) The dispersion curves of free CTW motions characteristic of bottom topography prolfile 6.

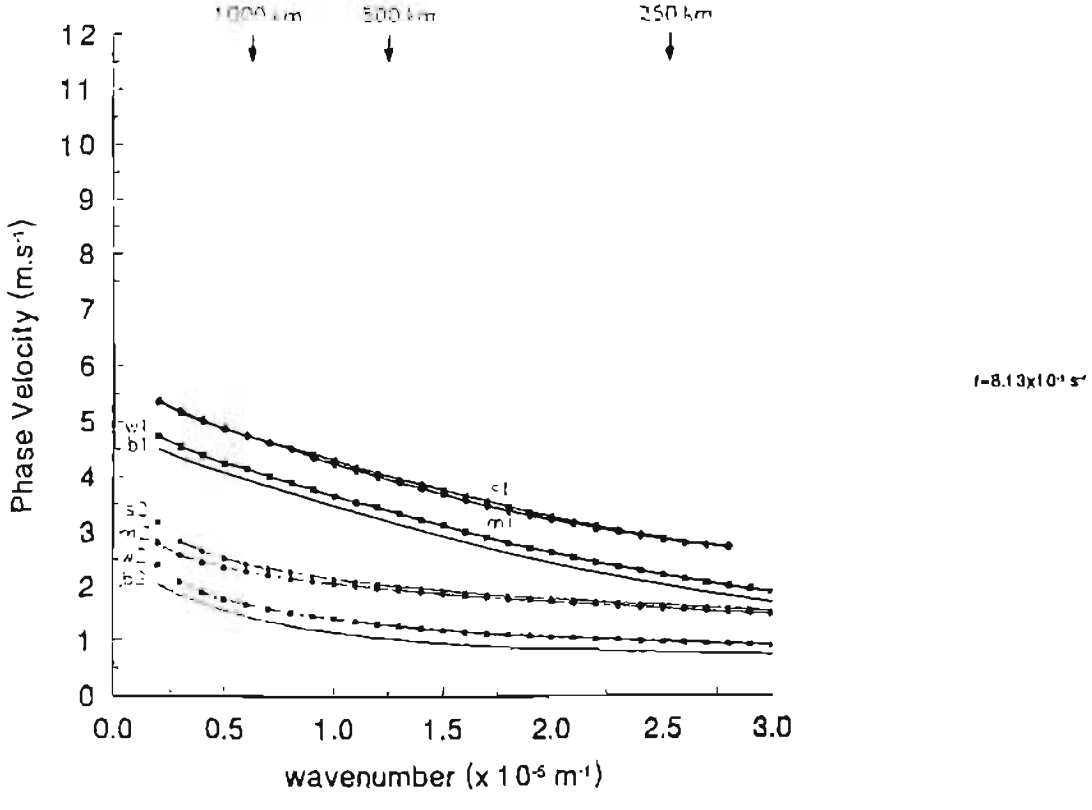

Fig B 6b) The phase velocities of free CTW motions characteristic of bottom topography prolfile 6.

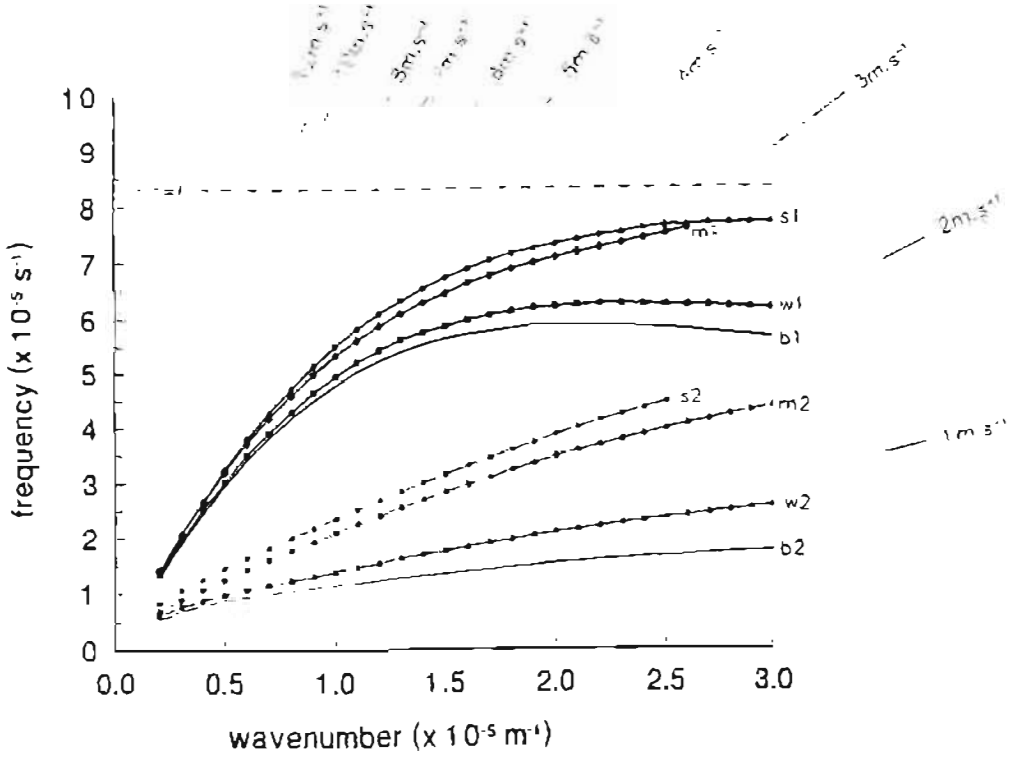

Fig B.7a) The dispersion curves of free CTW motions characteristic of bottom topography profile 7.

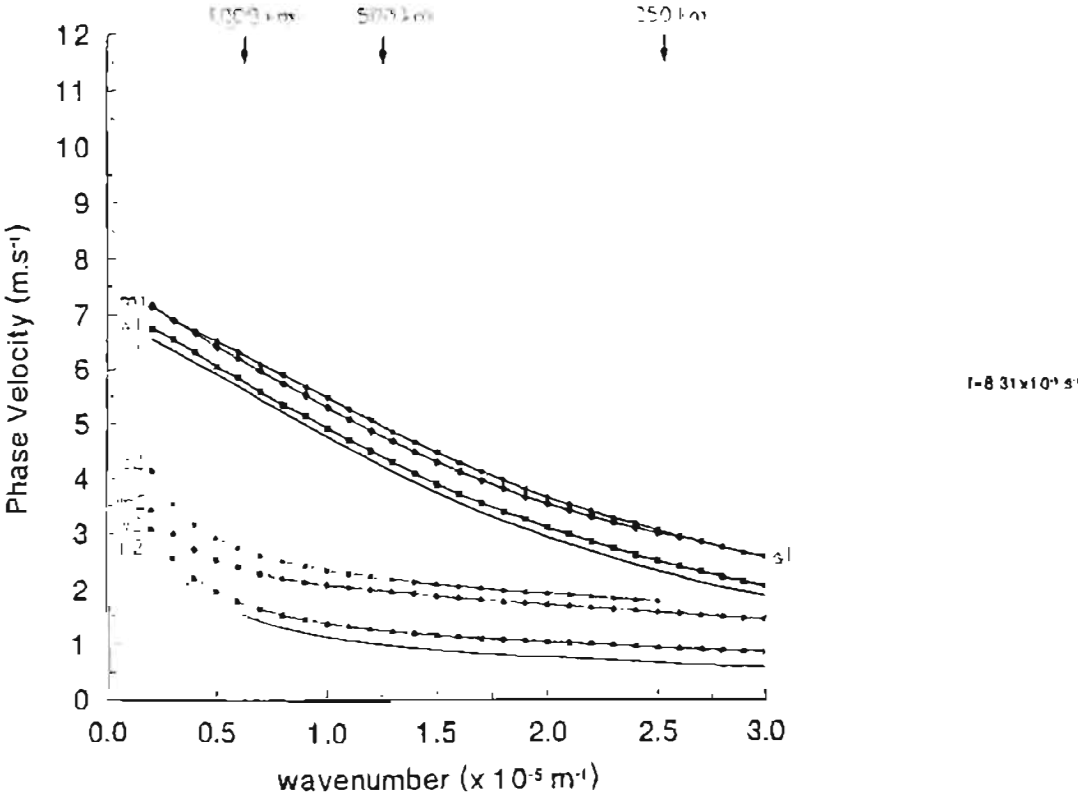

Fig B.7b) The phase velocities of free CTW motions characteristic of bottom topography profile 7

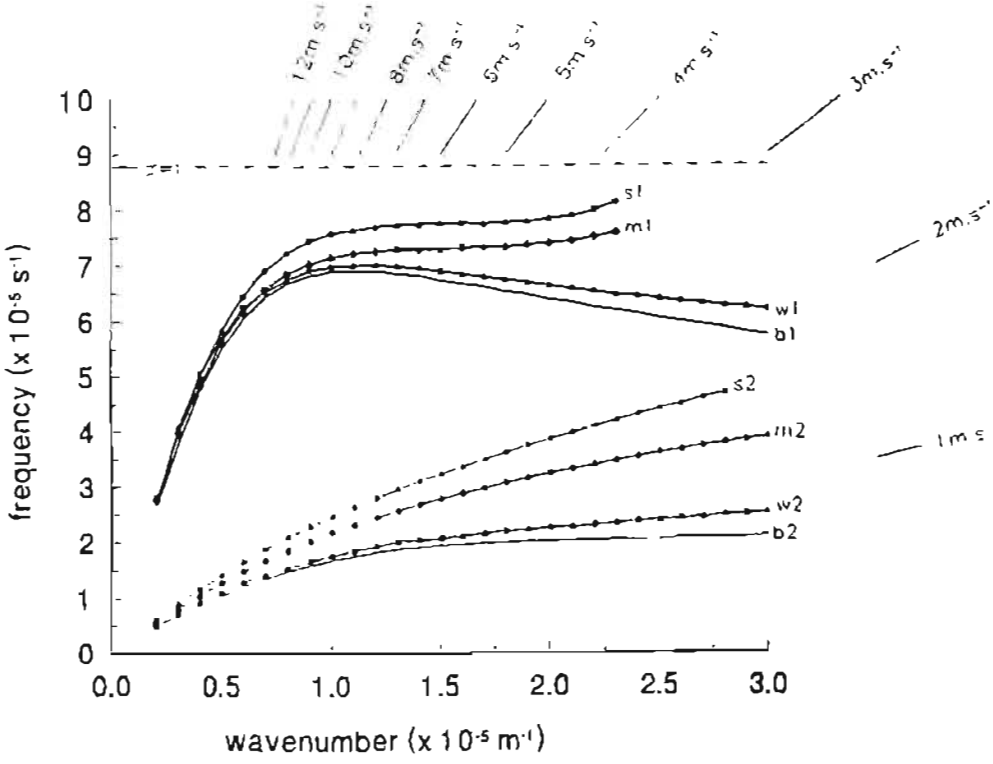

Fig B.8a) The dispersion curves of free CTW motions characteristic of bottom topography profile 8.

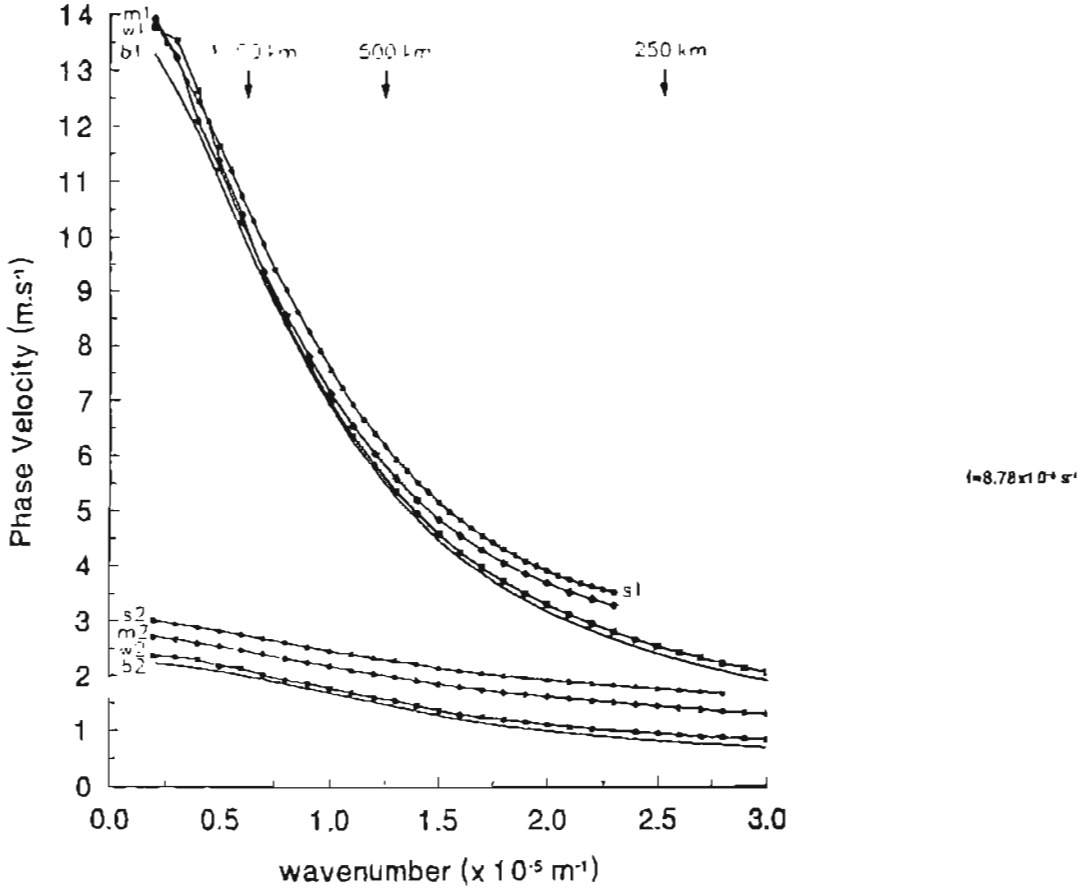

Fig B 8b) The phase velocities of free CTW motions characteristic of bottom topography profile 8.

APPENDIX C - Methods of time series analysis

The raw sea and atmospheric pressure times series in Chapter 5 are analysed using;

a) autospectra to describe the frequency characteristics of the atmospheric pressure and sea level time series,

b) cross-spectra, coherency and phase plots to characterise (in the frequency domain) the relationships that exist between atmospheric pressures at various sites and sea levels at various sites along the coastline, and

c) cross-correlation analyses to characterise (in the time domain) the relationships that exist between the various atmospheric pressure and sea level time series.

C-1 Autospectra

The methods used to estimate the autospectra (power spectral densities) of time series are described in many texts (for example, Jenkins and Watts, 1968; Bendat and Piersol, 1971; Otnes and Enochson, 1978 and Schumway, 1988). Here the autospectra have been calculated using the MATLAB signal processing toolbox (Krauss *et al.*, 1995). The MATLAB power spectral density routines utilise the averaged periodogram method of Welch (1967) where the input time series $x(t)$ of length $N\Delta t$ is split up into a n_{win} subseries, each of length $m=N/n_{win}$. A window of length m is used to taper the data in each of the subseries and the magnitude of the square of the Fast Fourier transform (FFT) of each "tapered" subseries is calculated and normalised according to the type of window used to taper the data. (A Hanning window is used for all data analyses in this thesis). The mean of these individual autospectral estimates provide smoothed autospectral estimates, $\hat{P}_{xx}(f)$, which are defined at $f = 1/(2m\Delta t)$, $2/(2m\Delta t)$,....., f_n . The quantity $f_n = 1/(2\Delta t)$, known as the Nyquist frequency, is the maximum resolvable frequency in the input time series. The frequency resolution for each estimate, $\hat{P}_{xx}(f)$, is given by the resolution bandwidth, $B_e = 1/(m\Delta t)$. The above method, which produces smoothed autospectral estimates at frequency intervals of $\Delta f = 1/(2m\Delta t) = B_e/2$, results in overlapping of smoothed autospectral estimates since each estimate, $\hat{P}_{xx}(f_0)$, represents of the power spectral density in a frequency range $f_0 - B_e/2 \leq f_0 \leq f_0 - B_e/2$.

For a time series of length $N\Delta t$, the number of degrees of freedom, ν, is given by $\nu = 2B_e m\Delta t = 2N/m$ and the normalised standard error, ε_T, by

$$\varepsilon_T = \sqrt{\frac{1}{Be\Delta t}} = \sqrt{\frac{m}{N}}$$

To keep the normalised standard error small it is necessary that $m \ll N$. In general m is chosen such that $m \leq N/10$ (that is $n_{win} = 10$). The values $n_{win} = 9$ and $m = N/9$ are chosen for the all of the data analyses in Chapter 5. The sampling distribution $\hat{P}_{xx}(f)$, after smoothing with a suitable window (in this case a Hanning window), is approximately chi-square with ν degrees of freedom. The 100(1-α) percent confidence interval for the estimates, $\hat{P}_{xx}(f)$, of the true autospectrum, $P_{xx}(f)$, is given by

$$\frac{\nu\ \hat{P}_{xx}(f)}{\chi^2_{\nu,\frac{\alpha}{2}}} \leq P_{xx}(f) \leq \frac{\nu\ \hat{P}_{xx}(f)}{\chi^2_{\nu,1-\frac{\alpha}{2}}}$$

where the chi-squared values may be obtained from tables in standard statistical texts. Here the values are calculated in MATLAB routines written using algorithms obtained from Numerical Recipes in C (Press *et al.*, 1989).

C-2 Cross-spectra, phase and coherence

The cross-spectra, phase and coherence of the atmospheric pressure and sea level time series are also calculated using the MATLAB signal processing toolbox. The cross-spectra are calculated in an analogous manner to the autospectra, except that here the individual estimates (before averaging) consist of the product of the FFT of the second series, *y(t)*, and the complex conjugate of the FFT of the first series, *x(t)*. The mean of these individual cross-spectral estimates provide the smoothed cross-spectral estimates, $\hat{P}_{xy}(f)$, which are defined at $f = 1/(2m\Delta t), 2/(2m\Delta t), \ldots\ldots, f_n$. These smoothed cross-spectral estimates may be expressed as

$$\hat{P}_{xy}(f) = \hat{C}_{xy}(f) - i\hat{Q}_{xy}(f)$$

where $\hat{C}_{xy}(f)$ is the co-spectrum and $\hat{Q}_{xy}(f)$ is the quadrature spectrum.

The confidence interval for the cross-spectral estimates is obtained in a manner analogous to those for the autospectral estimates and is provided directly by the MATLAB routines.

The phase behaviour between the two input time series is provided by the phase function which is estimated as

$$\hat{\theta}(f) = \tan^{-1}\left[\frac{-\hat{Q}_{xy}(f)}{\hat{C}_{xy}(f)}\right]$$

The $100(1-\alpha)$ percent confidence interval for phase function estimates is given by

$$\hat{\theta}_{xy}(f) - \Delta\hat{\theta}_{xy}(f) \;\le\; \theta_{xy}(f) \;\le\; \hat{\theta}_{xy}(f) + \Delta\hat{\theta}_{xy}(f)$$

where

$$\Delta\hat{\theta}_{xy}(f) = \sin^{-1}\left(\sqrt{F_{2,\nu-2,\alpha}\left(\frac{2}{\nu-2}\right)\left(\frac{1}{\hat{\gamma}^2_{xy}(f)} - 1\right)}\right)$$

$F_{2,\nu-2,\alpha}$ refers to F-distribution values obtainable from standard statistical tables. Here these values were calculated using MATLAB routines based on algorithms obtained from Numerical Recipes in C (Press *et al.*, 1989).

The coherency squared, $\gamma^2_{xy}(f)$, is defined as the square of the magnitude of the cross-spectrum normalised by the magnitude of the autospectra of the two input time series and is estimated as

$$\hat{\gamma}^2_{xy}(f) = \frac{\left|\hat{P}_{xy}(f)\right|^2}{\hat{P}_{xx}(f)\;\hat{P}_{yy}(f)}$$

The $100(1-\alpha)$ confidence interval for the coherence estimates, obtained using the Fischer z-transform, is

$$\tanh\left\{\hat{z}(f) - (\nu-2)^{-1} - \sigma_{\hat{z}}\, z_{\alpha/2}\right\} \le \gamma_{xy}(f) \le \tanh\left\{\hat{z}(f) - (\nu-2)^{-1} + \sigma_{\hat{z}}\, z_{\alpha/2}\right\}$$

where $\hat{z}(f) = \tanh^{-1}\left[\hat{\gamma}_{xy}(f)\right]$, $\nu = \dfrac{2N}{m}$ and $\sigma_{\hat{z}} = \sqrt{\dfrac{1}{\nu-2}}$

The estimates of $\hat{z}(f)$ and $\sigma_{\hat{z}}$ may be improved (Benignus, 1969 as quoted by Otnes and Enochson, 1978) by using a bias correction to obtain an improved estimate of coherence, $\tilde{\gamma}^2_{xy}(f)$, and an improved variance estimate, $\sigma_{\tilde{z}}$, where

$$\tilde{\gamma}^2_{xy}(f) = \hat{\gamma}^2_{xy}(f) - \frac{1}{2\nu}\left(1-\hat{\gamma}^2_{xy}(f)\right) \quad \text{and} \quad \sigma_{\tilde{z}} = \sqrt{\frac{1}{\nu-2}}\left[1-0.004^{\left\{1.6\,\hat{\gamma}^2_{xy}(f)+0.22\right\}}\right]$$

The improved confidence interval defined using these variables is given by

$$\tanh\left\{\tilde{z}(f)-(\nu-2)^{-1}-\sigma_{\tilde{z}}\,z_{\alpha/2}\right\} \le \gamma_{xy}(f) \le \tanh\left\{\tilde{z}(f)-(\nu-2)^{-1}+\sigma_{\tilde{z}}\,z_{\alpha/2}\right\}$$

where $\hat{z}(f) = \tanh^{-1}\left[\tilde{\gamma}^2_{xy}(f)\right]$

The confidence limits for the coherency squared is simply the square of the above limits. The significance of a given coherence squared estimate can be assessed by noting that the quantity

$$\hat{F}_{2,\nu-2,\alpha} = \frac{\hat{\gamma}^2_{xy}(f)}{\left[1-\hat{\gamma}^2_{xy}(f)\right]}\frac{\nu-2}{2}$$

has an approximate F-distribution with 2 and (ν-2) degrees of freedom under the hypothesis that $\hat{\gamma}^2_{xy}(f) = 0$. Therefore, if $\hat{F}_{2,\nu-2,\alpha} \ge F_{2,\nu-2,\alpha}$, then the coherence squared estimate is significant at the 100(1-α) significance level (Schumway, 1988).

C-3 Correlation Analysis

An unbiased estimate of the autocovariance function of a time series *x(t)* is given by

$$\hat{C}_{xx}(i\Delta t) = \frac{1}{N-|i|}\sum_{n=1}^{N-|i|}\left[x(n\Delta t)-\bar{x}\right]\left[x((n+i)\Delta t)-\bar{x}\right]$$

and similarly an unbiased estimate of the cross-covariance of *x(t)* and *y(t)* is given by

$$\hat{C}_{xy}(i\Delta t) = \frac{1}{N-|i|}\sum_{n=1}^{N-|i|}\left[x(n\Delta t)-\bar{x}\right]\left[y((n+i)\Delta t)-\bar{y}\right]$$

where $\bar{x}$ and $\bar{y}$ are the mean values of *x(t)* and *y(t)*, respectively and $i\Delta t$ is the lag number where $i = -(N-1), \ldots, 0, \ldots, (N-1)$.

The cross-correlation function, $r_{xy}(i\Delta l)$, is defined as the cross-covariance normalised by the autocovariances of $x(l)$ and $y(l)$ at zero lag and is estimated using

$$\hat{r}_{xy}(i\Delta l) = \frac{\hat{C}_{xy}(i\Delta l)}{\sqrt{\hat{C}_{xx}(0)\,\hat{C}_{yy}(0)}}$$

The standard error of the $\hat{r}_{xy}(i\Delta l)$ estimates is $s_r^2(i\Delta l) = \sqrt{1-\hat{r}_{xy}(i\Delta l)}$ and the residual variance of the $\hat{r}_{xy}(i\Delta l)$ estimates is $s_r^2(i\Delta l) = \sqrt{\frac{\nu-2}{1-\hat{r}_{xy}(i\Delta l)}}$

The test statistic to determine whether $\hat{r}_{xy}(i\Delta l)$ is significant at the 100(1-α) percent significance level is the t-statistic

$$\hat{t}(i) = \frac{\left|\hat{r}_{xy}(i\Delta l)\right|}{s_r(i\Delta l)} = \left|\hat{r}_{xy}(i\Delta l)\right| \sqrt{\frac{\nu-2}{1-\hat{r}_{xy}(i\Delta l)}}$$

If $\hat{t}(i) \geq t_{\nu-2,\frac{\alpha}{2}}$, then the null hypothesis of $\hat{r}_{xy}(i\Delta l) = 0$ is rejected and the correlation is significant at the 100(1-α) percent significance level

The 100(1−α) percent confidence interval for the cross-correlation estimates, obtained using the Fischer z-transform (Otnes and Enochson, 1978), is

$$\tanh\left\{\hat{z}(f) - \sigma_{\hat{z}}\, z_{\alpha/2}\right\} \leq r_{xy}(f) \leq \tanh\left\{\hat{z}(f) + \sigma_{\hat{z}}\, z_{\alpha/2}\right\}$$

where $\hat{z}(f) = \tanh^{-1}\left[\hat{r}_{xy}^2(f)\right]$ and $\sigma_{\hat{z}} = \sqrt{\frac{1}{\nu-2-i}}$

It is often assumed that the number of degrees of freedom, ν, are equal to the number of data points, N, in the time series In oceanographic time series this is rarely the case as there is usually significant autocorrelation within the data series. The true number of degrees of freedom may be determined using the method of Davis (1976) who defines a time scale, τ, which represents the length of time needed to gain a new degree of freedom in the data series. This quantity, used to determine the number of degrees of freedom, is calculated using the following expression

$$\tau = \sum_{i=-\infty}^{\infty} \hat{r}_{xx}(i\Delta l)\,\hat{r}_{yy}(i\Delta l)\,\Delta l$$

where $\hat{r}_{xx}(i\Delta t) = \dfrac{\hat{C}_{xx}(i\Delta t)}{\hat{C}_{xx}(0)}$ and $\hat{r}_{yy}(i\Delta t) = \dfrac{\hat{C}_{yy}(i\Delta t)}{\hat{C}_{yy}(0)}$ are the normalised auto-covariance functions of the time series x(t) and y(t).

In practise τ is calculated using

$$\tau = \sum_{i=-m}^{m} \hat{r}_{xx}(i\Delta t)\,\hat{r}_{yy}(i\Delta t)\,\Delta t$$

where m is large compared to the lag at which both $\hat{r}_{xx}(i\Delta t)$ and $\hat{r}_{yy}(i\Delta t)$ are statistically zero. It is usual in practise to set $m \leq N/10$ to avoid autocorrelations having large variances (due to the small number of points in the estimate). However, if it is not possible to increase the length of the data series such that $\hat{r}_{xx}(m)$ and $\hat{r}_{yy}(m)$ are statistically zero, a compromise value of $m = N/4$ may be chosen (de Cuevas, 1985) The appropriate value of τ is then the maximum of the cumulative summation $\Pi(j)$ where

$$\Pi(j) = \left[\hat{r}_{xx}(0)\,\hat{r}_{yy}(0)\right] + 2\sum_{i=1}^{j}\left[\hat{r}_{xx}(j)\,\hat{r}_{yy}(j)\right]\Delta t \qquad \text{for } j = 1, 2, \ldots, N/4.$$

The choice of $m = N/4$ is only justified if value of $\Pi(j)$ reaches a maximum in the range $1 \leq j \leq N/4$ or is only slowly increasing at $j = N/4$. The number of degrees of freedom are then calculated using

$$\nu = \frac{N\Delta t}{\tau}.$$

Using this value for ν, the significance of each cross-correlation estimate may be determined using the t-statistic defined earlier.

Sciremammano (1979) suggested an alternative approach where the $\hat{r}_{xy}(i\Delta t)$ values are normalised by the large lag standard error σ_{se} which is estimated as

$$\hat{\sigma}^2_{se}(i) = \frac{1}{N - |i|}\sum_{j=-m}^{m} \hat{r}_{xx}(j\Delta t)\,\hat{r}_{yy}(j\Delta t)\,\Delta t$$

Such a normalised cross-correlation defined as

$$\hat{r}^{n}_{xy}(i\Delta t) = \frac{\hat{r}_{xy}(i\Delta t)}{\hat{\sigma}_{se}},$$

is a normally distributed, zero mean, unit standard deviation variate that not only gives the strength of the cross-correlation but also directly provides a statistic which

determines the significance of the cross-correlation estimates. If $\hat{r}^{n}_{xy}(i\Delta t) \geq z_{\frac{\alpha}{2}}$ then the cross-correlation is significant at the $100(1-\alpha)$ percent significance level.

The presentation of correlations normalised by their large lag standard errors thus conveys much more information than the "standard" correlations normally reported because the normalisation compensates for the interplay of the dominant time scales of the input processes and the possible different lengths of the input time series. The greatest value of this method is the fact that it yields significance levels on inspection.

The method is thus particularly useful in comparing long records of environmental variables which have different time scales of variability which is a feature of the sea level observations at the different coastal sites around southern Africa. It is important to note that the above method is simply a different manner of presenting the data. Sciremammano (1979) has shown the above methodology to be equivalent to that proposed by Davis (1976).

APPENDIX D - The semi-implicit Euler forward-backward finite difference numerical scheme and cross-shelf open boundary conditions

D-1 The Euler forward-backward finite difference numerical scheme

The finite difference numerical scheme used in this investigation of forced continental shelf wave motions over the continental shelf off the west coast of southern Africa is based on the following homogenous, linear, *f*-plane, shallow water wave equations

$$\frac{\partial U}{\partial t} - fV = -gh\frac{\partial \eta}{\partial x} + \frac{1}{\rho}\left[\tau^{x}_{w} - \tau^{x}_{b}\right]$$

$$\frac{\partial V}{\partial t} + fU = -gh\frac{\partial \eta}{\partial y} + \frac{1}{\rho}\left[\tau^{y}_{w} - \tau^{y}_{b}\right]$$

$$\frac{\partial \eta}{\partial t} = -\left(\frac{\partial U}{\partial x} + \frac{\partial V}{\partial y}\right)$$

where it is assumed that

i) the sea level perturbation to water depth ratio is small, i.e. $\frac{\eta}{H} \ll 1$,

ii) non-linear effects are negligible, i.e. $\frac{U}{fX} \ll 1$, $\frac{V}{fY} \ll 1$ *or* $U \ll C_{ph}$, $V \ll C_{ph}$.

iii) atmospheric pressure forcing is negligible, i.e. $\left(f\frac{\partial \eta^{a}}{\partial t} \Big/ \frac{\tau_{w}}{\rho h}\frac{\partial h}{\partial x}\right) \ll 1$.

iv) the bottom friction is linear, i.e. $\tau^{x}_{b} = \frac{\rho r U}{h}$, $\tau^{y}_{b} = \frac{\rho r V}{h}$

The finite difference numerical scheme used is the semi-implicit Euler forward-backward scheme implemented on an staggered (Arakawa C-) grid with irregular cross-shore spacing (Δx increases offshore) and an regular alongshore spacing (Δy is constant). The detail of the finite difference grid is given in Fig. 6.1 (p127).

The finite difference approximation of the above shallow water wave equations on an staggered grid with irregular grid spacing in the offshore direction is as follow

$$\eta^{n+1}_{i,j} = \eta^{n}_{i,j} - \Delta t\left[\left(U^{n}_{i,j} - U^{n}_{i-1,j}\right)\Big/\Delta x_{i-1} + \left(V^{n}_{i,j} - V^{n}_{i,j-1}\right)\Big/\Delta y\right] \quad (D.1)$$

$$U_{i,j}^{n+1} = U_{i,j}^{n} + \Delta t \begin{bmatrix} -g\overline{h_{i,j}}\left(\eta_{i+1,j}^{n+1} - \eta_{i,j}^{n+1}\right)/\Delta v_i \\ +f\left\{(1-w_u)\left(V_{i,j}^{n} - V_{i,j-1}^{n}\right)/2 + w_u\left(V_{i+1,j}^{n} - V_{i+1,j-1}^{n}\right)/2\right\} \\ +\left\{(1-w_u)\left(\tau_w^x\right)_{i,j}^{n} + w_u\left(\tau_w^x\right)_{i+1,j}^{n}\right\}/\rho - \left(\tau_b^x\right)_{i,j}/\rho \end{bmatrix} \tag{D.2}$$

$$V_{i,j}^{n+1} = V_{i,j}^{n} + \Delta t \begin{bmatrix} -g\overline{\overline{h_{i,j}}}\left(\eta_{i,j+1}^{n+1} - \eta_{i,j}^{n+1}\right)/\overline{\Delta y} \\ -f\left\{(1-w_v)\left(U_{i,j}^{n+1} - U_{i-1,j+1}^{n+1}\right)/2 + w_v\left(U_{i,j}^{n+1} - U_{i,j+1}^{n+1}\right)/2\right\} \\ +\left\{\left(\tau_w^y\right)_{i,j+1}^{n} + \left(\tau_w^y\right)_{i,j}^{n}\right\}/2\rho - \left(\tau_b^y\right)_{i,j}/\rho \end{bmatrix} \tag{D.3}$$

where

$$\Delta u_i = \Delta x_{2i} + \Delta x_{2i-1}$$
$$\Delta v_i = \Delta x_{2i} + \Delta x_{2i-1}$$
$$x = \sum_{m=1}^{i} \overline{\Delta x_m}, \quad y = j\,\overline{\Delta y}$$
$$t = n\Delta t$$
$$w_u = \Delta x_{2i-1}/\Delta v_i$$
$$w_v = \Delta x_{2i-2}/\Delta u_{i-1}$$
$$\overline{h_{i,j}} = (1-w_u)h_{i,j} + w_u h_{i+1,j}$$
$$\overline{\overline{h_{i,j}}} = \left(h_{i,j+1} + h_{i,j}\right)/2$$
$$\left(\tau_b^x\right)_{i,j} = \rho r U_{i,j}^{n}/\overline{h_{i,j}}$$
$$\left(\tau_b^y\right)_{i,j} = \rho r V_{i,j}^{n}/\overline{\overline{h_{i,j}}}$$

and $\Delta u_i \approx \Delta v_i = \overline{\Delta x_i} \approx 2\Delta x_i$, $\overline{\Delta y} = 2\Delta y$ are the spacings between any two consecutive variables of the same type in the cross-shore and alongshore direction, respectively (see Fig 6.1, p127).

If one assumes a regular and equal grid spacing in both the cross-shore and alongshore directions (i.e $\overline{\Delta s} = \overline{\Delta x} = \overline{\Delta y}$) then the finite difference numerical scheme is significantly simplified and is given by the following set of finite difference equations

$$\eta_{i,j}^{n+1} = \eta_{i,j}^{n} - \Delta t/\overline{\Delta s}\left[\left(U_{i,j}^{n} - U_{i-1,j}^{n}\right) + \left(V_{i,j}^{n} - V_{i,j-1}^{n}\right)\right] \tag{D.4}$$

$$U_{i,j}^{n+1} = U_{i,j}^{n} + \Delta t \begin{bmatrix} -g\overline{h_{i,j}}\left(\eta_{i+1,j}^{n+1} - \eta_{i,j}^{n+1}\right)/\overline{\Delta x} \\ +f\left(V_{i,j}^{n} - V_{i,j-1}^{n} + V_{i+1,j}^{n} - V_{i+1,j-1}^{n}\right)/4 \\ +\left\{\left(\tau_w^x\right)_{i,j}^{n} + \left(\tau_w^x\right)_{i+1,j}^{n}\right\}/2\rho - \left(\tau_b^x\right)_{i,j}/\rho \end{bmatrix} \quad \text{(D.5)}$$

$$V_{i,j}^{n+1} = V_{i,j}^{n} + \Delta t \begin{bmatrix} -g\overline{\overline{h_{i,j}}}\left(\eta_{i,j+1}^{n+1} - \eta_{i,j}^{n+1}\right)/\overline{\Delta y} \\ -f\left(U_{i-1,j}^{n+1} - U_{i-1,j+1}^{n+1} + U_{i,j}^{n+1} - U_{i,j+1}^{n+1}\right)/4 \\ +\left\{\left(\tau_w^y\right)_{i,j+1}^{n} + \left(\tau_w^y\right)_{i,j}^{n}\right\}/2\rho - \left(\tau_b^y\right)_{i,j}/\rho \end{bmatrix} \quad \text{(D.6)}$$

where

$$t = n\Delta t$$
$$x = i\overline{\Delta s}, \quad y = j\overline{\Delta s}$$
$$\overline{h_{i,j}} = \left(h_{i,j} + h_{i+1,j}\right)/2$$
$$\overline{\overline{h_{i,j}}} = \left(h_{i,j+1} + h_{i,j}\right)/2$$
$$\left(\tau_b^x\right)_{i,j} = \rho r U_{i,j}^{n}/\overline{h_{i,j}}$$
$$\left(\tau_b^y\right)_{i,j} = \rho r V_{i,j}^{n}/\overline{\overline{h_{i,j}}}$$

D-2 Stability properties of the finite difference scheme

Ideally the finite difference scheme should be stable, neutral (i.e. the solution is not amplified or damped with each time step) and display the minimum of numerical dispersion. To determine the stability of the finite difference scheme on a staggered grid with uneven grid spacing, it is necessary to make the following approximations

$$\Delta u_i = \Delta u_{i-1} = 2\Delta x$$
$$\Delta v_i = \Delta v_{i-1} = 2\Delta x$$
$$\overline{\Delta x} = 2\Delta x$$
$$\overline{\Delta y} = 2\Delta y$$
$$(1 - w_u) = (1 - w_v) = \frac{1}{2}$$

For ease of manipulation the finite difference equations are rewritten using the indices as indicated in the grid in Fig D.1.

Excluding the wind forcing and bottom friction terms, the finite difference equations D.4 to D.6 may then be expressed as follows

$$\eta_{i,j}^{n+1} = \eta_{i,j}^{n} - \Delta t \left[\left(U_{i+1,j}^{n} - U_{i-1,j}^{n} \right) / 2\Delta x + \left(V_{i,j+1}^{n} - V_{i,j-1}^{n} \right) / 2\Delta y \right] \quad \text{(D.7)}$$

$$U_{i,j}^{n+1} = U_{i,j}^{n} + \Delta t \begin{bmatrix} -g\overline{h_{i,j}} \left(\eta_{i+1,j}^{n+1} - \eta_{i-1,j}^{n+1} \right) / 2\Delta x \\ +f \left(V_{i+1,j+1}^{n} + V_{i+1,j-1}^{n} + V_{i-1,j+1}^{n} + V_{i-1,j-1}^{n} \right) / 4 \end{bmatrix} \quad \text{(D.8)}$$

$$V_{i,j}^{n+1} = V_{i,j}^{n} + \Delta t \begin{bmatrix} -g\overline{\overline{h_{i,j}}} \left(\eta_{i,j+1}^{n+1} - \eta_{i,j-1}^{n+1} \right) / 2\Delta y \\ -f \left(U_{i+1,j+1}^{n+1} - U_{i+1,j-1}^{n+1} + U_{i-1,j+1}^{n+1} - U_{i-1,j-1}^{n+1} \right) / 4 \end{bmatrix} \quad \text{(D.9)}$$

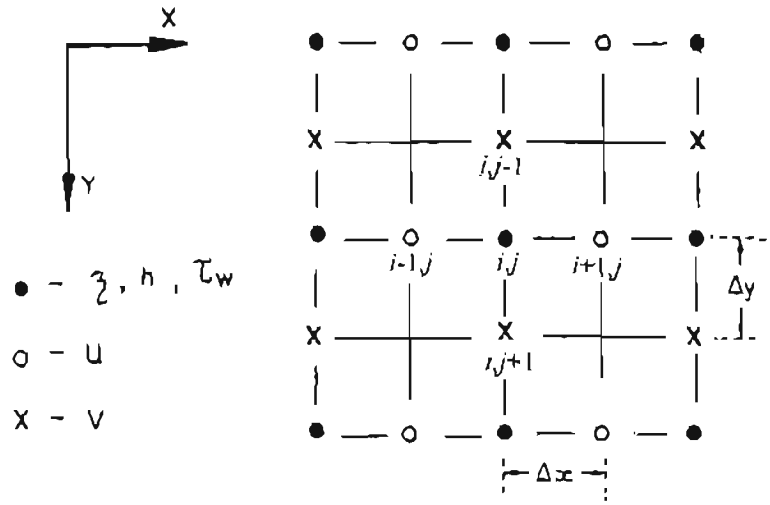

Fig D.1 *Staggered finite difference grid indicating the indices used to re-write the finite difference equations for ease of manipulation in the stability analysis of the semi-implicit Euler forward-backward finite difference scheme.*

A Von Neumann stability analysis (Mesinger and Arakawa, 1976) is undertaken to determine the stability and numerical dispersion properties of the above finite difference numerical scheme by making the following substitutions into equations D.7 to D.9

$$\left[U_{j,m}^{n+1}, V_{j,m}^{n+1}, \eta_{j,m}^{n+1} \right] = \lambda \left[U^{n}, V^{n}, \eta^{n} \right] e^{i(k\Delta x + l\Delta y)}$$

where $x = j\Delta x$, $y = m\Delta y$, $t = n\Delta t$ and λ is an amplification factor where $|\lambda|$ gives the growth of the numerical solution with each time step. Ideally the finite difference numerical scheme of the inviscid equations D.7 to D.9 should be neutral, where the

numerical solution is neither amplified or damped with each time step (i.e. $|\lambda| = 1$) The Von Neumann analysis shows that for a neutral and stable numerical scheme it is required that

$$\frac{\overline{\Delta x}}{\Delta t} \geq \sqrt{gh\left[\left(\frac{\overline{\Delta x}}{\overline{\Delta y}}\right)^2 + 1\right]} \quad or \quad \frac{\overline{\Delta y}}{\Delta t} \geq \sqrt{gh\left[\left(\frac{\overline{\Delta y}}{\overline{\Delta x}}\right)^2 + 1\right]} \qquad (D.10)$$

and $\Delta t \leq 2/f$

where $\overline{\Delta x} = 2\Delta x$, $\overline{\Delta y} = 2\Delta y$

When the grid spacings are equal (i.e. $\overline{\Delta x} = 2\Delta x$, $\overline{\Delta y} = 2\Delta y$) these stability criteria reduce to

$$\frac{\overline{\Delta x}}{\Delta t} \geq \sqrt{2\,gh} \quad or \quad \frac{\overline{\Delta y}}{\Delta t} \geq \sqrt{2\,gh} \qquad (D.11)$$

and $\Delta t \leq 2/f$

This stability criterion is commonly known as the Courant-Friederich-Lewy (CFL) condition. If linear bottom friction terms are included in the equations used in the stability analysis, the real solution is damped and consequently the numerical scheme is no longer expected to be neutral. A similar analysis to that above shows that the inclusion of linear bottom friction terms leads to $|\lambda|$ assuming a value of

$$|\lambda| = (1 + B) \quad \text{where} \quad B = \frac{-r\Delta t}{h}$$

This results in a "modified stability criterion" of

$$\frac{\overline{\Delta x}}{\Delta t} \geq \sqrt{\frac{4\,gh}{B_1}} \quad or \quad \frac{\overline{\Delta y}}{\Delta t} \geq \sqrt{\frac{4\,gh}{B_1}}$$

where $B_1 = \left(1 + \frac{B}{2}\right) + \sqrt{1 + B}$

D-3 Numerical Dispersion

The dispersion properties of external gravity waves in the finite difference equations (D 7 to D.9) differ from the dispersion properties of external gravity waves in the unforced, frictionless shallow water wave equations from which the finite difference

equations D 7 to D.9 are derived. This discrepancy in phase characteristics between the two is due to numerical dispersion (i.e. dispersion inherent to the finite difference numerical scheme). For the finite difference model to produce solutions that are representative of the set of continuum equations, one requires that the numerical dispersion be negligible. Consider a flat-bottomed ocean where the dispersion properties of an external gravity wave $\eta \propto e^{i(\sigma t - kx - hy)}$ in the continuum equations are given by

$$\sigma_c = \pm\sqrt{f^2 + \left(k^2 + \ell^2\right)gh}$$

The dispersion properties of the same wave in the discretised equations (D.7 to D.9) is given by

$$\sigma_n = \pm\frac{1}{\Delta t}\arctan\left(\frac{\lambda_{imaginary}}{\lambda_{real}}\right)$$

$$= \pm\frac{1}{\Delta t}\arctan\left(\frac{\sqrt{4\varepsilon - \varepsilon^2}}{2-\varepsilon}\right)$$

where

$$\varepsilon = \left(gh\Delta t^2\right)\left[\left(\frac{\sin k\Delta x}{\Delta x}\right)^2 + \left(\frac{\sin \ell\Delta y}{\Delta y}\right)^2 - \frac{f\Delta t}{4}\left(\frac{\sin 2k\Delta x \sin 2\ell\Delta y}{\Delta x\,\Delta y}\right)\right]$$

$$+ \left(f\Delta t \cos k\Delta x \cos \ell\Delta y\right)$$

The dispersion properties (and thus numerical dispersion) of the finite different numerical scheme are thus dependent on the spatial arrangement of the variables, the spatial increments Δx and Δy in the finite difference grid, and the time increment Δt

In Fig D.2, the percentage relative phase error due to numerical dispersion is expressed as a function of the cross-shore (k) and alongshore (ℓ) wavenumbers of the motion multiplied by the grid spacings Δx and Δy, respectively. Note that the shortest wavelengths resolved by the staggered grid are $\lambda_k = 4\Delta x$ ($k\Delta x = \pi/2$) and $\lambda_\ell = 4\Delta y$ ($k\Delta x = \pi/2$). The percentage relative phase error is calculated using

$$\%\text{ relative phase error} = 100\left(\frac{\sigma_c - \sigma_n}{\sigma_c}\right)$$

Fig D.2 indicates that the shortest resolvable wavelength motions ($\lambda_k = 4\Delta x$ and $\lambda_\ell = 4\Delta y$) are least accurately modelled by the finite difference numerical scheme. The relative phase error is as great as 30% for the shortest resolvable wavelength motions. Further, the dispersion properties of the finite difference scheme are such that these shortest resolvable wavelength motions have a zero group velocity (Mesinger and Arakawa, 1976). This is expected to cause problems in the numerical model should these short wavelength motions be introduced into the modelled domain. Inferior open boundary conditions, in particular, can introduce into the numerical domain short wavelength "noise" consisting of short wavelength motions having a zero group velocity. The longer wavelength motions have less significant relative phase errors and are accurately represented within the numerical model.

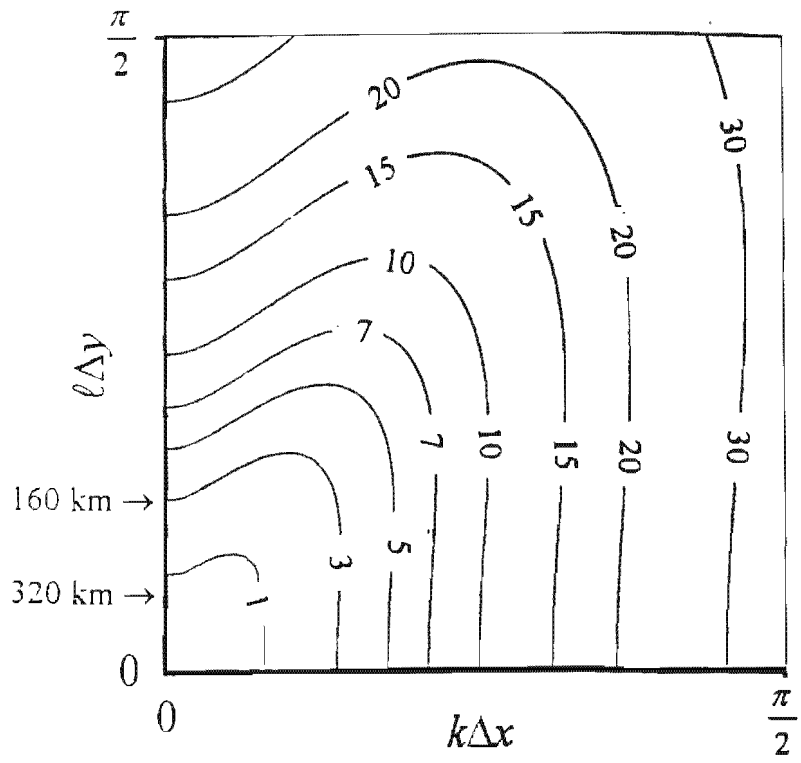

Fig D.2 *Contours of the percentage relative phase errors introduced by the numerical scheme expressed as a function of* kΔx *and* ℓΔy. *($k\Delta x$ = $\ell\Delta y$. = $\pi/2$ are the shortest waves resolved by the numerical grid)*

In Fig D.3 .the phase speed of a wave in the numerical model (C_n) is plotted as a percentage of its true phase speed (C_c) in the continuum equations. This relative phase speed is calculated using

$$\% \text{ relative phase speed} = 100\ (C_n / C_c)$$

A value of 100% represents complete accuracy of phase speeds in the numerical model. The longer wavelength motions are accurately represented, however the phase speeds of the shortest resolvable wavelengths are only 70% of their true magnitude in the continuum equations.

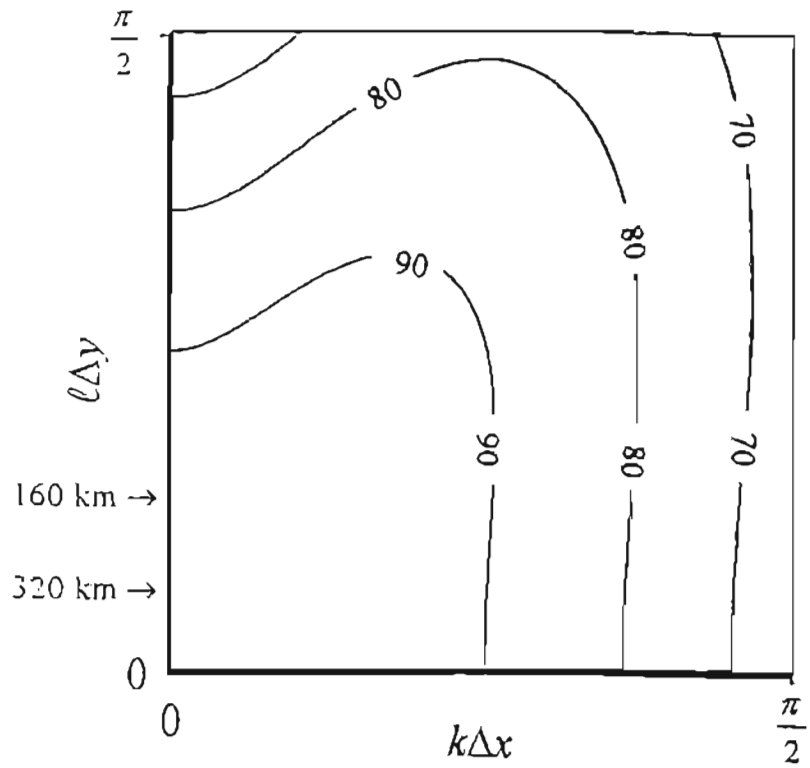

Fig D.3 *Contours of the percentage relative phase velocities in the finite difference numerical scheme expressed as a function of kΔx and ℓΔy. (kΔx = ℓΔy. = π/2 are the shortest waves resolved by the numerical grid)*

Since the phase properties of all but the shortest resolvable wavelengths are accurately represented within the numerical model, one can assume that the impact of numerical dispersion on the numerical model results is small. The only reason for concern are the shortest resolvable wavelengths which are poorly represented within the finite difference numerical model. This is confirmed by Foreman (1987) who compared analytical shelf wave dispersion curves for the above continuum equations with shelf wave dispersion properties typical of a number of finite difference schemes and grid configurations. He shows that, although the low frequency (non-dispersive) behaviour of shelf waves in the numerical models is acceptable, significant errors are apparent in the high frequency phase behaviour of modelled CTW and the 'resonance' frequencies (frequency maxima) in the numerical shelf wave dispersion curves are slightly lower

than the analytical shelf wave dispersion curves obtained from the continuum equations. He also shows that the magnitude of these errors are related to the nature of the underlying topography.

The above discussion underscores the importance of resolving the significant physical processes in numerical models of shelf circulation. A comprehensive discussion of the space and time scales that are required to be resolved in numerical models of shelf circulation is provided by Craig (1988).

D-4 - Cross-shelf open boundary conditions of the numerical model

The correct specification of open boundary conditions (OBC's) in the cross-shelf direction is very important as the OBC's in a numerical model can strongly influence the results in the interior of the numerical domain (e.g. Chapman, 1985; Røed and Cooper, 1986, 1987; Hayashi *et al.*, 1986). Ideally an OBC should allow disturbances originating in the interior of the computational domain to leave the computational domain without disturbing or causing any deterioration of the interior solution. In short, an OBC should satisfy the following requirements:

a) fluid motions such as propagating waves or advection should be unrestricted

b) the OBC should be numerically stable

c) the accuracy of the OBC should be adequate (i.e. have an accuracy of approximately the same order as the finite difference numerical scheme)

d) the OBC should be mathematically well (enough) posed, and

e) the OBC should be matched to the numerical model

A number of specialist reviews (Chapman, 1985; Røed and Cooper, 1986, 1987,) highlight both the effect the boundary conditions have on the interior solution and the effectiveness of the different open boundary conditions (OBC's) under different forcing functions. General conclusions are that the effects of a particular OBC may be felt far into the interior domain and that the performance of the different OBC's is strongly dependent on the type of forcing used.

The nature of continental shelf wave motions are such that the long wave motions are essentially non-dispersive and move anti-clockwise around the coast of southern Africa. Shorter wavelength motions, however, are strongly dispersive. In barotropic theory of CTW motions there exists a critical wavenumber, ℓ_{crit}, where the group velocity is zero (see dispersion curves in Appendix B). Motions with wavelengths exceeding ℓ_{crit}, all have a negative group velocity (i.e. the phase and group velocities of these motions are of opposite sign). Further, the dispersion properties of the shortest resolvable wavelengths in the barotropic finite difference numerical model are such that they have a zero group velocity. Thus, for short wavelength motions, the associated energy is not propagated away from the location where these motions are generated. Inferior open boundary conditions excite and cause reflection of short wavelength motions into the interior of the numerical model. Not only do these reflected short waves contaminate the solution in the interior of the numerical domain but the energy associated with these waves accumulates at the southern boundary of the numerical model and cause the model to become unstable due to the rapid growth of the solution in this region A large number of possible open boundary conditions (mainly "sponge" and pseudo-radiation boundary conditions) for the southern boundary of the numerical model have been investigated (for example Chapman, 1985; Røed and Smedstad, 1984; Røed and Cooper, 1986; 1987 and Hayashi *et al.*, 1986). These reviews suggest that the simplest open boundary conditions for the Euler forward-backward finite difference numerical model that satisfy all of the desired criteria for an open boundary condition are of the pseudo-radiation type based on the Sommerfeld radiation equation

$$\frac{\partial \phi}{\partial t} + C_{ph} \frac{\partial \phi}{\partial y} = f(\phi, t)$$

The open boundary conditions used to test the numerical model are

a) a modified Miller and Thorpe (1981) version of the Orlanski (1976) open boundary radiation condition where forward differences rather than centred differences are used in developing the numerical version of the OBC (Two versions of this OBC were tested, one where the maximum allowed phase velocity of motions leaving the grid are restricted to the local gravity wave

phase velocity of $\sqrt{gh_i}$ and the other were this phase velocity is restricted to the maximum allowable phase velocity in the grid of $\overline{\Delta y}/\Delta t$), and

b) the Camerlengo and O'Brien (1980) version of the same OBC. More complicated OBC's are available for numerical models where there is wind-forcing on the boundaries (Røed and Smedstad, 1984), however it was found that the Camerlengo and O'Brien (CO) OBC performed adequately for modelling dispersive CTW motions with forcing on the open boundaries. There are problems associated with this CO OBC such as emptying of the model basin (Røed and Cooper, 1986), however these do not seem to be limiting on the time scales (96 hours) for which the model was run. Greater detail of the properties of the above OBC's are given in the reviews mentioned above.

The detail of the two OBC,s is given below

(a) The "advection" OBC (Miller and Thorpe, 1981) - MT OBC

Here the boundary variable at the new time level $(n+1)$ is given by

$$\phi_{i,B}^{n+1} = \left(1 - \mu_B\right)\phi_{i,B}^{n} + \mu_B\left(\phi_{i,B-1}^{n}\right) \qquad \text{(D.12)}$$

where for version 1

$$\mu_B = \begin{cases} \mu_{local} & \mu_{est} > \mu_{local} \\ \mu_{est} & \text{if} \quad 0 \le \mu_{est} \le \mu_{local} \\ 0 & \mu_{est} < 0 \end{cases}, \qquad \text{(D.13)}$$

and for version 2

$$\mu_B = \begin{cases} 1 & \mu_{est} > 1 \\ \mu_{est} & \text{if} \quad 0 \le \mu_{est} \le 1 \\ 0 & \mu_{est} < 0 \end{cases} \qquad \text{(D.14)}$$

where

$$\mu_{local} = \sqrt{gh_i}\,\frac{\Delta t}{\overline{\Delta y}} \qquad \text{(D.15)}$$

$$\mu_{est} = -\frac{\Delta t}{\overline{\Delta y}}\,\frac{\left(\phi_{i,B-1}^{n} - \phi_{i,B-1}^{n-1}\right)}{\left(\phi_{i,B-1}^{n-1} - \phi_{i,B-2}^{n-1}\right)} \qquad \text{(D.16)}$$

The reflection of motions back into the numerical domain is proportional to the difference between the real phase speed of the motions leaving the computational domain and the numerically estimated phase speed. The estimate of μ_B may become

particularly large for small gradients of $\frac{\partial \phi}{\partial t}$ and $\frac{\partial \phi}{\partial y}$, leading to substantial reflection at the boundaries. It is for this reason that we limit the magnitude of μ_B such that $|\mu_B| \leq 1$.

(b) The simplified OBC (Camerlengo and O'Brien, 1980) - CO OBC

Camerlengo and O'Brien (1980) modified the above form of the OBC to obtain a simpler version where D.12 and D.16 hold but D.13/14 is given by

$$\mu_B = \begin{matrix} 1 \\ 0 \end{matrix} \quad \text{if} \quad \begin{matrix} \mu_{est} \geq 0 \\ \mu_{est} < 0 \end{matrix} \qquad \text{(D.17)}$$

In this version of the OBC any outgoing wave is assumed to be moving at a phase speed of $\Delta y / \Delta t$ which is the maximum phase speed possible in the numerical grid. This version of OBC is chosen for use in the finite difference model as it handles forced, dispersive waves adequately.